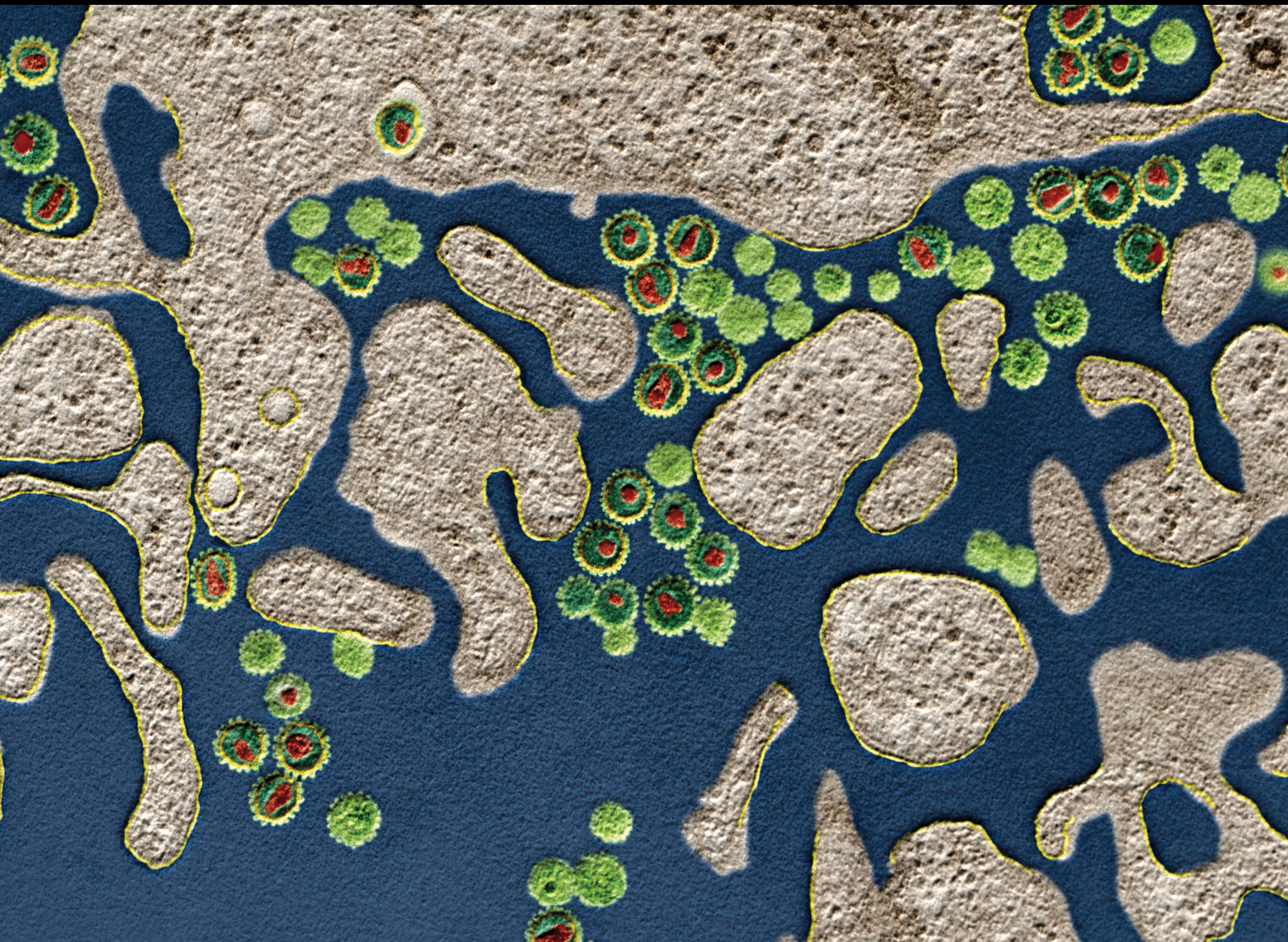


Translational Research Based on Pathogen-Derived Molecules Inducing Innate And Adaptive Immune Responses

Lead Guest Editor: Zhipeng Xu

Guest Editors: Xianyang Li, Biniam Mathewos, and Juming Yan





Translational Research Based on Pathogen-Derived Molecules Inducing Innate And Adaptive Immune Responses

**Translational Research Based on
Pathogen-Derived Molecules Inducing
Innate And Adaptive Immune
Responses**

Lead Guest Editor: Zhipeng Xu





Guest Editors: Xianyang Li, Biniam Mathewos, and
Juming Yan



Copyright © 2021 Hindawi Limited. All rights reserved.

This is a special issue published in "Journal of Immunology Research." All articles are open access articles distributed under the Creative Commons Attribution License, which permits unrestricted use, distribution, and reproduction in any medium, provided the original work is properly cited.

Associate Editors

Douglas C. Hooper , USA
Senthamil R. Selvan , USA
Jacek Tabarkiewicz , Poland
Baohui Xu , USA

Academic Editors




Nitin Amdare , USA
Lalit Batra , USA
Kurt Blaser, Switzerland
Dimitrios P. Bogdanos , Greece
Srinivasa Reddy Bonam, USA
Carlo Cavaliere , Italy
Cinzia Ciccacci , Italy
Robert B. Clark, USA
Marco De Vincentiis , Italy
M. Victoria Delpino , Argentina
Roberta Antonia Diotti , Italy
Lihua Duan , China
Nejat K. Egilmez, USA
Theodoros Eleftheriadis , Greece
Eyad Elkord , United Kingdom
Weirong Fang, China
Elizabeth Soares Fernandes , Brazil
Steven E. Finkelstein, USA
JING GUO , USA
Luca Gattinoni , USA
Alvaro González , Spain
Manish Goyal , USA
Qingdong Guan , Canada
Theresa Hautz , Austria
Weicheng Hu , China
Giannicola Iannella , Italy
Juraj Ivanyi , United Kingdom
Ravirajsinh Jadeja , USA
Peirong Jiao , China
Youmin Kang , China
Sung Hwan Ki , Republic of Korea
Bogdan Kolarz , Poland
Vijay Kumar, USA
Esther Maria Lafuente , Spain
Natalie Lister, Australia

Daniele Maria-Ferreira, Saint Vincent and the Grenadines

Eiji Matsuura, Japan
Juliana Melgaço , Brazil
Cinzia Milito , Italy
Prasenjit Mitra , India
Chikao Morimoto, Japan
Paulina Niedźwiedzka-Rystwej , Poland
Enrique Ortega , Mexico
Felipe Passero, Brazil
Anup Singh Pathania , USA
Keshav Raj Paudel, Australia
Patrice Xavier Petit , France
Luis Alberto Ponce-Soto , Peru
Massimo Ralli , Italy
Pedro A. Reche , Spain
Eirini Rigopoulou , Greece
Ilaria Roato , Italy
Suyasha Roy , India
Francesca Santilli, Italy
Takami Sato , USA
Rahul Shivahare , USA
Arif Siddiqui , Saudi Arabia
Amar Singh, USA
Benoit Stijlemans , Belgium
Hiroshi Tanaka , Japan
Bufu Tang , China
Samanta Taurone, Italy
Mizue Terai, USA
Ban-Hock Toh, Australia
Shariq M. Usmani , USA
Ran Wang , China
Shengjun Wang , China
Paulina Wlasiuk, Poland
Zhipeng Xu , China
Xiao-Feng Yang , USA
Dunfang Zhang , China
Qiang Zhang, USA
Qianxia Zhang , USA
Bin Zhao , China
Jixin Zhong , USA
Lele Zhu , China

Contents



SLC2A5 Correlated with Immune Infiltration: A Candidate Diagnostic and Prognostic Biomarker for Lung Adenocarcinoma

Lianxiang Luo , Jiating Su, Yushi Zheng, Fangfang Huang, Riming Huang , and Hui Luo 
Research Article (18 pages), Article ID 9938397, Volume 2021 (2021)



The Role and Function of Regulatory T Cells in *Toxoplasma gondii*-Induced Adverse Pregnancy Outcomes

Xuyang Gao , Yue Zhong , Yifan Liu , Runmin Ding , and Jinling Chen 
Review Article (11 pages), Article ID 8782672, Volume 2021 (2021)



Inhibition of NF- κ B/IL-33/ST2 Axis Ameliorates Acute Bronchiolitis Induced by Respiratory Syncytial Virus

Liwen Zhang, Yu Wan, Liang Ma, Kaihong Xu , and Baojin Cheng 
Research Article (11 pages), Article ID 6625551, Volume 2021 (2021)

Analysis of Lymphocyte Subpopulations and Cytokines in COVID-19-Associated Pneumonia and Community-Acquired Pneumonia

Guohong Liu, Xianghu Jiang, Xiaoqiao Zeng, Yunbao Pan , and Haibo Xu 
Research Article (9 pages), Article ID 6657894, Volume 2021 (2021)




1 α ,25-Dihydroxyvitamin D3 Supplementation during Pregnancy Is Associated with Allergic Rhinitis in the Offspring by Modulating Immunity

Liqing Zhang, Haifeng Ni , Zhen Zhou, Xiaoyang Yuan, Junbo Xia, Bo Jiang, and Yong Li 
Research Article (12 pages), Article ID 6638119, Volume 2021 (2021)



Identification of SHMT2 as a Potential Prognostic Biomarker and Correlating with Immune Infiltrates in Lung Adenocarcinoma

Lianxiang Luo , Yushi Zheng, Zhiping Lin, Xiaodi Li, Xiaoling Li, Mingyue Li, Liao Cui, and Hui Luo
Research Article (18 pages), Article ID 6647122, Volume 2021 (2021)






Application of Bionanomaterials in Tumor Immune Microenvironment Therapy

Jiawei Wang , Yan Bao , and Yandan Yao 
Review Article (10 pages), Article ID 6663035, Volume 2021 (2021)








High-Expressed Macrophage Scavenger Receptor 1 Predicts Severity Clinical Outcome in Transplant Patient in Idiopathic Pulmonary Fibrosis Disease

Mingfeng Zheng, Tian Tian, Jialong Liang, Shugao Ye, Jingyu Chen , and Yong Ji 
Research Article (11 pages), Article ID 6690100, Volume 2021 (2021)

Club Cell Protein 16 Attenuates CD16^{bright}CD62^{dim} Immunosuppressive Neutrophils in Damaged Tissue upon Posttraumatic Sepsis-Induced Lung Injury

Nils Becker , Philipp Störmann , Andrea Janicova, Kernt Köhler, Klemens Horst , Ildiko Rita Dunay, Claudia Neunaber , Ingo Marzi, Jan Tilmann Vollrath, and Bornha Relja 
Research Article (14 pages), Article ID 6647753, Volume 2021 (2021)

DHX37 Impacts Prognosis of Hepatocellular Carcinoma and Lung Adenocarcinoma through Immune Infiltration

Yanni Xu , Qiongchao Jiang , Hejun Liu , Xiaoyun Xiao , Dinghong Yang , Phei Er Saw , and Baoming Luo 

Research Article (20 pages), Article ID 8835393, Volume 2020 (2020)

Research Article

SLC2A5 Correlated with Immune Infiltration: A Candidate Diagnostic and Prognostic Biomarker for Lung Adenocarcinoma

Lianxiang Luo ^{1,2,3}, Jiating Su,⁴ Yushi Zheng,⁴ Fangfang Huang,⁵ Riming Huang ⁶,
and Hui Luo ^{1,2,3}

¹Southern Marine Science and Engineering Guangdong Laboratory (Zhanjiang), Zhanjiang, Guangdong 524023, China

²The Marine Biomedical Research Institute, Guangdong Medical University, Zhanjiang, Guangdong 524023, China

³The Marine Biomedical Research Institute of Guangdong Zhanjiang, Zhanjiang, Guangdong 524023, China

⁴The First Clinical College, Guangdong Medical University, Zhanjiang, Guangdong 524023, China

⁵Graduate School, Guangdong Medical University, Zhanjiang, Guangdong 524023, China

⁶Guangdong Provincial Key Laboratory of Food Quality and Safety, College of Food Science, South China Agricultural University, Guangzhou, China

Correspondence should be addressed to Lianxiang Luo; luolianxiang321@gdmu.edu.cn,
Riming Huang; huangriming@scau.edu.cn, and Hui Luo; luohui@gdmu.edu.cn

Received 28 March 2021; Accepted 20 August 2021; Published 23 September 2021

Academic Editor: Zhipeng Xu

Copyright © 2021 Lianxiang Luo et al. This is an open access article distributed under the Creative Commons Attribution License, which permits unrestricted use, distribution, and reproduction in any medium, provided the original work is properly cited.

Lung adenocarcinoma (LUAD) is a major subtype of lung cancer with a relatively poor prognosis, requiring novel therapeutic approaches. Great advances in new immunotherapy strategies have shown encouraging results in lung cancer patients. This study is aimed at elucidating the function of SLC2A5 in the prognosis and pathogenesis of LUAD by analyzing public databases. The differential expression of SLC2A5 in various tissues from Oncomine, GEPIA, and other databases was obtained, and SLC2A5 expression at the protein level in normal and tumor tissues was detected with the use of the HPA database. Then, we used the UALCAN database to analyze the expression of SLC2A5 in different clinical feature subgroups. Notably, in both Prognoscan and Kaplan-Meier plotter databases, we found a certain association between SLC2A5 and poor OS outcomes in LUAD patients. Studies based on the TIMER database show a strong correlation between SLC2A5 expression and various immune cell infiltrates and markers. The data analysis in the UALCAN database showed that the decreased promoter methylation level of SLC2A5 in LUAD may lead to the high expression of SLC2A5. Finally, we used the LinkedOmics database to evaluate the SLC2A5-related coexpression and functional networks in LUAD and to investigate their role in tumor immunity. These findings suggest that SLC2A5 correlated with immune infiltration can be used as a candidate diagnostic and prognostic biomarker in LUAD patients.

1. Introduction

Lung cancer is considered to be one of the most common cancers worldwide with high incidence rate and high mortality rate [1]. Non-small-cell lung cancer, including lung adenocarcinoma (LUAD) and lung squamous cell carcinoma, is the main type of lung cancer, accounting for nearly 85%; among them, LUAD is the most common histological subtype [2]. LUAD generally originates from the surrounding lung tissue [3] and is characterized by the formation of glands or ducts and the production of a large amount of mucus, with obvious

cellular and molecular characteristics [4]. Due to the high metastasis, recurrence, and drug resistance of LUAD, the curative effect of conventional treatment including surgery, radiotherapy, and chemotherapy is not so satisfactory, and the incidence of this aggressive disease is still surprisingly high [5, 6]. Therefore, it is urgent to find reliable biomarkers for the diagnosis and prognosis prediction of LUAD, which will contribute to the effective treatment of LUAD.

SLC2A5, namely, fructose transporter GLUT5 gene, is one of the key genes in the process of tumor development, whose regulation mechanism is the regulation of fructose

uptake and absorption and carbon absorption in cells [7]. Studies have found that the expression of SLC2A5 is closely related to the metabolism of tumor cells and tumor progression, especially the increase of SLC2A5 coding GLUT5 protein seems to be associated with the development and metastasis of LUAD [7]. According to recent reports, SLC2A5 is involved in the progression of a variety of cancers, including pancreatic cancer, breast cancer, small intestine carcinoma, and LUAD [7]. SLC2A5 can increase the flux of pentose phosphate pathway and protein synthesis by increasing fructose synthesis, thus promoting the growth of pancreatic cancer [8]. Jiang et al. [9] demonstrated that SLC2A5 can increase the risk of breast cancer development and metastasis by promoting fructose synthesis, which could induce lipoxygenase-12 and related fatty acid 12-HETE in breast cancer cells [9]. A study on acute myeloid leukemia (AML) showed that SLC2A5 upregulation occurs in AML, and blocking the pharmacological process of SLC2A5 regulating fructose uptake could improve the phenotype of leukemia [10]. Moreover, studies have shown that SLC2A5 are significantly upregulated in LUAD patients and that their overexpression is highly correlated with poor survival in LUAD patients [7]. However, whether SLC2A5 is a powerful biomarker of LUAD has not been given a clear answer. Also, the biological functions of SLC2A5 in LUAD remain to be determined.

As is known to us, inflammation is one of the major contributors to the tumor microenvironment [11], and the risk of cancer is greatly increased by viral and bacterial infection [12]. Previous studies have found increases in the expression of indoleamine 2,3-dioxygenase 1 (IDO1) associated with intestinal flora and the differentiation of gut secretion cells is related to inflammation, injury, infection, changes in flora, and so on, but with reduced SLC2A5 levels [13]. This may indicate that changes in SLC2A5 levels are associated with inflammation, viruses, flora changes, infection, etc., thus affecting tumor occurrence and/or progression. The above thinking may provide promising foundations and analysis for studying the role that SLC2A5 plays in lung cancer.

To better explore the role of SLC2A5 in LUAD, we learned the research ideas of Luo et al. in this study [14]. We first explored the differential expression of SLC2A5 in different organizations using databases like Oncomine and GEPIA. Meanwhile, the Human Protein Atlas (HPA) database was used to detect SLC2A5 expression in normal and tumor tissues. Moreover, we used the UALCAN database to analyze the expression of SLC2A5 in different clinical feature subgroups. PrognoScan database and Kaplan-Meier plotter were used to assess the relationship between SLC2A5 and prognosis of LUAD patients comprehensively. Tumor immunoassay resource (TIMER) database was used to further investigate the association between SLC2A5 expression levels and immune cell infiltration, different immune cell subsets markers in LUAD, and the UALCAN database was used to analyze the promoter methylation level of SLC2A5 in LUAD and the correlation between SLC2A5 expression level and different subgroups of LUAD patients. Finally, we used the LinkedOmics database to evaluate the SLC2A5-related coexpression and functional network of SLC2A5 in

LUAD and to investigate their role in tumor immunity. Our results provide a novel insight into the function of SLC2A5 in LUAD and a theoretical basis for the early diagnosis, prognosis, and targeted therapy of LUAD.

2. Materials and Methods

2.1. Oncomine Database Analysis. The web-based Oncomine database, whose data includes a microarray database of most human cancers, aims at facilitating cancer-related factor discovery from genome-wide expression analyses [15, 16]. In this study, following the methods of Ma et al. [17], we conducted Oncomine database analysis to assess SLC2A5 expression level based on the following criteria: (1) “gene: SLC2A5”; (2) “analysis type: cancer vs. normal”; (3) “cancer type: lung cancer”; (4) “data type: mRNA”; and (5) threshold settings: folding change = 2, P value = 0.05.

2.2. TIMER Database Analysis. By studying the research ideas of Luo et al. [14], the TIMER database is an effective tool to analyze the abundance of tumor-infiltrating immune cells from the target gene expression data [18–20]. Thus, this study analyzed the expression of SLC2A5 in LUAD patients and six types of infiltration of immune cells (B cells, CD4+ T cells, CD8+ T cells, neutrophils, macrophages, and dendritic cells). At the same time, the correlation between SLC2A5 expression and the genetic markers of tumor-infiltrating immune cells was also discussed.

2.3. GEPIA Database Analysis. The GEPIA (Gene Expression Profiling Interactive Analysis) web server has been a valuable and highly cited resource for gene expression analysis based on tumor and normal samples from TCGA and the GTEx databases [21–23]. So the expression of SLC2A5 in tumor and normal tissues of this study was further used to conduct with GEPIA, as shown in the box diagram.

2.4. UALCAN Database Analysis. In this study, UALCAN, an interactive web portal based on TCGA3RNA-seq and clinical data of 31 cancer types [24], was used to analyze the correlation between SLC2A5 expression and different clinical factors.

2.5. Kaplan-Meier Plotter Analysis. The Kaplan-Meier plotter is an online database including gene expression data and clinical data, which offers a means of exploring the impact of a wide variety of genes on patient survival in 21 different types of cancer [25, 26]. Therefore, this database was used to evaluate the prognostic value of SLC2A5 and explore the association between SLC2A5 expression and outcome in LUAD patients, as well as the impact of both clinicopathological factors and SLC2A5 on the outcome of patients with LUAD.

2.6. Human Protein Atlas Database Analysis. The Human Protein Atlas (HPA) [27, 28] provides a powerful platform to evaluate protein localization and expression in human cells, tissues, and organs [29]. Therefore, we used the database to analyze the protein expression and immunohistochemistry (IHC) of SLC2A5 in normal and LUAD tissues.

2.7. PrognScan Database Analysis. The PrognScan database offers a valuable tool for researchers assessing the biological relationship between gene expression and prognosis, which is of great help to accelerate our cancer research [30, 31]. This database was used to assess the relationship between SLC2A5 expression and patient outcome.

2.8. Meta-Analysis. Meta-analysis can evaluate the evidence and the effect indicators more accurately and objectively, so as to explain the heterogeneity of different research results [32, 33]. Therefore, meta-analysis was used to evaluate the overall prognostic significance of SLC2A5 in LUAD patients. HR and 95% CI were calculated to evaluate the correlation between SLC2A5 expression and the prognosis of LUAD patients. With the random effects model, the heterogeneity across multiple datasets was assessed by the Q test (I^2 statistics).

2.9. LinkedOmics Database Analysis. The LinkedOmics database contains multiomic cancer datasets for 32 cancer types and a total of 11,158 patients from TCGA project. This comprehensive and functional database also provides three key analysis modules including LinkFinder, LinkCompare, and LinkInterpreter [34] and an analysis toolkit (WebGestalt) [35, 36], which were applied in this study. Thus, LinkedOmics was used to sign and rank the data which was selected for GSEA to perform GO (BP, CC, and MF) and KEGG analysis in this study.

3. Results

3.1. High SLC2A5 Expression in LUAD. Oncomine and TIMER databases were used to evaluate the mRNA expression of SLC2A5 in multiple tumor tissues and normal tissues. Oncomine analysis results showed that in several solid tumors, the expression of SLC2A5 was more significant in lung cancer, lymphatic cancer, brain and CNS cancer, and breast cancer, while the expression rate of SLC2A5 in other cancers such as gastric cancer, ovarian cancer, and other cancers was lower (Figure 1(a)). Meanwhile, Oncomine analysis of LUAD and normal samples also showed that in different patient datasets (SLC2A5 expression in Su's dataset, Hou's dataset, Stearman's dataset, and Okayama's dataset), the expression of SLC2A5 in LUAD was higher than that in normal lung gland tissue (Figures 1(c)–1(f)). TIMER database analysis results revealed the SLC2A5 expression differences in all tumor tissues and adjacent normal tissues (Figure 1(b)): SLC2A5 expression in COAD (colon adenocarcinoma), KICH (renal cell carcinoma), KIRP (renal cell carcinoma), PRAD (prostate adenocarcinoma), and READ (rectal adenocarcinoma) was significantly lower than that in adjacent normal tissues; in contrast, SLC2A5 expression in LUAD (lung adenocarcinoma), UCEC (endometrial carcinoma), CHOL (cholangiocarcinoma), KIRC (renal clear cell carcinoma), LIHC (hepatocellular carcinoma), LUSC (lung squamous cell carcinoma), and ESCA (esophageal carcinoma) was significantly higher. Data mining of GEPIA and UALCAN databases was further confirmed. On the

one hand, GEPIA analysis confirmed that the expression of SLC2A5 in LUAD tissues was significantly upregulated compared with normal lung gland tissues ($P < 0.05$) (Figure 1(g)). On another, analysis in UALCAN examined the protein expression of SLC2A5 and found it was highly expressed in tumor tissues (Figure 1(h)). In addition, we also carried out immunohistochemistry (IHC) in the HPA database. As can be seen from Figure 1(i), the protein expression of SLC2A5 in normal tissues decreased significantly, while the protein level in tumor tissues increased significantly. According to the results of differential analysis of SLC2A5 above, SLC2A5 is highly expressed in LUAD, suggesting that abnormal expression of SLC2A5 may be closely related to the development, metastasis, and prognosis of LUAD.

3.2. Distribution of SLC2A5 Expression in Clinical Characteristic Subgroups. Using the UALCAN database to detect the distribution of SLC2A5 in different histological subtypes of LUAD, it was found that the expression of SLC2A5 in lung adenocarcinoma-not otherwise specified (NOS), lung adenocarcinoma mixed subtype (Mixed), lung clear cell adenocarcinoma (ClearCell), lung bronchioloalveolar carcinoma nonmucinous (LBC-Nonmucinous), lung solid pattern predominant adenocarcinoma (SolidPattern-Predominant), lung acinar adenocarcinoma (Acinar), lung bronchioloalveolar carcinoma mucinous (LBC-Mucinous), mucinous (colloid) carcinoma (Mucinous), lung papillary adenocarcinoma (Papillary), lung mucinous adenocarcinoma (Mucinous), lung micropapillary adenocarcinoma (Micropapillary), and lung signet ring adenocarcinoma (SignetRing) was significantly higher than that of normal LUAD (Figure 2(a)). Subgroup analysis based on sex, age, race, different lymph node metastasis status, and tumor stage showed that the expression level of SLC2A5 in LUAD patients increased relative to normal samples (Figures 2(b)–2(f)). At the same time, UALCAN analysis showed that there was statistical difference between SLC2A5 expression and each tumor stage ($P < 0.05$). And the distribution of SLC2A5 increased in all stages of tumor; however, the expression of SLC2A5 did not increase with the increase of tumor stage, that is to say, there was no linear relationship between the expression of SLC2A5 and tumor stage (Figure 2(f)). Moreover, as shown in Figure 2(e), SLC2A5 expression increased in LUAD patients with different lymph node metastasis status (N classification). Nevertheless, there is no significant difference in the distribution of SLC2A5 in N0, N1, and N2 classification, and it was highly expressed in N3. Notably, SLC2A5 expression is increased in different genders of LUAD patients, and different genders were also associated with SLC2A5 expression.

3.3. Prognosis Analysis of SLC2A5 Expression and LUAD and Meta-Analysis of SLC2A5 Overexpression and OS of LUAD. Next, we used the PrognScan database to explore the relationship between SLC2A5 expression and the prognosis of LUAD patients. It is found that there was a significant correlation between the prognosis of LUAD patients and the expression of SLC2A5 ($P < 0.05$) (Figures 3(a)–3(d)).

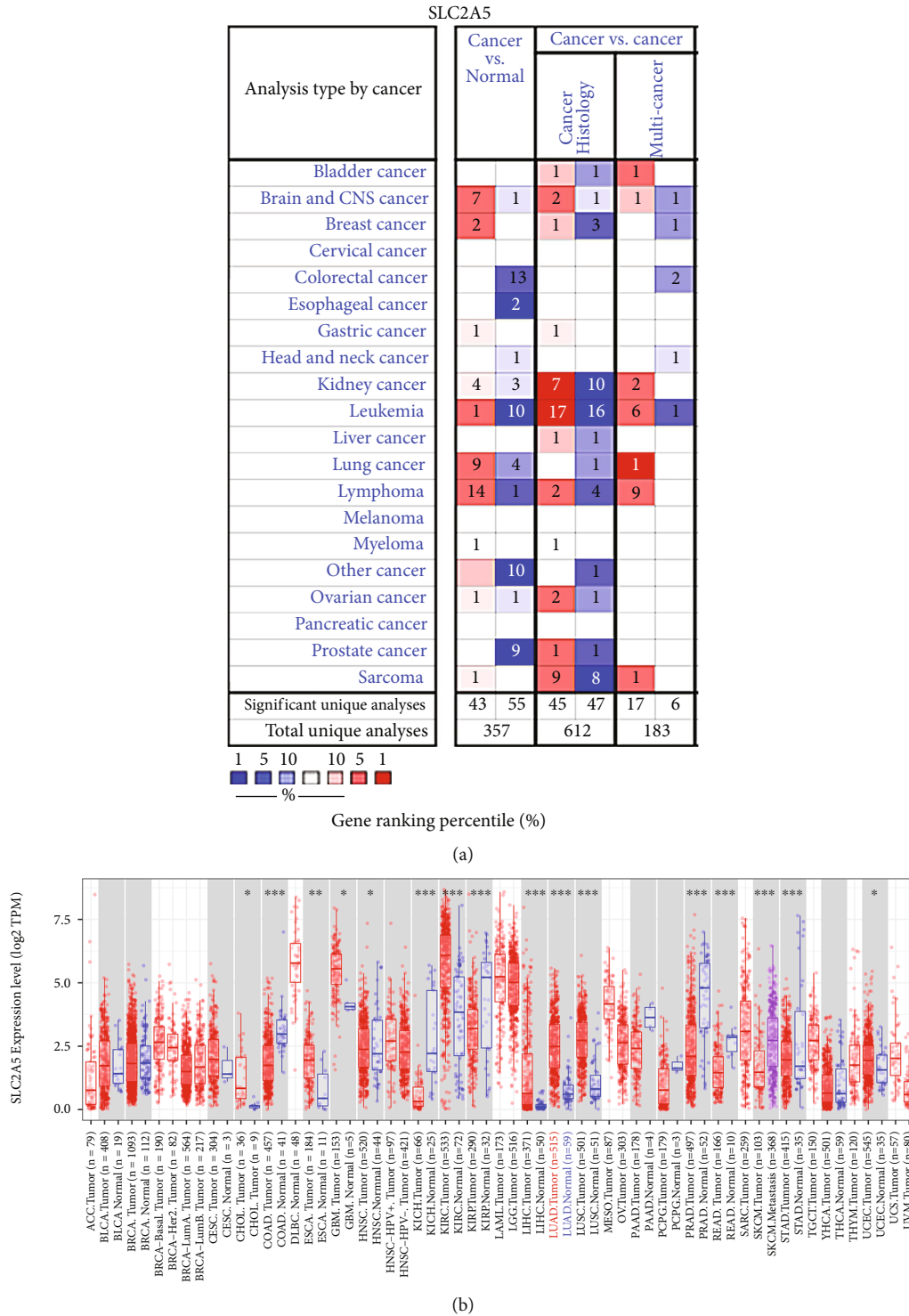


FIGURE 1: Continued.

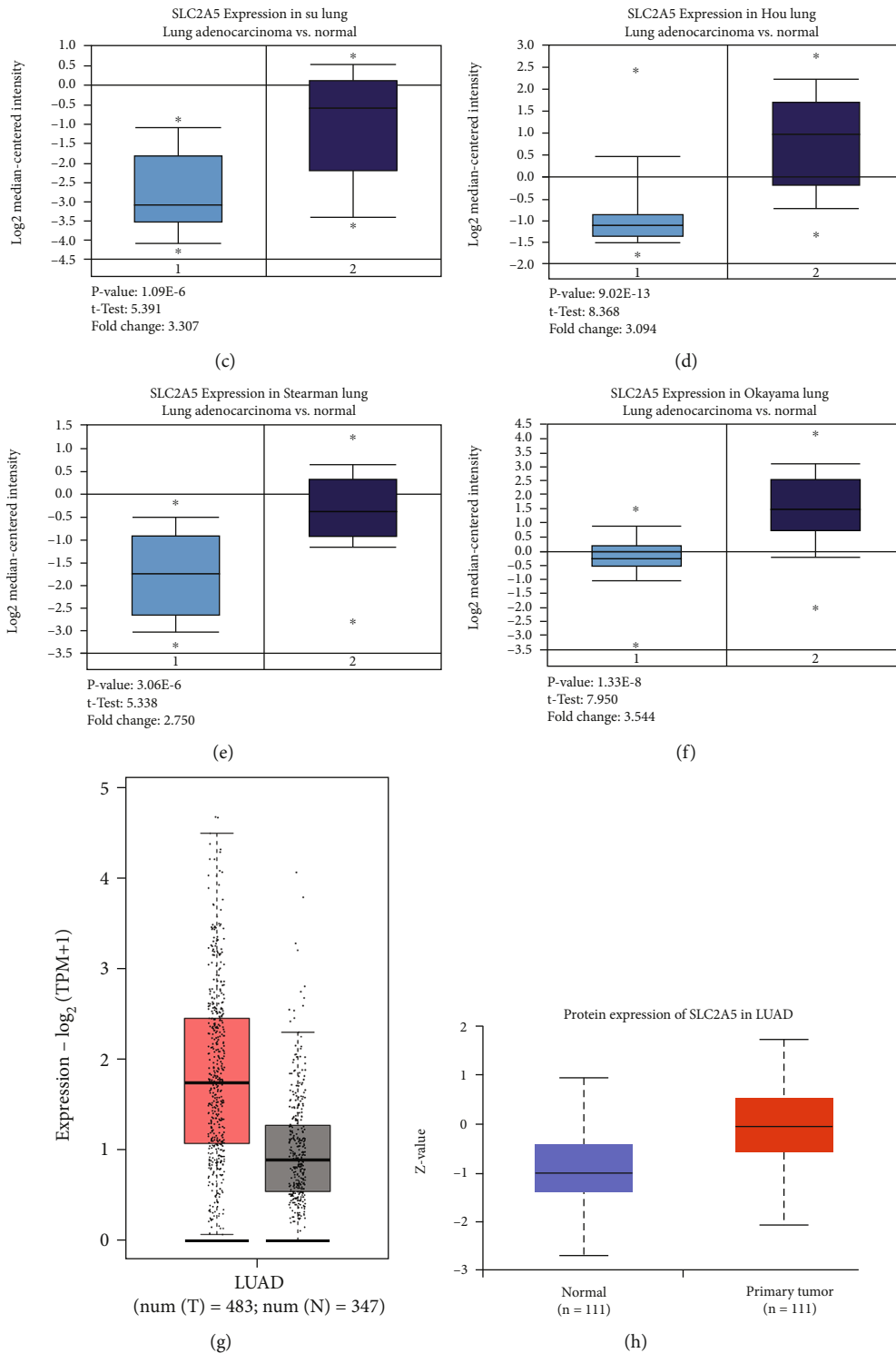


FIGURE 1: Continued.

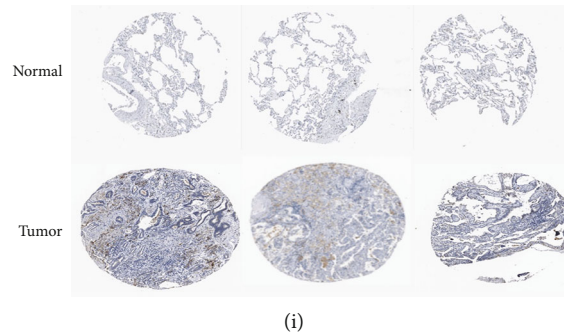


FIGURE 1: SLC2A5 is highly expressed in LUAD. (a) The expression level of SLC2A5 in different types of tumor tissues and normal tissues in the Oncomine database. (P value is 0.05, data type is mRNA, and gene ranking of all.) (b) The expression level of SLC2A5 in different types of tumor tissues and normal tissues in the TIMER database ($*P < 0.05$, $**P < 0.01$, and $***P < 0.001$). (c–f) The expression of SLC2A5 in LUAD is higher than that in normal tissues in different databases (SLC2A5 expression in Su’s dataset, Hou’s dataset, Stearman’s dataset, and Okayama’s dataset) in Oncomine. (g) High expression of SLC2A5 mRNA in LUAD tissues ($n = 483$) compared with the normal tissues ($n = 347$) in the GEPIA database. (h) High protein expression of SLC2A5 in LUAD tissues ($n = 111$) compared with the normal tissues ($n = 111$) in the UALCAN database. (i) Immunohistochemistry (IHC) of SLC2A5 expression in LUAD tissues and corresponding normal tissues based on HPA.

Interestingly, there are many other cancer types showing certain correlation between prognosis and SLC2A5 expression, including blood cancer, breast cancer, colorectal cancer, and eye cancer (Figures 3(e)–3(h)). To strengthen the persuasive power of association between SLC2A5 high expression and poor survival analysis results of LUAD patients, we conducted a meta-analysis of different datasets. Meta-analysis results have shown that the combined HR and 95% CI of survival analysis results associated with high SLC2A5 expression were 1.14 (1.06, 1.23), and no significant heterogeneity was observed in the 21 datasets ($I^2 = 36\%$, $P = 0.05$) (Figure 3(i)). Therefore, through the meta-analysis, we can safely conclude that high expression of SLC2A5 is a powerful predictor of adverse prognosis in LUAD patients.

Kaplan-Meier plotter was further used to validate SLC2A5 high expression prognosis. According to the median level of SLC2A5 expression in each group, the patients were divided into two groups. It was found that the increased expression of SLC2A5 was associated with the prognosis of LUAD patients ($P < 0.05$), and overall survival and first progression (FP) were also highly affected by the increased expression of SLC2A5 mRNA (OS: HR = 1.39, log-rank $P = 0.0055$; FP: HR = 1.77, log-rank $P = 0.00037$) (Figures 3(j) and 3(k)), suggesting that SLC2A5 may be a reliable biomarker for the prognosis of LUAD. Since SLC2A5 expression has an impact on the prognosis of LUAD patients, we next evaluated the correlation between SLC2A5 expression level and different clinical features of LUAD by using the Kaplan-Meier plotter database to explore its potential mechanism. The results are shown in Table 1, which showed that high SLC2A5 expression did not correlate with OS and FP in female (OS: HR = 1.15, $P = 0.4656$; FP: HR = 1.35, $P = 0.199$), stage 2 (OS: HR = 0.75, $P = 0.2407$; FP: HR = 1.15, $P = 0.6103$), AJCC stage T2 (OS: HR = 0.93, $P = 0.7933$; FP: HR = 0.86, $P = 0.6515$), AJCC stage N0 (OS: HR = 1.5, $P = 0.097$; FP: HR = 1.63, $P = 0.2142$), and AJCC stage N1 (OS: HR = 0.73, $P = 0.4358$; FP: HR = 1.06, $P = 0.8979$). However, in male (OS: HR =

1.46, $P = 0.0232$; FP: HR = 1.94, $P = 0.0028$), stage 1 (OS: HR = 1.62, $P = 0.0156$; FP: HR = 2.33, $P = 0.0007$), and exclude those never smoked (OS: HR = 2.68, $P = 6.7e - 05$; FP: HR = 2.05, $P = 0.0013$), high SLC2A5 mRNA expression correlated with both OS and FP. In conclusion, it is proved that most other factors can independently predict the prognosis of LUAD. Therefore, SLC2A5 may be a potential independent risk factor in LUAD.

3.4. Correlation between SLC2A5 Expression and Immune Cell Infiltration in LUAD. The TIMER database was used to analyze whether SLC2A5 high expression in LUAD tissues was associated with several major infiltrating immune cells. As the analysis results showed, the SLC2A5 expression level is correlated with B cell (Rho = 0.268, $P = 1.59e - 09$), CD8 T cell (Rho = 0.264, $P = 2.63e - 09$), CD4 T cell (Rho = -0.184, $P = 3.84e - 05$), neutrophil (Rho = -0.121, $P = 7.34e - 03$), dendritic cell (Rho = 0.105, $P = 2.00e - 02$), macrophage M1 (Rho = 0.171, $P = 1.38e - 04$), macrophage M2 (Rho = 0.194, $P = 1.40e - 05$), Tregs (Rho = 0.245, $P = 3.45e - 08$), and T cell follicular helper (Tfh) (Rho = -0.152, $P = 6.81e - 04$). As shown in the scatter plot (Figure 4(a)), SLC2A5 expression level was positively correlated with immune cells including B cell, CD8 T cell, Tregs, macrophage M2, macrophage M1, and DC cell and was negatively correlated with immune cells like neutrophil, Tfh, and CD8 T cell, suggesting that SLC2A5 expression level was closely correlated with LUAD immune infiltration. To further investigate the relationship between immune cell infiltration and SLC2A5 expression in LUAD, we further conducted Kaplan-Meier maps by using the TIMER database to evaluate the prognostic value of each of the six types of cells of the immune cells mentioned above (Figure 4(b)). We found that the expression of B cells (log-rank $P = 0$) and dendritic cells (log-rank $P = 0.048$) was significantly correlated with the prognosis of LUAD, which indicated that SLC2A5 plays an important role in regulating the infiltration of immune cells in LUAD, especially in the infiltration of B cells and dendritic cells.

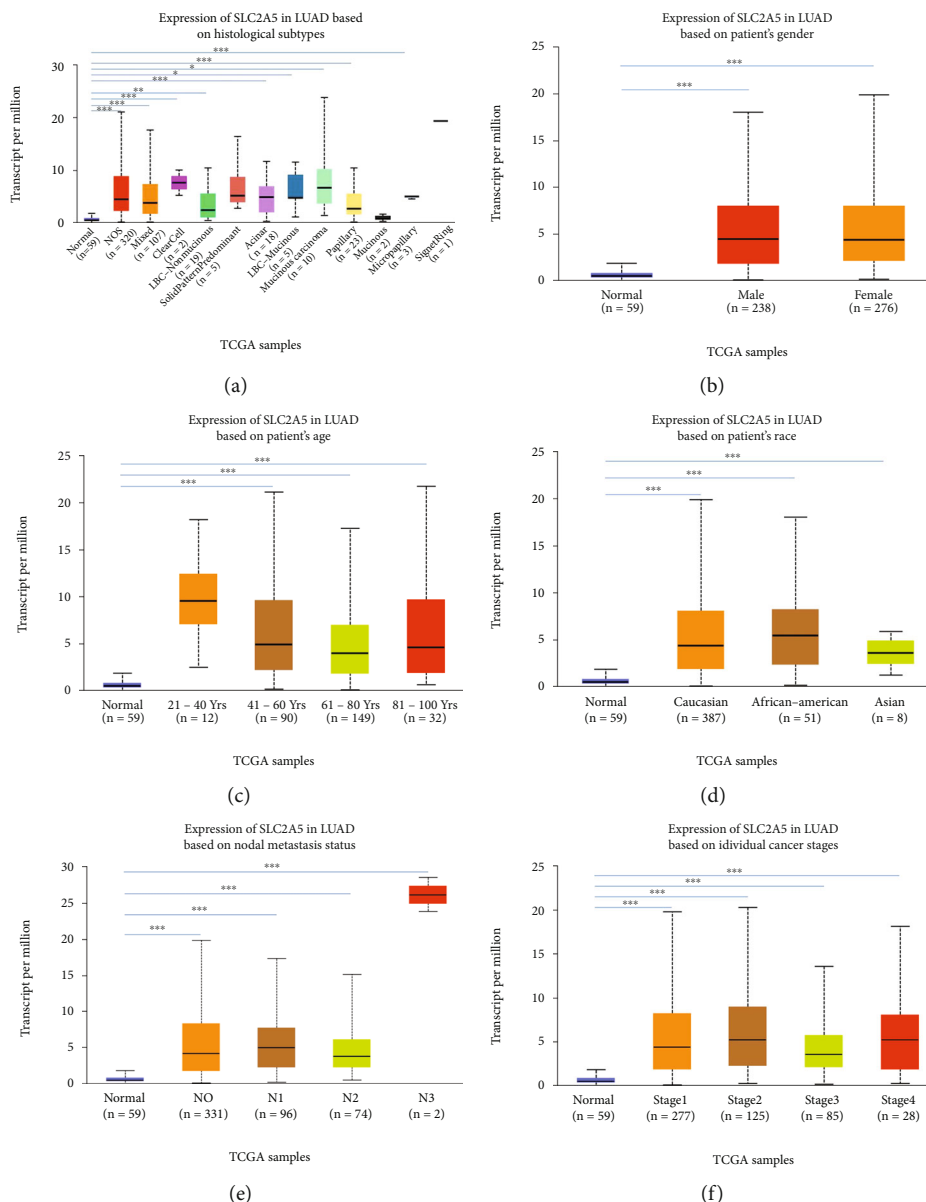


FIGURE 2: SLC2A5 expression in subgroups of clinical characteristics. (a) Expression of SLC2A5 in LUAD based on histological subtypes. (b) Expression of SLC2A5 in LUAD based on patient's gender. (c) Expression of SLC2A5 in LUAD based on patient's age. (d) Expression of SLC2A5 in LUAD based on patient's race. (e) Expression of SLC2A5 in LUAD based on nodal metastasis status. (f) Expression of SLC2A5 in LUAD based on individual cancer stages.

3.5. Correlation Analysis between SLC2A5 mRNA Levels and Different Subgroup Markers of Immune Cells. Next, based on the set of immunologic markers in LUAD, the TIMER database was used to further search the association between SLC2A5 expression and immune cell infiltration level. Specifically, targeting the special cell subsets (including CD8+ cells, T cells (general), B cells, monocytes, TAM, M1 macrophages, M2 macrophages, neutrophils, natural killer cells, and democratic cells), we evaluated the correlation between SLC2A5 expression and levels of parkers. At the same time, we also analyzed different subsets of T cells, namely, T helper 1 (Th1), T helper 2 (Th2), follicular helper T (TFH), T helper 17 (Th17), regulatory T (Tregs), and T cell exhaustion. Since the tumor purity of clinical samples affects

the immune osmotic analysis, we adjusted the results according to the tumor purity. The results showed that the expression of SLC2A5 in LUAD tissues was significantly related to the expression of most marker genes in immune osmotic cells (Table 2).

It was found that the expression of SLC2A5 in LUAD was significantly correlated with the expression of immune marker genes in CD8+ T cells, T cells, B cells, monocytes, TAM, and M2 macrophages. In particular, CD8A and CD8B of CD8+ T cells; CD3D, CD3E, and CD2 of T cells; CD19 and CD79A of B cells; CSF1R of monocytes; CCL2, CD68, and IL10 of TAMs; IRF5 of M1 macrophage; and CD163, VSIG4, and MS4A4A of M2 macrophage were all closely related to SLC2A5 level in LUAD ($P < 0.0001$).

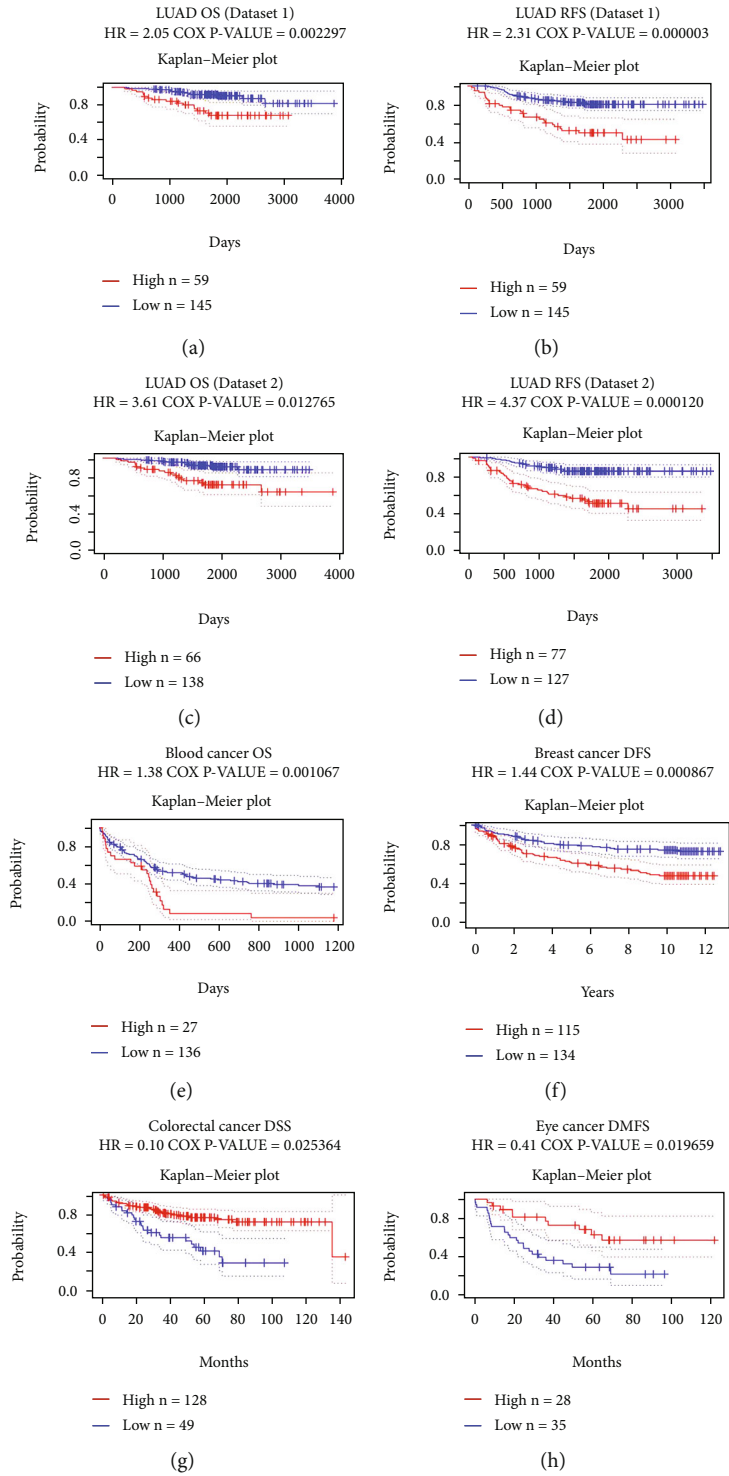


FIGURE 3: Continued.

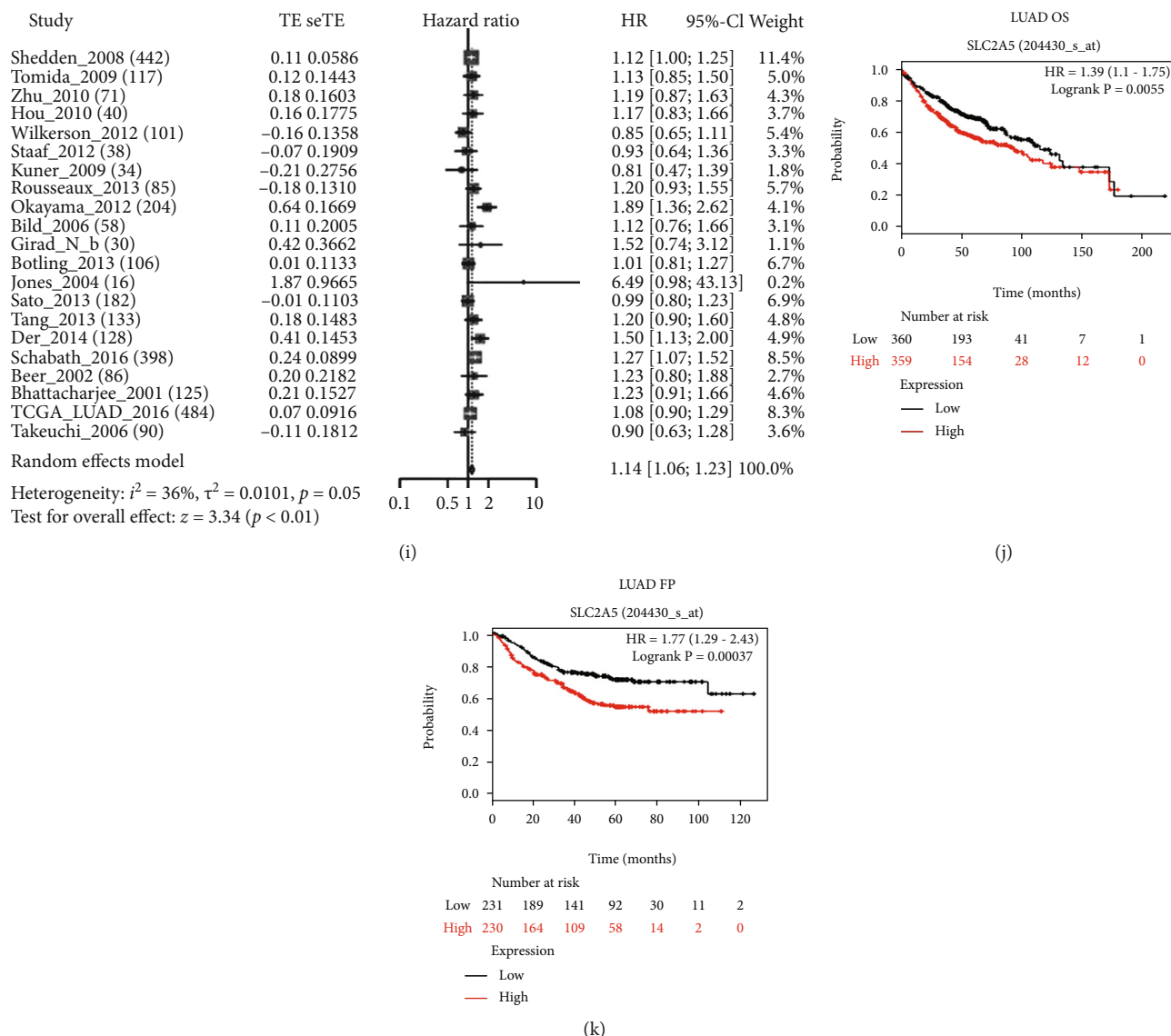


FIGURE 3: SLC2A5 is associated with survival outcome. (a–d) There was a significant correlation between prognosis in LUAD patients and expression of SLC2A5. (e–h) Several other types of cancer show a correlation between the patient’s prognostic period and the expression of SLC2A5. (i) Forest plot of survival analysis results associated with high SLC2A5 expression. (j, k) Survival analyses of SLC2A5 by the Kaplan-Meier plotter web tool. (j) Overall survival (OS) of LUAD ($P < 0.5$) on SLC2A5 gene expression. (k) First progression (FP) of LUAD ($P < 0.5$) on SLC2A5 gene expression. Survival differences are compared between patients with high and low (grouped according to median) expression of SLC2A5. The numbers below the figures denote the number of patients at risk in each group.

Moreover, high expression of SLC2A5 is associated with dense natural killer cell infiltration in LUAD. The expression of marker genes of natural killer cells (KIR2DL3, KIR2DL4, KIR3DL2, KIR3DL3, and KIR2DS4) was all significantly correlated with SLC2A5 expression, which suggests a close relationship between SLC2A5 expression and natural killer cell infiltration. In addition, for neutrophils, SLC2A5 expression was positively correlated with ITGAM and negatively correlated with CEACAM8. We also found that SLC2A5 expression is closely associated with TH1, Treg, and T cell failure marker genes (e.g., TBX21, STAT4, STAT1, IFNG, TNF, FOXP3, CCR8, STAT5B, TGFB1, PDCD1, LAG3,

havcr2, and GZMB), which further supports the close relationship between SLC2A5 expression and LUAD immune infiltration.

3.6. Analysis of SLC2A5 Promoter Methylation Levels in LUAD. A significant increase in SLC2A5 expression was found in LUAD through the above analysis. Consequently, we would conduct further studies to explore the causes of SLC2A5 elevation. Methylation is a significant event in epigenetic modification of the genome, and particularly, low global methylation can result in genomic instability and changes in gene transcription which may have an impact

TABLE 1: Correlation of SLC2A5 mRNA expression and clinical prognosis in LUAD with different important clinical characteristics by Kaplan-Meier plotter.

Factor	N	Overall survival ($n = 719$)		Progression-free survival ($n = 461$)		
		HR	P value	N	HR	P value
Sex						
Female	317	1.15 (0.79-1.68)	0.4656	235	1.35 (0.85-2.12)	0.199
Male	344	1.46 (1.05-2.03)	0.0232	226	1.94 (1.25-3.03)	0.0028
Stage						
1	370	1.62 (1.09-2.39)	0.0156	283	2.33 (1.41-3.86)	0.0007
2	136	0.75 (0.46-1.22)	0.2407	103	1.15 (0.67-2)	0.6103
3	24	1.46 (0.54-3.95)	0.4495	10	—	—
4	4	—	—	0	—	—
AJCC stage T						
1	123	2.06 (1.11-3.83)	0.0188	47	1.37 (0.31-6.11)	0.6808
2	105	0.93 (0.54-1.6)	0.7933	93	0.86 (0.46-1.62)	0.6515
3	4	—	—	2	—	—
4	0	—	—	0	—	—
AJCC stage N						
0	184	1.5 (0.93-2.42)	0.097	102	1.63 (0.75-3.55)	0.2142
1	44	0.73 (0.34-1.6)	0.4358	38	1.06 (0.43-2.62)	0.8979
2	3	—	—	2	—	—
AJCC stage M						
0	231	1.55 (1.04-2.31)	0.0315	142	1.77 (0.99-3.18)	0.0514
1	1	—	—	0	—	—
Smoking history						
Exclude those never smoked	246	2.68 (1.62-4.44)	$6.70E - 05$	243	2.05 (1.31-3.2)	0.0013
Only those never smoked	143	1.77 (0.78-4.06)	0.1686	143	2.32 (1.22-4.41)	0.0081

Bold values indicate $P < 0.05$.

on normal cell growth and increase the likelihood of tumorigenesis [37]. Therefore, we used the UALCAN database to verify the methylation level of SLC2A5 promoter in LUAD. As shown in Figure 5, the promoter methylation level of SLC2A5 in normal tissues is slightly lower than that in LUAD. Moreover, we conducted subgroup analyses of promoter methylation based on the patient's race, age, sex, tumor stage, and TP53 mutation status. The results showed that the promoter methylation was associated with gender, tumor stage, and TP53 mutation status in LUAD patients (Figures 5(b), 5(d), and 5(e)); however, there was no correlation between promoter methylation and LUAD patients who aged 21-40 or 81-100 and patients of African ethnicity (Figures 5(c) and 5(f)). These findings suggest that lower promoter DNA methylation may lead to high expression levels of SLC2A5 in LUAD.

3.7. Gene Enrichment Analysis and Gene Coexpression Network Construction. To better understand the biological implication of SLC2A5 in LUAD, the "LinkFinder" module in LinkedOmics database was used to examine the SLC2A5 coexpression pattern. As shown in Figure 6(a), it is indicated that 11,085 genes (red dots) were positively correlated with SLC2A5, while 8903 genes (green dots) were negatively correlated ($P < 0.05$). As shown in Figure 6(b), the first 50 pos-

itive and negative genes associated with SLC2A5 are shown in the form of heat map, and the network of them is also shown. SLC2A5 expression is strongly positively correlated with the expression of genes such as IL4I1 (positive rank #1, $r = 0.716$, $P = 3.59E - 82$), FCGR2B (positive rank #2, $r = 0.708$, $P = 1.45E - 79$), and GPR84 (positive rank #3, $r = 0.692$, $P = 1.49E - 74$), but negatively correlated with the expression of genes such as TOB1 (negative rank #1, $r = -0.430$, $P = 1.40E - 24$), SELENBP1 (negative rank #2, $r = -0.420$, $P = 2.15E - 23$), and IL17RE (negative rank #3, $r = -0.416$, $P = 6.06E - 23$). The annotation of gene set enrichment analysis (GSEA) indicates that SLC2A5-coexpressed genes are mainly involved in adaptive immune response, interferon-gamma production, positive regulation of cell activation, response to chemokine, myeloid dendritic cell activation, and other biological processes (Figure 6(c)). KEGG analysis results show that the genes are mainly enriched in *Staphylococcus aureus* infection, malaria, osteoclast differentiation, chemokine signaling pathway, NF-kappa B signaling pathway, and other pathways. In contrast, genes enriched in butanoate metabolism, ribosome, fatty acid degradation, propanoate metabolism, glycosylphosphatidylinositol (GPI) anchor biosynthesis, or others were inhibited (Figure 6(d)). Besides, we plotted the survival heat map of the genes significantly associated with SLC2A5

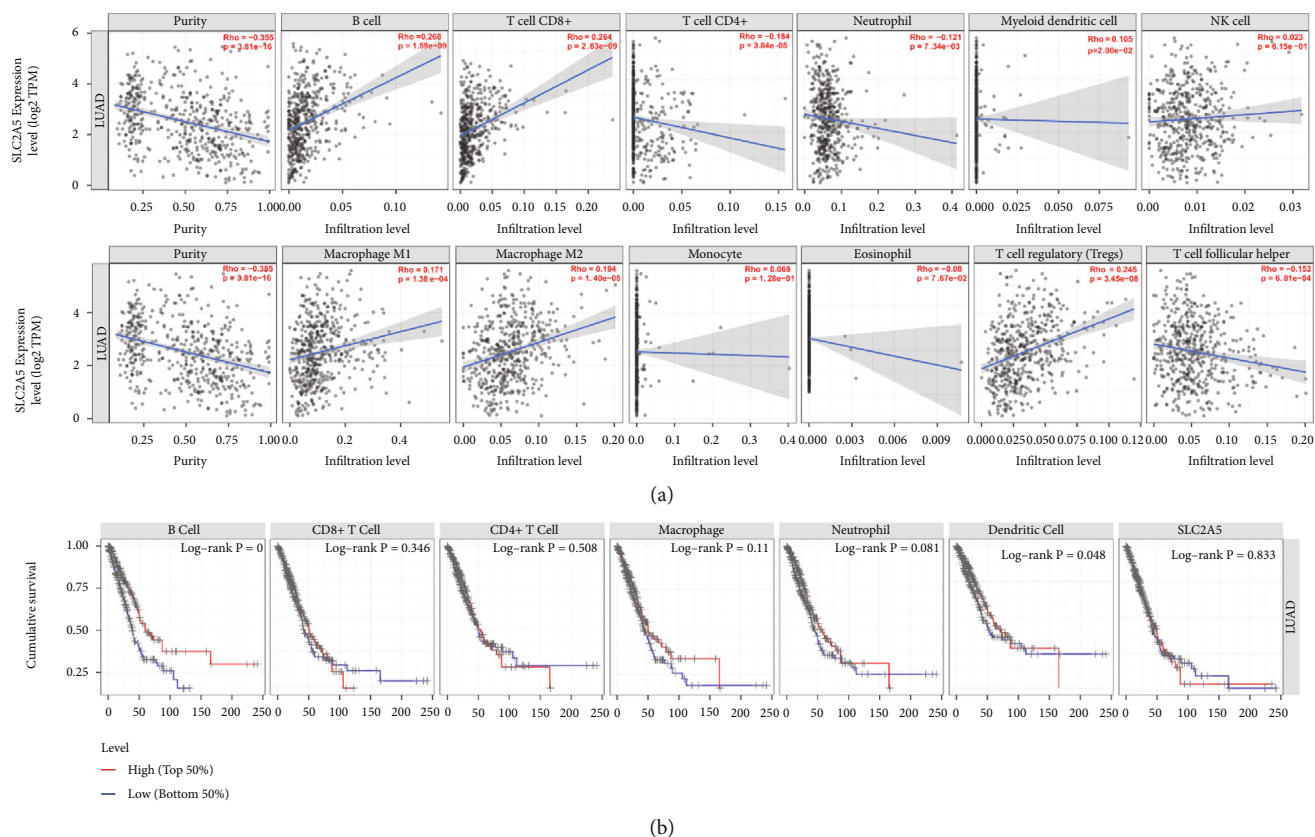


FIGURE 4: Correlation analysis between SLC2A5 expression and the infiltrating immune cells in LUAD. (a) Correlation of SLC2A5 expression with 12 types of immune infiltration cells obtained from TIMER (purity-corrected Spearman test). (b) Overall survival curve of the six types of cells produced by Kaplan-Meier estimator from TIMER. Survival differences are compared between patients with high and low (grouped according to median) infiltration of each kind of immune cells.

expression in Figures 6(e) and 6(f). As shown in the figure, only 4 of the first 50 positively related genes have lower risk ratios (HR), compared with 12/50 negative related genes which have low HR ($P < 0.05$). And all of these genes have a high probability of becoming risk ratio markers of LUAD.

4. Discussion

Lung cancer (LC) is a major health problem and one of the most common causes of tumor-related deaths. Its rapid growth requires excessive catabolism of major metabolic fuels [38]. In the presence of metabolic fuels in vivo, fructose can be easily used as a glucose substitute by LC cells in vivo by upregulating SLC2A5 [38]. This can be explained by the study of Norimichi et al. [39]. Therefore, SLC2A5-mediated fructose utilization in vivo must play an important role in the control of LC growth, especially in LUAD. However, if there is too much fructose in the gut, the unabsorbed fructose may lead to bacterial fermentation, leading to irritable bowel syndrome, resulting in inflammatory damage, flora disorders, bacterial infections, and other harmful consequences, which may affect the progress of tumor [40]. Although LUAD treatment strategies have improved significantly in recent decades, survival rates still remain unsatisfactory. Therefore, it is necessary to develop new prognostic biomarkers and therapeutic targets. In our study,

we explored the expression, prognostic role, and biological function of SLC2A5 in LUAD.

Results of our study found that SLC2A5 is highly expressed in LUAD tumor tissues and is also significantly associated with its prognosis. Moreover, each tumor stage also has high expression, at the same time, the correlation between SLC2A5 expression and prognosis based on different clinical characteristics indicates that SLC2A5 may be a potential independent biomarker for LUAD prognosis. Then, we analyzed the correlation between SLC2A5 and immune infiltration and the correlation between SLC2A5 and different subsets of immune cells. And it is also found that SLC2A5 is related to the major infiltrating immune cells and has a particularly strong effect on B cell and dendritic cell infiltration. Therefore, SLC2A5 infiltration in B cells and dendritic cells may be one of the factors of its prognostic ability. And then, we analyzed the effect of SLC2A5 expression on promoter methylation. Finally, we studied the SLC2A5 coexpression and regulatory networks. All the work above we do is aimed at guiding LUAD future research.

It is worth noting that different lymph node metastasis statuses (N classification) are highly correlated with SLC2A5 expression and SLC2A5 high expression occurred more significantly in N3 than in N0, N1, and N2, which suggests that SLC2A5 is mainly involved in the N3 stage of LUAD [17, 41] and that there may be a relationship between SLC2A5

TABLE 2: Correlation analysis between SLC2A5 and related genes and markers of immune cells in TIMER.

Description	Gene markers	LUAD				
		None	Cor	Purity	P value	
CD8+ T cell	CD8A		0.403		***	
	CD8B		0.343		***	
	CD3D		0.402		***	
T cell	CD3E		0.41		***	
	CD2		0.408		***	
B cell	CD19		0.391		***	
	CD79A		0.45		***	
Monocyte	CD86		0.599		0	
	CSF1R		0.525		***	
	CCL2		0.427		***	
TAM	CD68		0.469		***	
	IL10		0.424		***	
	NOS2		0.153		**	
M1 macrophage	IRF5		0.36		***	
	PTGS2		0.075		8.85E - 02	
	CD163		0.517		***	
M2 macrophage	VSIG4		0.435		***	
	MS4A4A		0.438		***	
	CEACAM8		-0.134		*	
Neutrophils	ITGAM		0.479		***	
	CCR7		0.255		***	
	KIR2DL1		0.189		***	
	KIR2DL3		0.256		***	
	KIR2DL4		0.464		***	
Natural killer cell	KIR3DL1		0.178		***	
	KIR3DL2		0.288		***	
	KIR3DL3		0.245		***	
	KIR2DS4		0.253		***	
	HLA-DPB1		0.209		***	
	HLA-DQB1		0.189		***	
	HLA-DRA		0.252		***	
	HLA-DPA1		0.226		***	
Dendritic cell	CD1C		-0.062		1.57E - 01	
	NRP1		0.187		***	
	ITGAX		0.561		***	
	TBX21		0.366		***	
	STAT4		0.307		***	
	Th1	STAT1		0.468		0
		IFNG		0.443		***
TNF			0.303		***	
Th2	GATA3		0.325		***	
	STAT6		-0.138		*	

TABLE 2: Continued.

Description	Gene markers	LUAD			
		None	LUAD	Purity	
		Cor	P value	Cor	P value
Tfh	STAT5A	0.39	***	0.291	***
	IL13	0.057	1.99E - 01	-0.019	6.71E - 01
	BCL6	0.098	2.65E - 02	0.092	4.14E - 02
	IL21	0.361	***	0.314	***
Th17	STAT3	0.104	1.80E - 02	0.115	1.07E - 02
	IL17A	0.201	***	0.13	*
Treg	FOXP3	0.48	0	0.389	***
	CCR8	0.434	***	0.351	***
	STAT5B	0.209	***	0.196	***
	TGFB1	0.308	***	0.219	***
	PDCD1	0.508	***	0.415	***
	CTLA4	0.485	0	0.388	***
T cell exhaustion	LAG3	0.499	0	0.413	***
	HAVCR2	0.572	0	0.507	***
	GZMB	0.567	***	0.491	***

TAM: tumor-associated macrophage; Th: T helper cell; Tfh: follicular helper T cell; Treg: regulatory T cell; Cor: R value of Spearman's correlation; none: correlation without adjustment; purity: correlation adjusted by purity. * $P < 0.01$; ** $P < 0.001$; *** $P < 0.0001$.

expression and LUAD disease outcomes, that is to say, the overexpression of SLC2A5 enhances the proliferation, migration, invasion, and tumorigenicity of cells and then closely affects the progress of LUAD [7]. Therefore, we used the PrognosScan database and its related data to carry out survival analysis and meta-analysis and found that high SLC2A5 expression may be associated with poor OS prognosis of LUAD. Additionally, analysis in the Kaplan-Meier plotter showed the correlation between SLC2A5 expression level and the different clinical features of the LUAD, which further demonstrated that SLC2A5 is an independent risk factor of LUAD. Therefore, our results suggest that SLC2A5 upregulation occurs in LUAD and is worthy of further clinical validation as a potential diagnostic and prognostic marker.

Our study found that SLC2A5 expression level was closely related to B cell and dendritic cell infiltration. Subsequently, Kaplan-Meier analysis found certain correlation between B cells and LUAD prognosis and between dendritic cells and LUAD prognosis. These findings suggest that B cell and dendritic cell infiltration may be key factors in SLC2A5 with prognostic value. Next, in the correlation analysis between SLC2A5 and several immune characteristics, we found that most of the marker genes in immune-infiltrating cells were also associated with high SLC2A5 expression. As the most important prognostic factors of SLC2A5, the gene markers of B cells and dendritic cells were associated with SLC2A5 (correlation between these genes and SLC2A5: $P < 0.0001$). It is worth noting that all the marker genes of natural killer cell (KIR2DL1, KIR2DL3, KIR2DL4, KIR3DL1, KIR3DL2, KIR3DL3, and KIR2DS4) are correlated with the high expression of SLC2A5. These

marker genes may affect the occurrence and development of LUAD by regulating the activity and effector function of NK cells. In conclusion, this analysis provides a detailed description of the relationship between SLC2A5 and immune characteristics in LUAD patients, indicating that SLC2A5 is a key factor of immune escape in the tumor microenvironment. In addition, the correlation between SLC2A5 and B cells and dendritic cells and their related markers is also very important for the prognosis of LUAD patients. For example, as the literature [42] shows, SLC2A5 could inhibit the development of human normal adjacent lung adenocarcinoma cytoplasmic pre-B cells. The network mechanism includes Golgi apparatus of AP1M2_1; cell cycle of CUL7, SAC3D1; protein amino acid dephosphorylation of STYXL1; pro-B cell-cell differentiation of SOX4_3; and FAD biosynthesis of FLAD1. Therefore, the correlation between SLC2A5 and B cells and their related markers is very important for the prognosis of LUAD patients. At the same time, it is worth noting that SLC2A5 may be a key factor in mediating dendritic cell therapy, which needs further study.

To investigate the reasons for the increase of SLC2A5 in LUAD, we studied the methylation level of SLC2A5 in the LUAD and found that the methylation level of promoters in the LUAD decreased. Therefore, SLC2A5 may be activated and upregulated by its hypomethylation, which may explain a certain degree elevation of SLC2A5 in LUAD. Among the results of gene enrichment analysis, we found that the biological processes of SLC2A5 and its related genes mainly belong to the immune response of the body, such as adaptive immune response, lymphocyte activation, leukocyte activation, differentiation and migration, and other processes related to immunity. Therefore, SLC2A5 may play a

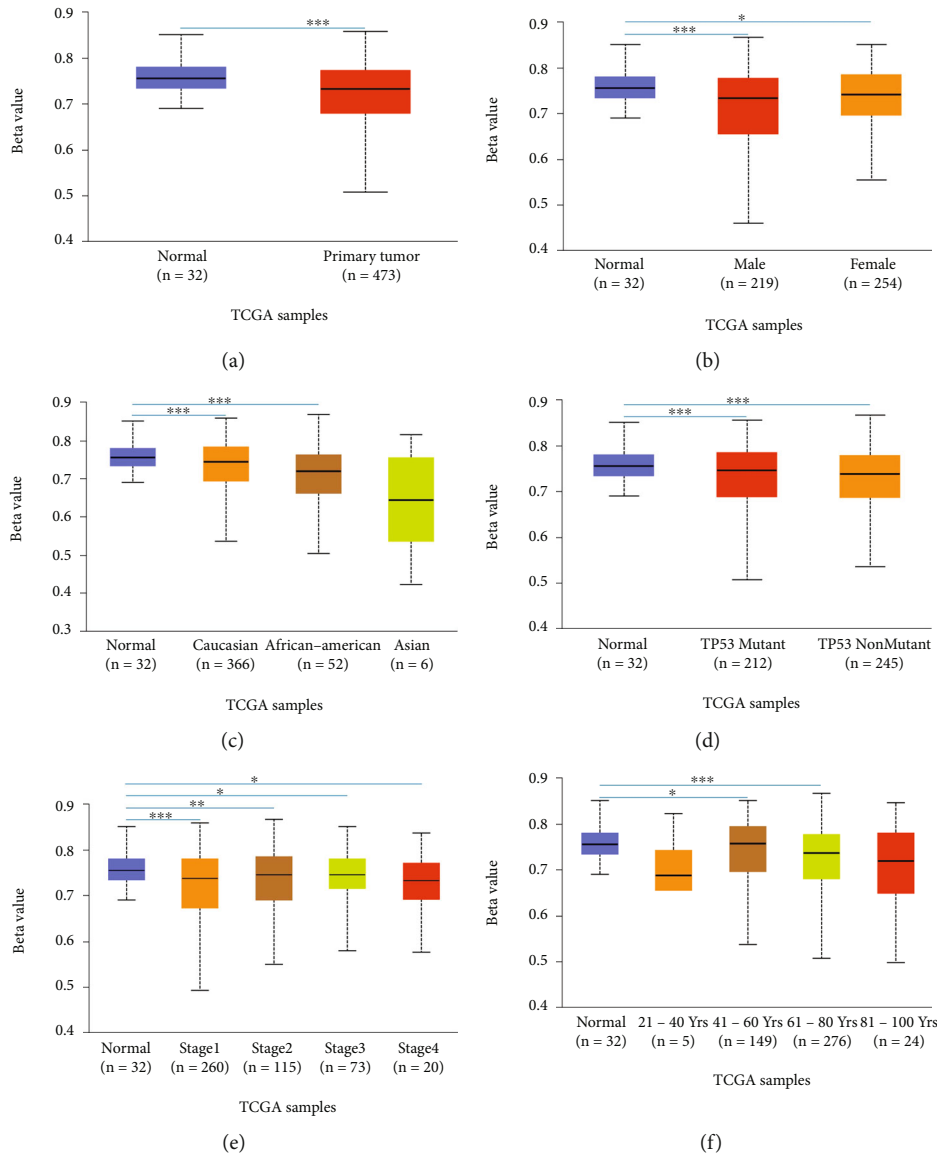


FIGURE 5: Promoter methylation levels of SLC2A5 in LUAD. Promoter methylation levels of SLC2A5 were low in (a)–(f). LUAD: (a) sample type, (b) gender, (c) race, (d) TP53 mutation status, (e) individual cancer stages, and (f) age (**P* < 0.05, ***P* < 0.01, and ****P* < 0.001).

vital role in the immune microenvironment of LUAD by participating in the immune response and possibly regulating immune cells such as B cells and T cells and interferon γ , interleukin-10, interleukin-12, and other immune regulatory factors. Last but not least, in the construction of the gene coexpression network, we can see that the expression of IL4I1, FCGR2B, and GPR84 has the strongest positive correlation with the expression of SLC2A5, while the expression of TOB1, SELENBP1, and IL17RE has the strongest negative correlation with the expression of gene coexpression. According to some relevant paper, the role of IL4I1 in escaping tumor immune response can be achieved by participating in the fine control of adaptive immune of B and T cells [43]. The mouse model of CD8T cell-FCGR2B deletion established by Anna et al. demonstrated the intrinsic coinhibitory function of Fc γ RIIB (FCGR2B) in regulating the immunity of CD8 T cells [44]. As a member of the metabolic

G protein-coupled receptor family, results of Recio et al. have shown that when the body is in an inflammatory state, GPR84 could act as an enhancer of inflammatory signals in macrophages, resulting in increased expression of key inflammatory cytokines and chemokines [45]. The evidence above may explain that SLC2A5 and its related genes are mainly enriched in KEGG pathways related to inflammatory response such as NF-kappa B signaling pathway and Toll receptor signaling pathway. With regard to genes negatively associated with SLC2A5, a previous study showed that overexpression of TOB1 significantly inhibited the proliferation and metastasis of lung cancer cells [46]. TOB1 could inhibit the proliferation and metastasis of lung cancer cells through a series of downstream regulators, including cyclin D1, AKT signal transduction, BCL-2, BCL-XL, and SMAD4 [47]. SELENBP1 is a direct target for transcription factor Nkx2-1, which can inhibit tumor clonal growth and migration

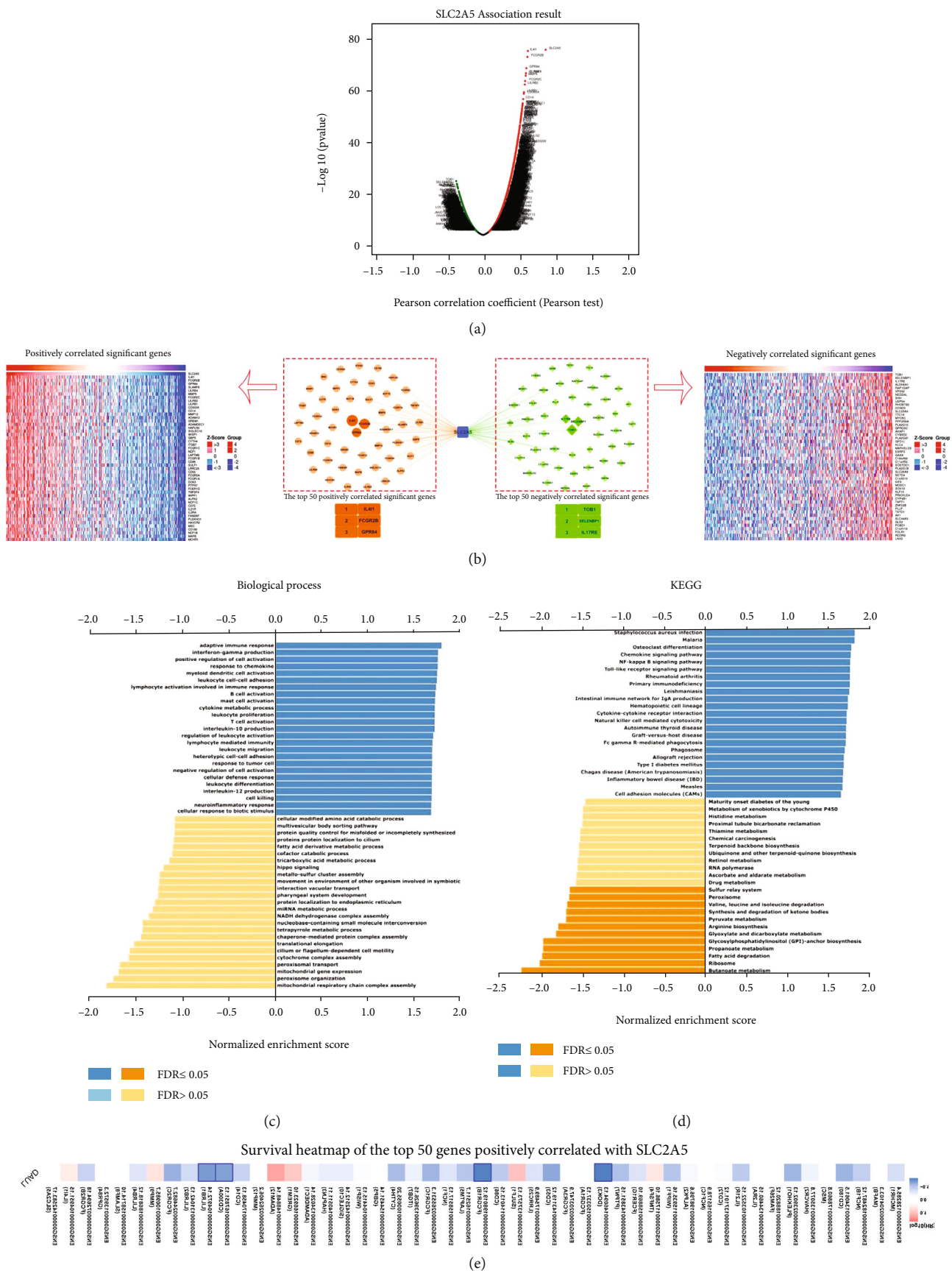


FIGURE 6: Continued.

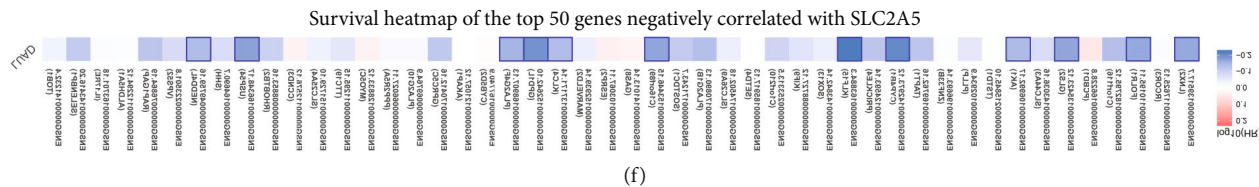


FIGURE 6: SLC2A5 coexpression genes in LUAD (LinkedOmics database). (a) The global SLC2A5 highly correlated genes were identified by the Pearson test in LUAD. Red and green dots represent positively and negatively significantly correlated genes with SLC2A5, respectively. (b) Heat maps and network showing the top 50 genes positively and negatively correlated with SLC2A5 in LUAD. (c, d) Significantly enriched GO: biological process annotations and KEGG pathways of SLC2A5 in LUAD. (e, f) Survival heat maps of the top 50 genes positively and negatively correlated with SLC2A5 in LUAD. The survival heat maps show the hazard ratios in the logarithmic scale (\log_{10}) for different genes. The red and blue blocks denote higher and lower risks, respectively. The rectangles with frames mean the significant unfavorable and favorable results in prognostic analyses ($P < 0.05$).

and inhibit malignant progression of LUAD in vivo. Thus, SELENBP1 is an important inhibitor of lung tumor growth and plays a role in the positive feedback loop of Nkx2-1 [48]. The loss of the expression of this gene may be associated with poor prognosis in lung cancer patients. As a marker cytokine for TH17 cell subsets [49], IL17RE may help to reshape tumor microenvironment and tumor growth/survival [50]. These evidences prove that when the expression of SLC2A5 increases, the body may regulate some biological processes by affecting the expression of positive and negative related genes, thus affecting the condition of patients with lung adenocarcinoma. However, in this study, all the analyses in this paper are based on servers or databases, which may be different in specific experiments. It will be important to verify the analysis results through experiments in our future research.

5. Conclusions

In conclusion, this study provides comprehensive evidence for the value of SLC2A5 in lung cancer progression and its potential as a biological target and prognostic predictor of LUAD. Our findings suggest that the upregulation of SLC2A5 in LUAD predicts adverse outcomes in the overall survival of patients, possibly due to multiple physiological processes affecting SLC2A5 expression. Furthermore, we found a significant correlation between SLC2A5 and most immune features. Nevertheless, attention needs to be paid to the link among SLC2A5 and B cells and dendritic cells and their associated markers, which may be a new direction for future LUAD research.

Data Availability

The data that support the findings of this study are available from the corresponding author upon reasonable request.

Consent

Consent is not applicable.

Conflicts of Interest

The authors declare that they have no competing interests.

Authors' Contributions

LX Luo, H Luo, and RM Huang conceived the idea; LX Luo, JT Su, YS Zheng, and FF Huang contributed to the acquisition, analysis, and interpretation of data. LX Luo and JT Su wrote the manuscript; LX Luo, H Luo, and RM Huang reviewed the paper and provided comments, and all authors reviewed the manuscript.

Acknowledgments

This project was supported by the Administration of Traditional Chinese Medicine of Guangdong Province (20201180 and 20211223), Science and Technology Special Project of Zhanjiang (2019A01009), Basic and Applied Basic Research Program of Guangdong Province (2019A1515110201), Program of Department of Natural Resources of Guangdong Province (Nos. GDNRC [2020]038 and [2021]53), and Discipline Construction Project of Guangdong Medical University (4SG21004G).

References

- [1] A. Jemal, F. Bray, M. M. Center, J. Ferlay, E. Ward, and D. Forman, "Global cancer statistics," *CA: A Cancer Journal for Clinicians*, vol. 61, pp. 69–90, 2011.
- [2] L. Zhang, W. Fan, L. Xu et al., "Rab27b is a potential indicator for lymph node metastasis and unfavorable prognosis in lung adenocarcinoma," *Disease Markers*, vol. 2018, Article ID 7293962, 8 pages, 2018.
- [3] V. M. L. de Sousa and L. Carvalho, "Heterogeneity in lung cancer," *Pathobiology*, vol. 85, pp. 96–107, 2018.
- [4] J.-T. Zhang, Y.-C. Lin, B.-F. Xiao, and B.-T. Yu, "Overexpression of family with sequence similarity 83, member A (FAM83A) predicts poor clinical outcomes in lung adenocarcinoma," *Medical Science Monitor*, vol. 25, pp. 4264–4272, 2019.
- [5] R. S. Heist and J. A. Engelman, "SnapShot: non-small cell lung cancer," *Cancer Cell*, vol. 21, no. 3, pp. 448–448.e2, 2012.
- [6] Q. Qi, Y. Hou, A. Li, Y. Sun, S. Li, and Z. Zhao, "Yifei Tongluo, a Chinese herbal formula, suppresses tumor growth and metastasis and exerts immunomodulatory effect in Lewis lung carcinoma mice," *Molecules (Basel, Switzerland)*, vol. 24, no. 4, p. 731, 2019.

- [7] Y. Weng, X. Fan, Y. Bai et al., "SLC2A5 promotes lung adenocarcinoma cell growth and metastasis by enhancing fructose utilization," *Cell Death Discovery*, vol. 4, no. 1, p. 38, 2018.
- [8] H. Liu, D. Huang, D. L. McArthur, L. G. Boros, N. Nissen, and A. P. Heaney, "Fructose induces transketolase flux to promote pancreatic cancer growth," *Cancer Research*, vol. 70, pp. 6368–6376, 2010.
- [9] Y. Jiang, Y. Pan, P. R. Rhea et al., "A sucrose-enriched diet promotes tumorigenesis in mammary gland in part through the 12-lipoxygenase pathway," *Cancer Research*, vol. 76, pp. 24–29, 2016.
- [10] W.-L. Chen, Y.-Y. Wang, A. Zhao et al., "Enhanced fructose utilization mediated by SLC2A5 is a unique metabolic feature of acute myeloid leukemia with therapeutic potential," *Cancer Cell*, vol. 30, pp. 779–791, 2016.
- [11] D. A. Dixon, F. F. Blanco, A. Bruno, and P. Patrignani, "Mechanistic aspects of COX-2 expression in colorectal neoplasia," *Recent Results in Cancer Research*, vol. 191, pp. 7–37, 2013.
- [12] Y.-Y. Hsieh, S.-Y. Tung, H.-Y. Pan et al., "Increased Abundance of *Clostridium* and *Fusobacterium* in Gastric Microbiota of Patients with Gastric Cancer in Taiwan," *Scientific Reports*, vol. 8, no. 1, pp. 158–158, 2018.
- [13] D. M. Alvarado, B. Chen, M. Iticovici et al., "Epithelial indoleamine 2,3-dioxygenase 1 modulates aryl hydrocarbon receptor and notch signaling to increase differentiation of secretory cells and alter mucus-associated microbiota," *Gastroenterology*, vol. 157, no. 4, pp. 1093–1108.e11, 2019.
- [14] L. Luo, M. Li, J. Su, X. Yao, and H. Luo, *FURIN Correlated with Immune Infiltration Serves as a Potential Biomarker in SARS-CoV-2 Infection-Related Lung Adenocarcinoma*, 2021.
- [15] D. R. Rhodes, S. Kalyana-Sundaram, V. Mahavisno et al., "OncoPrint 3.0: genes, pathways, and networks in a collection of 18,000 cancer gene expression profiles," *Neoplasia*, vol. 9, no. 2, pp. 166–180, 2007.
- [16] D. R. Rhodes, J. Yu, K. Shanker et al., "ONCOMINE: a cancer microarray database and integrated data-mining platform," *Neoplasia*, vol. 6, pp. 1–6, 2004.
- [17] C. Ma, H. Luo, J. Cao, C. Gao, X. Fa, and G. Wang, "Independent prognostic implications of RRM2 in lung adenocarcinoma," *Journal of Cancer*, vol. 11, no. 23, pp. 7009–7022, 2020.
- [18] B. Li, E. Severson, J.-C. Pignon et al., "Comprehensive analyses of tumor immunity: implications for cancer immunotherapy," *Genome Biology*, vol. 17, p. 174, 2016.
- [19] T. Li, J. Fan, B. Wang et al., "TIMER: a web server for comprehensive analysis of tumor-infiltrating immune cells," *Cancer Research*, vol. 77, pp. e108–e110, 2017.
- [20] T. Li, J. Fu, Z. Zeng et al., "TIMER2.0 for analysis of tumor-infiltrating immune cells," *Nucleic Acids Research*, vol. 48, no. W1, pp. W509–w514, 2020.
- [21] C. Li, Z. Tang, W. Zhang, Z. Ye, and F. Liu, "GEPIA2021: integrating multiple deconvolution-based analysis into GEPIA," *Nucleic Acids Research*, vol. 49, no. W1, pp. W242–w246, 2021.
- [22] Z. Tang, B. Kang, C. Li, T. Chen, and Z. Zhang, "GEPIA2: an enhanced web server for large-scale expression profiling and interactive analysis," *Nucleic Acids Research*, vol. 47, no. W1, pp. W556–w560, 2019.
- [23] Z. Tang, C. Li, B. Kang, G. Gao, C. Li, and Z. Zhang, "GEPIA: a web server for cancer and normal gene expression profiling and interactive analyses," *Nucleic Acids Research*, vol. 45, no. W1, pp. W98–w102, 2017.
- [24] D. S. Chandrashekar, B. Bashel, S. A. H. Balasubramanya et al., "UALCAN: a portal for facilitating tumor subgroup gene expression and survival analyses," *Neoplasia*, vol. 19, pp. 649–658, 2017.
- [25] G. X. Hou, P. Liu, J. Yang, and S. Wen, "Mining expression and prognosis of topoisomerase isoforms in non-small-cell lung cancer by using OncoPrint and Kaplan-Meier plotter," *PLoS One*, vol. 12, no. 3, article e0174515, 2017.
- [26] Á. Nagy, A. Lánckzy, O. Menyhárt, and B. Györfy, "Validation of miRNA prognostic power in hepatocellular carcinoma using expression data of independent datasets," *Scientific Reports*, vol. 8, no. 1, p. 9227, 2018.
- [27] M. Uhlen, L. Fagerberg, B. M. Hallstrom et al., "Tissue-based map of the human proteome," *Science*, vol. 347, no. 6220, article 1260419, 2015.
- [28] M. Uhlen, C. Zhang, S. Lee et al., "A pathology atlas of the human cancer transcriptome," *Science*, vol. 357, 2017.
- [29] A. Lánckzy, Á. Nagy, G. Bottai et al., "miRpower: a web-tool to validate survival-associated miRNAs utilizing expression data from 2178 breast cancer patients," *Breast Cancer Research and Treatment*, vol. 160, pp. 439–446, 2016.
- [30] A. Elfilali, S. Lair, C. Verbeke, P. La Rosa, F. Radvanyi, and E. Barillot, "ITACA: a new database for integrated tumor transcriptome array and clinical data analysis," *Nucleic Acids Research*, vol. 34, pp. D613–D616, 2006.
- [31] H. Mizuno, K. Kitada, K. Nakai, and A. Sarai, "PrognoScan: a new database for meta-analysis of the prognostic value of genes," *BMC Medical Genomics*, vol. 2, no. 1, p. 18, 2009.
- [32] L. Askie and M. Offringa, "Systematic reviews and meta-analysis," *Seminars in Fetal & Neonatal Medicine*, vol. 20, no. 6, pp. 403–409, 2015.
- [33] A. P. Siddaway, A. M. Wood, and L. V. Hedges, "How to do a systematic review: a best practice guide for conducting and reporting narrative reviews, meta-analyses, and meta-syntheses," *Annual Review of Psychology*, vol. 70, no. 1, pp. 747–770, 2019.
- [34] Y. Miyazawa, T. Uekita, N. Hiraoka et al., "CUB domain-containing protein 1, a prognostic factor for human pancreatic cancers, promotes cell migration and extracellular matrix degradation," *Cancer Research*, vol. 70, pp. 5136–5146, 2010.
- [35] S. V. Vasaikar, P. Straub, J. Wang, and B. Zhang, "LinkedOmics: analyzing multi-omics data within and across 32 cancer types," *Nucleic Acids Research*, vol. 46, pp. D956–d963, 2018.
- [36] J. Wang, S. Vasaikar, Z. Shi, M. Greer, and B. Zhang, "WebGestalt 2017: a more comprehensive, powerful, flexible and interactive gene set enrichment analysis toolkit," *Nucleic Acids Research*, vol. 45, no. W1, pp. W130–w137, 2017.
- [37] H. Dan, S. Zhang, Y. Zhou, and Q. Guan, "DNA methyltransferase inhibitors: catalysts for antitumor immune responses," *Oncotargets and Therapy*, vol. 12, pp. 10903–10916, 2019.
- [38] W.-L. Chen, X. Jin, M. Wang et al., "GLUT5-mediated fructose utilization drives lung cancer growth by stimulating fatty acid synthesis and AMPK/mTORC1 signaling," *JCI Insight*, vol. 5, no. 3, 2020.
- [39] N. Nomura, G. Verdon, H. J. Kang et al., "Structure and mechanism of the mammalian fructose transporter GLUT5," *Nature*, vol. 526, no. 7573, pp. 397–401, 2015.
- [40] K. Iizuka, "The role of carbohydrate response element binding protein in intestinal and hepatic fructose metabolism," *Nutrients*, vol. 9, no. 2, p. 181, 2017.

- [41] L. Luo, Y. Zheng, M. Li et al., "TMPRSS2 correlated with immune infiltration serves as a prognostic biomarker in prostatic adenocarcinoma: implication for the COVID-2019," *Frontiers in Genetics*, vol. 11, p. 575770, 2020.
- [42] J. You, L. Wang, J. Huang et al., "Low glucose transporter SLC2A5-inhibited human normal adjacent lung adenocarcinoma cytoplasmic pro-B cell development mechanism network," *Molecular and Cellular Biochemistry*, vol. 399, pp. 71–76, 2015.
- [43] V. Molinier-Frenkel, A. Prévost-Blondel, and F. Castellano, "The IL4I1 enzyme: a new player in the immunosuppressive tumor microenvironment," *Cell*, vol. 8, no. 7, p. 757, 2019.
- [44] A. B. Morris, C. R. Farley, D. F. Pinelli et al., "Signaling through the Inhibitory Fc Receptor FcγRIIB Induces CD8⁺ T Cell Apoptosis to Limit T Cell Immunity," *Immunity*, vol. 52, no. 1, pp. 136–150.e6, 2020.
- [45] C. Recio, D. Lucy, G. S. D. Purvis et al., "Activation of the immune-metabolic receptor GPR84 enhances inflammation and phagocytosis in macrophages," *Frontiers in Immunology*, vol. 9, p. 1419, 2018.
- [46] Y. Jiao, K. K. Sun, L. Zhao, J. Y. Xu, L. L. Wang, and S. J. Fan, "Suppression of human lung cancer cell proliferation and metastasis *in vitro* by the transducer of ErbB-2.1 (TOB1)," *Acta Pharmacologica Sinica*, vol. 33, no. 2, pp. 250–260, 2012.
- [47] W. J. Shangguan, H. T. Liu, Z. J. Que, F. F. Qian, L. S. Liu, and J. H. Tian, "TOB1-AS1 suppresses non-small cell lung cancer cell migration and invasion through a ceRNA network," *Experimental and Therapeutic Medicine*, vol. 18, pp. 4249–4258, 2019.
- [48] D. R. Caswell, C. H. Chuang, R. K. Ma, I. P. Winters, E. L. Snyder, and M. M. Winslow, "Tumor suppressor activity of Selenbp1, a direct Nkx2-1 target, in lung adenocarcinoma," *Molecular Cancer Research*, vol. 16, no. 11, pp. 1737–1749, 2018.
- [49] S. L. Gaffen, "Structure and signalling in the IL-17 receptor family," *Nature Reviews. Immunology*, vol. 9, no. 8, pp. 556–567, 2009.
- [50] R. M. Gorczynski, "IL-17 signaling in the tumor microenvironment," *Advances in Experimental Medicine and Biology*, vol. 1240, pp. 47–58, 2020.

Review Article

The Role and Function of Regulatory T Cells in *Toxoplasma gondii*-Induced Adverse Pregnancy Outcomes

Xuyang Gao , Yue Zhong , Yifan Liu , Runmin Ding , and Jinling Chen 

Department of Pathogen Biology, School of Medicine, Nantong University, Nantong, 226001 Jiangsu, China

Correspondence should be addressed to Jinling Chen; chenchennt@ntu.edu.cn

Received 30 April 2021; Revised 22 June 2021; Accepted 29 July 2021; Published 19 August 2021

Academic Editor: Zhipeng Xu

Copyright © 2021 Xuyang Gao et al. This is an open access article distributed under the Creative Commons Attribution License, which permits unrestricted use, distribution, and reproduction in any medium, provided the original work is properly cited.

Infection with *Toxoplasma gondii* (*T. gondii*) during the pregnant period and its potentially miserable outcomes for the fetus, newborn, and even adult offspring continuously occur worldwide. People acquire infection through the consumption of infected and undercooked meat or contaminated food or water. *T. gondii* infection in pregnant women primarily during the gestation causes microcephaly, mental and psychomotor retardation, or death. Abnormal pregnancy outcomes are mainly associated with regulatory T cell (Treg) dysfunction. Tregs, a special subpopulation of T cells, function as a vital regulator in maintaining immune homeostasis. Tregs exert a critical effect on forming and maintaining maternal-fetal tolerance and promoting fetal development during the pregnancy period. Forkhead box P3 (Foxp3), a significant functional factor of Tregs, determines the status of Tregs. In this review, we summarize the effects of *T. gondii* infection on host Tregs and its critical transcriptional factor, Foxp3.

1. Introduction

T. gondii is an obligate intracellular parasite with a complicated life cycle, belonging to apicomplexa. *T. gondii* requires two hosts, mammals including human acting as intermediate hosts and cats, which are definitive hosts [1]. People acquire infection by eating undercooked meats or dairy products which contain cysts or pseudocyst of *T. gondii* or by contacting with water contaminated with feces of cats that involve *T. gondii* oocysts [2]. *T. gondii* in an individual with normal immunity is in a state of latent infection and produces no obvious clinical effect. Nevertheless, an individual with compromised immunity possibly suffers from ocular toxoplasmosis and fatal diseases of the central nervous system like encephalitis. Contracting *T. gondii* during the pregnancy, which is a state of immunological tolerance, might be a lethal factor for the fetus. The overall risk of congenital infection from primary *T. gondii* infection varies from 20% to 50% without treatment [3]. Based on the seroprevalence study in Central and Southern Italy from 2013 to 2017, the prevalence of pregnant women remains 13.8%, although pregnant women are conscious of the importance of hygiene and diet

to prevent primary *T. gondii* infection [4]. *T. gondii* tachyzoites infect fetuses and cause potentially tragic outcomes such as microcephaly, intrauterine growth restriction, or death [5] (Figure 1). And the severity of *T. gondii* infection is closely associated with gestational age [6]. Chorioallantoic attachment did not occur until embryonic day (E) 8.5 during the development of mouse placenta. At this stage, trophoblast cells of the chorionic plate and mesoderm cells of allantois begin to interdigitate to generate villi [7]. Villous explantation has high resistance to pathogen infection [8]. Therefore, *Toxoplasma* infection, which occurs in the early pregnancy, enhances the possibility of miscarriage.

Normal pregnancy is a special immune phenomenon, similar to allotransplantation. Many mechanisms protect the fetus from the maternal immune system, including the nonclassical MHC molecules expressed on trophoblast cells, the complement system, tryptophan catabolism by the action of enzyme indoleamine 2,3-dioxygenase (IDO), T cell apoptosis, and suppressive function of CD4⁺ CD25⁺ Tregs [9]. Among them, Tregs are documented as important regulators in maintaining normal pregnancy [10]. Tregs modulate the immune response mainly by secreting inhibitory

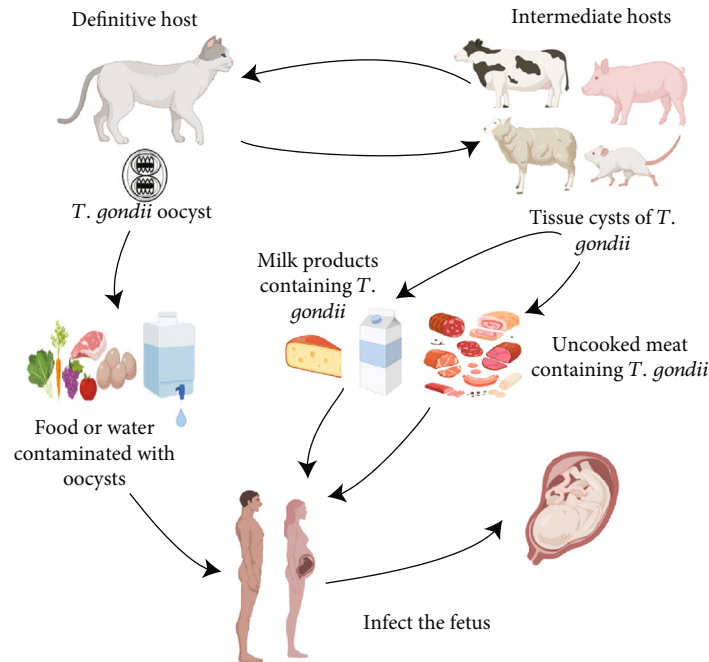


FIGURE 1: Life cycle and spread of *T. gondii* between people and animal. Feline is the definitive host. Intermediate hosts will infect by ingesting the water source of *T. gondii* oocyst deposited in cat feces or animal meat and milk products containing cysts or pseudocysts. Pregnant women infected during the gestation period will bring about adverse outcomes because *T. gondii* can be transmitted to the fetus through the placenta.

factors such as transforming growth factor- β (TGF- β) and interleukin-10 (IL-10) or inhibiting inflammatory cytokines produced by Th1/Th17 cells, such as interferon- γ (IFN- γ), IL-17, and IL-23, in order to protect against their harmful effects [11, 12].

Pregnant women infected with *T. gondii* during the gestation period will lead to decidual Treg depletion in number and downregulation in function on the maternal-fetal interface [13]. In our laboratory, previous research has shown that the decrease in the number and function of Tregs of pregnant mice results from *T. gondii* excreted-secreted antigens [14], which break immune tolerance of normal pregnancy and finally cause abortion during early pregnancy [15]. In this article, we review the role of Tregs and the underlying mechanism in *T. gondii*-induced adverse pregnancy outcomes.

2. Destructions of Placental Structure by *T. gondii* Infection

Human placenta, a critical organ with multiple functions like endocrine and immune reaction, consists of its umbilical cord, amnion, parenchyma, and chorion. Chorion differentiates into floating and anchoring villi. Floating villi are formed by an inner layer of cytotrophoblasts (CTBs) where a layer of syncytiotrophoblasts (SYN) covers, while anchoring villi attach itself to maternal decidual tissue via extravillous trophoblasts (EVTs). EVT's straightly invade the decidua basalis and thus anchor the placenta into the uterine implantation site, in which the EVT's directly contact with maternal immune cells. The maternal-fetal interface is composed of CTBs and SYN that are formed via the fusion of the underlying CTBs. SYN on both floating and anchoring villi consti-

tutes the outermost cell layer and thereby forms the critical interface between maternal and fetal blood [16]. The syncytiotrophoblast layer has high resistance to *T. gondii* infection. *T. gondii* rarely goes across the syncytiotrophoblast layer *in vivo* [17]. When syncytium is damaged, it would allow for pathogen to enter the villous core [18]. The influence might be dependent on the gestation time as well, for the layer of subsyncytial CTBs becomes thinner and discontinuous in part after the first trimester. Although *T. gondii* replicates well in underlying subsyncytial CTBs, it fails to colonize SYN [18]. Those indicate that *T. gondii* might invade subsyncytial CTBs only if the syncytiotrophoblast layer ruptures (Figure 2).

In the process of placentation, trophoblast cells from implanted blastocyst invade the mother's endometrium. Endometrial stromal cells differentiate through a process called decidualization, which contributes to trophoblast invasion [19]. According to the contact pattern between the trophoblast and endometrium, the placentae of eutherians are classified in epitheliochorial, endotheliochorial, and hemochorial placentae. In hematochorionic placentas of human and mice, the fetal membrane is in direct contact with maternal tissue and blood [20]. To maintain successful pregnancy, the deep placentation implies proper recognition and tolerance of semiallogeneic fetuses, in which maternal immune cells play a key role. Tregs infiltrate into the decidua of pregnancy and play a crucial role in fetal tolerance, trophoblast invasion, and tissue and vascular remodeling, along with other leukocytes (macrophages, NK cells, and dendritic cells) [21].

Brito et al. infected BALB/c mice with *T. gondii* type II strain (ME49) [22]. Histopathological analysis showed that *T. gondii* was generally detected in the muscularis at the early

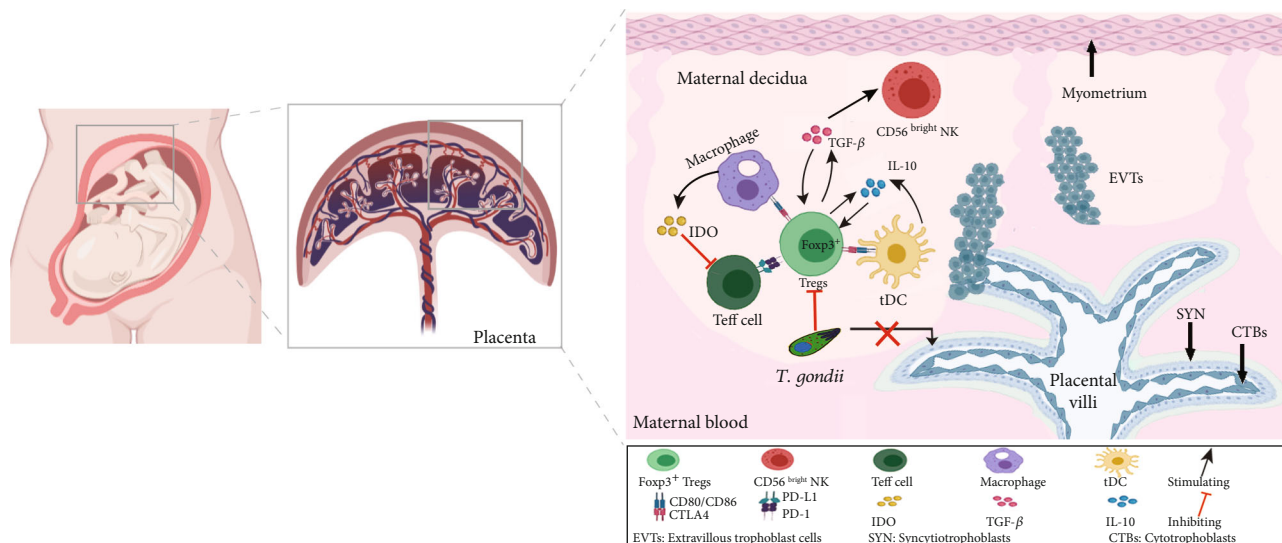


FIGURE 2: Mechanism of maternal-fetal immune regulation. The maternal-fetal interface is composed of CTBs and SYN, formed by the fusion of underlying CTBs. SYN, the key interface between the blood and fetal barrier, is highly resistant to *T. gondii*. *T. gondii* rarely goes across SYN. *T. gondii* infection affects maternal-fetal immune regulation by affecting maternal regulatory immune cells, mainly by inhibiting Tregs. CTBs: cytotrophoblasts; SYN, syncytiotrophoblasts; EVTs: extravillous trophoblasts; Teff cell: effector T; tDC: tolerance-inducing DC; images were created with BioRender.

gestation period, and a small number of *T. gondii* were found in the decidua on the 14th day of gestation. On the 18th day of gestation, necrosis appeared at the maternal-fetal interface and *T. gondii* could be observed in the placenta. 2000 freshly sporulated oocysts of *T. gondii* M4 were administered orally to Churra sheep during the pregnancy [23]. From 7 to 11 days after infection, abortion occurred in pregnant ewes. The placenta with different degrees of autolytic edema could be seen under the microscope. Histological examination revealed infarction and thrombus formation of the villi of the placental corpuscle wall, which caused fetal hypoxia damage and was related to acute abortion. Fadaam et al. found that *T. gondii* could be detected in the fetal brain, lung, and placenta. And inflammatory pathological changes of trophoblastic cells in the placenta, trophoblast edema, hemorrhage, and fibrinoid necrosis were observed, indicating that *T. gondii* during the pregnancy was transmitted to the fetus through the placenta, affecting pathological changes of placental structure and further damaging trophoblast cells of the placenta [24]. In addition, pathologic examination revealed necrotic granuloma in the villous stroma leading to fetal autolysis in pregnant women infected with *T. gondii* [25]. A normal mouse placenta consists of the maternal decidua and the fetal embryo-derived compartments, containing the junctional zone and labyrinth zone [26]. Nearly all of the embryos and placentas in pregnant mice exhibited a necrotic and hemorrhagic appearance at the early stage of pregnancy following the administration of antigens from *T. gondii* [14]. The function of the labyrinth zone in the mouse placenta is to be equivalent to that of the chorionic villus of the human placenta. The labyrinth zone of the mouse placenta displayed the classical interhemal barrier, breaking fetal blood vessels and maternal lacunae upon the administration of antigens from *T. gondii* [14]. Hence, destructions of the

placental structure may partially account for the adverse pregnancy triggered by *T. gondii*.

3. Effects of *T. gondii* Infection on Maternal-Fetal Immune Regulation

3.1. Maternal-Fetal Immune Regulation. Normal pregnancy is, to a great extent, dependent on maternal immune tolerance, as the fetus consists of the tissue-specific as well as paternally inherited antigens. Balance between inactivation of alloreactive effector cells and/or clone deletion and immune suppression triggered by regulatory immune cells constitute maternal immune tolerance. Innate regulatory immune cells including alternatively activated/regenerative-type macrophages (M2), tolerance-inducing DCs (tDCs), and CD56^{bright} CD16⁻ decidual NK cells (dNK) interact with adaptive cells comprising Tregs to constitute a key network that maintain a successful pregnancy [27].

Macrophages have a capacity for immunosuppressive activity and production of cytokine besides antigen presentation. According to the function and repertoire of cytokine production, macrophages are generally classified into two significant subpopulations: M1 and M2. M1 macrophages are an inflammatory-type presenting antigen, producing proinflammatory cytokine and nitric oxide (NO) as well as reactive oxygen species (ROS). M2 macrophages, which are induced by Th2 cytokines like IL-4 and IL-13, are alternatively activated/regenerative type that exert an immunosuppressive function and promote immune tolerance and tissue remodeling at the maternal-fetal interface [21]. M2 macrophages play immunosuppressive roles by abundant production of IL-10 and IDO, accompanied with prostaglandin-E2 (PGE2) which limits the activation of cytotoxic leukocytes [28]. IDO produced by M2 is mediated by

Tregs via cytotoxic T-lymphocyte-associated protein 4 (CTLA-4) expressed on Treg surface. The shift from M2 to M1 phenotype during pregnancy is linked to adverse pregnancy outcomes like miscarriages or preeclampsia [29].

The DCs orchestrate T cell activation and differentiation via presenting antigen and providing costimulatory signaling. Placental formation during the early pregnancy is correlated with immature DCs with tolerogenic capacity. DCs induce Treg differentiation along with abundant production of IL-10 during the pregnancy [30]. Additionally, Tregs produce heme oxygenase-1 (HO-1) to maintain the immature state of DCs, which further induces Treg formation via higher level of IL-10 [31]. DCs produce IDO and TGF- β to interact with CTLA-4 expressed on Tregs, which inhibit allo-gen-specific T cell activity, improve Treg differentiation, and further break Treg/Teff balance.

Both uterine and decidual NK cells exert their immunoregulatory functions in the process of placental vascularization and formation during the early pregnancy. Imbalance between regulatory CD56^{bright} NK cells and cytotoxic CD56^{dim} may impair maternal immune tolerance. The decreased CD56^{bright}/CD56^{dim} NK cell ratio is bound up with adverse pregnancy outcomes like recurrent pregnancy loss [32]. Tregs are implicated in the regulation of cell phenotype and generation of dNK cells via inhibiting cytotoxicity of NK cells in a TGF- β -dependent manner and suppressing the release of IL-15 from DCs. Similarly, TGF- β produced by Tregs shifts NK cell from the peripheral CD56^{dim} to decidual-like CD56^{bright} phenotype. NK cells improve Treg homeostasis via alleviating Th17 cell responses through secreting IFN- γ and promoting Treg development.

Early studies have shown that Th1/Th2 intercellular immune balance and Th2 cell predominance are involved in the mechanisms of maintaining normal pregnancy [33, 34]. Cytokines, secreted by Th2 like IL-4 and IL-6, can induce trophoblast cells to release hCG and stimulate the production of progesterone [35], which in turn stimulates Th2 cells to reduce the secretion of Th1 cytokines [36]. However, in knockout mouse models that cannot secrete Th2 cytokines, abortion is not always possible [37], indicating that Th2 cytokines are not essential for the maintenance of normal pregnancy [38]. In recent years, studies have suggested that Th17/Treg cell balance is closely related to the formation and maintenance of maternal-fetal tolerance [39]. Th17 mainly mediates the immune response by secreting proinflammatory cytokines like IL-17 and IL-22 and specifically expresses the transcription factors orphan nuclear receptor (ROR γ t) and signal transducer and activator of transcription 3 (STAT3). IL-35, a newly discovered anti-inflammatory cytokine secreted by Tregs, functions as a regulator by promoting Treg amplification and inhibiting Th17 differentiation [40]. IL-35 suppresses the production of IL-17, but the levels of IL-35 and IL-35/IL-17 in patients with recurrent abortion are significantly lower than normal [41]. It follows that the deviation of Th17 will enhance the maternal immune response to the fetus, which is not conducive to the maintenance of normal pregnancy [10].

The pathogenic effects of *T. gondii* mainly contain the direct action of *T. gondii* and the immunopathological

response triggered by *T. gondii* antigen. Abortion caused by *T. gondii* infection is predominately related to the disruption of the maternal-fetal interface immune balance induced by *T. gondii* antigen in early pregnancy [42]. *T. gondii* ESA are soluble antigens that stick to and invade host cells in the early stage of *T. gondii* infection, and are excreted or secreted during intracellular proliferation [43]. It has strong immunogenicity [44], which can induce the host to provoke humoral and cellular immune responses and cause immune response [45]. The influence of ESA on the host is similar to the host directly infected with *T. gondii*. Pregnant mice injected with ESA could result in abortion during the early stage of pregnancy, accompanied with decreased levels of CD4⁺CD25⁺ Tregs and Foxp3 in the spleen and placenta [13]. Therefore, fetal resorption mediated by *T. gondii* is largely owing to immunopathological reaction rather than the direct effect of *T. gondii* proliferation in the uterus.

3.2. Characteristics and Mechanisms of Regulatory T Cells.

Tregs, accounting for 5-10% of the total CD4⁺ T cell pool and expressing T cell receptors (TCR), are mostly distinct from that of conventional CD4⁺CD25⁺ T cells. Tregs derive from two different populations that exert synergy effect to enhance peripheral immune tolerance [46, 47]: (1) CD4⁺CD25⁺ Foxp3⁺ natural regulatory T (nTreg) cells, enriched with an anti-self-biased TCR repertoire, differentiate from immature precursors in the thymus and enhance immune tolerance to self-antigens [48] and (2) induced regulatory T (iTreg) cells, developed from naive conventional CD4⁺CD25⁺ T cells after antigen encounter with specific factors such as TGF- β and IL-2 and act as effective Tregs to suppress the immune response [49].

Tregs can be activated by self-antigens as well as non-self-antigens [50]. Activated Tregs have the capacity of inhibiting T cell proliferation in specific and nonspecific antigen manners. Notably, the inhibitory function of Tregs is not limited to the adaptive immune system but impacts the activation and function of innate immune cells such as monocytes, neutrophils, macrophages, and dendritic cells [51]. Various mechanisms by which Tregs maintain self-tolerance as well as suppress autoimmune responses and chronic inflammation are involved: (1) Tregs kill target cells via a granzyme B-dependent, perforin-independent pathway [52]; (2) Tregs modulate target cells via binding to the corresponding receptor of target cells such as CTLA-4 and PD-1 [53, 54]; (3) Tregs play immunosuppressive roles via secreting immune regulatory factors like TGF- β , IL-10, or IL-4 [55, 56]; and (4) Tregs inhibit target cells by exosome-carried microRNAs [57].

3.3. Regulatory T Cells during Normal Pregnancy.

Tregs usually proliferate in the early stage of pregnancy with the enhanced immunosuppressive ability, which will continue until the end of pregnancy [58]. Aluvihare et al. firstly demonstrated an increase in the number of Tregs during normal pregnancy in an animal model, and the lack of Tregs eventually causes abortion [59]. The decreased number of Tregs was observed in mice prone to abortion, which can be prevented through adoptive transfer of Tregs from the spleen of normal

pregnant mice [60]. The number of Tregs was reduced in patients prone to recurrent spontaneous abortion as well [61, 62], indicating that Tregs push forward an immense influence on maintaining normal human pregnancy. In the early pregnancy, the number of Tregs increases gradually and reaches the highest level when trophoblast cells invade the decidua, suggesting that Tregs are involved in regulating the uterine immune response to the placenta [54, 63]. Studies have shown that Tregs mainly rely on three mechanisms to promote implantation and embryo development [64]. Firstly, Tregs can prevent effector T (Teff) cells from damaging the fetus in an antigen-dependent trophoblastic cytotoxic manner by secreting IL-10, TGF- β , CTLA-4, and PD-1 [35, 64, 65]. Secondly, Tregs can regulate other cells like M2-type macrophages and tDCs [66]. Tregs induce M2 macrophages and tDCs to express IDO, which can decrease Th1 cells [67]. Thirdly, Tregs have vascular regulation function [68], which is crucial for normal placental development and placental pathway with sufficient maternal blood. When Tregs were deficient, changes in uterine spiral arteries and placental hemodynamics were not conducive to fetal development [67, 69]. In addition, unexplained infertility and abortion are linked to the deficiency of the number and function of Tregs [54]. The expression of Foxp3 mRNA in the endometrium is very low in patients with unexplained infertility, suggesting that the differentiation ability of uterine T cells into Treg phenotypes is impaired, thereby affecting fertility [70].

Hence, the number and function of Tregs increase during the normal pregnancy and impair in the pregnancy failure, indicating that Tregs is extremely crucial during pregnancy (Figure 2).

3.4. The Role of Tregs on *T. gondii* Infection-Induced Abortion. Tregs are associated with adverse pregnancy induced by *T. gondii* as well. *T. gondii* infection results in a decreased number of decidua Tregs, accompanied with decreased levels of immune-related functional molecules like IL-10 and TGF- β [71]. In addition, study has shown that acute *T. gondii* infection can directly inhibit Treg proliferation [72].

3.4.1. *T. gondii* Induces a Decrease in the Number of Tregs. It has been found that the number of Tregs in the spleen and placenta was reduced in a *T. gondii*-infected pregnant mouse model [10]. The decreased number of Tregs is associated with apoptosis triggered by *T. gondii* infection [73]. IL-10 is an important cytokine to maintain normal pregnancy, and the hyposecretion of IL-10 in the decidua is correlated with adverse pregnancy [74]. Some studies indicate that IL-10 can regulate the expression of various apoptotic factors to prevent apoptosis [75, 76]. Lao et al. established an *T. gondii* infection animal model using recombinant IL-10 (rIL-10) and IL-10-deficient mice [77]. It was found that cleaved caspase-3 and caspase-8 were upregulated in decidua Tregs in the IL-10^{-/-} group, while those were decreased in the rIL-10 treatment group along with improved pregnant outcomes, indicating that IL-10 has the capacity of inhibiting the apoptosis of decidua Tregs and improving adverse pregnant outcomes.

The severity of adverse pregnant outcomes upon primary infection with *T. gondii* is bound up with the gestational time. *T. gondii* infection in the early stage of pregnancy can more possibly cause abortion than that in the late pregnancy in the mouse model, and the main reason is the apoptosis rate of Tregs induced by *T. gondii* infection in the early stage of pregnancy [78]. *T. gondii* infection can result in a decrease in the number of Tregs in the mouse placenta and spleen [10]. A significant decrease in mortality was observed through adoptive transfer of normal mouse CD4⁺ Tregs to *T. gondii*-infected mice [79], indicating that maintaining a certain number of Tregs is crucial to improve the adverse results caused by *T. gondii* infection.

Estradiol is implicated in several aspects of pregnancy, suggesting its indispensable role in pregnancy. Qiu et al. demonstrated that the decreased number of Tregs induced by *T. gondii* infection is attributed to Treg apoptosis mediated by *T. gondii* [78]. Compared with late pregnancy, the rate of Treg apoptosis was enhanced in the early pregnancy, accompanied with reduced PD-1 expression. Estradiol (E2) *in vitro* could provide protection against apoptosis and enhance PD-1 expression on Tregs through estradiol receptor (ER) in a dose-dependent manner. Simultaneously, E2 administration in nonpregnant mice could ameliorate the apoptosis rate of Tregs induced by *T. gondii* infection, accompanied with the potentiated expression of PD-1 on Tregs. E2 might help support the immune tolerance and improve the adverse pregnancy via targeting on Tregs. Those findings verify the role of Tregs in *T. gondii*-induced adverse pregnancy.

3.4.2. *T. gondii* Induces Dysfunction of Tregs. Tregs play an immunosuppressive role through CTLA-4 and PD-1 binding to the target cell surface [80, 81] as well as secreting cytokines IL-10 and TGF- β [77, 82], which are important for protective tolerance induced by Tregs during the pregnancy. CTLA-4 expression in a decidual membrane is positively correlated with the secretion of anti-inflammatory cytokines, indicating the significant immunosuppressive activity of CTLA-4 at the maternal-fetal interface [83]. Additionally, the combination of CTLA-4 and its ligand CD80/CD86 can induce IDO expression, and IDO will further promote maternal-fetal immune tolerance [84]. When CTLA-4 is deficient, the function of Tregs will decrease [80]. PD-1 is another important factor for Tregs to induce fetal protection in a mouse model [85]. PD-1 binds to PD-L1 expressed on trophoblastic cells [86], which can transmit inhibitory signals down to exert immunosuppressive effects. Though PD-1 blockade has no significant effect on Treg number, it could induce the impairment of Treg function in recurrent early abortion. Blocking PD-1 by injection of monoclonal antibody can cause fetal loss in pregnant mice, which is linked with insufficiency of Treg function and amplification of Teff [87]. Research has shown that the expression levels of CTLA-4, PD-1, TGF- β , and IL-10 in Tregs from pregnant mice with abortion induced by *T. gondii* infection are downregulated, while the levels of the inflammatory cytokines are increased [73]. High level of IFN- γ instead leads to maternal immune response of fetal abortion [88], and the adoptive transfer of Tregs from

healthy pregnancy mice can improve the adverse pregnant outcomes caused by *T. gondii* infection.

3.5. Signaling Pathways of Suppressing Foxp3 Caused by Excreted-Secreted Antigens. The continuous stability and high expression of Foxp3 are the key to the development of Tregs. Foxp3, an acknowledged character of Tregs, is implicated in the establishment and maintenance of Tregs and takes charge of maintaining immune homeostasis [89]. In patients with recurrent spontaneous abortion, the expression of Foxp3 protein in peripheral blood and decidual tissues is significantly less than that in normal pregnant women [90]. In addition, the expression of Foxp3 in women with unexplained infertility was associated with a lower number or percentage of Tregs in endometrial tissue [70]. Previous studies in our laboratory have shown that ESA could suppress Foxp3 expression both *in vivo* and *in vitro* and inhibit the function of Tregs, thereby causing abortion [14]. We all know that the regulation of Foxp3 is relatively complicated, including the TGF- β /Smad pathway, the interleukin-2 receptor/signal transducer and activator of transcription (IL-2R/STAT) pathway, and the phosphatidylinositol 3-kinase/protein kinase B/mammalian target of rapamycin (PI3K-AKT-mTOR) pathway.

TGF- β signaling plays an indispensable role in the early development of Tregs [91] and is a necessity to maintain the number of Tregs in peripheral lymphatic tissue [92]. TGF- β , binding with TGF- β type II receptor (T β RII), induces phosphorylation of T β RII and activates its kinase activity, which further activates Smad2 and Smad3 protein by phosphorylation. And then, phosphorylated Smad2 and Smad3 bind to Smad4, form the Smad complexes, and transfer into the nucleus, thereby regulating Foxp3 expression [93]. Our previous study revealed that Chinese 1 strain of *T. gondii* ESA could suppress Foxp3 by inhibiting Smad2 and Smad3 phosphorylation in pregnant mice [14]. Meanwhile, the overexpression of Smad2/Smad3/Smad4 can partially offset the inhibition of Foxp3 induced by ESA. It can be seen that ESA directly inhibits the expression of T β RII, suppresses the activation of Smad2/Smad3/Smad4 signaling pathway, and negatively modulates Foxp3, causing abortion. Treatment with TGF- β can prominently improve adverse pregnant outcomes caused by *T. gondii* infection [94]. The TGF- β /Smad signaling pathway can enhance the differentiation, development and function of Tregs, regulate Foxp3, and inhibit high levels of maternal-fetal inflammation triggered by *T. gondii* infection.

Besides the TGF- β /Smad signaling pathway, IL-2R is also essential for the development of Tregs and the transcription of Foxp3 [95]. IL-2R/Janus kinase 3 (JAK3)/STAT signaling pathway is associated with the development and functional maintenance of Tregs [96]. Binding to the corresponding receptor, heterodimerization of the cytoplasmic domain, IL-2 induces the activation of JAK3, which activates STATs by phosphorylation, mainly STAT5. A previous study has shown that ESA of *T. gondii* suppresses Foxp3 by directly inhibiting IL-2R, JAK3, and the phosphorylation of STAT3 and STAT5, while overexpression of STAT3/STAT5 can partially attenuate the inhibitory effect of ESA on Foxp3 [97]. Therefore, ESA of

T. gondii inhibits Foxp3 via the IL-2R/JAK3/STAT signaling pathway, thus suppressing Treg function.

The PI3K-AKT-mTOR signaling pathway mediates cell proliferation, differentiation, and apoptosis [98]. Tregs are sensitive to PI3K activation, and PI3K activation will down-regulate the expression of Foxp3, thus negatively affecting Treg function, while inducible T cell costimulator (ICOS) can activate negative regulators of PI3K such as TANK binding kinase 1 (TBK1) [55] to maintain the normal function of Tregs [99]. The activation of PI3K produces the second messenger phosphoinositide 3 kinase (PIP3), which binds to the intracellular signal protein AKT. Activated AKT induces the phosphorylation of mTOR, affects the expression of cytokine in T cells, and exerts a critical immunosuppression function. The PI3K-AKT-mTOR pathway negatively regulates Foxp3 via inactivating the transcription factor Forkhead O3a [100]. ESA can inhibit Foxp3 by upregulating PI3K, AKT, and mTOR [101], leading to downregulation of the immune function of Tregs.

Foxp3 functions as a key regulator in the development and function of Tregs. ESA of *T. gondii* can inhibit Foxp3 via suppressing the expression of T β RII and IL-2R, cutting the phosphorylation levels of Smads and STATs. Moreover, ESA can suppress Foxp3 by upregulating PI3K, AKT, and mTOR as well (Figure 3). The suppression of Foxp3 expression indicates the downregulation of Treg function, leading to adverse pregnancy.

4. Role of Tregs in Long-Term Effects of *T. gondii* Infection on the Fetus

T. gondii infection largely causes abortion in the early pregnancy, whereas its infection that occurred in the late pregnancy mainly induces neuropsychiatric diseases and behavior alterations in humans and rodents [102]. *T. gondii* infection increases vulnerability to schizophrenia, which is evidenced by the fact that the risk of schizophrenia among individuals prenatally exposed to *T. gondii* was more than twice that of healthy subjects. Consistent with these results, immunoglobulin G levels of *T. gondii* were closely linked to schizophrenia risk [72]. Several underlying mechanisms are involved, including enhanced testosterone [103], increased dopamine and decreased serotonin [104], and different immune alterations [105]. Hellmer and Nystrom reported that dysregulation of infant acetylcholine, dopamine, and melatonin may be responsible for autism spectrum disorders (ASD) [106]. Immune imbalance is a causal factor of schizophrenia as well. Alterations of circulating CD4⁺ T lymphocytes were observed in individuals with schizophrenia [105]. A similar finding was demonstrated in an independent sample in which the neuroinflammation triggered by CD4⁺ T cells could impact the central nervous system [107]. Neurotransmitters like dopamine are postulated to critical regulators of T cell functions [108]. In parallel, gene variants of dopamine receptor were largely linked to the amount of CD4⁺ T cells rather than CD8⁺ T cells [109].

Tregs are susceptible to dopamine and cyclic AMP levels in lymph cells [79]. Dopamine receptor D5 (DRD5) signaling strengthens suppressive capacity of Tregs, thereby mitigating

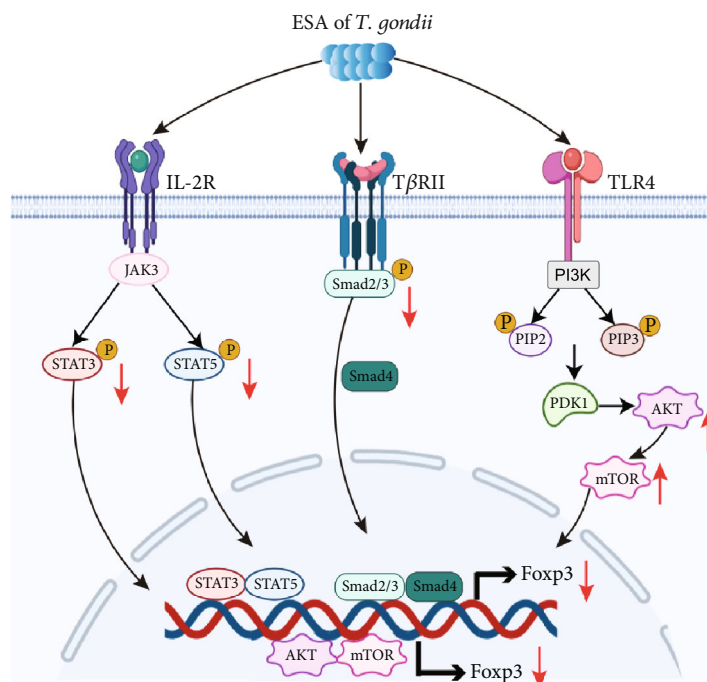


FIGURE 3: Mechanism of inhibiting Foxp3 by excreted-secreted antigens of *T. gondii*. ESA can inhibit the expression of Foxp3 by inducing the deactivation of IL-2R, inhibiting the expression of JAK3, and reducing the phosphorylation levels of STAT3 and STAT5. Furthermore, ESA may inactivate T β R11 and further suppress the levels of p-Smad2, p-Smad3, and Smad4 in order to downregulate the expression of Foxp3. In addition, ESA can upregulate the expression of PI3K/AKT/mTOR via TLR4, resulting in the decrease of Foxp3 expression. ESA: excreted-secreted antigens; Foxp3: forkhead box p3; IL-2R: interleukin 2 receptor; JAK3: Janus kinase 3; STAT3: signal transducer and activator of transcription 3; T β R11: TGF- β type II receptor; TLR4: Toll-like receptor 4; PI3K: phosphatidylinositol 3-kinase; AKT: protein kinase B; mTOR: mammalian target of rapamycin.

the manifestation of experimental autoimmune encephalomyelitis (EAE). Additionally, the anti-inflammatory effect of DRD5 signaling in Tregs is bound up with increased glucocorticoid-induced tumor necrosis factor receptor-related protein (GITR) expression, which can contribute to Treg expansion [110]. Simultaneously, Tregs have a neuroprotective capacity via promoting neurotrophic factor expression and repressing the synthesis of proinflammatory cytokines as well as ROS, which could impair the higher-order brain functions and thereby contribute to the progressive brain alterations [111]. Xu et al. established an animal model of maternal immune activation by the injection of *T. gondii* soluble tachyzoite antigen (STAg) on E 14.5 [112]. Consistent with our previous study, *T. gondii* antigen failed to induce abortion in the late pregnancy period [14]. At 3 days after injection, the decreased Tregs but increased Th1 and Th17 cells in the spleen of pregnant mice were observed, indicating that STAg could exert a proinflammatory T cell immune profile [112]. Offspring exposure to STAg-triggered MIA exhibited impaired-communicative capacity and anxiety-like behaviors as well as deficits in social behaviors. Isolated CD4⁺CD25⁺ Tregs from PBS-treated (_CTregs) and STAg-triggered MIA (_{MIA}Tregs) of mother mice were intravenously transferred into adult progeny at the age of 8 weeks, respectively. Treg transfer could effectively reverse autism-related manifestations. Noteworthy, _{MIA}Tregs appeared to have greater efficacy on immune suppression than _CTregs in the brain of offspring. *T. gondii*-activated

maternal Tregs could rescue behavior abnormalities in the offspring of adult mice induced by maternal immune activation. Therefore, sufficient Tregs not only prevent against the miscarriage but improve behavior abnormalities in the offspring of adult mice induced by *T. gondii*.

5. Conclusions and Future Directions

T. gondii infection can invade the placental tissue in different ways and destroy maternal-fetal immune tolerance during the pregnancy, which can lead to maternal immune rejection, affect fetal growth, and cause abortion or other pregnancy complications. Tregs play a vital role in the immune regulation of pregnancy [113], and the decline in the number or function of Tregs is associated with adverse pregnancy. As a critical functional molecule of Tregs, Foxp3 expression directly determines the state of Tregs. Extensive studies have been done to unravel the role of Tregs in different types of adverse pregnancy through mouse models. Treg transfer might be a potential therapeutic to treat adverse pregnancy, especially behavior abnormalities in the offspring of adult mice induced by maternal immune activation. The signaling pathways regulating Foxp3 expression can be targeted to recovery from adverse pregnancy as well.

Conflicts of Interest

All authors state that they have no conflicts of interest.

Acknowledgments

This study was funded by the Science and Technology Innovation and Demonstration Promotion Project of Natural Science Foundation of Nantong City (MS22020001), National Undergraduate Innovation and Entrepreneurship Training Program of China (202010304059Z); and Undergraduates Training Programs of Innovation and Entrepreneurship of Jiangsu Province (202110304099Y).

References

- [1] S. Lourido, “_Toxoplasma gondii_,” *Trends in Parasitology*, vol. 35, no. 11, pp. 944–945, 2019.
- [2] A. Barragan and L. David Sibley, “Migration of _Toxoplasma gondii_ across biological barriers,” *Trends in Microbiology*, vol. 11, no. 9, pp. 426–430, 2003.
- [3] M. Ferrucci and G. Dall’Ara, “Immunological indexes of receptivity and seroconversion for rubella and toxoplasmosis in the province of Ferrara, Italy,” *Annali Sclavo; rivista di microbiologia e di immunologia*, vol. 22, no. 4, pp. 606–623, 1980.
- [4] D. Fanigliulo, S. Marchi, E. Montomoli, and C. M. Trombetta, “Toxoplasma gondii in women of childbearing age and during pregnancy: seroprevalence study in Central and Southern Italy from 2013 to 2017,” *Parasite*, vol. 27, p. 2, 2020.
- [5] D. M. Feldman, R. Keller, and A. F. Borgida, “Toxoplasmosis, parvovirus, and cytomegalovirus in pregnancy,” *Clinics in Laboratory Medicine*, vol. 36, no. 2, pp. 407–419, 2016.
- [6] H. R. Storchilo, H. H. A. Rezende, T. C. Gomes et al., “Basic heel prick test: inclusion of screening, diagnosis and criteria for early confirmation of congenital infection by Toxoplasma gondii,” *Revista do Instituto de Medicina Tropical de São Paulo*, vol. 61, 2019.
- [7] L. Anson-Cartwright, K. Dawson, D. Holmyard, S. J. Fisher, R. A. Lazzarini, and J. C. Cross, “The glial cells missing-1 protein is essential for branching morphogenesis in the chorioallantoic placenta,” *Nature Genetics*, vol. 25, no. 3, pp. 311–314, 2000.
- [8] C. Tscherning-Casper, N. Papadogiannakis, M. Anvret et al., “The trophoblastic epithelial barrier is not infected in full-term placentae of human immunodeficiency virus-seropositive mothers undergoing antiretroviral therapy,” *Journal of Virology*, vol. 73, no. 11, pp. 9673–9678, 1999.
- [9] I. Guleria and M. Sayegh, “Maternal acceptance of the fetus: true human tolerance,” *Journal of immunology*, vol. 178, no. 6, pp. 3345–3351, 2007.
- [10] H. Zhang, X. Hu, X. Liu, R. Zhang, Q. Fu, and X. Xu, “The Treg/Th17 imbalance in Toxoplasma gondii-infected pregnant mice,” *American Journal of Reproductive Immunology*, vol. 67, no. 2, pp. 112–121, 2012.
- [11] D. Arranz-Solis, D. Mukhopadhyay, and J. J. P. Saeij, “_Toxoplasma_ effectors that affect pregnancy outcome,” *Trends in Parasitology*, vol. 37, no. 4, pp. 283–295, 2021.
- [12] J. Kwak-Kim, S. Bao, S. K. Lee, J. W. Kim, and A. Gilman-Sachs, “Immunological modes of pregnancy loss: inflammation, immune effectors, and stress,” *American Journal of Reproductive Immunology*, vol. 72, no. 2, pp. 129–140, 2014.
- [13] Y. Y. Ge, L. Zhang, G. Zhang et al., “In pregnant mice, the infection of Toxoplasma gondii causes the decrease of CD4⁺CD25⁺-regulatory T cells,” *Parasite Immunology*, vol. 30, no. 9, pp. 471–481, 2008.
- [14] J. Chen, C. Huang, D. Zhu et al., “Chinese 1 strain of Toxoplasma gondii excreted-secreted antigens negatively modulate Foxp3 via inhibition of the TGF β s/Smad2/Smad3/Smad4 pathway,” *Journal of Cellular and Molecular Medicine*, vol. 21, no. 9, pp. 1944–1953, 2017.
- [15] J. L. Chen, Y. Y. Ge, J. Zhang et al., “The dysfunction of CD4⁺CD25⁺ regulatory T cells contributes to the abortion of mice caused by Toxoplasma gondii excreted-secreted antigens in early pregnancy,” *PLoS One*, vol. 8, no. 7, p. e69012, 2013.
- [16] N. Arora, Y. Sadovsky, T. S. Dermody, and C. B. Coyne, “Microbial vertical transmission during human pregnancy,” *Cell Host & Microbe*, vol. 21, no. 5, pp. 561–567, 2017.
- [17] Y. Shiono, H. S. Mun, N. He et al., “Maternal-fetal transmission of _Toxoplasma gondii_ in interferon- γ deficient pregnant mice,” *Parasitology International*, vol. 56, no. 2, pp. 141–148, 2007.
- [18] J. R. Robbins, V. B. Zeldovich, A. Poukchanski, J. C. Bootbroyd, and A. I. Bakardjiev, “Tissue barriers of the human placenta to infection with Toxoplasma gondii,” *Infection and Immunity*, vol. 80, no. 1, pp. 418–428, 2012.
- [19] J. S. Hunt, “Stranger in a strange land,” *Immunological Reviews*, vol. 213, no. 1, pp. 36–47, 2006.
- [20] P. Vogel, “The current molecular phylogeny of Eutherian mammals challenges previous interpretations of placental evolution,” *Placenta*, vol. 26, no. 8–9, pp. 591–596, 2005.
- [21] M. K. Jena, N. Nayak, K. Chen, and N. R. Nayak, “Role of macrophages in pregnancy and related complications,” *Archivum Immunologiae et Therapiae Experimentalis (Warsz)*, vol. 67, no. 5, pp. 295–309, 2019.
- [22] C. Brito, T. Silva, M. Castro et al., “Toxoplasma gondii infection reduces serum progesterone levels and adverse effects at the maternal-foetal interface,” *Parasite Immunology*, vol. 42, no. 2, p. e12690, 2020.
- [23] P. Castaño, M. Fuertes, I. Ferre et al., “Placental thrombosis in acute phase abortions during experimental Toxoplasma gondii infection in sheep,” *Veterinary Research*, vol. 45, no. 1, pp. 9–9, 2014.
- [24] N. Fadaam, “Placental and fetal tissue structural changes resulting from congenital toxoplasmosis,” *WORLD JOURNAL OF PHARMACY AND PHARMACEUTICAL SCIENCES*, vol. 5, pp. 216–233, 2016.
- [25] E. Yavuz, F. Aydın, A. Seyhan et al., “Granulomatous villitis formed by inflammatory cells with maternal origin: a rare manifestation type of placental toxoplasmosis,” *Placenta*, vol. 27, no. 6–7, pp. 780–782, 2006.
- [26] J. Chen, Y. Liang, P. Yi et al., “Outcomes of congenital Zika disease depend on timing of infection and maternal-fetal interferon action,” *Cell Reports*, vol. 21, no. 6, pp. 1588–1599, 2017.
- [27] S. Liu, L. Diao, C. Huang, Y. Li, Y. Zeng, and J. Y. H. Kwak-Kim, “The role of decidual immune cells on human pregnancy,” *Journal of Reproductive Immunology*, vol. 124, pp. 44–53, 2017.
- [28] T. Nagamatsu and D. J. Schust, “The immunomodulatory roles of macrophages at the maternal-fetal interface,” *Reproductive Sciences*, vol. 17, no. 3, pp. 209–218, 2010.
- [29] Y. Xu, R. Romero, D. Miller et al., “An M1-like macrophage polarization in decidual tissue during spontaneous preterm

- labor that is attenuated by rosiglitazone treatment,” *Journal of Immunology*, vol. 196, no. 6, pp. 2476–2491, 2016.
- [30] A. Wakkach, N. Fournier, V. Brun, J. P. Breitmayer, F. Cottrez, and H. Groux, “Characterization of dendritic cells that induce tolerance and T regulatory 1 cell differentiation in vivo,” *Immunity*, vol. 18, no. 5, pp. 605–617, 2003.
- [31] A. Schumacher, P. O. Wafula, A. Teles et al., “Blockage of heme oxygenase-1 abrogates the protective effect of regulatory T cells on murine pregnancy and promotes the maturation of dendritic cells,” *PLoS One*, vol. 7, no. 8, p. e42301, 2012.
- [32] B. Guerrero, F. Hassouneh, E. Delgado, J. G. Casado, and R. Tarazona, “Natural killer cells in recurrent miscarriage: an overview,” *Journal of Reproductive Immunology*, vol. 142, p. 103209, 2020.
- [33] B. Polese, V. Grیدهlet, E. Araklioti, H. Martens, S. Perrier dâ €™Hauterive, and V. Geenen, “The endocrine milieu and CD4 T-lymphocyte polarization during pregnancy,” *Frontiers in Endocrinology*, vol. 5, p. 106, 2014.
- [34] J. R. Wilczynski, “Th1/Th2 cytokines balance—_yin_ and _yang_ of reproductive immunology,” *European Journal of Obstetrics, Gynecology, and Reproductive Biology*, vol. 122, no. 2, pp. 136–143, 2005.
- [35] S. Saito, “Cytokine network at the feto-maternal interface,” *Journal of Reproductive Immunology*, vol. 47, no. 2, pp. 87–103, 2000.
- [36] G. AbdulHussain, F. Azizieh, M. Makhseed, and R. Raghupathy, “Effects of progesterone, dydrogesterone and estrogen on the production of Th1/Th2/Th17 cytokines by lymphocytes from women with recurrent spontaneous miscarriage,” *Journal of Reproductive Immunology*, vol. 140, p. 103132, 2020.
- [37] G. Chaouat, N. Lédée-Bataille, S. Zourbas et al., “Cytokines, implantation and early abortion: re-examining the Th1/Th2 paradigm leads to question the single pathway, single therapy concept,” *American Journal of Reproductive Immunology*, vol. 50, no. 3, pp. 177–186, 2003.
- [38] A. C. Zenclussen, “Regulatory T cells in pregnancy,” *Springer Seminars in Immunopathology*, vol. 28, no. 1, pp. 31–39, 2006.
- [39] A. S. Figueiredo and A. Schumacher, “The T helper type 17/regulatory T cell paradigm in pregnancy,” *Immunology*, vol. 148, no. 1, pp. 13–21, 2016.
- [40] J. J. Liu, L. Zhang, F. F. Zhang et al., “Influence of miR-34a on preeclampsia through the Notch signaling pathway,” *European Review for Medical and Pharmacological Sciences*, vol. 23, no. 3, pp. 923–931, 2019.
- [41] Z. S. Ozkan, D. Deveci, M. Simsek, F. Ilhan, A. Risvanli, and E. Sapmaz, “What is the impact of SOCS3, IL-35 and IL17 in immune pathogenesis of recurrent pregnancy loss?,” *The Journal of Maternal-Fetal & Neonatal Medicine*, vol. 28, no. 3, pp. 324–328, 2015.
- [42] M. Owen, M. Clarkson, and A. J. Trees, “Acute phase Toxoplasma abortions in sheep,” *The Veterinary Record*, vol. 142, no. 18, pp. 480–482, 1998.
- [43] I. Prigione, S. Chiesa, P. Taverna et al., “T cell mediated immune responses to *Toxoplasma gondii* in pregnant women with primary toxoplasmosis,” *Microbes and Infection*, vol. 8, no. 2, pp. 552–560, 2006.
- [44] G. Saadatnia, Z. Mohamed, F. Ghaffarifar, E. Osman, Z. K. Moghadam, and R. Noordin, “Toxoplasma gondii excretory secretory antigenic proteins of diagnostic potential,” *APMIS*, vol. 120, no. 1, pp. 47–55, 2012.
- [45] O. Assossou, F. A. S. Besson, J. P. Rouault et al., “Characterization of an excreted/secreted antigen form of 14-3-3 protein in *Toxoplasma gondii* tachyzoites,” *FEMS Microbiology Letters*, vol. 234, no. 1, pp. 19–25, 2004.
- [46] J. Yang, P. Wei, J. Barbi et al., “The deubiquitinase USP44 promotes Treg function during inflammation by preventing FOXP3 degradation,” *EMBO reports*, vol. 21, no. 9, p. e50308, 2020.
- [47] A. Mohr, R. Malhotra, G. Mayer, G. Gorochov, and M. Miyara, “Human FOXP3⁺ T regulatory cell heterogeneity,” *Clinical & Translational Immunology*, vol. 7, no. 1, p. e1005, 2018.
- [48] M. Dominguez-Villar and D. A. Hafler, “Regulatory T cells in autoimmune disease,” *Nature Immunology*, vol. 19, no. 7, pp. 665–673, 2018.
- [49] P. Georgiev, L.-M. Charbonnier, and T. A. Chatila, “Regulatory T cells: the many faces of Foxp3,” *Journal of Clinical Immunology*, vol. 39, no. 7, pp. 623–640, 2019.
- [50] V. Kumar, “Homeostatic control of immunity by TCR peptide-specific Tregs,” *The Journal of Clinical Investigation*, vol. 114, no. 9, pp. 1222–1226, 2004.
- [51] X. Ke, J. Wang, L. Li, I. H. Chen, H. Wang, and X. F. Yang, “Roles of CD4⁺CD25^{high} FOXP3⁺ Tregs in lymphomas and tumors are complex,” *Frontiers in Bioscience*, vol. Volume, no. 13, pp. 3986–4001, 2008.
- [52] D. C. Gondek, L. F. Lu, S. A. Quezada, S. Sakaguchi, and R. J. Noelle, “Cutting edge: contact-mediated suppression by CD4⁺CD25⁺ regulatory cells involves a granzyme B-dependent, perforin-independent mechanism,” *Journal of Immunology*, vol. 174, no. 4, pp. 1783–1786, 2005.
- [53] B. Zhang, S. Chikuma, S. Hori, S. Fagarasan, and T. Honjo, “Nonoverlapping roles of PD-1 and FoxP3 in maintaining immune tolerance in a novel autoimmune pancreatitis mouse model,” *Proceedings of the National Academy of Sciences of the United States of America*, vol. 113, no. 30, pp. 8490–8495, 2016.
- [54] M. Ghaebi, M. Nouri, A. Ghasemzadeh et al., “Immune regulatory network in successful pregnancy and reproductive failures,” *Biomedicine & Pharmacotherapy*, vol. 88, pp. 61–73, 2017.
- [55] C. Pedros, Y. Zhang, J. K. Hu et al., “A TRAF-like motif of the inducible costimulator ICOS controls development of germinal center T_{FH} cells via the kinase TBK1,” *Nature Immunology*, vol. 17, no. 7, pp. 825–833, 2016.
- [56] J. Alijotas-Reig, E. Llurba, and J. M. Gris, “Potentiating maternal immune tolerance in pregnancy: a new challenging role for regulatory T cells,” *Placenta*, vol. 35, no. 4, pp. 241–248, 2014.
- [57] W. Y. Yang, Y. Shao, J. Lopez-Pastrana, J. Mai, H. Wang, and X. F. Yang, “Pathological conditions re-shape physiological Tregs into pathological Tregs,” *Burns & Trauma*, vol. 3, no. 1, 2015.
- [58] S. E. Ander, M. S. Diamond, and C. B. Coyne, “Immune responses at the maternal-fetal interface,” *Science Immunology*, vol. 4, no. 31, p. eaat6114, 2019.
- [59] V. R. Aluvihare, M. Kallikourdis, and A. G. Betz, “Regulatory T cells mediate maternal tolerance to the fetus,” *Nature Immunology*, vol. 5, no. 3, pp. 266–271, 2004.
- [60] J. Wang, J. Yang, Y. Yan et al., “Effect of adoptive transfer of CD4⁺CD25⁺Foxp3⁺ Treg induced by trichostatin A on the

- prevention of spontaneous abortion,” *Journal of Reproductive Immunology*, vol. 131, pp. 30–35, 2019.
- [61] L. P. Jin, Q. Y. Chen, T. Zhang, P. F. Guo, and D. J. Li, “The CD4⁺CD25^{bright} regulatory T cells and CTLA-4 expression in peripheral and decidual lymphocytes are down-regulated in human miscarriage,” *Clinical Immunology*, vol. 133, no. 3, pp. 402–410, 2009.
- [62] B. Liu, H. Wu, Q. Huang, M. Li, and X. Fu, “Phosphorylated STAT3 inhibited the proliferation and suppression of decidual Treg cells in unexplained recurrent spontaneous abortion,” *International Immunopharmacology*, vol. 82, p. 106337, 2020.
- [63] R. Pijnenborg, J. M. Bland, W. B. Robertson, and I. Brosens, “Uteroplacental arterial changes related to interstitial trophoblast migration in early human pregnancy,” *Placenta*, vol. 4, no. 4, pp. 397–413, 1983.
- [64] S. A. Robertson, A. S. Care, and L. M. Moldenhauer, “Regulatory T cells in embryo implantation and the immune response to pregnancy,” *The Journal of Clinical Investigation*, vol. 128, no. 10, pp. 4224–4235, 2018.
- [65] A. L. Mellor, J. Sivakumar, P. Chandler et al., “Prevention of T cell-driven complement activation and inflammation by tryptophan catabolism during pregnancy,” *Nature Immunology*, vol. 2, no. 1, pp. 64–68, 2001.
- [66] L. R. Guerin, J. R. Prins, and S. A. Robertson, “Regulatory T-cells and immune tolerance in pregnancy: a new target for infertility treatment?,” *Human Reproduction Update*, vol. 15, no. 5, pp. 517–535, 2009.
- [67] A. S. Care, S. L. Bourque, J. S. Morton, E. P. Hjartarson, S. A. Robertson, and S. T. Davidge, “Reduction in regulatory T cells in early pregnancy causes uterine artery dysfunction in mice,” *Hypertension*, vol. 72, no. 1, pp. 177–187, 2018.
- [68] J. Ye, Y. Wang, Z. Wang et al., “Circulating Th1, Th2, Th9, Th17, Th22, and Treg levels in aortic dissection patients,” *Mediators of Inflammation*, vol. 2018, Article ID 5697149, 10 pages, 2018.
- [69] S. Nadkarni, J. Smith, A. N. Sferruzzi-Perri et al., “Neutrophils induce proangiogenic T cells with a regulatory phenotype in pregnancy,” *Proceedings of the National Academy of Sciences of the United States of America*, vol. 113, no. 52, pp. E8415–E8424, 2016.
- [70] M. J. Jasper, K. P. Tremellen, and S. A. Robertson, “Primary unexplained infertility is associated with reduced expression of the T-regulatory cell transcription factor Foxp3 in endometrial tissue,” *Molecular Human Reproduction*, vol. 12, no. 5, pp. 301–308, 2006.
- [71] H. Zhang, L. Cui, L. Ren et al., “The role of decidual PD-1⁺ Treg cells in adverse pregnancy outcomes due to *Toxoplasma gondii* infection,” *Inflammation*, vol. 42, no. 6, pp. 2119–2128, 2019.
- [72] G. Oldenhove, N. Bouladoux, E. A. Wohlfert et al., “Decrease of Foxp3⁺ Treg cell number and acquisition of effector cell phenotype during lethal infection,” *Immunity*, vol. 31, no. 5, pp. 772–786, 2009.
- [73] Y. Liu, M. Zhao, X. Xu et al., “Adoptive transfer of Treg cells counters adverse effects of *Toxoplasma gondii* infection on pregnancy,” *The Journal of Infectious Diseases*, vol. 210, no. 9, pp. 1435–1443, 2014.
- [74] F. Y. Azizieh and R. Raghupathy, “IL-10 and pregnancy complications,” *Clinical and Experimental Obstetrics & Gynecology*, vol. 44, no. 2, pp. 252–258, 2017.
- [75] M. Zhao, R. Zhang, X. Xu et al., “IL-10 reduces levels of apoptosis in *Toxoplasma gondii*-infected trophoblasts,” *PLoS One*, vol. 8, no. 2, p. e56455, 2013.
- [76] C. D. Thompson, J. C. Zurko, B. F. Hanna, D. J. Hellenbrand, and A. Hanna, “The therapeutic role of interleukin-10 after spinal cord injury,” *Journal of Neurotrauma*, vol. 30, no. 15, pp. 1311–1324, 2013.
- [77] K. Lao, M. Zhao, Z. Li et al., “IL-10 regulate decidual Tregs apoptosis contributing to the abnormal pregnancy with *Toxoplasma gondii* infection,” *Microbial Pathogenesis*, vol. 89, pp. 210–216, 2015.
- [78] J. Qiu, R. Zhang, Y. Xie et al., “Estradiol attenuates the severity of primary *Toxoplasma gondii* infection-induced adverse pregnancy outcomes through the regulation of Tregs in a dose-dependent manner,” *Frontiers in Immunology*, vol. 9, p. 1102, 2018.
- [79] J. E. Olgún, J. Fernández, N. Salinas et al., “Adoptive transfer of CD4⁺Foxp3⁺ regulatory T cells to C57BL/6J mice during acute infection with *Toxoplasma gondii* down modulates the exacerbated Th1 immune response,” *Microbes and Infection*, vol. 17, no. 8, pp. 586–595, 2015.
- [80] N. Mitsui, C. Schwab, and B. Grimbacher, “What did we learn from CTLA-4 insufficiency on the human immune system?,” *Immunological Reviews*, vol. 287, no. 1, pp. 33–49, 2019.
- [81] L. M. Francisco, P. T. Sage, and A. H. Sharpe, “The PD-1 pathway in tolerance and autoimmunity,” *Immunological Reviews*, vol. 236, no. 1, pp. 219–242, 2010.
- [82] H. Jonuleit, E. Schmitt, H. Kakirman, M. Stassen, J. Knop, and A. H. Enk, “Infectious tolerance,” *The Journal of Experimental Medicine*, vol. 196, no. 2, pp. 255–260, 2002.
- [83] S. Wang, F. Sun, M. Li et al., “The appropriate frequency and function of decidual Tim-3⁺CTLA-4⁺CD8⁺ T cells are important in maintaining normal pregnancy,” *Cell Death & Disease*, vol. 10, no. 6, p. 407, 2019.
- [84] N. Miwa, S. Hayakawa, S. Miyazaki et al., “IDO expression on decidual and peripheral blood dendritic cells and monocytes/macrophages after treatment with CTLA-4 or interferon- γ increase in normal pregnancy but decrease in spontaneous abortion,” *Molecular Human Reproduction*, vol. 11, no. 12, pp. 865–870, 2005.
- [85] P. O. Wafula, A. Teles, A. Schumacher et al., “Original article: PD-1 but not CTLA-4 blockage abrogates the protective effect of regulatory T cells in a pregnancy murine model,” *American Journal of Reproductive Immunology*, vol. 62, no. 5, pp. 283–292, 2009.
- [86] A. Habicht, S. Dada, M. Jurewicz et al., “A link between PDL1 and T regulatory cells in fetomaternal tolerance,” *Journal of Immunology*, vol. 179, no. 8, pp. 5211–5219, 2007.
- [87] F. D’Addio, L. V. Riella, B. G. Mfarrej et al., “The link between the PDL1 costimulatory pathway and Th17 in fetomaternal tolerance,” *Journal of Immunology*, vol. 187, no. 9, pp. 4530–4541, 2011.
- [88] L. F. Si, S. Y. Zhang, C. S. Gao, S. L. Chen, J. Zhao, and X. C. Cheng, “Effects of IFN- γ on IL-18 expression in pregnant rats and pregnancy outcomes,” *Asian-Australasian Journal of Animal Sciences*, vol. 26, no. 10, pp. 1399–1405, 2013.
- [89] L. Lu, J. Barbi, and F. Pan, “The regulation of immune tolerance by FOXP3,” *Nature Reviews. Immunology*, vol. 17, no. 11, pp. 703–717, 2017.
- [90] W. Hou, Z. Li, Y. Li et al., “Correlation between protein expression of FOXP3 and level of FOXP3 promoter

- methylation in recurrent spontaneous abortion,” *The Journal of Obstetrics and Gynaecology Research*, vol. 42, no. 11, pp. 1439–1444, 2016.
- [91] M. Liu, S. Li, and M. O. Li, “TGF- β control of adaptive immune tolerance: a break from Treg cells,” *Bioessays*, vol. 40, no. 11, p. e1800063, 2018.
- [92] Y.-J. Tang, J. Xiao, X. R. Huang et al., “Latent transforming growth factor- β 1 protects against bleomycin-induced lung injury in mice,” *American journal of respiratory cell and molecular biology*, vol. 51, no. 6, pp. 761–771, 2014.
- [93] N. Pang, F. Zhang, X. Ma et al., “TGF- β /Smad signaling pathway regulates Th17/Treg balance during *Echinococcus multilocularis* infection,” *International Immunopharmacology*, vol. 20, no. 1, pp. 248–257, 2014.
- [94] M. Zhao, H. Zhang, X. Liu, Y. Jiang, L. Ren, and X. Hu, “The effect of TGF- β on Treg cells in adverse pregnancy outcome upon *Toxoplasma gondii* infection,” *Frontiers in Microbiology*, vol. 8, p. 901, 2017.
- [95] T. Chinen, A. K. Kannan, A. G. Levine et al., “An essential role for the IL-2 receptor in T_{reg} cell function,” *Nature Immunology*, vol. 17, no. 11, pp. 1322–1333, 2016.
- [96] J. D. Goldstein, A. Burlion, B. Zaragoza et al., “Inhibition of the JAK/STAT signaling pathway in regulatory T cells reveals a very dynamic regulation of Foxp3 expression,” *PLoS One*, vol. 11, no. 4, p. e0153682, 2016.
- [97] J. Chen, C. Huang, D. Zhu et al., “Excreted-secreted antigens of *Toxoplasma gondii* inhibit Foxp3 via IL-2R γ /JAK3/Stats pathway,” *Journal of Cellular Biochemistry*, vol. 119, no. 12, pp. 10176–10185, 2018.
- [98] L. Gao, Y. Dong, R. Lin, Y. Meng, F. Wu, and L. Jia, “The imbalance of Treg/Th17 cells induced by perinatal bisphenol A exposure is associated with activation of the PI3K/Akt/mTOR signaling pathway in male offspring mice,” *Food and Chemical Toxicology*, vol. 137, p. 111177, 2020.
- [99] C. A. O’Brien and T. H. Harris, “ICOS-deficient and ICOS YF mutant mice fail to control *Toxoplasma gondii* infection of the brain,” *PLoS One*, vol. 15, no. 1, p. e0228251, 2020.
- [100] W. Ouyang, O. Beckett, Q. Ma, J. H. Paik, R. A. DePinho, and M. O. Li, “Foxo proteins cooperatively control the differentiation of Foxp3⁺ regulatory T cells,” *Nature Immunology*, vol. 11, no. 7, pp. 618–627, 2010.
- [101] J. Chen, L. Hu, J. Wang et al., “*Toxoplasma gondii* excreted-secreted antigens suppress Foxp3 via PI3K-AKT-mTOR signaling pathway,” *Journal of Cellular Biochemistry*, vol. 120, no. 9, pp. 16044–16051, 2019.
- [102] J. Flegr, “How and why *Toxoplasma* makes us crazy,” *Trends in Parasitology*, vol. 29, no. 4, pp. 156–163, 2013.
- [103] A. Lim, V. Kumar, S. A. Hari Dass, and A. Vyas, “*Toxoplasma gondii* infection enhances testicular steroidogenesis in rats,” *Molecular Ecology*, vol. 22, no. 1, pp. 102–110, 2013.
- [104] J. Xiao, Y. Li, E. Prandovszky et al., “MicroRNA-132 dysregulation in *Toxoplasma gondii* infection has implications for dopamine signaling pathway,” *Neuroscience*, vol. 268, pp. 128–138, 2014.
- [105] B. J. Miller and D. R. Goldsmith, “Towards an immunophenotype of schizophrenia: progress, potential mechanisms, and future directions,” *Neuropsychopharmacology: official publication of the American College of Neuropsychopharmacology*, vol. 42, no. 1, pp. 299–317, 2017.
- [106] K. Hellmer and P. Nystrom, “Infant acetylcholine, dopamine, and melatonin dysregulation: neonatal biomarkers and causal factors for ASD and ADHD phenotypes,” *Medical Hypotheses*, vol. 100, pp. 64–66, 2017.
- [107] S. Najjar and D. M. Pearlman, “Neuroinflammation and white matter pathology in schizophrenia: systematic review,” *Schizophrenia Research*, vol. 161, no. 1, pp. 102–112, 2015.
- [108] F. Contreras, C. Prado, H. González et al., “Dopamine receptor D3 signaling on CD4⁺T cells favors Th1- and Th17-mediated immunity,” *Journal of Immunology*, vol. 196, no. 10, pp. 4143–4149, 2016.
- [109] M. Cosentino, M. Ferrari, N. Kustrimovic, E. Rasini, and F. Marino, “Influence of dopamine receptor gene polymorphisms on circulating T lymphocytes: a pilot study in healthy subjects,” *Human Immunology*, vol. 76, no. 10, pp. 747–752, 2015.
- [110] F. Osorio-Barrios, C. Prado, F. Contreras, and R. Pacheco, “Dopamine receptor D5 signaling plays a dual role in experimental autoimmune encephalomyelitis potentiating Th17-mediated immunity and favoring suppressive activity of regulatory T-cells,” *Frontiers in Cellular Neuroscience*, vol. 12, p. 192, 2018.
- [111] G. Anderson, M. Berk, S. Dodd et al., “Immuno-inflammatory, oxidative and nitrosative stress, and neuroprogressive pathways in the etiology, course and treatment of schizophrenia,” *Progress in Neuro-Psychopharmacology and Biological Psychiatry*, vol. 42, pp. 1–4, 2013.
- [112] Z. Xu, X. Zhang, H. Chang et al., “Rescue of maternal immune activation-induced behavioral abnormalities in adult mouse offspring by pathogen-activated maternal T_{reg} cells,” *Nature Neuroscience*, vol. 24, no. 6, pp. 818–830, 2021.
- [113] D. A. Clark, “The importance of being a regulatory T cell in pregnancy,” *Journal of Reproductive Immunology*, vol. 116, pp. 60–69, 2016.

Research Article

Inhibition of NF- κ B/IL-33/ST2 Axis Ameliorates Acute Bronchiolitis Induced by Respiratory Syncytial Virus

Liwen Zhang,¹ Yu Wan,¹ Liang Ma,² Kaihong Xu ¹ and Baojin Cheng ¹

¹Department of Pediatrics, The Second People's Hospital of Changzhou, Affiliated Hospital of Nanjing Medical University, China

²Department of Digestive Disease, The First People's Hospital of Changzhou, the Third Affiliated Hospital of Soochow University, China

Correspondence should be addressed to Kaihong Xu; xukaihongerke@sina.cn and Baojin Cheng; chengbaojinerke@aliyun.com

Received 16 December 2020; Revised 4 June 2021; Accepted 16 July 2021; Published 4 August 2021

Academic Editor: Zhipeng Xu

Copyright © 2021 Liwen Zhang et al. This is an open access article distributed under the Creative Commons Attribution License, which permits unrestricted use, distribution, and reproduction in any medium, provided the original work is properly cited.

Background/Aim. Bronchiolitis is a common acute lower respiratory tract infectious disease in infants. Respiratory syncytial virus (RSV) infection is one of the main causes. Bronchiolitis can lead to a significant increase in the incidence of asthma in young children, but the mechanism of bronchiolitis transforming into asthma is still unclear. The study was aimed at investigating the role of NF- κ B/IL-33/ST2 axis on RSV-induced acute bronchiolitis. **Methods.** A total of 40 infants diagnosed with acute bronchiolitis infected by RSV, and 20 normal infants were included in this study. BALB/c mice (6-8 weeks old, 20 ± 1.1 g) were used as study models. Enzyme-linked immunosorbent assay (ELISA), quantitative real time PCR, western blot analysis, immunohistochemical staining, and flow cytometry analysis were performed to examine relevant indicators. **Results.** IL-33 level was significantly elevated, and Th1/Th2 ratio is imbalance after in infants with acute bronchiolitis. In vivo study, we found that NF- κ B/IL-33/ST2 axis is mediated the Th2 cytokine levels and BAL cell number induced by RSV. Acute bronchiolitis induced by RSV in a mouse model is attenuated after inhibition of NF- κ B/IL-33/ST2 pathway. Moreover, we also confirmed that macrophages are important sources of IL-33 and are regulated by NF- κ B pathway in RSV-induced mice. **Conclusion.** We confirmed that inhibition of NF- κ B/IL-33/ST2 axis could attenuate acute bronchiolitis by RSV infected. Our findings not only demonstrate the potential role of IL-33 antibody in attenuating RSV-induced lung damage but also provide a new insight into better prevention of RSV-induced asthma by mediating NF- κ B/IL-33/ST2 axis.

1. Introduction

Asthma is a respiratory disease involving a variety of inflammatory mediators and cytokines, which has been a serious threat to human health [1]. Numerous studies have shown that viral infection can directly invade 75-300 μ m bronchioles, causing necrosis and exfoliation of epithelial cells of bronchioles, infiltration of peripheral lymphocytes, glandular hyperplasia, increased mucus secretion, and narrowing or even blockage of the lumen [2, 3]. Repeated or persistent viral infection eventually leads to chronic airway inflammation and airway hyperreflex [4].

Respiratory syncytial virus (RSV), as the main pathogen of bronchiolitis and pneumonia in infants and young children, is one of the main causes of asthma in young patients [5]. Previous reports showed that RSV infection accounts

for 80-85% and 75-80% of asthma cases in children and adults, respectively [6, 7]. Another important reason RSV can induce asthma is that it can activate T helper 2 (Th2) cell-related cytokines such as IL-4, IL-5, and IL-10 and break the body's immune balance [8, 9]. Recent studies have found that the treatment of cytokines secreted by Th2 cells can effectively alleviate the symptoms of acute asthma attack, while the reduction of cytokines secreted by Th1 cells does not significantly alleviate the symptoms of asthma [8, 10]. These findings enrich and improve the classic Th1/Th2 imbalance theory in asthma.

IL-33 is a recently discovered proinflammatory cytokine with a variety of biological functions. It belongs to the IL-1 family with a molecular weight of about 1800 and is located on human 9p24.1 chromosome [11]. Current studies have shown that IL-33 not only induces Th0 cells to differentiate

TABLE 1: Sequences of primers for PCR.

Genes	Forward primer	Reverse primer
IL-33	5'-GTCGCCCTGGTACCAGTCCAG-3'	5'-AGGCCTGGCCCGAGTTGTCAG-3'
IL-4	5'-GGCCCGCTATTTGTTTGGTCA-3'	5'-GCTCCTCCCTTGCTTACCAG-3'
IL-10	5'-TAGACGCGCTGGGCGACAG-3'	5'-GTCGCCCCCTAACGCCGTAA-3'
GAPDH	5'-TTCGAAGCACCGGTCCC-3'	5'-TCTCAAGAGCAGCTCCAGT-3'

into Th2 cells but also promotes the secretion of Th2-related cytokines IL-4, IL-5, IL-6, and IL-10 in vitro and in vivo [12, 13]. In the study of children with asthma, it was found that the proportion of Th2 cells and the level of IL-33 in serum increased significantly, which were positively correlated with the level of autoantibody IgE in vivo [14].

Suppression of tumorigenesis 2 (ST2) receptor can specifically bind to IL-33 in two forms; one is transmembrane ST2 (ST2L), mainly expressed on Th2 surface, and the other is soluble ST2, which can compete with ST2L and bind to IL-33, leading to the decrease of IL-33 function [13]. When ST2 is combined with IL-33, it activates the NF- κ B signaling pathway and promotes the release of Th2 cytokines such as IL-4, IL-5, and IL-10 [15]. However, the role of IL-33/ST2 and NF- κ B in RSV-induced bronchitis is still unclear.

In our present study, we explored the expression of IL-33 in serum of acute bronchiolitis infants and in lung tissues of RSV-induced mice and investigated its role on Th1/Th2 cell ratio in acute bronchiolitis infants and RSV infected mice. Moreover, we demonstrated that NF- κ B/IL-33/ST2 axis is involved in the RSV-induced acute bronchiolitis. Our results suggested that IL-33, ST2, and NF- κ B can serve as therapeutic targets in the treatment of RSV infected asthma.

2. Materials and Methods

2.1. Reagents and Antibodies. Respiratory syncytial virus (RSV) was purchased from Hipower Pharmaceutical (Hipower Pharmaceutical, Guangzhou, China). Fetal bovine serum (FBS) and Dulbecco's modified Eagle's medium (DMEM) were obtained from GIBCOBRL (Gibco, CA, USA). Anti-IL-33 antibody and anti-IgG were obtained from Santa Cruz Biotechnology (SantaCruz, CA, USA). Soluble ST2 (sST2) was purchased from KeyGEN (KeyGEN, Nanjing, China). Pyrrolidine dithiocarbamic acid ammonium salt (PDTC) was obtained from Beyotime (Beyotime, Shanghai, China). Antibodies of p50, p65, ST2, and GAPDH were purchased from Cell Signaling Technology (CST, CA, USA). Lipofectamine 2000 and Opti-MEM were purchased from Invitrogen (Carlsbad, CA, USA). Trizol was obtained from Invitrogen (Carlsbad, CA, USA). Western blot detection chemiluminescence reagents were purchased from Thermo Scientific (Thermo Scientific, CA, USA).

2.2. Study Subjects. A total of 40 infants from the Second People's Hospital of Changzhou, Affiliated Hospital of Nanjing Medical University between 2016 and 2018 diagnosed with acute bronchiolitis infected by RSV and 20 normal infants were included in this study. The diagnosis of acute bronchi-

olitis was based on the latest diagnostic guidelines [16]. The venous blood samples of all the selected cases were taken before treatment and used for later experiments. All cases were excluded from congenital heart disease, cardiopulmonary dysplasia, immunodeficiency, and other serious diseases. The present study was approved by the ethics committee of the Second People's Hospital of Changzhou, Affiliate Hospital of Nanjing Medical University (No. SPH1904880). The written informed consent was obtained from all parents of subjects.

2.3. Animal Experiments. BALB/c mice (6-8 weeks old, 20 ± 1.1 g) were randomly divided into six groups: normal control (NC), respiratory syncytial virus (RSV), anti-IgG + RSV, anti-IL-13 + RSV, sST2 + RSV, and PDTC+RSV. Protocols for the RSV-induced mouse models were as previously described [17]. The mice in the RSV infection group were anesthetized by intraperitoneal injection of 3% pentobarbital sodium 0.1 ml/kg, followed by nasal drip of RSV with 100 ml 10^6 PFU on 6 consecutive days, while the mice in the control group were anesthetized by nasal drip of the same dose of saline. The anti-IgG + RSV, anti-IL-33 + RSV, sST2 + RSV, and PDTC+RSV groups were pretreated with anti-Rabbit IgG antibody and anti-Mouse IL-33 antibody (30 μ g/mouse) by intranasal injection 100 μ l 2 h, Ribavirin, sST2, and PDTC by intraperitoneal injection 2 h before challenge with RSV on 3 consecutive days.

All the mice were killed and sampled on 3, 5, and 7 days after RSV infected; the present study was approved by the ethics committee of the Second People's Hospital of Changzhou, Affiliate Hospital of Nanjing Medical University (No. CZ0004-1732).

Serum samples were taken from the spleen of mice after execution, and erythrocytes were removed. The cells were suspended in 10 ml of HBSS wash buffer and counted by a blood cell counter. The cell suspension was centrifuged at 4°C for 10 min at 200 g. Then, the supernatant was discarded, and the precipitate was mixed at a ratio of 0.9 ml of MACS buffer per 10^8 cells. 0.1 ml of magnetic beads (CD90) was added per 10 cells and incubate for 15 min at 4°C in order to extract total T cells. After centrifugation and cell suspension at 4°C, 200 g for 10 min, sufficient MACS buffer was added to the precipitate to reach a concentration of 10^8 cells/ml and mix well. Pass the cells through 30 μ m nylon mesh or 40 μ m prepreparation membrane. Rinse the filter with 0.1 ~ 0.4 ml of MACS buffer. Place the cells into the upper sample channel of autoMACS. Select the possel program so that the labeled cells will elute from the positive lane.

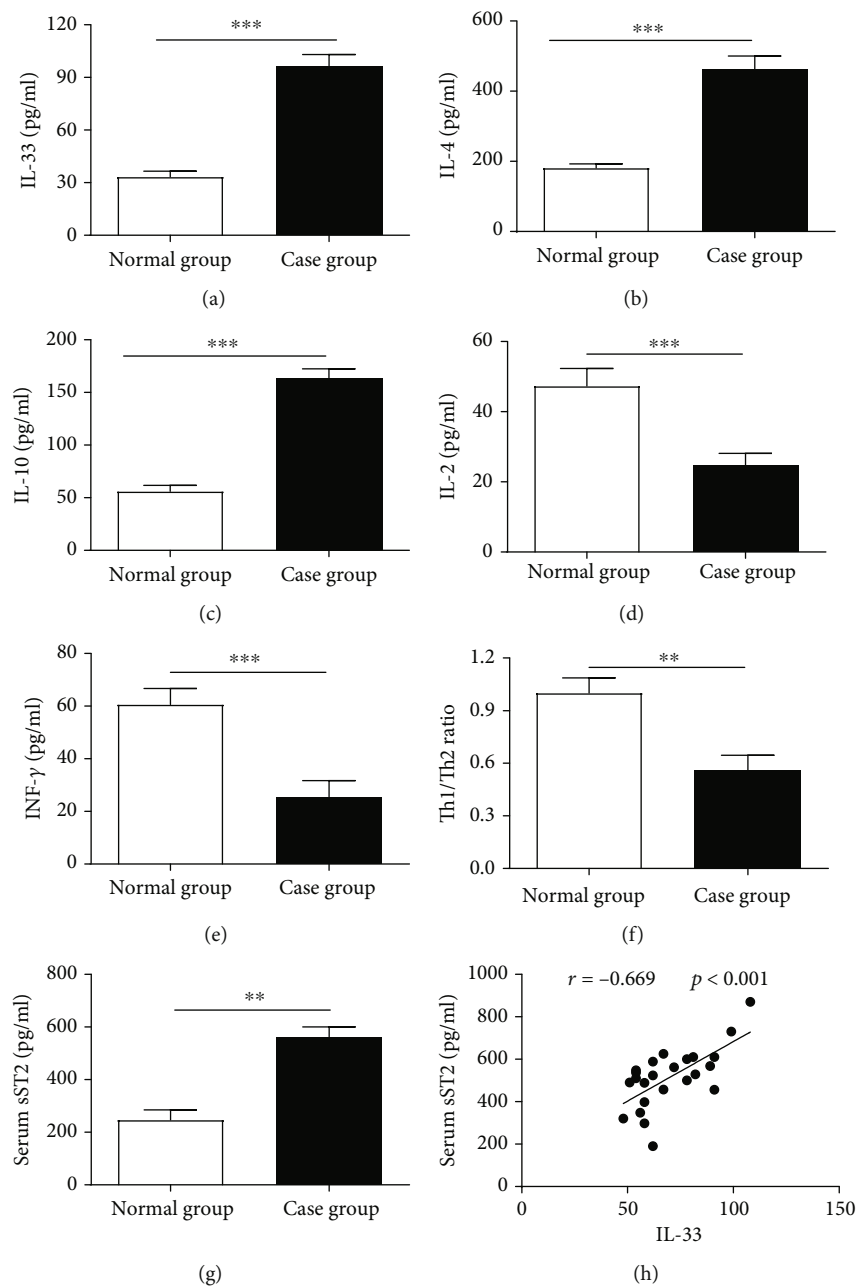


FIGURE 1: IL-33 expression is elevated, and Th1/Th2 ratio is imbalance in infants with acute bronchiolitis. (a) ELISA assay was used to detect the production of IL-33 in serum. (b, c) The levels of Th2-related cytokines IL-4 and IL-10 were examined by ELISA assay. (d, e) The levels of Th1-related cytokines IL-2 and INF- γ were examined by ELISA assay. (f) Cell flow cytometry was used to detect the ratio of Th1/Th2 cells. (g) ELISA assay was used to detect the production of ST2 in serum. (h) Correlation analysis is used to calculate the correlation between IL-33 and ST2 in serum. All data were expressed as the mean \pm SD ($n = 3$). Each value of * $p < 0.05$, ** $p < 0.01$, and *** $p < 0.001$ was deemed to have significant differences.

2.4. Enzyme-Linked Immunosorbent Assay (ELISA). The levels of IL-33, IL-4, IL-10, IL-2, INF- γ , and ST2 in infant serum were examined by specific ELISA kits (Cloud Clone Corp, Wuhan, China) according to manufacturer's instructions.

2.5. Extraction and Detection of Bronchoalveolar Lavage Fluid (BALF). PBS (1 ml) was injected into the trachea after the separation of surrounding connective tissue and repeated

for 3 times, and the rinsed PBS was recovered. Collected lavage fluid for inflammatory cell counting, and stored lavage fluid at -20°C for cell flow cytometry assay detection.

2.6. Quantitative Real Time PCR. Total RNA was extracted from lung tissues by using Trizol (Invitrogen). Superscript II (Invitrogen) was used to carry out reverse transcription qualified with 400 ng according to the manufacturer's instructions. For quantitative real time PCR, SYBR Green

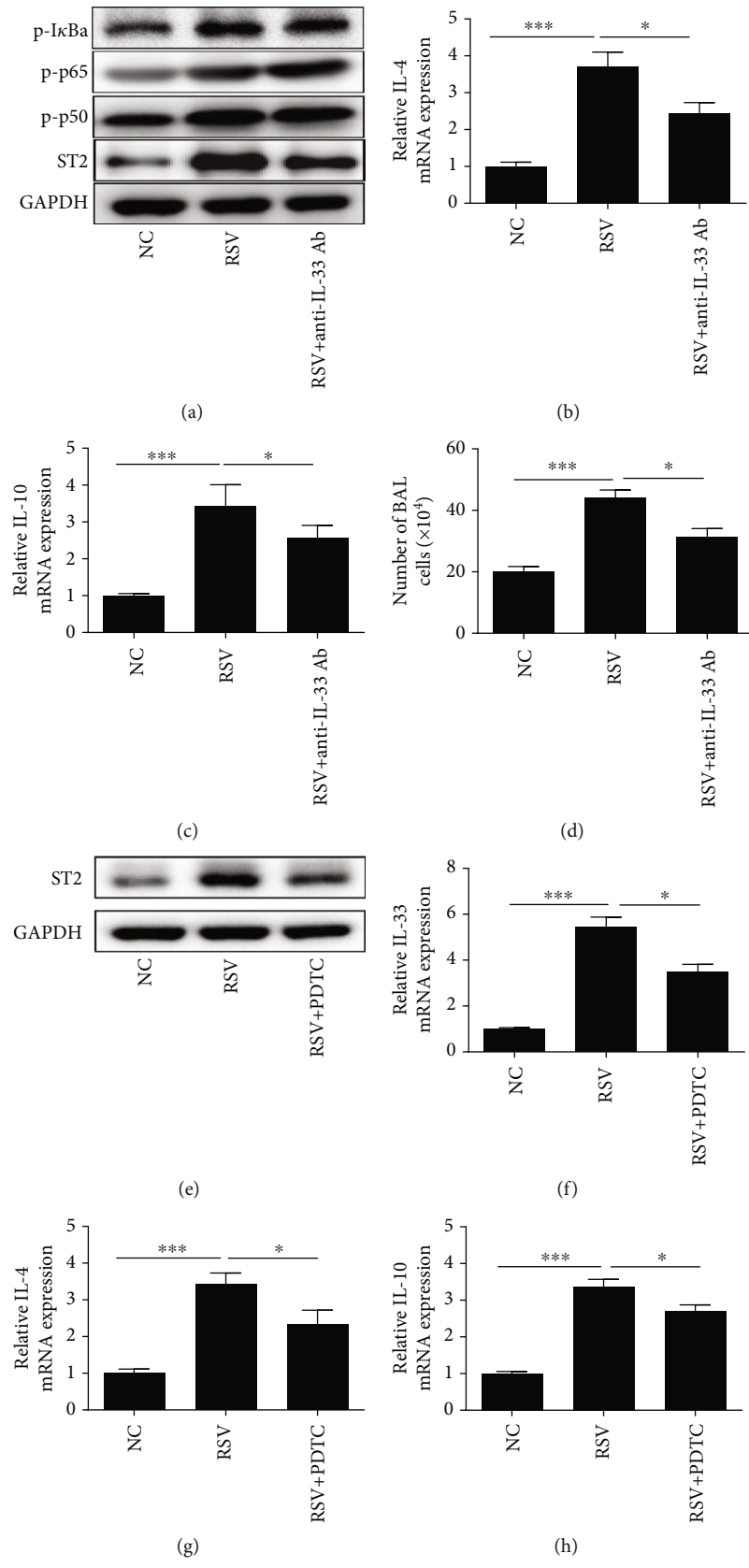


FIGURE 2: Continued.

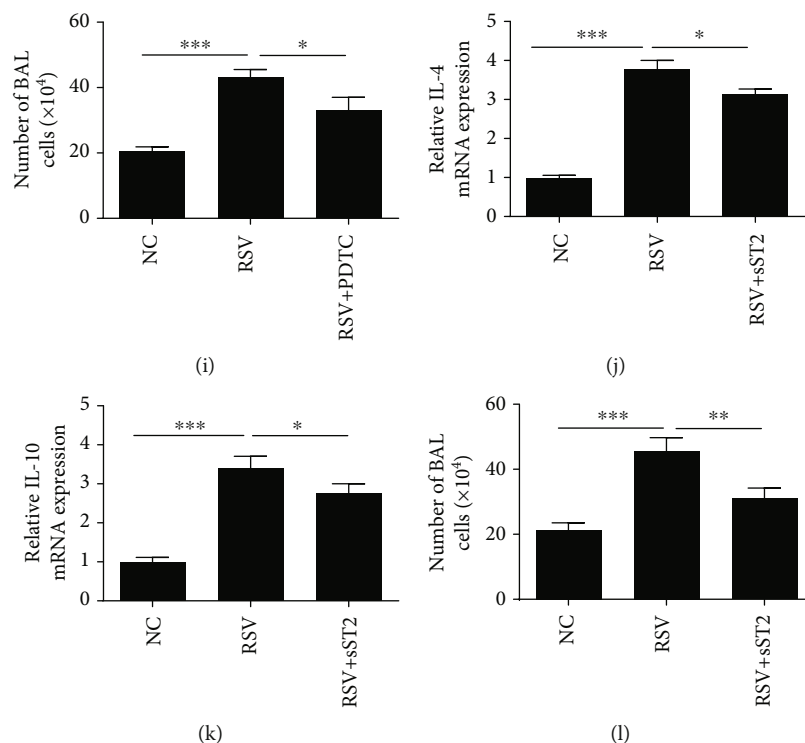


FIGURE 2: NF- κ B/IL-33/ST2 axis is mediated the Th2 cytokine levels and BAL cell number induced by RSV. (a) Western blot analysis was performed to examine the abundance of p-I κ Ba, ST2, p-p65, and p-p50. (b, c) RT-PCR analysis was used to examine the mRNA expression of Th2-related cytokines IL-4 and IL-10 after IL-33 antibody treatment. (d) Inflammatory cell number of bronchoalveolar lavage fluid after IL-33 antibody treatment. (e) ST2 protein abundance was examined by western blot analysis. (f) The IL-33 mRNA expression in lung tissues was detected by RT-PCR. (g, h) RT-PCR analysis was used to examine the mRNA expression of Th2-related cytokines IL-4 and IL-10 after PDTC treatment. (i) Inflammatory cell number of bronchoalveolar lavage fluid after PDTC treatment. (j, k) PCR analysis was used to examine the mRNA expression of Th2-related cytokines IL-4 and IL-10 after sST2 treatment. (l) Inflammatory cell number of bronchoalveolar lavage fluid after sST2 treatment. All data were expressed as the mean \pm SD ($n = 3$). Each value of * $p < 0.05$, ** $p < 0.01$, and *** $p < 0.001$ was considered to be significant differences.

Master Mix (Roche) and ABI-7900 system were used, and GAPDH functioned as a loading control. Primers of related genes are listed in Table 1.

2.7. Western Blot Analysis. Protein samples were prepared, followed with the SDS polyacrylamide gel electrophoresis, and protein was subsequently transferred onto PVDF membranes. For further detection of related genes, the following antibodies were used: I κ B, p65, p50, ST2, and GAPDH. Membranes were blocking in 5% BSA for 2 h at room temperature prior to incubation with primary antibody at 4°C overnight. Membranes were washed 10 min for three times in TBST and then cultured with secondary antibody (1:5000) (CST, CA, USA) at -20°C for 2 h. Then, membranes were washed 20 min for three times with TBST. The blots were detected with an ECL plus reagent (Thermo Scientific, Waltham, USA).

2.8. Immunohistochemical Staining. The lung tissues in different treatment groups were collected separately and were stained with a rabbit monoclonal anti-mouse IL-33, p65, and ST2 antibody overnight at room temperature, washed, then incubated with the secondary Ab (CST, CA, USA) for 2 h, and washed again. The specific detail steps were per-

formed according to DAB substrate kit (Thermo Scientific, Ma, USA).

2.9. Flow Cytometry Analysis. Peripheral blood samples and single cell suspension from lung tissue of mice were collected. FITC, anti-CD30, anti-CD49, and CD11 antibodies were added in samples in turn according to the concentration of the instructions. The 100 P1 antibody system fully suspended the cells and incubated on ice for 30 min under the condition of dark. Add 2% FBS and PBS 1 ml/tube, gently whirl, 1500 rpm, 4°C centrifuge for 5 minutes, discard supernatant; repeat this step once. Stored at 2% FBS. PBS overhanging cells were detected and analyzed using the FlowJo software (version 7.6.5).

2.10. Statistical Analysis. Continuous variables were shown as “means \pm SD.” For multiple comparisons, One-way ANOVA was performed using the SPSS 22.0 software (SPSS, Inc., USA), and p value < 0.05 was considered significant statistically.

3. Results

3.1. IL-33 Level Is Significantly Elevated and Th1/Th2 Ratio Is Imbalance after RSV Infection in Infants. It was reported that

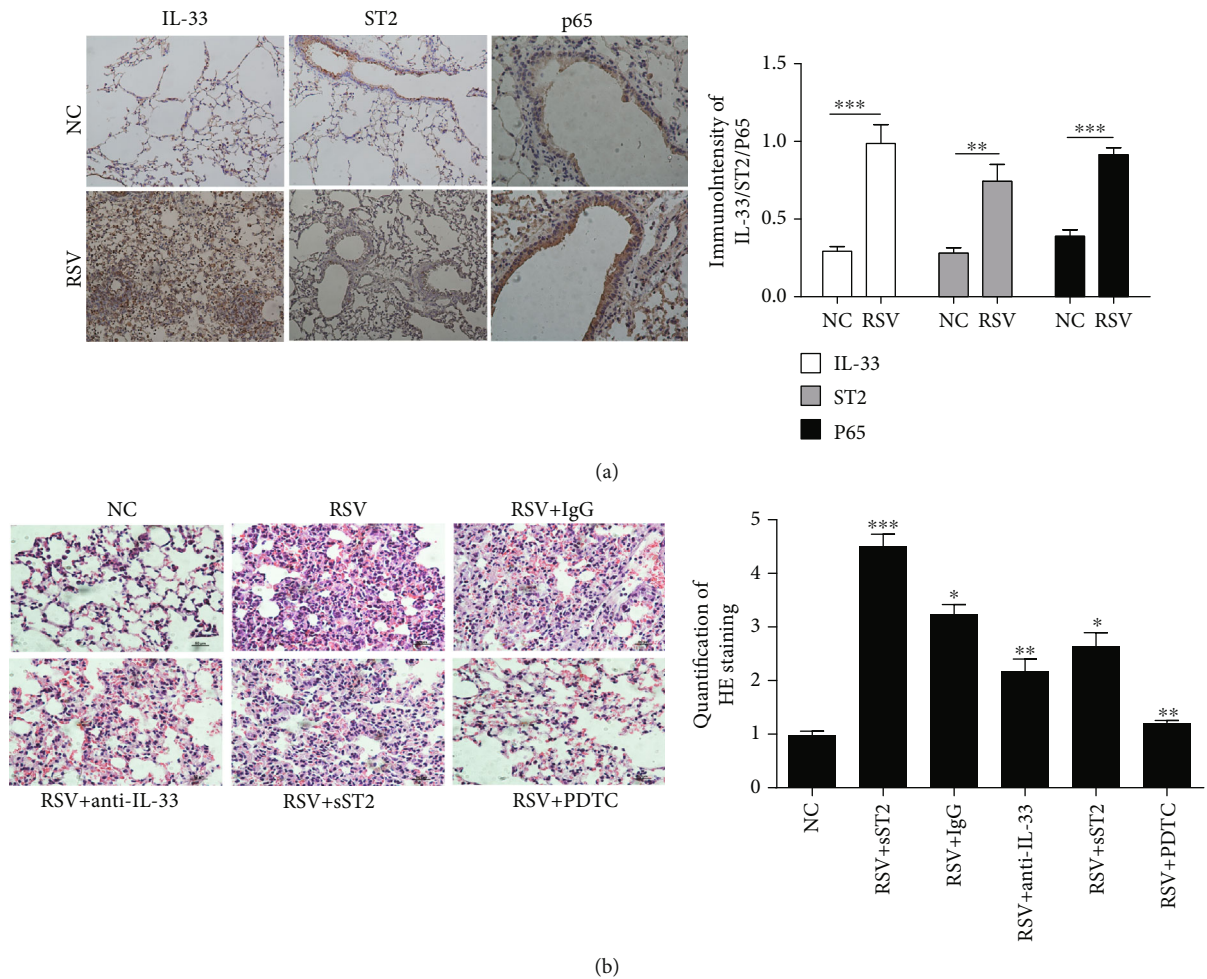


FIGURE 3: RSV-induced mouse model is attenuated after inhibition of NF- κ B/IL-33/ST2 pathway. (a) Immunohistochemical analysis of IL-33, ST2, and p65 abundance in saline-exposed control mice (NC); RSV-treated mice (RSV) was performed (original magnification $\times 400$, scale bar $100\ \mu\text{m}$) and scored (right graph). (b) H&E staining of lung tissue in different group mice was analyzed by Image-proplus 6.0 (original magnification $\times 400$). The data are presented as mean \pm SEM and were analyzed by Student's *t*-test (NC group, $n = 8$; RSV group, $n = 7$; RSV + IgG = 6; RSV + IL-33 antibody = 6; RSV + PDTC = 7; RSV + sST2 = 8). Each value of $*p < 0.05$, $**p < 0.01$, and $***p < 0.001$ was considered to be significant differences.

the production of Th2 cytokines IL-4 and IL-10 was promoted by IL-33 [18], and Th2 immune response was described to influence the pathogenesis of respiratory syncytial virus (RSV) acute bronchiolitis [19]. Firstly, the expression of IL-33 in serum of acute bronchiolitis infants infected by RSV was examined by ELISA assay; we found that IL-33 concentrations in AVB infants were significantly increased compared to normal subjects (Figure 1(a)). Acute bronchiolitis elicited increased levels of IL-4 and IL-10 (Figures 1(b) and 1(c)) but decreased level of IFN- γ and IL-2 (Figures 1(d) and 1(e)). We also examined that the ratio of Th1 and Th2 cell was lowered in peripheral blood of acute bronchiolitis than normal infants by flow cytometry (Figure 1(f)). In addition, infants with acute bronchiolitis had a 2.87-fold higher level of serum (sST2) than those normal cases (Figure 1(g)). The ST2 protein expression was positively correlated ($r = 0.669$, $p < 0.001$) with IL-33 production in acute bronchiolitis cases (Figure 1(h)).

3.2. NF- κ B/IL-33/ST2 Axis Is Mediated the Th2 Cytokine Levels and BAL Cell Number Induced by RSV. Previous studies have shown that NF- κ B is involved in the process of RSV-induced acute bronchiolitis [20], and NF- κ B inhibitor dimethyl fumarate inhibited IL-33 production [21], but its specific mechanism is unclear. Moreover, sST2 is another mode of existence of ST2. It is reported that sST2 can competently bind with IL-33, interfere with the coupling of IL-33 and ST2, and then inhibit the biological effects of IL-33. To confirm whether the level of Th2 cytokines IL-4 and IL-10 was mediated by IL-33, we used anti-IL-33 antibody by intranasal injection $30\ \mu\text{g}/\text{mouse}$ 2 h before challenge with RSV on 3 consecutive days (14, 15, and 16). Western blot analysis showed that abundances of ST2, p-I κ Ba, p-p65, and p-p50 were all induced by RSV, and ST2 abundance was markedly inhibited after treated with anti-IL-33 antibody prior to expose to RSV. However, the abundance of I κ Ba, p65, and p50 was not significantly decreased in the anti-IL-33+ RSV

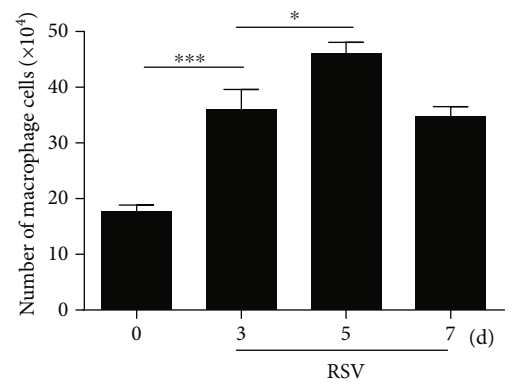
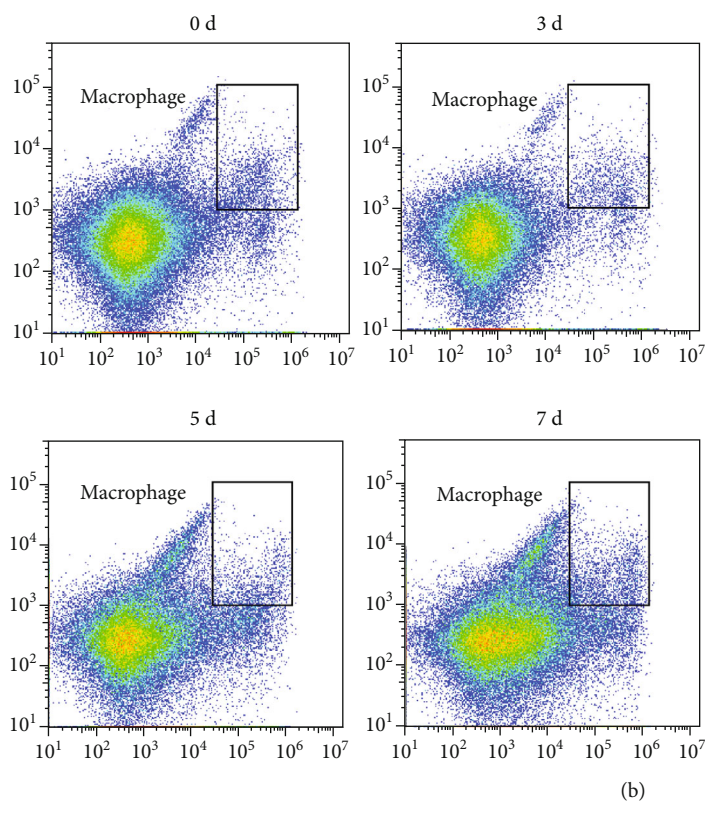
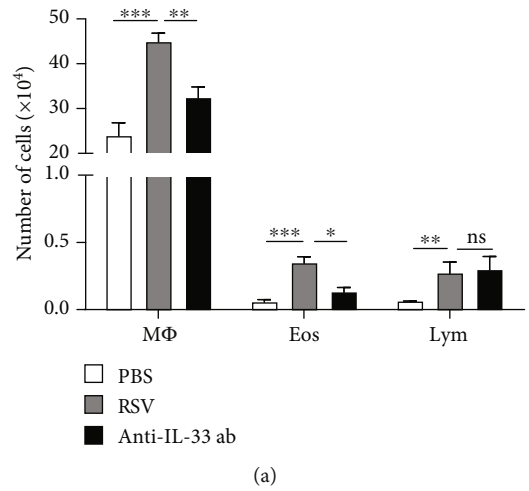


FIGURE 4: Continued.

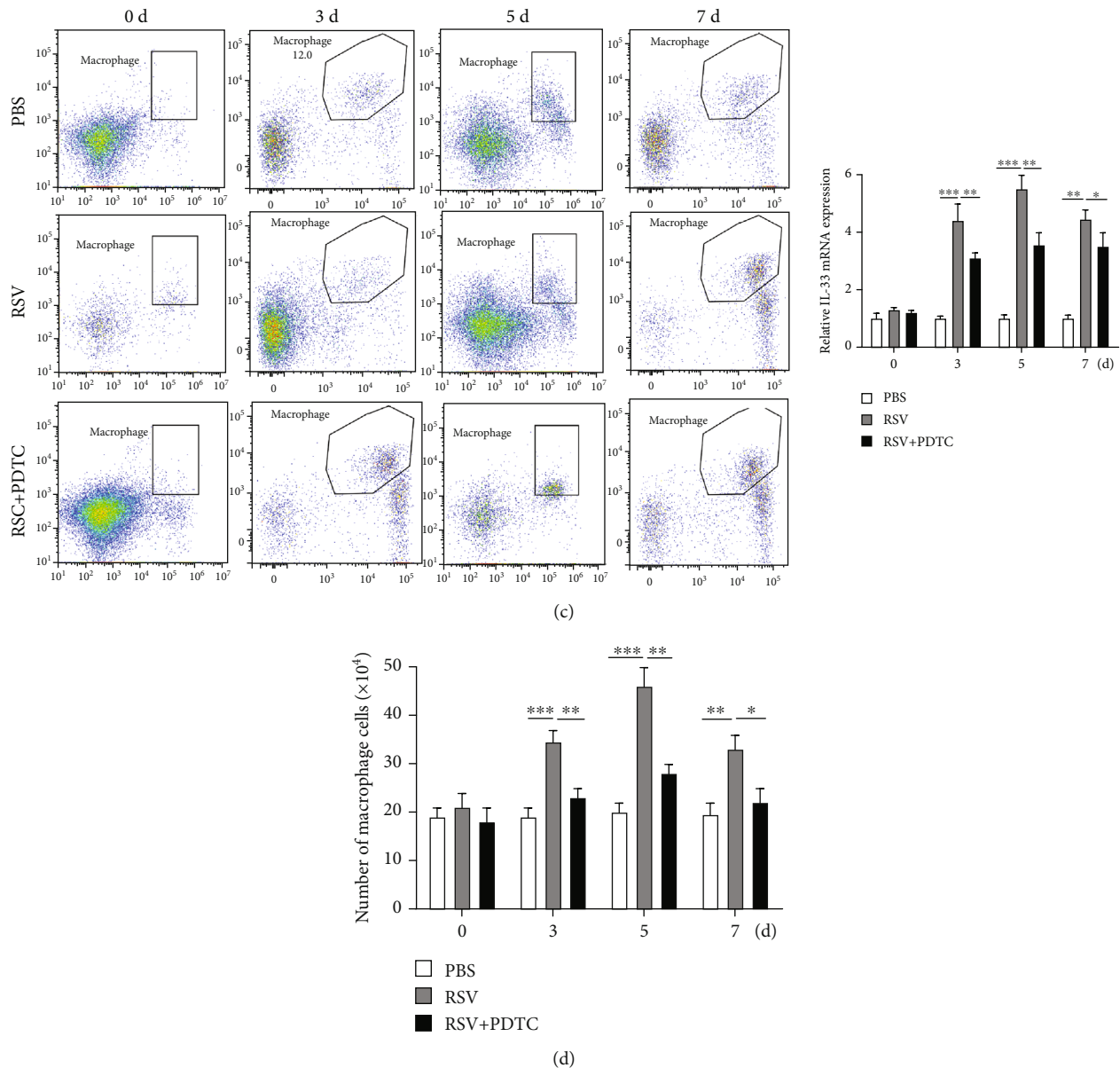


FIGURE 4: Macrophages are important sources of IL-33 and are regulated by NF- κ B pathway in RSV-induced mice. (a) The number of alveolar macrophages, lymphocyte, and eosinophils in BAL of mice. (b) Flow cytometry analysis was performed to sort alveolar macrophages at different times after RSV infection. (c) Flow cytometry analysis was performed to sort alveolar macrophages at different times after RSV + PDTC treatment. (d) The IL-33 expression in alveolar macrophages at different times after RSV + PDTC treatment was examined by RT-PCR analysis. All data were expressed as the mean \pm SD ($n = 3$). Each value of * $p < 0.05$, ** $p < 0.01$, and *** $p < 0.001$ was considered to be significant differences.

groups (Figure 2(a)). The mRNA expression of Th2 cytokines IL-4 and IL-10 elevated by RSV in lung tissues was significantly decreased in the anti-IL-33+ RSV groups (Figures 2(b) and 2(c)). Moreover, IL-33 antibody strongly suppressed the BAL cells activated by RSV (Figure 2(d)). In order to further verify whether there is a relationship between NF- κ B and IL-33, we used NF- κ B specific inhibitors (PDTC) to inject the mice prior 2h to activate by RSV. As shown in Figures 2(e) and 2(f), the protein abundances of the ST2 and mRNA expression of IL-33 in mouse lung tissues induced by RSV were elevated and were significantly inhibited in the PDTC+RSV groups.

Consistent with the role of IL-33 antibody, the mRNA expression of Th2 cytokines IL-4 and IL-10 elevated by RSV in lung tissues was also significantly inhibited in the PDTC+ RSV groups (Figures 2(g) and 2(h)). Besides, PDTC treatment strongly suppressed the BAL cells activated by RSV (Figure 2(i)). Furthermore, the levels of IL-4 and IL-10 (Figures 2(j) and 2(k)), and BAL cells (Figure 2(l)) elevated in the RSV groups were significantly inhibited in the RSV + sST2 groups. However, the abundance of IL-33 and NF- κ B (p-p50, p-p65, and p-I κ Ba) increased in the RSV groups was not suppressed in the sST2 + RSV groups.

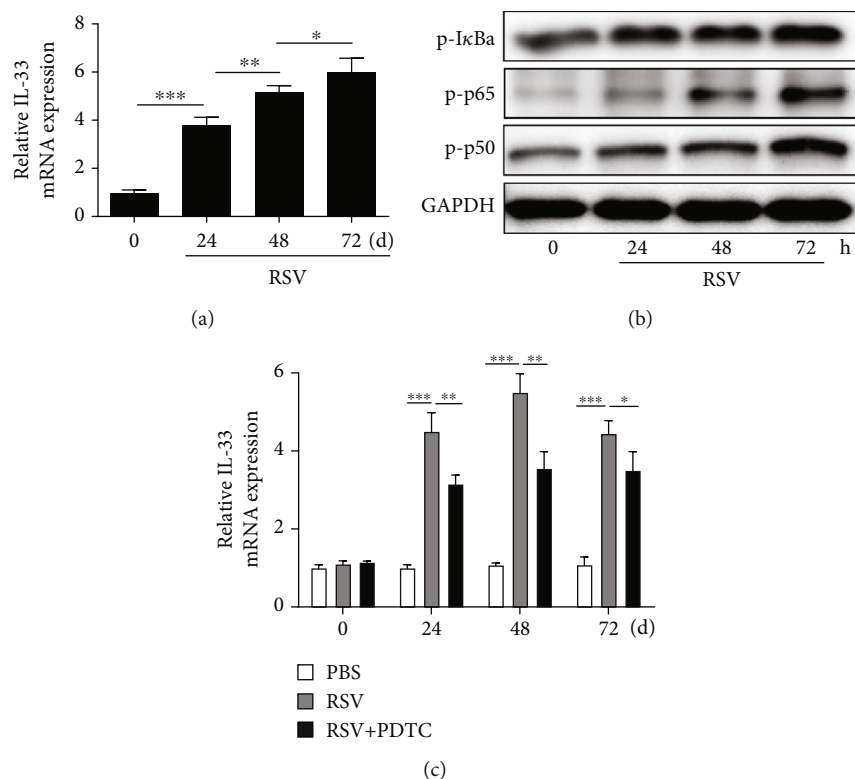


FIGURE 5: RSV-induced IL-33 expression was inhibited through NF- κ B pathway in vitro. (a) RT-PCR analysis was performed to examine the IL-33 expression in RAW264.7 cells at different time after RSV-induced. (b) Western blot analysis was performed to examine the abundance of I κ Ba, p65, and p50. (c) The IL-33 expression in macrophages at different times after RSV + PDTC treatment was examined by RT-PCR analysis. All data were expressed as the mean \pm SD ($n = 3$). Each value of $*p < 0.05$, $**p < 0.01$, and $***p < 0.001$ was considered to be significant differences.

3.3. Acute Bronchiolitis Induced by RSV in a Mouse Model Is Attenuated after Inhibition of NF- κ B/IL-33/ST2 Pathway. To further confirm the role of NF- κ B/IL-33/ST2 pathway in RSV-induced AVB in a mouse model, immunohistochemical staining was performed in this study. Representative IL-33, ST2, and p65 immunostaining was examined in saline-exposed control mice (NC) and RSV-treated mice (RSV). Immunostaining results showed that the abundances of IL-33, ST2, and p65 were all increased in acute bronchiolitis induced by RSV than NC groups (Figure 3(a)). In addition, HE staining assay indicated that RSV significantly thickened the trachea wall, widened intercellular space, and enhanced inflammatory cell infiltration which was attenuated by anti-IL-13 antibody, PDTC, and sST2 treatment, representatively (Figure 3(b)).

3.4. Macrophages Are Important Sources of IL-33 and Are Regulated by NF- κ B Pathway in RSV-Induced Mice. To further clarify the main cellular source of increased IL-33 secretion after RSV infection, inflammatory cells in BAL were classified and counted. We found that the number of alveolar macrophages and eosinophils in BAL mice increased significantly after RSV infection (Figure 4(a)); flow cytometry analysis showed that the number of macrophages was the largest and reached the peak on the fifth day after RSV infection (Figure 4(b)). We further verified whether NF- κ B pathway was involved in RSV-induced macrophage number and IL-

33 production in macrophages; we found that both the number of macrophages and expression of IL-33 increased in the RSV groups were reduced in the PDTC+RSV groups (Figures 4(c) and 4(d)).

3.5. RSV-Induced IL-33 Expression Was Inhibited through NF- κ B Pathway In Vitro. To further validate the role of NF- κ B pathway on the production of IL-33 in RSV infected macrophages, RAW264.7 macrophage line was used in this study. RT-PCR analysis showed that the IL-33 expression induced by RSV was markedly elevated after 24 h and at a time-dependent manner (Figure 5(a)). Consistent with the above results, the protein abundance of I κ Ba, p65, and p50 was also increased at a time-dependent manner in RSV-induced macrophages (Figure 5(b)). Furthermore, the expression of IL-33 increased in RSV activated RAW264.7 cells was significantly inhibited by PDTC (Figure 5(c)).

4. Discussion

Respiratory syncytial virus infection can aggravate airway inflammation and promote the occurrence and development of asthma [22]. If effective treatment measures are not taken in time, children with acute bronchiolitis may suffer from repeated wheezing and develop asthma in the future, which seriously affects pulmonary function and brings heavy mental and economic burden to their families and society [23].

IL-33 can promote helminth infection and alleviate atherosclerosis by promoting Th2 immune response [11]. In the process of airway inflammation induced by RSV, IL-33 and its specific receptor of ST2 increased significantly [24]. However, the role of IL-33/ST2 pathway on RSV-induced acute bronchiolitis and its molecular mechanism is unknown. In our study, we demonstrated that the levels of IL-33 and Th2-related cytokines IL-4 and IL-10 in RSV infected acute bronchiolitis in serum of infants were significantly increased. Besides, the Th1-associated cytokines IL-2 and INF- γ and Th1/Th2 cell ratio were markedly reduced in infant serum of acute bronchiolitis. Furthermore, RSV-induced Th2-related cytokines IL-4 and IL-10 in lung tissues were decreased by IL-33 antibody treatment. In addition, we also found that the increase of inflammatory cells in lung tissue infected by RSV was inhibited by IL-33 antibody. These data indicated that IL-33 plays an important role in acute bronchiolitis infants infected by RSV.

ST2 is one of the receptors of IL-1 family and widely expressed in many kinds of cells, especially mast cells and helper T cells [25]. Without proinflammatory stimulation, IL-33 only exists in the nucleus of inflammation and immune cells. In many disease processes, activated and released IL-33 can play an important role by combining with ST2 [26, 27]. In addition, soluble ST2 (sST2) as a bait receptor of IL-33 can directly bind to IL-33 and inhibit the biological function of IL-33 [28, 29]. In this study, we confirmed that the ST2 gene expression was positively correlated with IL-33 production in acute bronchiolitis cases. Both IL-33 antibody and sST2 could reversed RSV-induced Th2-related cytokine and pulmonary inflammatory damage. In addition, ST2 abundance can be inhibited in vivo and in vitro by IL-33 antibody treatment. Our results suggested that IL-33/ST2 pathway is mediated the RSV-induced acute bronchiolitis and maybe the potential targets for the prevention of asthma after acute bronchiolitis in infants.

Many kinds of cells can secrete IL-33 after stimulating inflammation. In addition to nonimmune cells such as epithelial cells and fibroblasts, macrophages, dendritic cells, and mast cells can also secrete IL-33 after stimulation [30]. In recent years, increasing evidences indicate that innate immune cells may be an important source of IL-33 in the process of respiratory viral infection [30]. By flow cytometry analysis, we found that inflammatory cells increased significantly after RSV infection in mice, mainly macrophages, and the IL-33 expression in macrophages was elevated markedly. In addition, we also found that IL-33 antibody could reduce the number of macrophages induced by RSV. These results indicated that RSV increases the number of macrophages and leads to the increase of IL-33 secretion; IL-33 could also further promote the increase of macrophages.

Although evidence showed that IL-33 plays a biological role through NF- κ B pathway [20], IL-33 antibody treatment did not inhibit the expression of NF- κ B pathway induced by RSV in our study, so we speculate that the NF- κ B pathway is not mediated by the inhibitory effect of IL-33 antibody on RSV-induced lung damage. Interestingly, we found that NF- κ B inhibitors can reduce RSV-induced lung damage in mice, and we also found that NF- κ B inhibitors can reduce the

abundance of IL-33 in vivo and in vitro. This finding indicated that the NF- κ B pathway is mainly involved in the process of RSV-induced IL-33 secretion in mice.

In conclusion, we confirmed that NF- κ B/IL-33/ST2 axis is mediated the acute bronchiolitis by RSV infected. Our findings not only demonstrate the potential role of IL-33 antibody in attenuating RSV-induced lung damage but also provide a new insight into better prevention of RSV-induced asthma by mediating NF- κ B/IL-33/ST2 axis.

Data Availability

All data collection and analysis were conducted under double-blind and supported by The Second People's Hospital of Changzhou, Affiliated Hospital of Nanjing Medical University.

Conflicts of Interest

There are no conflicts of interest.

Authors' Contributions

Liwen Zhang designed and performed the in vivo experiments, analyzed the data, and wrote the manuscript. Yu Wan and Liang Ma are responsible for collecting clinical blood samples and detecting inflammatory markers; they are also responsible for in vitro studies. Kaihong Xu participated in the animal experiments. Baojin Cheng designed and supervised the study and performed the manuscript editing. Liwen Zhang and Yu Wan contributed equally to this work.

Acknowledgments

This study was supported by grants from the Research Project of Jiangsu Provincial Commission of Health and Family Planning (No. H201547), the Major Scientific and Technological Project of Changzhou City Commission of Health and Family Planning (No. ZD201612), the Scientific and Technological Project of Nanjing Medical University (No. 2017NJMU042), the National Natural Science Foundation of China (No. 81700500), and the Applied Basic Research Programs of Science, Technology Department of Changzhou city (CJ20160031).

Supplementary Materials

Uncropped western blotting image. (*Supplementary Materials*)

References

- [1] E. M. Abrams, A. B. Becker, and S. J. Szefer, "Where does worsening asthma end and an asthma exacerbation begin?," *Annals of Allergy, Asthma & Immunology*, vol. 123, no. 4, pp. 329-330, 2019.
- [2] J. P. Lynch, R. B. Werder, Z. Loh et al., "Plasmacytoid dendritic cells protect from viral bronchiolitis and asthma through semaphorin 4a-mediated T reg expansion," *The Journal of Experimental Medicine*, vol. 215, no. 2, pp. 537-557, 2018.

- [3] L. Petrarca, R. Nenna, A. Frassanito et al., "Acute bronchiolitis: influence of viral co-infection in infants hospitalized over 12 consecutive epidemic seasons," *Journal of Medical Virology*, vol. 90, no. 4, pp. 631–638, 2018.
- [4] S. M. Teo, H. H. F. Tang, D. Mok et al., "Airway microbiota dynamics uncover a critical window for interplay of pathogenic bacteria and allergy in childhood respiratory disease," *Cell Host & Microbe*, vol. 24, no. 3, pp. 341–352.e5, 2018, e5.
- [5] R. P. Tórtora, M. A. A. M. Guimarães, L. M. de Souza et al., "Adenovirus species C detection in children under four years of age with acute bronchiolitis or recurrent wheezing," *Journal of Clinical Virology*, vol. 73, pp. 77–80, 2015.
- [6] A. M. Nathan, F. Rani, R. J. Y. Lee et al., "Clinical risk factors for life-threatening lower respiratory tract infections in children: a retrospective study in an urban city in Malaysia," *PLoS One*, vol. 9, no. 10, article e111162, 2014.
- [7] J. Teeratakulpisarn, C. Pientong, T. Ekalaksananan, H. Ruangsiripiyakul, and R. Uppala, "Rhinovirus infection in children hospitalized with acute bronchiolitis and its impact on subsequent wheezing or asthma: a comparison of etiologies," *Asian Pacific Journal of Allergy and Immunology*, vol. 32, no. 3, pp. 226–234, 2014.
- [8] J. Y. Chung, T. H. Han, J. S. Kim, S. W. Kim, C. G. Park, and E. S. Hwang, "Th1 and Th2 cytokine levels in nasopharyngeal aspirates from children with human bocavirus bronchiolitis," *Journal of Clinical Virology*, vol. 43, no. 2, pp. 223–225, 2008.
- [9] X. Hu, X. Li, C. Hu et al., "Respiratory syncytial virus exacerbates OVA-mediated asthma in mice through C5a-C5aR regulating CD4⁺T cells immune responses," *Scientific Reports*, vol. 7, no. 1, article 15207, 2017.
- [10] T. Jartti, M. Paul-Anttila, P. Lehtinen et al., "Systemic T-helper and T-regulatory cell type cytokine responses in rhinovirus vs. respiratory syncytial virus induced early wheezing: an observational study," *Respiratory Research*, vol. 10, no. 1, p. 85, 2009.
- [11] Y. Liang, N. Yang, G. Pan, B. Jin, S. Wang, and W. Ji, "Elevated IL-33 promotes expression of MMP2 and MMP9 via activating STAT3 in alveolar macrophages during LPS-induced acute lung injury," *Cellular & Molecular Biology Letters*, vol. 23, no. 1, p. 52, 2018.
- [12] C. M. Finlay, A. M. Stefanska, K. P. Walsh et al., "Helminth products protect against autoimmunity via innate type 2 cytokines IL-5 and IL-33, which promote eosinophilia," *Journal of Immunology, Virus Research and Experimental Chemotherapy*, vol. 196, no. 2, pp. 703–714, 2016.
- [13] H. Y. Lee, C. K. Rhee, J. Y. Kang et al., "Blockade of IL-33/ST2 ameliorates airway inflammation in a murine model of allergic asthma," *Experimental Lung Research*, vol. 40, no. 2, pp. 66–76, 2014.
- [14] X. Han, R. Chai, F. Qi et al., "Natural helper cells mediate respiratory syncytial virus-induced airway inflammation by producing type 2 cytokines in an IL-33-dependent manner," *Immunotherapy*, vol. 9, no. 9, pp. 715–722, 2017.
- [15] H. Yin, P. Li, F. Hu, Y. Wang, X. Chai, and Y. Zhang, "IL-33 attenuates cardiac remodeling following myocardial infarction via inhibition of the p38 MAPK and NF- κ B pathways," *Molecular Medicine Reports*, vol. 9, no. 5, pp. 1834–1838, 2014.
- [16] J. J. Zorc and C. B. Hall, "Bronchiolitis: recent evidence on diagnosis and management," *Pediatrics*, vol. 125, no. 2, pp. 342–349, 2010.
- [17] A. Tahamtan, Y. Samieipoor, F. S. Nayeri et al., "Effects of cannabinoid receptor type 2 in respiratory syncytial virus infection in human subjects and mice," *Virulence*, vol. 9, no. 1, pp. 217–230, 2018.
- [18] M. de Martinis, L. Ginaldi, M. M. Sirufo et al., "IL-33/vitamin D crosstalk in psoriasis-associated osteoporosis," *Frontiers in Immunology*, vol. 11, article 604055, 2021.
- [19] J. E. Vargas, A. P. D. de Souza, B. N. Porto et al., "Immuno-modulator plasmid projected by systems biology as a candidate for the development of adjunctive therapy for respiratory syncytial virus infection," *Medical Hypotheses*, vol. 88, pp. 86–90, 2016.
- [20] K. Fink, A. Duval, A. Martel, A. Soucy-Faulkner, and N. Grandvaux, "Dual role of NOX2 in respiratory syncytial virus- and Sendai virus-induced activation of NF- κ B in airway epithelial cells," *Journal of Immunology*, vol. 180, no. 10, pp. 6911–6922, 2008.
- [21] S. Demyanets, C. Kaun, R. Pentz et al., "Components of the interleukin-33/ST2 system are differentially expressed and regulated in human cardiac cells and in cells of the cardiac vasculature," *Journal of Molecular and Cellular Cardiology*, vol. 60, pp. 16–26, 2013.
- [22] X. Carbonell-Estrany, "RSV prevention in infancy and asthma in later life," *The Lancet Respiratory Medicine*, vol. 6, no. 7, article e31, 2018.
- [23] D. You, D. T. Siefker, B. Shrestha, J. Saravia, and S. A. Cormier, "Building a better neonatal mouse model to understand infant respiratory syncytial virus disease," *Respiratory Research*, vol. 16, no. 1, p. 91, 2015.
- [24] S. Zeng, J. Wu, J. Liu, F. Qi, and B. Liu, "IL-33 receptor (ST2) signalling is important for regulation of Th2-mediated airway inflammation in a murine model of acute respiratory syncytial virus infection," *Scandinavian Journal of Immunology*, vol. 81, no. 6, pp. 494–501, 2015.
- [25] A. Bayes-Genis, J. L. Januzzi, H. K. Gaggin et al., "ST2 pathogenic profile in ambulatory heart failure patients," *Journal of Cardiac Failure*, vol. 21, no. 4, pp. 355–361, 2015.
- [26] X. Liu, L. Zhu, X. Lu et al., "IL-33/ST2 pathway contributes to metastasis of human colorectal cancer," *Biochemical and Biophysical Research Communications*, vol. 453, no. 3, pp. 486–492, 2014.
- [27] S. M. Jung, J. Lee, S. Y. Baek et al., "The interleukin 33/ST2 axis in patients with primary Sjögren syndrome: expression in serum and salivary glands, and the clinical association," *The Journal of Rheumatology*, vol. 42, no. 2, pp. 264–271, 2015.
- [28] S. E. Piper, R. A. Sherwood, G. F. Amin-Youssef, A. M. Shah, and T. A. McDonagh, "Serial soluble ST2 for the monitoring of pharmacologically optimised chronic stable heart failure," *International Journal of Cardiology*, vol. 178, pp. 284–291, 2015.
- [29] K. Broch, A. K. Andreassen, T. Ueland et al., "Soluble ST2 reflects hemodynamic stress in non-ischemic heart failure," *International Journal of Cardiology*, vol. 179, pp. 378–384, 2015.
- [30] B. M. Matta, J. M. Lott, L. R. Mathews et al., "IL-33 is an unconventional alarmin that stimulates IL-2 secretion by dendritic cells to selectively expand IL-33R/ST2⁺ regulatory T cells," *Journal of Immunology*, vol. 193, no. 8, pp. 4010–4020, 2014.

Research Article

Analysis of Lymphocyte Subpopulations and Cytokines in COVID-19-Associated Pneumonia and Community-Acquired Pneumonia

Guohong Liu,¹ Xianghu Jiang,² Xiaojiao Zeng,² Yunbao Pan ,² and Haibo Xu ¹

¹Department of Radiology, Zhongnan Hospital of Wuhan University, Wuhan University, Wuhan, Hubei, China

²Department of Laboratory Medicine, Zhongnan Hospital of Wuhan University, Wuhan University, Wuhan, Hubei, China

Correspondence should be addressed to Yunbao Pan; panyunbao@outlook.com and Haibo Xu; xuhaibo11202021@126.com

Received 13 December 2020; Revised 11 March 2021; Accepted 17 April 2021; Published 12 June 2021

Academic Editor: Zhipeng Xu

Copyright © 2021 Guohong Liu et al. This is an open access article distributed under the Creative Commons Attribution License, which permits unrestricted use, distribution, and reproduction in any medium, provided the original work is properly cited.

Background. The 2019 novel coronavirus SARS-CoV-2 caused large outbreaks of COVID-19 worldwide. COVID-19 resembles community-acquired pneumonia (CAP). Our aim was to identify lymphocyte subpopulations to distinguish between COVID-19 and CAP. **Methods.** We compared the peripheral blood lymphocytes and their subsets in 296 patients with COVID-19 and 130 patients with CAP. Parameters for independent prediction of COVID-19 were calculated by logistic regression. **Results.** The main lymphocyte subpopulations ($CD3^+CD4^+$, $CD16^+CD56^+$, and $CD4^+/CD8^+$ ratio) and cytokines (TNF- α and IFN- γ) of COVID-19 patients were significantly different from that of CAP patients. $CD16^+CD56^+$ %, $CD4^+/CD8^+$ ratio, $CD19^+$, and $CD3^+CD4^+$ were identified as predictors of COVID-19 diagnosis by logistic regression. In addition, the $CD3^+CD4^+$ counts, $CD3^+CD8^+$ counts, and TNF- α are independent predictors of disease severity in patients. **Conclusions.** Lymphopenia is an important part of SARS-CoV-2 infection, and lymphocyte subsets and cytokines may be useful to predict the severity and clinical outcomes of the disease.

1. Introduction

COVID-19 is a newly emerging disease with high infection rates, unclear pathogenesis, rapid disease progression, and relatively high incidence of mortality. COVID-19 has affected many countries, with the World Health Organization (WHO) reporting 122536880 confirmed cases and 2703780 deaths up to March 21, 2021, globally [1].

Most of the early reports are classified cases as COVID-19 based on the clinical case definition, but specific laboratory confirmation could be made following recognition of SARS-CoV-2 as the pathogen [2]. As the COVID-19 epidemic surges across the globe, researchers are struggling to understand a key epidemiological puzzle—what percentage of infected people have mild or no symptoms and may pass the virus on to others. Some preliminary and detailed estimates of these clandestine cases suggest that they may account for about 60% of all infections [3]. The symptoms COVID-19 appears to cause are similar to other causes of community-acquired pneumonia (CAP), such as fever, cough, shortness of breath, dyspnoea, chest tightness, and

diarrhea [4, 5]. Distinguishing COVID-19 from other causes of CAP is one of the main challenges of the COVID-19 outbreak. Our group and others have previously reported numerous hematological abnormalities in COVID-19 [5–8]. Prominent amongst the abnormalities is lymphopenia; although, lymphocyte subsets have not been reported in most studies.

In this study, lymphocyte subsets were examined in a cohort of 296 COVID-19 patients and 130 CAP patients. The present study is aimed at evaluating the ability of lymphocyte subsets and cytokines for distinguishing COVID-19 from CAP.

2. Materials and Methods

2.1. Patients and Data Collection. The 296 COVID-19 patients presented to our hospital from Feb 1, 2020, to Mar 10, 2020. All patients were laboratory confirmed to be SARS-CoV-2 infected by real-time RT-PCR. The CAP group consisted of 130 patients who visited our hospital from January 2019 to November 2019. The inclusion criteria included

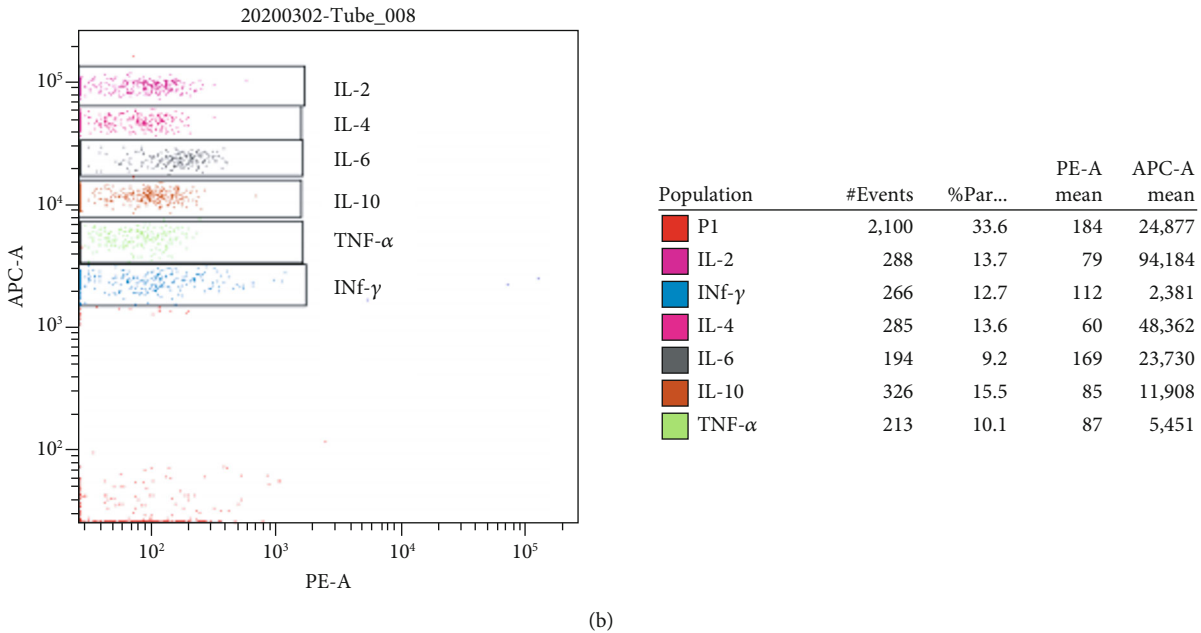
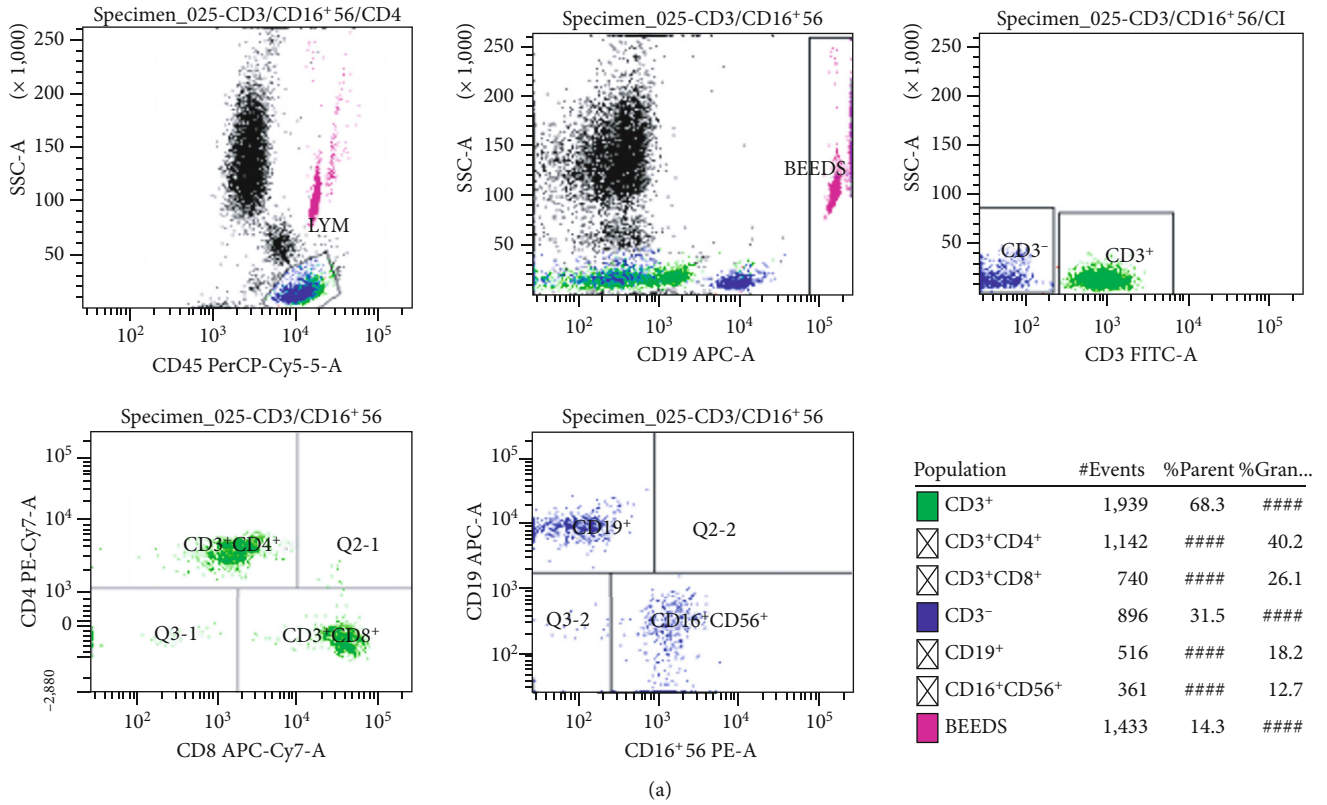


FIGURE 1: Flow cytometry analysis template to detect the CD3⁺, CD3⁺CD4⁺, CD3⁺CD8⁺, CD19⁺, and CD16⁺CD56⁺ cells (a) and 6 kinds of cytokines (b) in one tube simultaneously.

the following: (a) pneumonia was defined as pulmonary infiltration and one or more of the following symptoms: fever (body temperature $\geq 38.0^{\circ}\text{C}$), cough with or without sputum discharge, dyspnea, or changes in breathing sounds by auscultation; (b) complete patient records of lymphocyte subsets; and (c) hospital patients. The exclusion criteria were as follows: (a) patients lacking data on clinical lymphocyte sub-

sets and (b) outpatient patients. During that hard time, 244 (82.4%) COVID-19 patients took antiviral medicine at home, but none of the COVID-19 patients received immunomodulating drugs before visiting the hospital. All the COVID-19 patients received blood sampling after the onset of symptoms. The clinical data collected from the patients was approved by the Ethics Committee of Zhongnan Hospital

TABLE 1: Laboratory values of COVID-19 patients and CAP patients.

Variable	CAP (n = 130)	COVID-19 (n = 296)	<i>p</i>
Age (years)	50 (32-72)	53 (41-64)	0.230
Gender (M/F)	80/50	152/144	0.057
CD3 ⁺	936.37 (322.75-1187.5)	973.11 (596.75-1274)	0.673
CD19 ⁺	248.5 (55.25-285.5)	184.43 (92-246)	0.152
CD3 ⁺ CD4 ⁺	426.42 (133.25-580.25)	579.1 (334-766.5)	<0.001
CD3 ⁺ CD8 ⁺	462.48 (123.75-540.75)	368.9 (212.75-488)	0.106
CD16 ⁺ CD56 ⁺	183.98 (64.25-227.5)	238.59 (107.75-304.25)	0.007
4/8 ratio	1.47 (0.57-1.73)	1.81 (1.19-2.21)	0.015
CD3 ⁺ % lym	67.5 (60.1-77.19)	67.8 (62.43-74.87)	0.802
CD19 ⁺ % lym	16.69 (7.41-22.32)	14 (8.6-17.8)	0.024
CD3 ⁺ CD4 ⁺ % lym	31.79 (21.81-39.57)	40.38 (33.72-46.49)	<0.001
CD3 ⁺ CD8 ⁺ % lym	31.87 (21.18-39.42)	25.7 (20-31.4)	<0.001
CD16 ⁺ CD56 ⁺ % lym	14.6 (7.21-19.4)	16.75 (9.68-22.2)	0.038

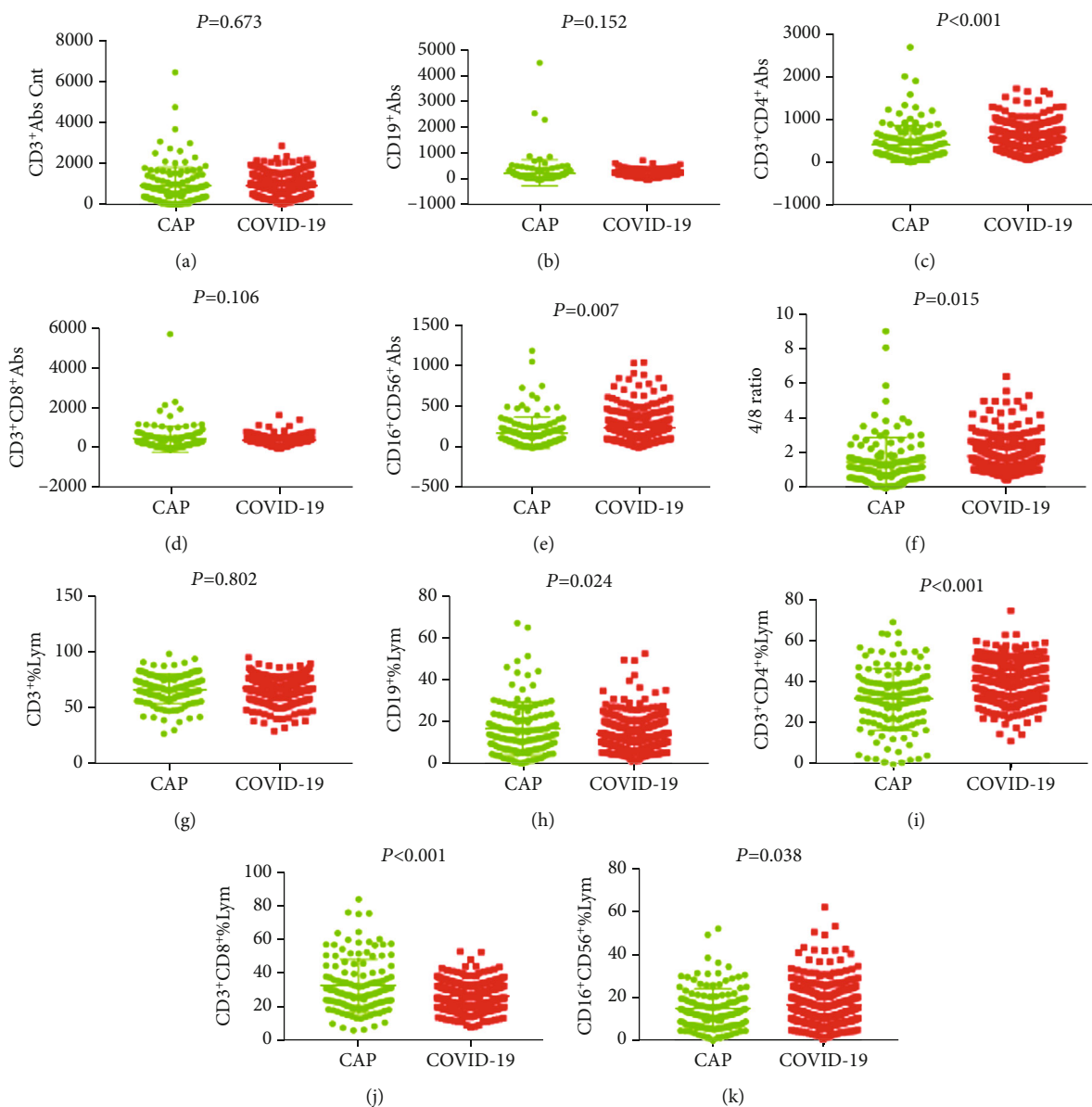


FIGURE 2: General characteristics of lymphocyte subpopulations between CAP patients and COVID-19 patients.

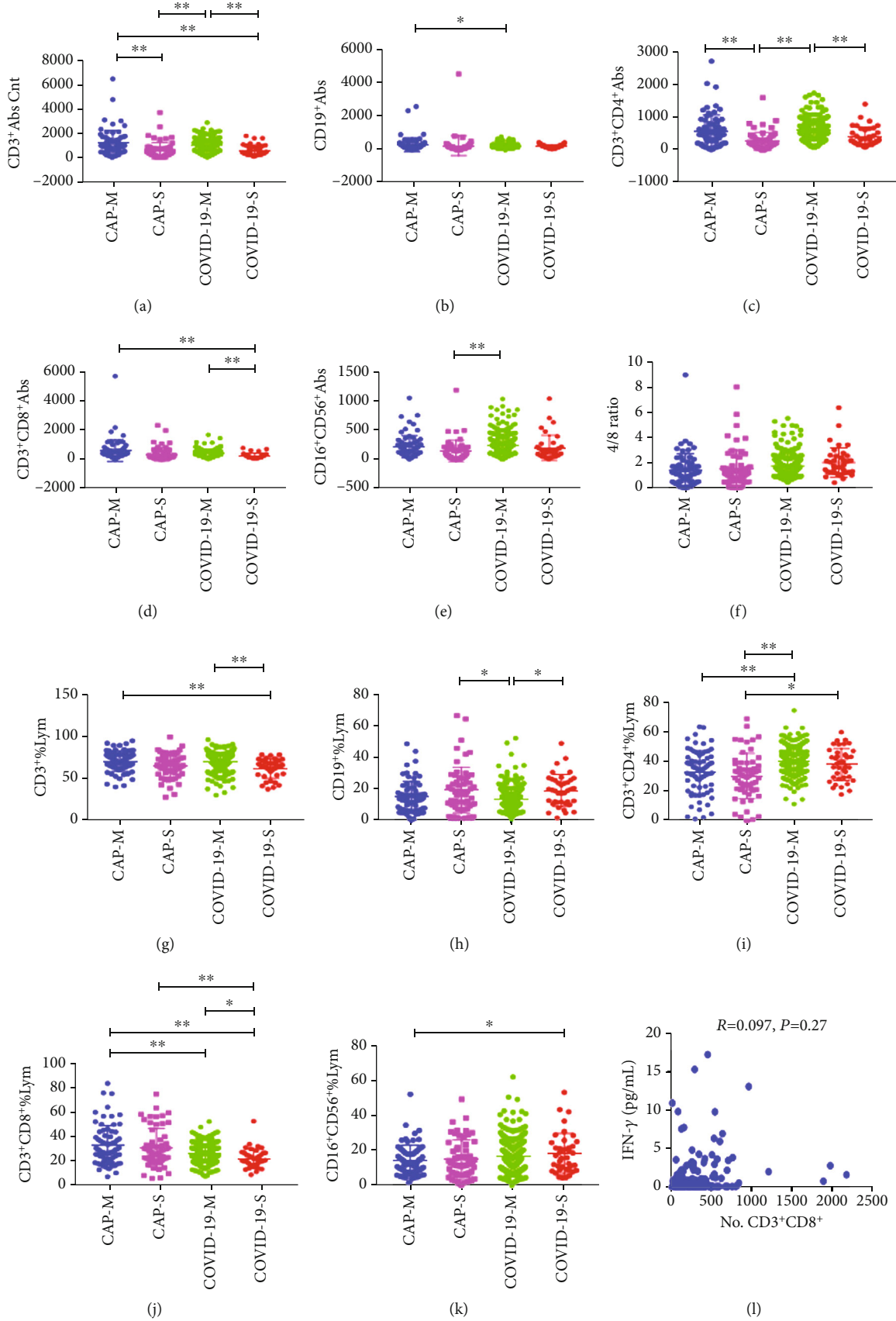


FIGURE 3: General characteristics of lymphocyte subpopulations in mild CAP patients (CAP-M), severe CAP patients (CAP-S), mild COVID-19 patients (COVID-19-M), and severe COVID-19 patients (COVID-19-S). * $p < 0.05$, ** $p < 0.01$.

TABLE 2: Abnormal laboratory results for COVID-19 patients and CAP patients.

Variate	COVID-19 (n = 296)	CAP (n = 130)	p
CD3 ⁺			<0.001
Normal	185 (62.5%)	56 (43.1%)	
High	0 (0%)	2 (1.5%)	
Low	111 (37.5%)	72 (55.4%)	
CD19 ⁺			0.032
Normal	81 (27.4%)	35 (26.9%)	
High	0 (0%)	3 (2.3%)	
Low	215 (72.6%)	92 (70.8%)	
CD3 ⁺ CD4 ⁺			<0.001
Normal	217 (73.3%)	59 (45.4%)	
High	0 (0%)	1 (0.8%)	
Low	79 (26.7%)	70 (53.8%)	
CD3 ⁺ CD8 ⁺			0.216
Normal	140 (47.3%)	55 (42.3%)	
High	0 (0%)	1 (0.8%)	
Low	156 (52.7%)	74 (56.9%)	
CD16 ⁺ CD56 ⁺			0.008
Normal	129 (43.6%)	39 (30%)	
Low	167 (56.4%)	91 (70%)	
4/8 ratio			<0.001
Normal	169 (57.1%)	58 (44.6%)	
High	88 (29.7%)	26 (20%)	
Low	39 (13.2%)	46 (35.4%)	
CD3 ⁺ % lym			0.679
Normal	153 (51.7%)	70 (53.8%)	
High	139 (47%)	57 (43.8%)	
Low	4 (1.4%)	3 (2.3%)	
CD19 ⁺ % lym			0.004
Normal	164 (55.4%)	66 (50.8%)	
High	15 (5.1%)	19 (14.6%)	
Low	117 (39.5%)	45 (34.6%)	
CD3 ⁺ CD4 ⁺ % lym			<0.001
Normal	106 (35.8%)	69 (51.1%)	
High	189 (63.9%)	45 (36.7%)	
Low	1 (0.3%)	16 (12.2%)	
CD3 ⁺ CD8 ⁺ % lym			<0.001
Normal	264 (89.2%)	88 (67.7%)	
High	15 (5.1%)	34 (26.2%)	
Low	17 (5.7%)	8 (6.2%)	
CD16 ⁺ CD56 ⁺ % lym			0.018
Normal	231 (78%)	88 (67.7%)	
High	16 (5.4%)	5 (3.8%)	
Low	49 (16.6%)	37 (28.5%)	

TABLE 3: Multivariate predictors of COVID-19 versus CAP.

Variate	OR	95% CI	p
CD3 ⁺ CD4 ⁺ % lym	0.951	0.637-1.422	0.808
CD19 ⁺ % lym	1.048	0.805-1.363	0.729
CD3 ⁺ % lymcnt	0.871	0.54-1.402	0.569
CD16 ⁺ CD56 ⁺ % lym	1.338	1.032-1.736	0.028
CD3 ⁺ CD8 ⁺ % lym	1.334	0.886-2.009	0.167
4/8 ratio	1.538	1.166-2.028	0.002
CD19 ⁺	0.743	0.566-0.975	0.032
CD3 ⁺ CD4 ⁺	1.822	1.417-2.343	<0.001
CD16 ⁺ CD56 ⁺	1.102	0.838-1.449	0.488
CD3 ⁺	1.174	0.776-1.778	0.447
CD3 ⁺ CD8 ⁺	0.834	0.636-1.094	0.19

of Wuhan University. The Ethics Committee waived written informed consent for emerging infectious diseases.

2.2. Lymphocyte Subpopulation Test. Fasting whole blood from every patient was collected aseptically by venipuncture into ethylenediamine tetraacetic acid (EDTA) collection tubes for the quantification of the main lymphocyte subpopulations. Whole blood was incubated with BD Multitest 6-color TBNK reagent and then lysed with BD FACS™ lysing solution. Lymphocyte subpopulations were acquired and analyzed with BD FACSCanto clinical software. The BD Multitest 6-color TBNK reagent contains the following antibodies to identify and count different lymphocyte subsets: CD3 FITC was used for T lymphocyte identification, CD16 and CD56 PE for NK lymphocyte identification, CD45 PerCP-Cy™5.5 for lymphocyte population identification, CD4 PE-Cy™7 for T-helper/inducer lymphocyte identification and CD19 APC B lymphocyte identification, and CD8 APC-Cy7 for inhibitory/toxic T lymphocyte subset identification. The final results can be easily observed in the flow cytometry template we established (Figure 1(a)).

Generally, we pipette 20 μ L of BD Multitest 6-color TBNK reagent into the bottom of the BD Trucount tube and then pipette 50 μ L of well-mixed, anticoagulated whole blood into the bottom of the tube. Cap the tube and vortex gently to mix followed by incubating for 15 minutes in the dark at room temperature (20°C–25°C). We add 450 μ L of 1X BD FACS lysing solution to the tube and incubate the tube for 15 minutes in the dark at room temperature. The samples were then analyzed on the flow cytometer. Absolute counts are calculated by BD FACSCanto clinical software using the following formula.

$$\frac{\# \text{events in cell population}}{\# \text{events in absolute count bead region}} \times \frac{\# \text{beads/test} *}{\text{test volume}} = \text{cell population absolute count} \quad (1)$$

*This value is found on the BD Trucount tube foil pouch label and can vary from lot to lot.

TABLE 4: Multivariate predictors of lymphocyte subsets on disease severity.

Variate	COVID-19			CAP and COVID-19		
	OR	95% CI	<i>p</i>	OR	95% CI	<i>p</i>
4/8 ratio	0.901	0.531-1.527	0.698	1.083	0.762-1.539	0.657
CD16 ⁺ CD56 ⁺ % lym	0.851	0.519-1.395	0.522	1.068	0.774-1.474	0.688
CD16 ⁺ CD56 ⁺ abs	1.212	0.744-1.975	0.441	1.133	0.811-1.583	0.463
CD19 ⁺ % lym	0.874	0.552-1.386	0.568	0.911	0.677-1.226	0.539
CD19 ⁺ abs	0.622	0.387-1	0.05	0.744	0.528-1.049	0.092
CD3 ⁺ % lymcnt	0.585	0.287-1.194	0.141	0.864	0.542-1.378	0.54
CD3 ⁺ abs cnt	0.873	0.425-1.796	0.713	1.277	0.821-1.988	0.278
CD3 ⁺ CD4 ⁺ % lym	0.938	0.402-2.186	0.881	0.93	0.597-1.448	0.747
CD3 ⁺ CD4 ⁺ abs	2.046	1.328-3.151	0.001	2.515	1.862-3.397	<0.001
CD3 ⁺ CD8 ⁺ % lym	1.041	0.546-1.984	0.904	1.161	0.767-1.757	0.48
CD3 ⁺ CD8 ⁺ abs	2.218	1.288-3.819	0.004	1.539	1.126-2.103	0.007

2.3. Cytokine Analysis. This method involved Multiplex Cytometric Bead Array (CBA) for quantitative analysis of 6 kinds of cytokines, including tumor necrosis factor-alpha (TNF- α), interferon-gamma (IFN- γ), IL-6, IL-2, IL-4, and IL-10. The multiplex CBA was performed according to the manufacturer's instructions. Briefly, 25 μ L serum was mixed with an equal volume of capture beads and incubated with 25 μ L of PE-binding antibodies in the dark at room temperature for 2.5 hours. The beads were then centrifuged at 200 g for 5 min, and the supernatant was gently aspirated and resuscitated with phosphate buffer brine (PBS) (100 μ L). The CBA was addressed in a flow cytometer (BD) and analyzed by clinical software. The final result can be easily observed in the flow cytometry template we have established (Figure 1(b)).

2.4. Statistical Analysis. Statistical analysis was performed using SPSS (Version 22.0, SPSS, Inc., Chicago, IL, USA). Statistical analysis for the results was performed using the Student *t*-test. A *p* value <0.05 was considered statistically significant.

3. Results

A total of 296 COVID-19 patients (152male vs. 144female), with a mean age of 53 years and 130 CAP patients (80male vs. 50female), with a mean age of 50 years that were hospitalized at Zhongnan Hospital of Wuhan University, were enrolled in the study. Among the 130 CAP patients, 76 (58.5%) patients had bacterial pneumonia, 31 (23.8%) had viral pneumonia, 5 (3.8%) patients had fungal pneumonia, 5 (3.8%) patients had mycoplasma pneumonia, and 13 (10.0%) patients had pneumocystosis or other infection. The mean values of lymphocyte subpopulations indexes in COVID-19 patients and CAP patients were demonstrated in Table 1 and Figures 1 and 2. The mean values of CD19⁺% and CD3⁺CD8⁺% in COVID-19 patients were significantly lower than those in patients with CAP. The mean values of CD3⁺CD4⁺, CD16⁺CD56⁺, CD4/CD8 ratio, CD3⁺CD4⁺%, and CD16⁺CD56⁺% in COVID-19 patients

were significantly higher than those in patients with CAP. The mean values of CD3⁺, CD19⁺, and CD3⁺CD8⁺ were not significantly different between the COVID-19 group and CAP group.

In the mild group (71 CAP and 257 COVID-19), COVID-19 patients showed decreased CD19⁺, CD3⁺CD8⁺%, and increased CD3⁺CD4⁺%, compared with that of CAP patients. Similarly, in the severe patients (59 CAP and 39 COVID-19), COVID-19 patients had increased CD3⁺CD4⁺% and decreased CD3⁺CD8⁺%, compared with that of CAP patients (Figure 3).

The proportion of patients with abnormal lymphocyte subpopulations is shown in Table 2. Both COVID-19 patients and CAP patients had lymphopenia. A higher percentage of CAP patients showed reduced CD3⁺, CD3⁺CD4⁺, reduced CD16⁺CD56⁺, reduced CD4⁺/CD8⁺ ratio, increased CD19⁺%, and normal CD3⁺CD4⁺% compared with the COVID-19 patients. Logistic regression analysis showed that laboratory indicators could independently distinguish between COVID-19 and CAP. The ORs of the factors to predict COVID-19 versus CAP were demonstrated in Table 3. The CD16⁺CD56⁺%, CD4⁺/CD8⁺ ratio, CD19⁺, and CD3⁺CD4⁺ independently discriminating COVID-19 from CAP. In addition, the CD3⁺CD4⁺ and CD3⁺CD8⁺ counts are independent predictors of disease severity in the COVID-19 group and the combined COVID-19 and CAP group (Table 4).

In this study, we also analyzed 6 kinds of cytokines data in 92 COVID-19 patients and 38 CAP patients (Figures 1(b) and 4). TNF- α and IFN- γ had lower level in COVID-19 patients compared with the CAP patients. However, we found that IFN- γ levels were not correlated with CD8⁺ cytotoxic T lymphocytes in COVID-19 patients based on the database analysis, suggesting that decreased IFN- γ is not caused by CD8⁺ cytotoxic T lymphocytes (Figure 3(l)). As to IL-6, IL-2, IL-4, and IL-10, we did not find significant difference between the two groups. Logistic regression analysis revealed that TNF- α independently discriminate disease severity in COVID-19 patients (Table 5).

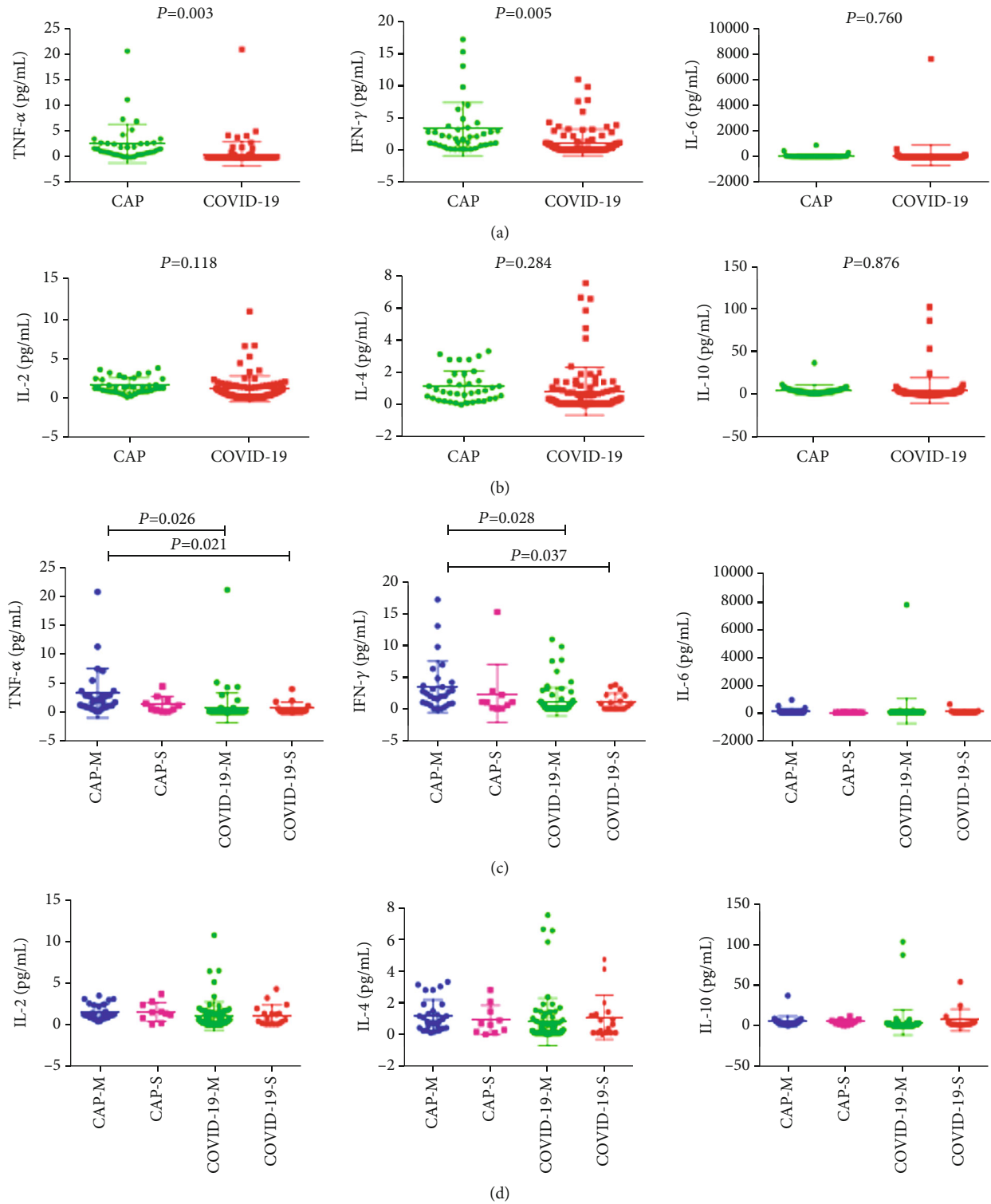


FIGURE 4: General characteristics of cytokines in patients with mild CAP (CAP-M), severe CAP (CAP-S), mild COVID-19 (COVID-19-M), and severe COVID-19 (COVID-19-S). * $p < 0.05$, ** $p < 0.01$.

4. Discussion

The interaction between COVID-19 and the immune system is complex. In the current study, lymphocyte subsets and cytokines were examined in COVID-19 and CAP patients. A significant proportion of COVID-19 patients had reduced

lymphocyte subpopulations. This study confirmed the lymphopenia observed in most of the other series of COVID-19 cases [5–7]. The data discussed here extend these observations, showing that the $CD3^+CD4^+$ and $CD16^+CD56^+$ lymphocyte counts were higher but the $TNF-\alpha$ and $IFN-\gamma$ were lower in COVID-19 patients compared with those of CAP patients.

TABLE 5: Multivariate predictors of cytokines on disease severity.

Variate	COVID-19			CAP and COVID-19		
	OR	95% CI	<i>p</i>	OR	95% CI	<i>p</i>
IFN- γ	1.04	0.76-1.423	0.807	1.017	0.865-1.195	0.841
IL-10	1.187	0.996-1.414	0.055	1.01	0.982-1.038	0.503
IL-2	0.626	0.203-1.926	0.414	1.021	0.461-2.26	0.96
IL-4	1.794	0.971-3.315	0.062	1.265	0.823-1.942	0.283
IL-6	0.998	0.996-1	0.092	0.999	0.997-1.001	0.306
TNF- α	0.361	0.138-0.941	0.037	0.874	0.694-1.101	0.254

The most commonly used lymphocyte subsets are currently detected, including T lymphocytes (CD3⁺), B lymphocytes (CD19⁺), NK cells (CD16⁺⁵⁶⁺), helper T lymphocytes (CD3⁺CD4⁺), and suppressor T lymphocytes (CD3⁺CD8⁺). Percentages and absolute counts of T and B lymphocytes and the ratio of helper/inducer versus suppressor/cytotoxic T cells provide valuable information on immune status for a number of patient conditions [7]. Helper T lymphocytes cells can help B cells secrete antibodies and regulate the immune response of other T cells [9]. It can release IL-2, IFN- γ , IL-4, and other cytokines and activate macrophages and NK cells [10]. Suppressor T lymphocytes cells often exhibit cytotoxic activity and are the major cytotoxic effector cells. As the main immune cells of the body's natural immune system, NK lymphocytes have been shown to be cytotoxic to certain tumors and viruses [11, 12]. Secreted antibodies and mediator humoral immune response are the major functions of B lymphocytes. Activated B lymphocytes can secrete antigens and induce T cell immunity.

Lymphopenia is an important part of COVID-19, and the lymphocyte count may be used to predict the severity of the disease and clinical outcome. Total and subset lymphopenia also occurs in other human coronavirus SARS infections [13]. Experimental coronavirus 229E infections resulted in lymphopenia in humans [14]. The lymphopenia in COVID-19 may be attributed to direct viral invasion and destruction of lymphocytes from SARS-CoV-2. However, studies suggest that the human receptor for COVID-19 could be angiotensin-converting enzyme 2 (ACE2) [15]. ACE2 is the functional cellular receptor for the SARS-CoV-2 but does not express in B or T lymphocytes [16, 17]. This suggests that lymphopenia in COVID-19 is not directly infected and destroyed by SARS-CoV-2 and requires further study.

Other possible explanations for lymphopenia are lymphocyte isolation in the lung where SARS-CoV-2 damage is most pronounced [18], or cytokine-mediated altered lymphocyte transport [7]. Coronavirus 229E can induce apoptosis of monocytes/macrophages in vitro [19]. It is not clear whether different strains of SARS-CoV-2 induce lymphocyte apoptosis. SARS-CoV-2-induced immunosuppression may be predisposed to secondary infection, especially in severely ill patients, and it remains to be determined whether there are any long-term effects on humoral or cell-mediated immunity.

Our findings demonstrated that lymphocyte subsets features, especially CD16⁺CD56⁺%, CD4⁺/CD8⁺ ratio, CD19⁺, and CD3⁺CD4⁺ independently predicted the differentiation

of COVID-19 and CAP. The CD3⁺CD4⁺, CD3⁺CD8⁺ counts, and TNF- α are independent predictors of disease severity. Thus, detection of lymphocyte subsets and cytokines provides new insights into the pathogenesis of COVID-19 and CAP, which is helpful to understand the immune function of patients and is worthy of popularization and application.

Data Availability

The data used to support the findings of this study are included within the article.

Conflicts of Interest

The authors have no conflicts of interest to declare.

Authors' Contributions

Guohong Liu and Xianghu Jiang contributed equally to this work and should be considered as co-first authors.

Acknowledgments

We acknowledge all health-care workers involved in the diagnosis and treatment of patients in Wuhan.


References

- [1] WHO, *Weekly epidemiological update on COVID-19*, 2021, <https://www.who.int/publications/m/item/weekly-epidemiological-update-on-covid-19—23-march-2021>.
- [2] F. Yu, L. Yan, N. Wang et al., "Quantitative detection and viral load analysis of SARS-CoV-2 in infected patients," *Clinical Infectious Diseases*, vol. 71, no. 15, pp. 793–798, 2020.
- [3] J. Qiu, "Covert coronavirus infections could be seeding new outbreaks," *Nature*, 2020.
- [4] N. Yu, W. Li, Q. Kang et al., "Clinical features and obstetric and neonatal outcomes of pregnant patients with COVID-19 in Wuhan, China: a retrospective, single-centre, descriptive study," *The Lancet Infectious Diseases*, vol. 20, no. 5, pp. 559–564, 2020.
- [5] T. Chen, D. I. Wu, H. Chen et al., "Clinical characteristics of 113 deceased patients with coronavirus disease 2019: retrospective study," *BMJ*, vol. 368, p. m1091, 2020.
- [6] G. Zhang, J. Zhang, B. Wang, X. Zhu, Q. Wang, and S. Qiu, "Analysis of clinical characteristics and laboratory findings of 95 cases of 2019 novel coronavirus pneumonia in Wuhan, China: a retrospective analysis," *Respiratory Research*, vol. 21, no. 1, p. 74, 2020.

- [7] G. Chen, D. Wu, W. Guo et al., "Clinical and immunological features of severe and moderate coronavirus disease 2019," *The Journal of Clinical Investigation*, vol. 130, no. 5, pp. 2620–2629, 2020.
- [8] Y. Pan, G. Ye, X. Zeng et al., "Can routine laboratory tests discriminate SARS-CoV-2-infected pneumonia from other causes of community-acquired pneumonia?" *Clinical and Translational Medicine*, vol. 10, no. 1, pp. 161–168, 2020.
- [9] S. H. Cho, A. L. Raybuck, J. Blagih et al., "Hypoxia-inducible factors in CD4(+) T cells promote metabolism, switch cytokine secretion, and T cell help in humoral immunity," *Proceedings of the National Academy of Sciences of the United States of America*, vol. 116, no. 18, pp. 8975–8984, 2019.
- [10] T. Kido, K. Ishiwata, M. Suka, and H. Yanagisawa, "Inflammatory response under zinc deficiency is exacerbated by dysfunction of the T helper type 2 lymphocyte-M2 macrophage pathway," *Immunology*, vol. 156, no. 4, pp. 356–372, 2019.
- [11] C. Zhang, X. M. Wang, S. R. Li et al., "NKG2A is a NK cell exhaustion checkpoint for HCV persistence," *Nature Communications*, vol. 10, no. 1, p. 1507, 2019.
- [12] C. Zhang, Y. Hu, and C. Shi, "Targeting natural killer cells for tumor immunotherapy," *Frontiers in Immunology*, vol. 11, p. 60, 2020.
- [13] C. K. Fan, K. M. Yieh, M. Y. Peng, J. C. Lin, N. C. Wang, and F. Y. Chang, "Clinical and laboratory features in the early stage of severe acute respiratory syndrome," *Journal of Microbiology, Immunology, and Infection*, vol. 39, no. 1, pp. 45–53, 2006.
- [14] K. A. Callow, H. F. Parry, M. Sergeant, and D. A. J. Tyrrell, "The time course of the immune response to experimental coronavirus infection of man," *Epidemiology and Infection*, vol. 105, no. 2, pp. 435–446, 1990.
- [15] M. Letko, A. Marzi, and V. Munster, "Functional assessment of cell entry and receptor usage for SARS-CoV-2 and other lineage B betacoronaviruses," *Nature Microbiology*, vol. 5, no. 4, pp. 562–569, 2020.
- [16] W. Li, M. J. Moore, N. Vasilieva et al., "Angiotensin-converting enzyme 2 is a functional receptor for the SARS coronavirus," *Nature*, vol. 426, no. 6965, pp. 450–454, 2003.
- [17] I. Hamming, W. Timens, M. L. C. Bulthuis, A. T. Lely, G. J. Navis, and H. van Goor, "Tissue distribution of ACE2 protein, the functional receptor for SARS coronavirus. A first step in understanding SARS pathogenesis," *The Journal of Pathology*, vol. 203, no. 2, pp. 631–637, 2004.
- [18] Z. Xu, L. Shi, Y. Wang et al., "Pathological findings of COVID-19 associated with acute respiratory distress syndrome," *The Lancet respiratory medicine*, vol. 8, no. 4, pp. 420–422, 2020.
- [19] A. R. Collins, "In vitro detection of apoptosis in monocytes/macrophages infected with human coronavirus," *Clinical and Diagnostic Laboratory Immunology*, vol. 9, no. 6, pp. 1392–1395, 2002.

Research Article

1 α ,25-Dihydroxyvitamin D3 Supplementation during Pregnancy Is Associated with Allergic Rhinitis in the Offspring by Modulating Immunity

Liqing Zhang,¹ Haifeng Ni ,² Zhen Zhou,² Xiaoyang Yuan,² Junbo Xia,² Bo Jiang,² and Yong Li ²

¹Department of Otolaryngology, Tongxiang First People's Hospital, Tongxiang, Zhejiang 314500, China

²Department of Otolaryngology, Affiliated Hangzhou First People's Hospital, Zhejiang University School of Medicine, Hangzhou, Zhejiang 310006, China

Correspondence should be addressed to Haifeng Ni; nihaifeng138@163.com and Yong Li; leeyung828@sina.com

Received 5 November 2020; Revised 1 March 2021; Accepted 25 March 2021; Published 15 April 2021

Academic Editor: Zhipeng Xu

Copyright © 2021 Liqing Zhang et al. This is an open access article distributed under the Creative Commons Attribution License, which permits unrestricted use, distribution, and reproduction in any medium, provided the original work is properly cited.

Background. Maternal supplementation with 1 α ,25-dihydroxyvitamin D3 (VD3) has immunologic effects on the developing fetus through multiple pathways. This study was aimed at investigating the effects of VD3 supplementation on immune dysregulation in the offspring during allergic rhinitis. **Methods.** Different doses of VD3 as well as control were given to pregnant female mice. Ovalbumin (OVA) challenge and aluminum hydroxide gel in sterile saline were used to induce allergic rhinitis in offspring mice. Nasal lavage fluids (NLF) were collected, and eosinophils were counted in NLF 24 hours after the OVA challenge. Th1, Th2, Th17, and Treg subtype-relevant cytokines, including IFN- γ , IL-4, IL-10, IL-17, TGF- β , and OVA-IgE levels from the blood and NLF of offspring mice, were detected by the enzyme-linked immunosorbent assay (ELISA) method. The Treg subtype was analyzed by flow cytometry. Treg cells were purified from offspring and were adoptively transferred to OVA-sensitized allogenic offspring mice. The outcomes were assessed in allogenic offspring. **Results.** Our data showed that VD3 supplementation significantly decreased the number of eosinophils, basophils, and lymphocytes in the peripheral blood and NLF. The proportion of CD4⁺CD25⁺FoxP3⁺Tregs had a positive correlation with VD3 in a dose-dependent manner. The levels of serum IgE, IL-4, and IL-17 were decreased while the expressions of IFN- γ , IL-10, and TGF- β were significantly enhanced in VD3 supplementation groups. Adoptive transfer CD4⁺CD25⁺FoxP3⁺Tregs of VD3 supplementation groups promoted Th1 and suppressed Th2 responses in the offspring during allergic rhinitis. **Conclusion.** Our findings indicated that low dose VD3 supply in pregnant mice's diet suppressed Th2 and Th17 responses in allergic rhinitis by elevating the Th1 subtype and the proportion of CD4⁺CD25⁺FoxP3⁺Tregs in offspring. It suggested that low dose VD3 supply may have the potential to act as a new therapeutic strategy for allergic rhinitis.

1. Introduction

Allergic rhinitis (AR) is one of the most common allergic diseases with progressively increasing prevalence, which affects 36%-40% of children and 10%-30% of adults [1, 2]. AR is a hypersensitivity disease mediated by specific IgE in response to allergens, which is characterized by a destructive balance of Th1 (T helper type 1)/Th2 (T helper type 2) cytokine with Th2 skewing [3]. Although both environmental

factors and genetic susceptibility are confirmed to play critical roles in the development of AR [4], its exact pathogenesis remains unknown.

1 α ,25-Dihydroxyvitamin D3 (VD3) was initially characterized for its role in bone metabolism, but recent researches confirmed that it also could regulate the function of various immunocytes and nonimmune cells, including monocytes, dendritic cells, T and B lymphocytes, epithelial cells, and so on [5]. Furthermore, VD3 receptors have also been identified

in almost all immunocytes. Most of the immunocytes can also convert vitamin D into VD3 by expressing VD3-activating enzymes [6, 7].

Recent studies have investigated the relationship between the level of VD3 and the incidence of AR [8, 9]. AR incidence was found to decline as VD3 levels increased [10]. A Norwegian study found similar results in women but converse results in men [11]. However, the other study showed that no association between VD3 levels and the incidence of AR has been found [12]. Hence, the relationship between VD3 levels and AR incidences remains unclear, and the role of VD3 in AR appears to be more complex. VD3 deficiency during pregnancy is fairly prevalent in most countries. It was reported that maternal VD3 status during pregnancy may affect the developing immune system of the offspring [13]. For example, a few studies showed that maternal VD3 intake from foods during pregnancy decreased the risk of AR in less than 5-year-old children [14, 15]. However, the other reports showed that intake of VD3 in pregnant women did not have any effects on the incidence of AR in children [16], even increasing the incidence of AR in adulthood [17, 18]. Evidently, the relationship between the VD3 maternal intake during pregnancy and the AR incidence of its offspring should be confirmed by further experiments.

CD4⁺CD25⁺FoxP3⁺Tregs cells have been shown to be critical in the maintenance of immune responses and T cell homeostasis, which suppresses Th2 responses in allergic conditions [19]. Low dose VD3 could promote the proliferation of CD4⁺CD25⁺FoxP3⁺Tregs to induce antigen-specific tolerance in immune-mediated conditions [20]. As we know, naïve T cells can change into different subtypes like Th1, Th2, Th17, and Treg in different culture conditions [21, 22]. Th1, Th2, Th17, and Treg characterize with specific transcription factors and cytokines, which are T-bet and IFN- γ for Th1, GATA-3 and IL-4 for Th2, RoRyt and IL-12 for Th17, Foxp3 and CD25 for Treg. Therefore, VD3 supplementation may disrupt the balance of these T lymphocyte subtypes.

Based on these previous studies, we hypothesize that low dose VD3 may suppress Th2 responses to allergens in AR by elevating CD4⁺CD25⁺FoxP3⁺Tregs. In this study, pregnant female mice were supplemented with different low doses of VD3 first; the Th1, Th2, and Th17 responses to allergens in offspring mice were assessed; and the quantity and ability of CD4⁺CD25⁺FoxP3⁺Tregs in offspring mice were detected. The aim of this study was to investigate the optimal dose of VD3 as a supplement for pregnant mice's diet to successfully decrease the allergic rhinitis incidence of their offspring via regulating T lymphocyte functions.

2. Methods

2.1. Animals and Reagents. A total of 25 eight-week-old female BALB/c mice were purchased from the Animal Resources Centre (Nanjing, China). The animals were raised in a constant-temperature environment at $22 \pm 2^\circ\text{C}$, with a regular 12-hour light/dark cycle. Ovalbumin (OVA) and VD3 were obtained from Sigma (St. Louis, Mo, USA). The enzyme-linked immunosorbent assay (ELISA) kits for mouse VD3, IL-4, IL-10, IFN- γ , IL-17, TGF- β , and OVA-IgE were

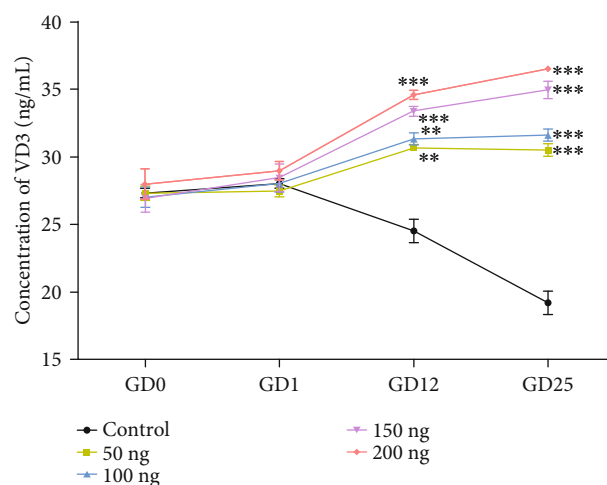


FIGURE 1: The response of the serum VD3 levels of pregnant mice to different doses of VD3. There was a positive dose-dependent manner between the supplementation time and the concentration of VD3. Values are mean \pm SEM ($n = 5$). GD: gestation day. ** $P < 0.01$ vs. control and *** $P < 0.001$ vs. control.

obtained from Abcam (Cambridge, MA, USA). Mouse Treg Flow Kit (FOXP3 Alexa Fluor[®] 488/CD4 APC/CD25 PE) was purchased from BioLegend, San Diego, CA.

2.2. Mating, Parturition, Offspring, and Preparation of Animal Model. The female mice were allowed to mate with males at a 2:1 ratio, and mating was confirmed by observing the vaginal smear. Female mice showing sperm in the smear were separated on the day of detection, and this was considered as gestation day (GD) 0. The day on which mice were born before 4:00 pm was designated as postnatal day (PND) 0. Offspring mice remained with their mothers until weaned at PND 21. Twenty-five pregnant female mice were randomly divided into 5 groups ($n = 5$). The control group received subcutaneous injections of 1 mL of 0.9% saline; the 50 ng, 100 ng, 150 ng, and 200 ng VD3 groups were correspondingly given 50 ng, 100 ng, 150 ng, and 200 ng (diluting to 1 mL used 0.9% saline, equal to 100, 200, 300, and 400 IU/kg/daily) VD3 by subcutaneous injections once a day during pregnancy. Blood was obtained from the pregnant female mice to test the level of VD3 at GD 0, 1, 12, and 25.

2.3. Sensitization and Challenge for Offspring Mice. To establish allergic rhinitis mouse models, six-week-old offspring were first sensitized with an intraperitoneal injection of 50 μg OVA and 5 mg aluminum hydroxide gel in sterile saline from days 0 to 2. After systemic sensitization, mice were locally challenged by intranasal instillation with 50 μg OVA and 50 μL phosphate-buffered saline (PBS) into their nostrils from day 7 to day 12. After the last challenge, frequency of sneezing and nose rubbing behavior was recorded for at least 15 min.

2.4. Eosinophil Counts in Nasal Lavage Fluid. Nasal lavage fluids (NLF) were collected 24 hours after the last intranasal challenge with OVA through a pulmonary lavage technique

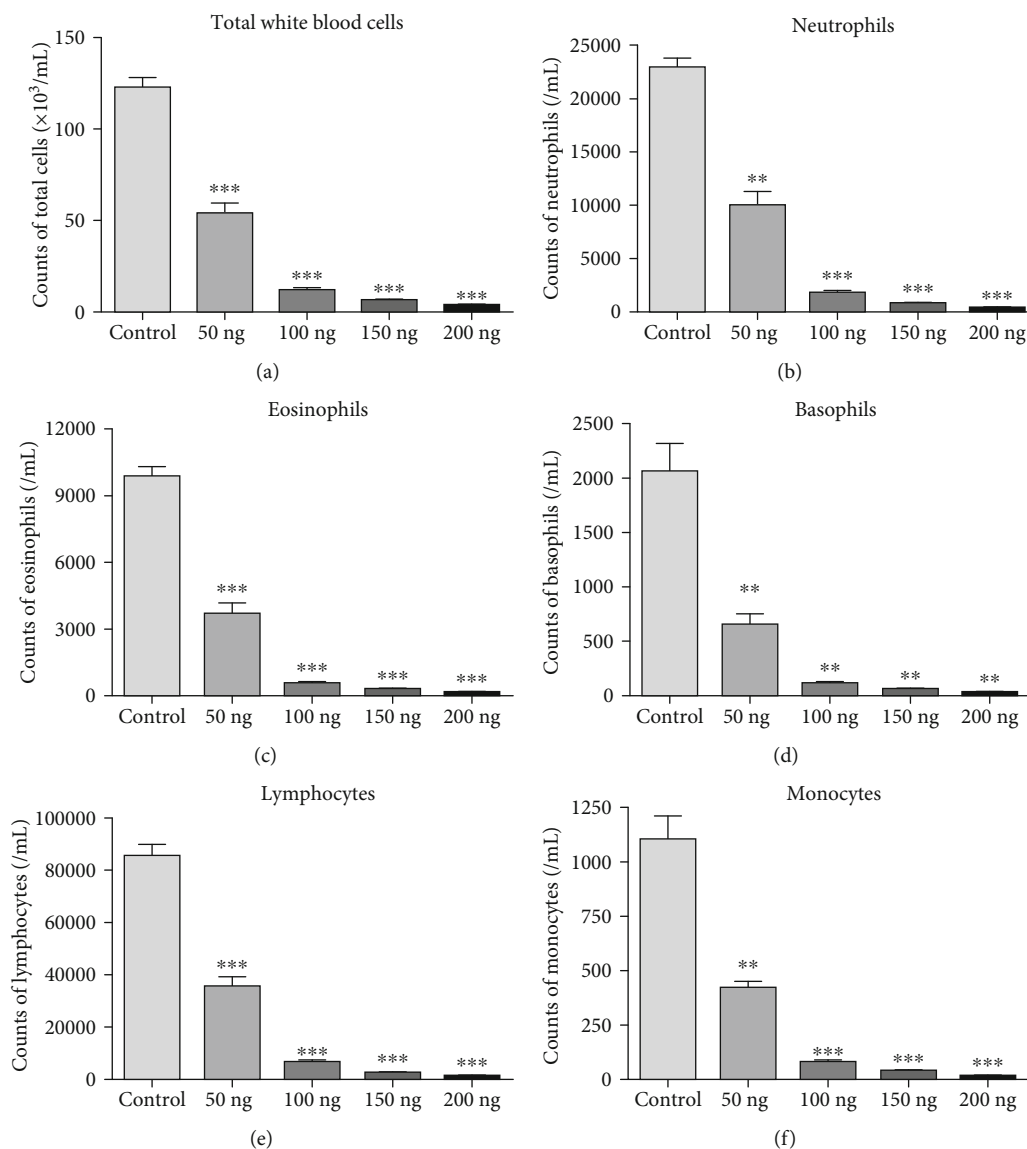


FIGURE 2: Immune cells were counted in offspring mice from VD3-treated group: (a) total white blood cells, (b) neutrophils, (c) eosinophils, (d) basophils, (e) lymphocytes, and (f) monocytes were counted by mouse cell count machine from peripheral blood of offspring mice. * $P < 0.05$ VD3 treatment vs. control; ** $P < 0.01$ VD3 treatment vs. control; *** $P < 0.001$ VD3 treatment vs. control.

with sterile saline. Total cell numbers in NLF were determined in duplicates with a hemocytometer. Eosinophils were stained with the Wright-Giemsa and 500 cells were counted in total from each sample at a magnification of $\times 200$ (oil immersion).

2.5. Serum OVA-Specific IgE and Cytokine Detection in Peripheral Blood and Nasal Mucosa Tissues. Blood (0.1 mL) and nasal mucosa tissue were collected from offspring mice. The serum was obtained from blood by centrifugation at 3000 revolutions per minute (rpm) for 10 minutes at 4°C . The nasal mucosa was homogenated and centrifuged at 3000 rpm for 10 minutes at 4°C , and the supernatants were collected for cytokine detection. The levels of IL-4, IL-10, IFN- γ , and OVA-IgE in peripheral blood and nasal mucosa tissues were assessed by an ELISA kit.

2.6. The Analysis of $\text{CD4}^+\text{CD25}^+\text{FoxP3}^+$ Tregs by Flow Cytometry. The flow cytometry assay was carried out according to the manufacturer's guidelines. Briefly, spleens from offspring were processed to prepare splenocytes. A Mouse Treg Flow Kit was used to double stain the collected and enriched CD4^+ T cells with fluorescence-conjugated antibodies (CD25-phycoerythrin and CD4-allophycocyanin); then, the cells were stained with Alexa Fluor 488-conjugated FoxP3 antibody. $\text{CD4}^+\text{CD25}^+\text{FoxP3}^+$ Tregs were analyzed by flow cytometry.

2.7. Adoptive Transfer of $\text{CD4}^+\text{CD25}^+\text{FoxP3}^+$ Tregs into OVA-Sensitized Allogenic Offspring. Briefly, $\text{CD4}^+\text{CD25}^+\text{FoxP3}^+$ Tregs were purified from offspring in each group and 5×10^4 cells were resuspended in 0.2 mL 0.9% saline and then were

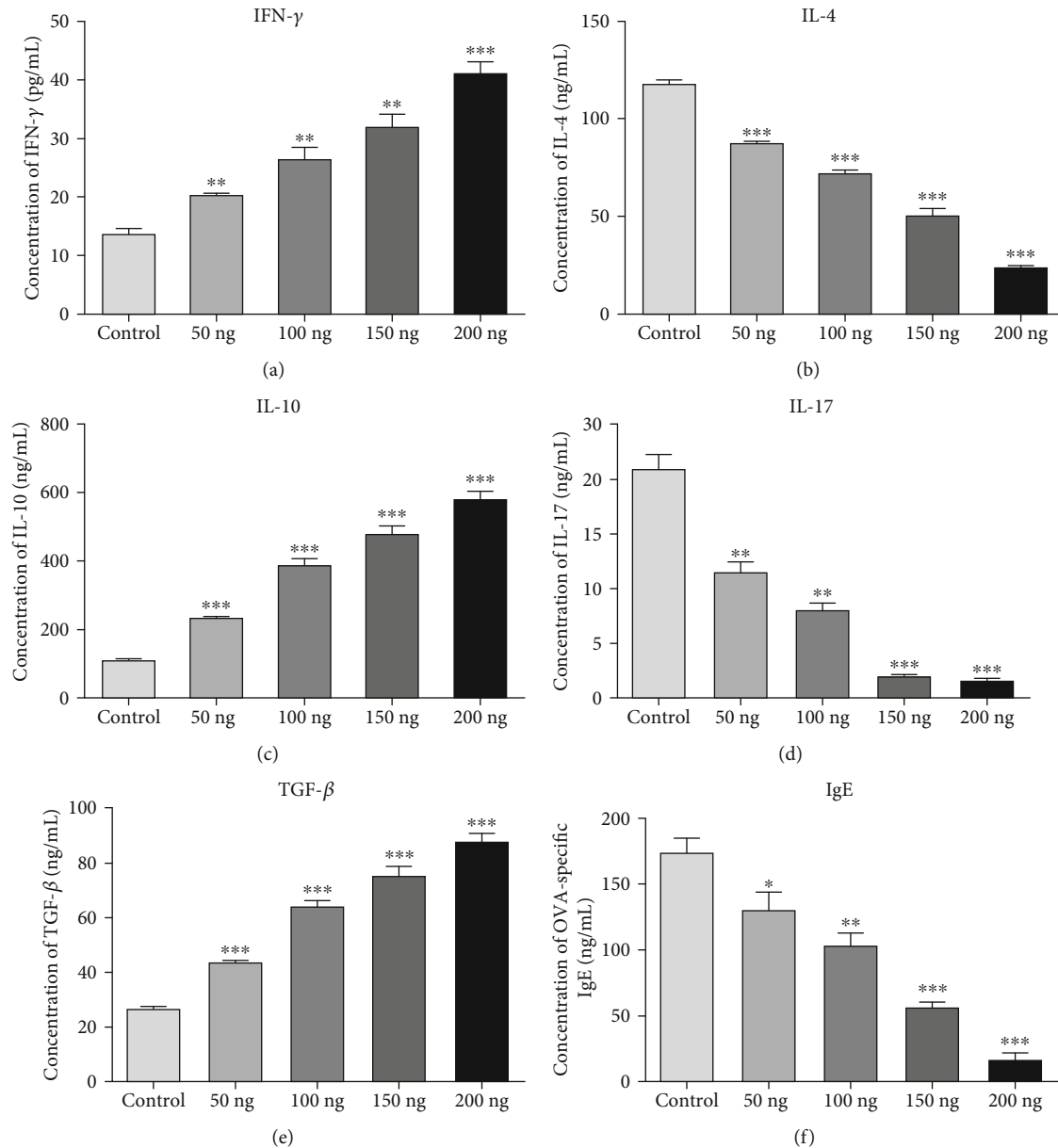


FIGURE 3: Cytokines were measured by ELISA in offspring mice from VD3-treated groups: (a) IFN- γ , (b) IL-4, (c) IL-10, (d) IL-17, (e) TGF- β , and (f) IgE from peripheral blood of offspring mice in VD3-treated and control groups were measured by ELISA. * $P < 0.05$ vs. control, ** $P < 0.01$ vs. control, and *** $P < 0.001$ vs. control.

adoptively transferred through the tail vein of a corresponding group of OVA-sensitized allogenic offspring. 24 hours later, the same outcomes were assessed in allogenic offspring.

2.8. Statistical Analysis. All statistical analyses were performed using the GraphPad Prism 5.0 (San Diego, CA, USA) and SPSS 21.0 version (Chicago, IBM Inc., USA). Data are expressed as the mean \pm SEM. Statistical significance of the pregnancy supplementation days and level of serum VD3 administration was calculated using two-way ANOVA with Bonferroni post hoc tests. Independent-sample T test was used to compare between each VD3 group and the control group. Pearson's correlation analysis was used to determine if there was a correlation between the aforementioned

parameters. * $P < 0.05$, ** $P < 0.01$, and *** $P < 0.001$ were considered statistically significant.

2.9. Ethics Approval and Consent to Participate. All animal care and experimental protocols were approved by the Institutional Animal Care and Use Committee (INHA 150309-351-2). The study was approved by the local ethics committee of Hangzhou First People's Hospital, China (approval ID: 201710701).

3. Results

3.1. Serum VD3 levels of Pregnant Mice. The serum VD3 levels in pregnant mice after different doses of VD3 injection

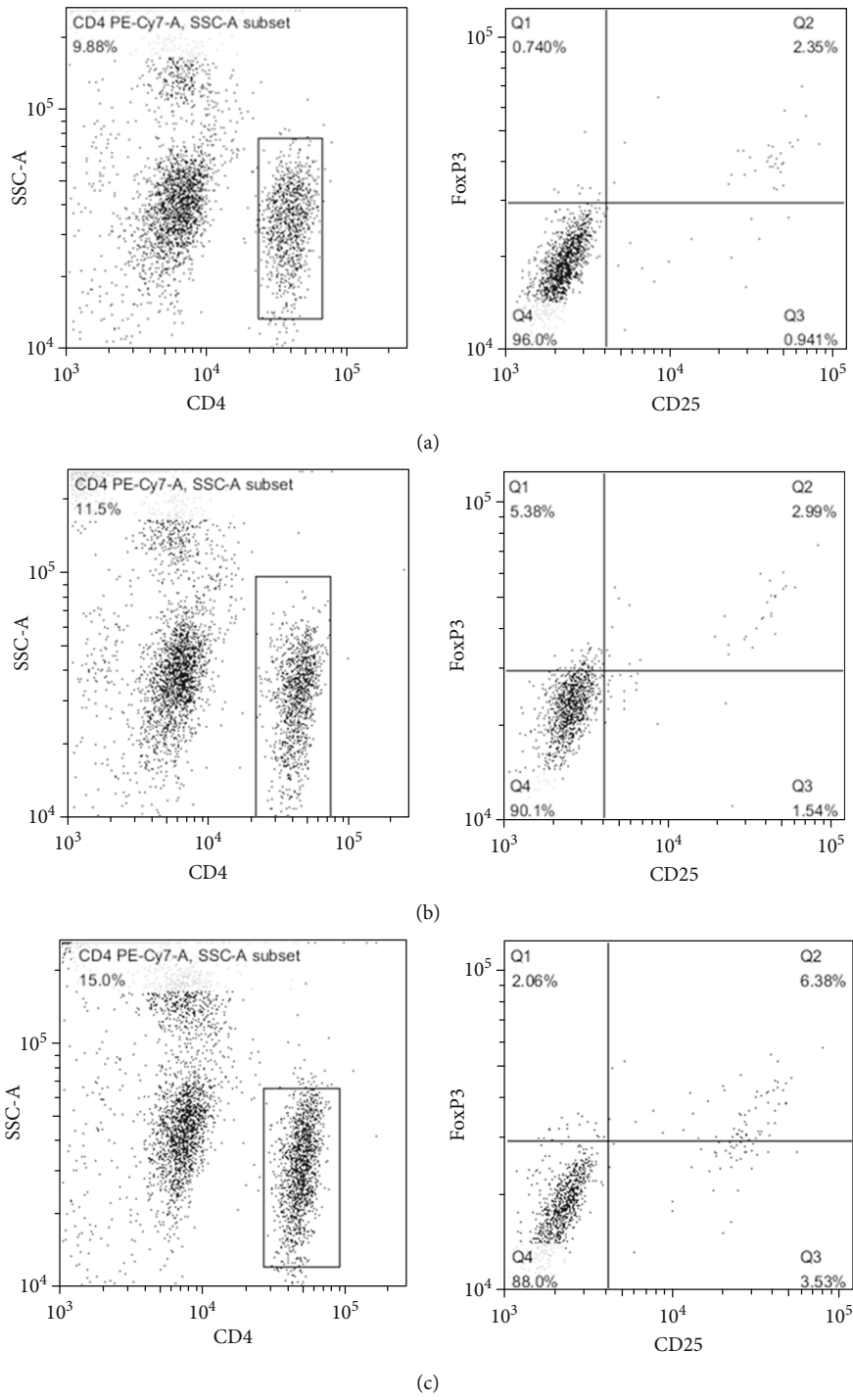


FIGURE 4: Continued.

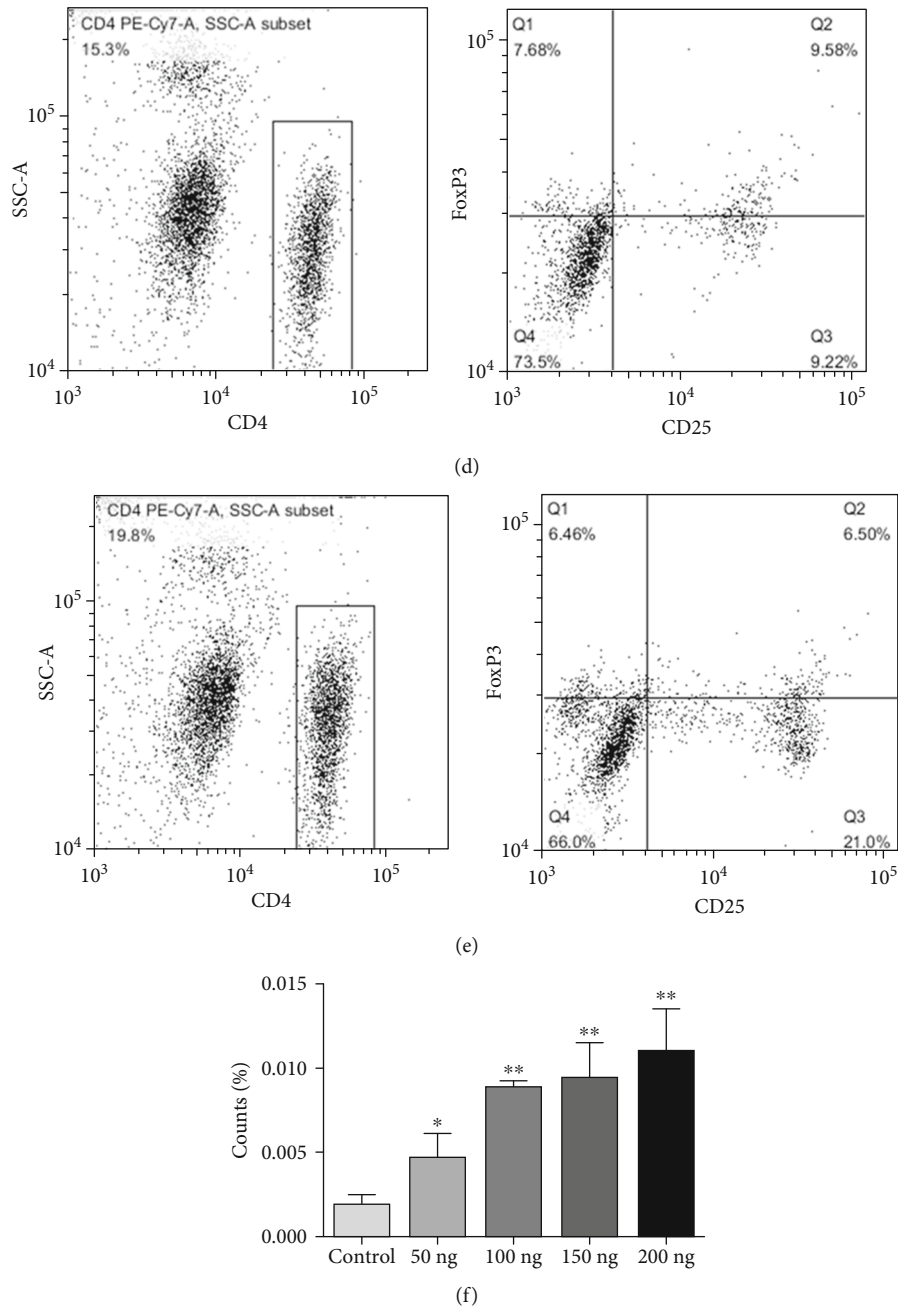


FIGURE 4: The proportion of $CD4^+CD25^+FoxP3^+$ Tregs in VD3 groups from offspring. Compared with control group (a), the proportion of $CD4^+CD25^+FoxP3^+$ Tregs was elevated in VD3 groups (b) 50 ng, (c) 100 ng, (d) 150 ng, and (e) 200 ng groups) from offspring in a dose dependency (f). Values are mean \pm SEM ($n = 5$), * $P < 0.05$ vs. control and ** $P < 0.01$ vs. control.

are illustrated in Figure 1. We found that the VD3 levels of pregnant mice were the same baseline at GD0 and GD1. During pregnancy, the VD3 concentration persistently decreased in the control group; however, it stably increased in all VD3 groups. Compared with the control group, the serum VD3 levels in the VD3 group had no significant difference at GD0 and GD1. However, significant differences were found at GD12 and GD25. Furthermore, the levels of VD3 in pregnant mice were increased in a supplementation time and the concentration in a VD3-dependent manner.

3.2. VD3 Maternal Supplementation Influenced Immune Response of the Offspring during AR. To investigate the effects of VD3 maternal supplementation on immune response, we measured immune cell profiles in the peripheral blood of offspring mice. The results are shown in Figures 2(a)–2(f). Total white blood cells, neutrophils, eosinophils, basophils, lymphocytes, and monocytes were significantly decreased in a VD3 dose-dependent manner. We further detected the levels of $IFN-\gamma$, IL-4, IL-10, IL-17, $TGF-\beta$, and IgE in peripheral blood by ELISA (Figure 3). It was found that the levels of

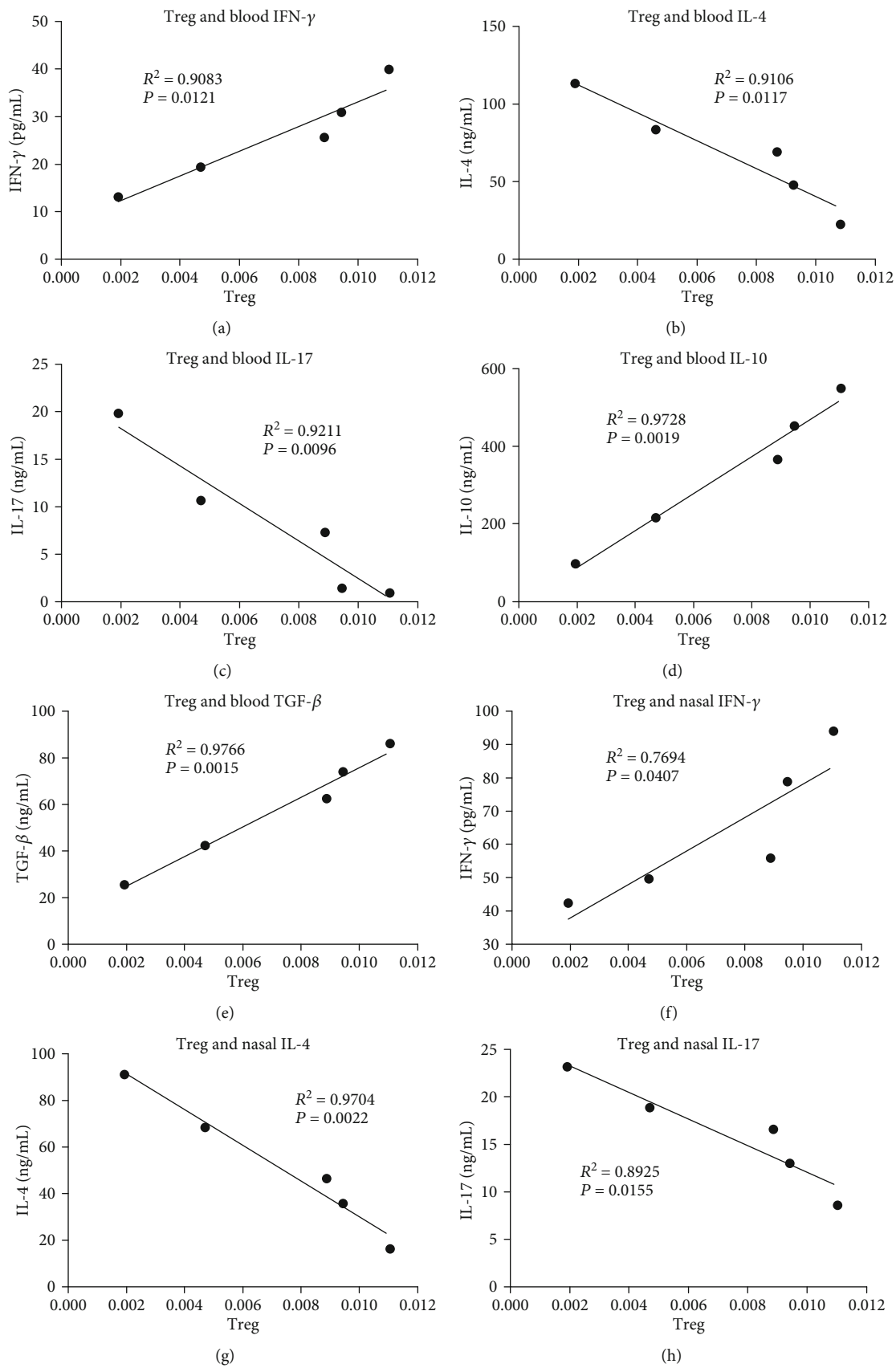


FIGURE 5: Continued.

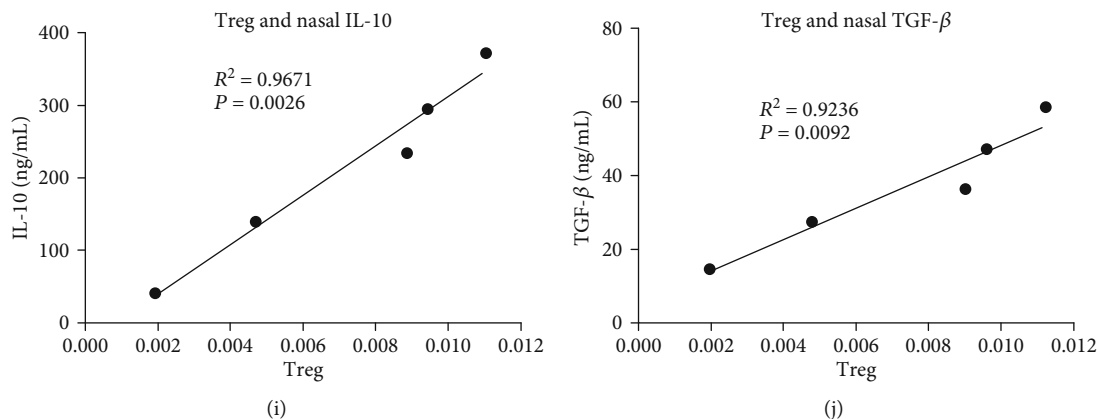


FIGURE 5: The correlation analyses of cytokine levels and the Treg cell number were analyzed in allogenic offspring after transferring $CD4^+CD25^+FoxP3^+$ Tregs from offspring in VD3 groups. (a) Treg and IFN- γ , (b) Treg and IL-4, (c) Treg and IL-17, (d) Treg and IL-10, and (e) Treg and TGF- β from peripheral blood of offspring mice with VD3 administration were analyzed for their correlation. (f) Treg and IFN- γ , (g) Treg and IL-4, (h) Treg and IL-17, (i) Treg and IL-10, and (j) Treg and TGF- β from NLF of offspring mice with VD3 administration were analyzed for their correlation.

IFN- γ , IL-10, and TGF- β in the peripheral blood of offspring mice were dramatically elevated with VD3 administration (Figures 3(a), 3(c), and 3(e)). In contrast, IL-4 and IL-17 levels were markedly declined in a VD3 dose-dependent manner (Figures 3(b) and 3(d)). We also found that there was a positive correlation between the IgE and IL-4 levels in the peripheral blood with a VD3 supplementation dose (Figure 3(f)).

3.3. The Proportion of $CD4^+CD25^+FoxP3^+$ Tregs in VD3 Treated Groups from Offspring by Flow Cytometry. In addition, we also analyzed $CD4^+CD25^+FoxP3^+$ Tregs by flow cytometry. Compared with the control group, the proportion of $CD4^+CD25^+FoxP3^+$ Tregs was elevated (Figures 4(a)–4(e)). There was also a positive correlation between the $CD4^+CD25^+FoxP3^+$ Tregs proportion and the VD3 supplementation dose (Figure 4(f)).

3.4. Adoptive Transfer $CD4^+CD25^+FoxP3^+$ Tregs from Offspring of VD3 Groups Reduce Serum IgE, Th2, and IL-17 Cytokine and Increase Th1 Cytokine in OVA-Sensitized Allogenic Offspring. To investigate whether the effects of vitamin D3 maternal supplementation on immune regulation depends on Treg cells, we transferred $CD4^+CD25^+FoxP3^+$ Tregs from VD3 groups to OVA-sensitized allogenic offspring. After the adoptive transfer of $CD4^+CD25^+FoxP3^+$ Tregs to allogenic offspring, there was a positive correlation between the number of Tregs and IFN- γ or IL-10 or TGF- β in either the peripheral blood (Figures 5(a), 5(d), and 5(e)) or NLF (Figures 5(f), 5(i), and 5(j)) from the VD3 group compared with the control group. In contrast, the levels of IL-4 and IL-17 in the peripheral blood (Figures 5(b) and 5(c)) and NLF (Figures 5(g) and 5(h)) had a negative correlation with the adoptively transferred Treg cell number increase in VD3-treated groups compared with the control group. We further explored the relationship among IFN- γ , IL-4, IL-10, IL-17, and TGF- β cytokines in a Treg cell adoptive transfer (Figure 6). The

results showed that the IL-4 and IL-17 levels with IFN- γ had a negative correlation (Figures 6(a) and 6(c)) in Treg cell adoptive transferred groups in VD3-treated mice. In contrast, there was a positive correlation between IFN- γ and IL-10 or TGF- β (Figures 6(b) and 6(d)). We also found that there was a negative correlation between IL-4 and IL-10 (Figure 6(e)), IL-4 and TGF- β (Figure 6(g)), IL-10 and IL-17 (Figure 6(h)), and TGF- β and IL-17 (Figure 6(j)) in Treg-transferred mice. There was a positive correlation between IL-4 and IL-17 (Figure 6(f)) and IL-10 and TGF- β (Figure 6(i)). The results indicated that Treg cell transfer promoted Th1, but inhibited Th2 and Th17 cell development.

4. Discussion

Although the associations between VD3 and clinical outcomes have been identified, there has been much less progress in elucidating the underlying *in vivo* biologic mechanism for this association. In this study, we found that VD3 was gradually decreased in the control group during pregnancy, while VD3 was gradually increased in all VD3 groups. This phenomenon was dose-dependent on the supplementation time and the concentration of VD3. Thus, maternal VD3 supplementation during pregnancy could remarkably increase serum VD3 levels.

Several studies *in vitro* found that VD3 could directly promote mature B-cell apoptosis [7]. Furthermore, VD3 also could inhibit antigen-specific B-cell proliferation and antibody secretion. Milovanovic et al. demonstrated that VD3 inhibited IgE production by B-cell [23]. Another study also reported that VD3 supplementation at weaning significantly reduced the serum IgE levels [13]. In our study, we also confirmed that the levels of serum IgE in the peripheral blood were significantly decreased in the offspring of the VD3 group compared with the control group. On the contrary, Matheu et al. reported that IgE production was increased in allergic airway disease mice that were treated early with VD3 [24]. Interestingly, Drozdenko et al. found that there

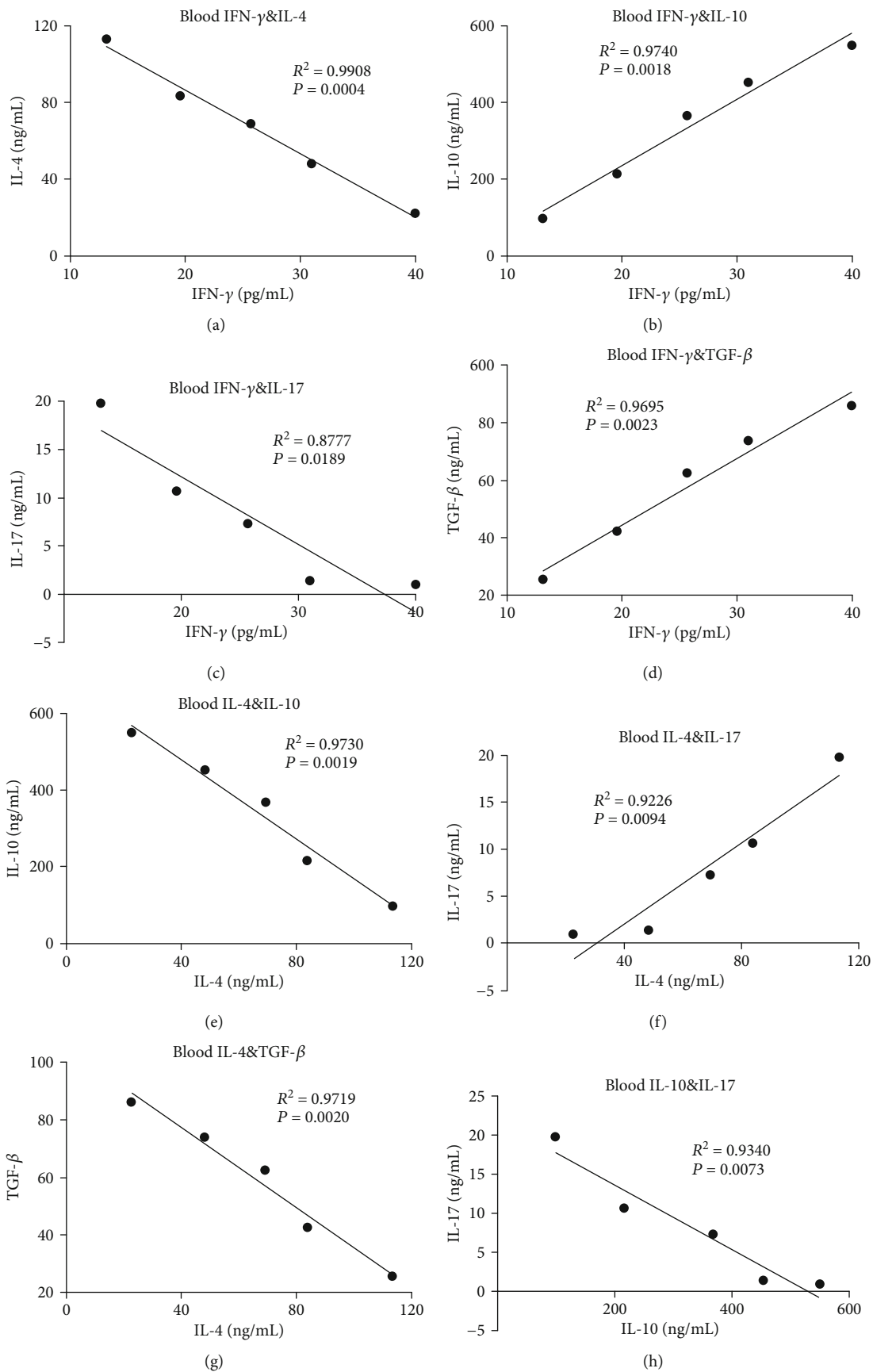


FIGURE 6: Continued.

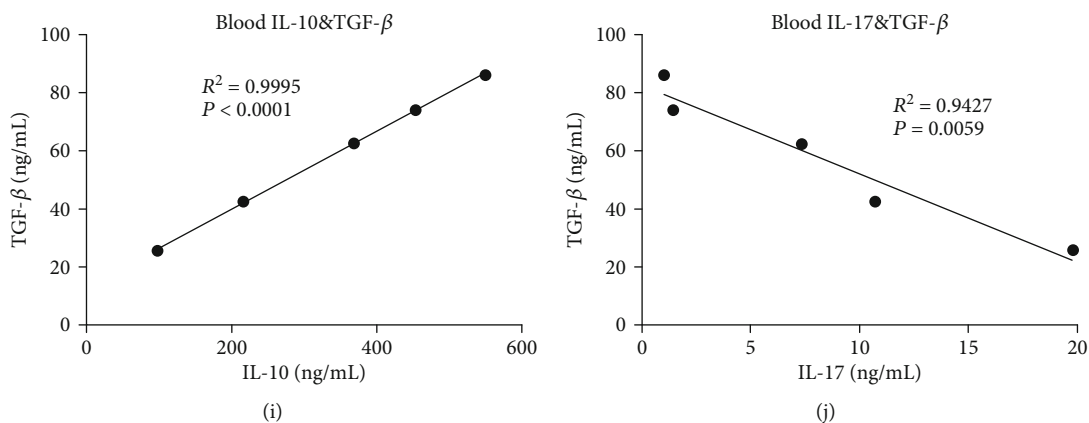


FIGURE 6: The correlation analyses of cytokines from peripheral blood were analyzed in allogenic offspring after transferring $CD4^+CD25^+FoxP3^+$ Tregs: (a) IFN- γ and IL-4, (b) IFN- γ and IL-10, (c) IFN- γ and IL-17, (d) IFN- γ and TGF- β , (e) IL-4 and IL-10, (f) IL-4 and IL-17, (g) IL-4 and TGF- β , (h) IL-10 and IL-17, (i) IL-10 and TGF- β , and (j) TGF- β and IL-17 from peripheral blood of offspring mice with Treg cells transferred in VD3 administration were analyzed for their correlation.

were no significant differences in the frequencies of antibody secreting plasma cells and serum immunoglobulin concentrations in humans after VD3 intake [25]. Similarly, our results also found that maternal VD3 supply during pregnancy significantly decreased serum IgE levels of the offspring in a dose-dependent manner. Furthermore, serum IgE levels have a positive correlation with IL-4 and IL-17 levels and a negative correlation with IL-10, TGF- β , and IFN- γ levels in offspring. As we know, IFN- γ , IL-4, and IL-17 are secreted from Th1, Th2, Th17, respectively [26, 27]. Our result revealed that VD3 might promote Th1, but inhibited Th2 and Th17 cell development.

It was reported that VD3 could recruit eosinophils to noninflammatory sites by regulating C-X-C chemokine receptor type 4 expression [28]. El-Shazly and Lefebvre demonstrated that VD3 modulated a novel inflammatory crosstalk between NK cells and eosinophils via the IL-15/IL-8 axis [29]. Yip et al. also confirmed that VD3 regulated mast cell function and played an anti-inflammatory effect *in vitro* and *in vivo* [30]. Matheu et al. reported that early treatment with VD3 significantly ameliorated eosinophil infiltration in bronchoalveolar lavage fluid and lung tissue with inferior levels of IL-5 [24]. Another study also reported that VD3 supply at weaning significantly reduced pulmonary eosinophilia [13]. In our study, we also confirmed that maternal VD3 supply during pregnancy significantly decreased eosinophils, neutrophils, basophils, lymphocytes, and monocytes in the peripheral blood and NLF of the offspring in a dose-dependent manner with statistical difference. This result indicated that VD3 administration can significantly decrease IgE secreting cells.

The study showed a clear efficacy of the food supplement VD3 in the relief of the signs and symptoms of seasonal allergic rhinitis and in the reduction of the consumption of anti-allergic drugs [31]. Compared with sensitized mice without specific immunotherapy or specific immunotherapy alone, the levels of IL-4 were reduced by VD3 plus specific immunotherapy [32]. Perinatal VD3 deficiency alone promoted Th2 skewing and reduced IL-10-secreting T regulatory cells.

Furthermore, perinatal VD3 deficiency contributed to asthma severity with worse eosinophilic inflammation and airway remodeling in neonates. Importantly, supplementation with VD3 improves both of these pathological abnormalities [13]. In our study, the same results were found wherein maternal VD3 supply during pregnancy significantly increased Th1 cytokine IFN- γ levels and reduced Th2 cytokine IL-4 and Th17 cytokine IL-17 levels of the offspring in a dose-dependent manner. Ozkara et al. reported similar results that VD3 levels showed a negative correlation with IL-4 levels and a positive correlation with IFN- γ levels in nasal polyposis patients together with allergic rhinitis [33]. $CD4^+CD25^+FoxP3^+$ Tregs have been confirmed to play a pivotal role in allergic diseases such as asthma, hay fever, and allergic rhinitis [34]. $CD4^+CD25^+FoxP3^+$ Tregs were capable of suppressing Th2 responses to allergens in allergic conditions [35]. The positive correlation between VD3 and Foxp3 $^+$ Tregs in the airways was observed in a severe pediatric asthma cohort. Equally, *in vitro* VD3 could selectively expand Foxp3 $^+$ Tregs [20]. On the other hand, VD3-induced IL-10 production by T cells and IL-10 together with VD3 also acted as a positive autocrine factor for further IL-10 production [36]. VD3 also promotes regulatory immune pathways via generation of tolerogenic antigen presenting cells and Foxp3 $^+$ Tregs or IL-10 [37]. In our study, we confirmed that *in vivo* absolute numbers of $CD4^+CD25^+FoxP3^+$ Tregs in the offspring from pregnant mice with different doses of VD3 were remarkably elevated in a dose-dependent manner. Furthermore, the proportion of $CD4^+CD25^+FoxP3^+$ Tregs has a positive correlation with IL-10, TGF- β , and IFN- γ levels, and a negative correlation with IL-4, IL-17, and IgE levels in offspring. In addition, we examined the expression of cytokines in the allogenic offspring after adoptively transferring $CD4^+CD25^+FoxP3^+$ Tregs cells from VD3 supplementation offspring. Our results indicated that VD3 strengthens the ability of $CD4^+CD25^+FoxP3^+$ Tregs to suppress Th2 and Th17 responses and enhance Th1 responses. These results further clarified that the effects of VD3 supplementation during pregnancy on immune regulation was dependent on $CD4^+CD25^+FoxP3^+$ Tregs. Our results

were consistent with the results of Gorman and Vijayendra reports *in vitro* and *in vivo* [38]. The present study indicated that low dose VD3 supplementation during pregnancy might suppress Th2 responses and enhance Th1 responses to OVA-induced AR by elevating the absolute numbers and strengthening the ability of CD4⁺CD25⁺FoxP3⁺Tregs in offspring. It is suggested that VD3 supplementation or expansion of allergen-specific CD4⁺CD25⁺FoxP3⁺Tregs has the potential to be a new therapeutic strategy for AR.

5. Conclusion

Our results showed the relationship between VD3 and the immune system; VD3 and allergic diseases *in vivo* were inconsistent with those *in vitro*. The ability of VD3 supplementation to result in clinical improvement may vary with the dosing regimen or have different effects on different populations. VD3 can significantly elevate the Treg cell number and might promote Th1 but inhibit Th2 and Th17 cell production.

Data Availability

All data collection and analysis were conducted under double blind and were supported by the Affiliated Hangzhou First People's Hospital, Zhejiang University School of Medicine. We will provide the original data at any time if necessary. Dr. Haifeng Ni and Dr. Yong Li are responsible for the data.

Ethical Approval

We would like to thank the Institutional Review Board of the Hangzhou First People's Hospital for assistance in obtaining informed consent for this study.

Conflicts of Interest

The authors have declared no conflict of interest.

Authors' Contributions

Liqing Zhang and Haifeng Ni contributed equally to this work.

Acknowledgments

This study was supported by grants from the Medical and Health Foundation Project of Zhejiang Province, China (Grant Numbers: 2015KYB294, 2020KY689, and 2021KY870).

References

- [1] S. Hong, D. K. Son, W. R. Lim et al., "The prevalence of atopic dermatitis, asthma, and allergic rhinitis and the comorbidity of allergic diseases in children," *Environmental Health and Toxicology*, vol. 27, article e2012006, 2012.
- [2] M. D. Seidman, R. K. Gurgel, S. Y. Lin et al., "Clinical practice guideline: allergic rhinitis executive summary," *Otolaryngology and Head and Neck Surgery*, vol. 152, no. 2, pp. 197–206, 2015.
- [3] Y. Zhang and L. Zhang, "Prevalence of allergic rhinitis in china," *Allergy, Asthma & Immunology Research*, vol. 6, no. 2, pp. 105–113, 2014.
- [4] J. Bousquet, H. J. Schünemann, B. Samolinski et al., "Allergic rhinitis and its impact on asthma (ARIA): achievements in 10 years and future needs," *The Journal of Allergy and Clinical Immunology*, vol. 130, no. 5, pp. 1049–1062, 2012.
- [5] A. Assa, L. Vong, L. J. Pinnell, N. Avitzur, K. C. Johnson-Henry, and P. M. Sherman, "Vitamin D deficiency promotes epithelial barrier dysfunction and intestinal inflammation," *The Journal of Infectious Diseases*, vol. 210, no. 8, pp. 1296–1305, 2014.
- [6] Y. Moran-Auth, M. Penna-Martinez, F. Shoghi, E. Ramos-Lopez, and K. Badenhoop, "Vitamin D status and gene transcription in immune cells," *The Journal of Steroid Biochemistry and Molecular Biology*, vol. 136, pp. 83–85, 2013.
- [7] Y. Wang, J. Zhu, and H. F. DeLuca, "Where is the vitamin D receptor?," *Archives of Biochemistry and Biophysics*, vol. 523, no. 1, pp. 123–133, 2012.
- [8] J. W. Jung, J. Y. Kim, S. H. Cho, B. W. Choi, K. U. Min, and H. R. Kang, "Allergic rhinitis and serum 25-hydroxyvitamin D level in Korean adults," *Annals of Allergy, Asthma & Immunology*, vol. 111, no. 5, pp. 352–357, 2013.
- [9] A. Bonanno, S. Gangemi, S. la Grutta et al., "25-Hydroxyvitamin D, IL-31, and IL-33 in children with allergic disease of the airways," *Mediators of Inflammation*, vol. 2014, Article ID 520241, 10 pages, 2014.
- [10] M. Wjst, "Introduction of oral vitamin D supplementation and the rise of the allergy pandemic," *Allergy, Asthma & Clinical Immunology*, vol. 5, no. 1, p. 8, 2009.
- [11] X. M. Mai, Y. Chen, C. A. Camargo Jr., and A. Langhammer, "Serum 25-hydroxyvitamin D levels and self-reported allergic rhinitis in Norwegian adults - the HUNT study," *Allergy*, vol. 69, no. 4, pp. 488–493, 2014.
- [12] H. M. Cheng, S. Kim, G. H. Park et al., "Low vitamin D levels are associated with atopic dermatitis, but not allergic rhinitis, asthma, or IgE sensitization, in the adult Korean population," *The Journal of Allergy and Clinical Immunology*, vol. 133, no. 4, pp. 1048–1055, 2014.
- [13] D. R. Miller, S. W. Turner, D. Spiteri-Cornish et al., "Maternal vitamin D and E intakes during early pregnancy are associated with airway epithelial cell responses in neonates," *Clinical and Experimental Allergy*, vol. 45, no. 5, pp. 920–927, 2015.
- [14] M. Erkkola, M. Kaila, B. I. Nwaru et al., "Maternal vitamin D intake during pregnancy is inversely associated with asthma and allergic rhinitis in 5-year-old children," *Clinical and Experimental Allergy*, vol. 39, no. 6, pp. 875–882, 2009.
- [15] S. Bunyavanich, S. L. Rifas-Shiman, T. A. Platts-Mills et al., "Prenatal, perinatal, and childhood vitamin D exposure and their association with childhood allergic rhinitis and allergic sensitization," *Journal of Allergy and Clinical Immunology*, vol. 137, no. 4, pp. 1063–1070.e2, 2016.
- [16] E. Maslova, S. Hansen, C. B. Jensen, A. L. Thorne-Lyman, M. Strom, and S. F. Olsen, "Vitamin D intake in mid-pregnancy and child allergic disease - a prospective study in 44,825 Danish mother-child pairs," *BMC Pregnancy Childbirth*, vol. 13, no. 1, p. 199, 2013.
- [17] E. HYPPÖNEN, U. SOVIO, M. WJST et al., "Infant vitamin d supplementation and allergic conditions in adulthood: northern Finland birth cohort 1966," *Annals of the New York Academy of Sciences*, vol. 1037, pp. 84–95, 2004.
- [18] O. Back, H. K. Blomquist, O. Hernell, and B. Stenberg, "Does vitamin D intake during infancy promote the development of

- atopic allergy?," *Acta Dermato-Venereologica*, vol. 89, no. 1, pp. 28–32, 2009.
- [19] K. T. Nouri-Aria, "Foxp3 expressing regulatory T-cells in allergic disease," *Advances in Experimental Medicine and Biology*, vol. 665, pp. 180–194, 2009.
- [20] E. S. Chambers, D. Suwannasaen, E. H. Mann et al., "1 α ,25-Dihydroxyvitamin D₃ in combination with transforming growth factor- β increases the frequency of Foxp3+regulatory T cells through preferential expansion and usage of interleukin-2," *Immunology*, vol. 143, no. 1, pp. 52–60, 2014.
- [21] J. Wu, E. del Duca, M. Espino et al., "RNA sequencing keloid transcriptome associates keloids with Th2, Th1, Th17/Th22, and JAK3-skewing," *Frontiers in Immunology*, vol. 11, article 597741, 2020.
- [22] M. Garcia de Oliveira, F. da Ressureicao Sgnotto, T. Rodrigues de Sousa, B. O. Fagundes, A. Duarte, and J. R. Victor, "Preconceptional immunization with an allergen inhibits offspring thymic Th17 cells maturation without influence on Th1 and Th2 cells," *European Cytokine Network*, vol. 31, no. 3, pp. 113–117, 2020.
- [23] M. Milovanovic, G. Heine, W. Hallatschek, B. Opitz, A. Radbruch, and M. Worm, "Vitamin D receptor binds to the ϵ germline gene promoter and exhibits transrepressive activity," *Journal of Allergy and Clinical Immunology*, vol. 126, no. 5, pp. 1016–1023.e4, 2010.
- [24] V. Matheu, O. Back, E. Mondoc, and S. Issazadeh-Navikas, "Dual effects of vitamin D-induced alteration of T_H1/T_H2 cytokine expression: enhancing IgE production and decreasing airway eosinophilia in murine allergic airway disease," *The Journal of Allergy and Clinical Immunology*, vol. 112, no. 3, pp. 585–592, 2003.
- [25] G. Drozdenko, G. Heine, and M. Worm, "Oral vitamin D increases the frequencies of CD38+ human B cells and ameliorates IL-17-producing T cells," *Experimental Dermatology*, vol. 23, no. 2, pp. 107–112, 2014.
- [26] J. Kitazawa, F. Kimura, A. Nakamura et al., "Alteration in endometrial helper T-cell subgroups in chronic endometritis," *American Journal of Reproductive Immunology*, vol. 85, no. 3, article e13372, 2021.
- [27] S. A. Sakyi, T. A. Buckman, D. Antwi-Berko et al., "Intracytoplasmic expression of IL-6 and IL-17A in circulating CD4+ T cells are strongly associated with and predict disease activity in rheumatoid arthritis: a case-control study in Ghana," *International Journal of Rheumatology*, vol. 2020, Article ID 2808413, 9 pages, 2020.
- [28] Y. Hiraguchi, H. Tanida, M. Sugimoto et al., "1,25-Dihydroxyvitamin D₃ upregulates functional C-x-C chemokine receptor type 4 expression in human eosinophils," *International Archives of Allergy and Immunology*, vol. 158, no. 1, pp. 51–57, 2012.
- [29] A. E. El-Shazly and P. P. Lefebvre, "Modulation of NK cell autocrine-induced eosinophil chemotaxis by interleukin-15 and vitamin D₃: a possible NK-eosinophil crosstalk via IL-8 in the pathophysiology of allergic rhinitis," *Mediators of Inflammation*, vol. 2011, Article ID 373589, 5 pages, 2011.
- [30] K. H. Yip, N. Kolesnikoff, C. Yu et al., "Mechanisms of vitamin D₃ metabolite repression of IgE-dependent mast cell activation," *Journal of Allergy and Clinical Immunology*, vol. 133, no. 5, pp. 1356–1364.e14, 2014.
- [31] R. Ariano, "Efficacy of a novel food supplement in the relief of the signs and symptoms of seasonal allergic rhinitis and in the reduction of the consumption of anti-allergic drugs," *Acta Bio-Medica*, vol. 86, no. 1, pp. 53–58, 2015.
- [32] G. Heine, C. Tabeling, B. Hartmann et al., "25-Hydroxyvitamin D₃ promotes the long-term effect of specific immunotherapy in a murine allergy model," *Journal of Immunology*, vol. 193, no. 3, pp. 1017–1023, 2014.
- [33] S. Ozkara, E. Keles, N. Ilhan, H. Gungor, I. Kaygusuz, and H. C. Alpay, "The relationship between Th1/Th2 balance and 1 α ,25-dihydroxyvitamin D₃ in patients with nasal polyposis," *European Archives of Oto-Rhino-Laryngology*, vol. 269, no. 12, pp. 2519–2524, 2012.
- [34] G. Xu, Z. Mou, H. Jiang et al., "A possible role of CD4+CD25+ T cells as well as transcription factor Foxp3 in the dysregulation of allergic rhinitis," *The Laryngoscope*, vol. 117, no. 5, pp. 876–880, 2007.
- [35] J. L. Kreindler, C. Steele, N. Nguyen et al., "Vitamin D₃ attenuates Th2 responses to *Aspergillus fumigatus* mounted by CD4+ T cells from cystic fibrosis patients with allergic bronchopulmonary aspergillosis," *Journal of Clinical Investigation*, vol. 120, no. 9, pp. 3242–3254, 2010.
- [36] J. Correale, M. C. Ysraelit, and M. I. Gaitan, "Immunomodulatory effects of vitamin D in multiple sclerosis," *Brain*, vol. 132, no. 5, pp. 1146–1160, 2009.
- [37] L. E. Jeffery, F. Burke, M. Mura et al., "1,25-Dihydroxyvitamin D₃ and IL-2 combine to inhibit T cell production of inflammatory cytokines and promote development of regulatory T cells expressing CTLA-4 and FoxP3," *Journal of Immunology*, vol. 183, no. 9, pp. 5458–5467, 2009.
- [38] A. Vijayendra Chary, R. Hemalatha, M. Seshacharyulu, M. Vasudeva Murali, D. Jayaprakash, and K. B. Dinesh, "Vitamin D deficiency in pregnant women impairs regulatory T cell function," *The Journal of Steroid Biochemistry and Molecular Biology*, vol. 147, pp. 48–55, 2015.

Research Article

Identification of SHMT2 as a Potential Prognostic Biomarker and Correlating with Immune Infiltrates in Lung Adenocarcinoma

Lianxiang Luo ^{1,2}, Yushi Zheng,³ Zhiping Lin,⁴ Xiaodi Li,³ Xiaoling Li,⁵ Mingyue Li,⁶ Liao Cui,⁷ and Hui Luo¹

¹The Marine Biomedical Research Institute, Guangdong Medical University, Zhanjiang 524023, China

²The Marine Biomedical Research Institute of Guangdong Zhanjiang, Zhanjiang, Guangdong 524023, China

³The First Clinical College, Guangdong Medical University, Zhanjiang 524023, China

⁴The Orthopedic Department, The Affiliated Hospital of Guangdong Medical University, Zhanjiang 524023, China

⁵Animal Experiment Center, Guangdong Medical University, Zhanjiang 524023, China

⁶Department of Pathology and Laboratory Medicine, Perelman School of Medicine, University of Pennsylvania, Philadelphia, PA19104, USA

⁷Guangdong Key Laboratory for Research and Development of Natural Drugs, Guangdong Medical University, Zhanjiang, Guangdong 524023, China

Correspondence should be addressed to Lianxiang Luo; luolianxiang321@gdmu.edu.cn

Received 15 November 2020; Revised 19 February 2021; Accepted 10 March 2021; Published 8 April 2021

Academic Editor: Zhipeng Xu

Copyright © 2021 Lianxiang Luo et al. This is an open access article distributed under the Creative Commons Attribution License, which permits unrestricted use, distribution, and reproduction in any medium, provided the original work is properly cited.

It has attracted growing attention that the role of serine hydroxy methyl transferase 2 (SHMT2) in various types of cancers. However, the prognostic role of SHMT2 in lung adenocarcinoma (LUAD) and its relationship with immune cell infiltration is not clear. In this study, the information of mRNA expression and clinic data in LUAD were, respectively, downloaded from the GEO and TCGA database. We conducted a biological analysis to select the signature gene SHMT2. Online databases including Oncomine, GEPIA, TISIDB, TIMER, and HPA were applied to analyze the characterization of SHMT2 expression, prognosis, and the correlation with immune infiltration in LUAD. The mRNA expression and protein expression of SHMT2 in LUAD tissues were higher than in normal tissue. A Kaplan-Meier analysis showed that patients with lower expression level of SHMT2 had a better overall survival rate. Multivariate analysis and the Cox proportional hazard regression model revealed that SHMT2 expression was an independent prognostic factor in patients with LUAD. Meanwhile, the gene SHMT2 was highly associated with tumor-infiltrating lymphocytes in LUAD. These results suggest that the SHMT2 gene is a promising candidate as a potential prognostic biomarker and highly associated with different types of immune cell infiltration in LUAD.

1. Introduction

Lung cancer is the most common cancer and the main reason of cancer-related death, leading to a rising public concern worldwide. Lung cancer is divided into nonsmall cell lung cancer (NSCLC) and small cell lung cancer (SCLC). NSCLC accounts for approximately 85% of all lung cancers [1], which contain two main types: lung squamous cell carcinoma (LUSC) and lung adenocarcinoma (LUAD). LUAD is the most common histological subtype of NSCLC diagnosed, followed by LUSC. As the most common histological subtype, LUAD frequently occurs in females and nonsmoking

people, with no obvious clinical symptoms in the early stage, but shared some common symptoms with other respiratory diseases, resulting in difficulty in identification of lung cancer. In addition, LUAD has an average 5-year survival rate of less than 20% [2] due to its metastasis at early stages. Therefore, there is an urgent need to identify new diagnostic and prognostic biomarkers for LUAD to increase the efficacy of early diagnosis.

Serine hydroxy methyl transferase (SHMT) is an essential enzyme in the conversion between serine and glycine as well as one-carbon metabolism, providing the important precursors for protein and nucleic acid synthesis for cancer growth

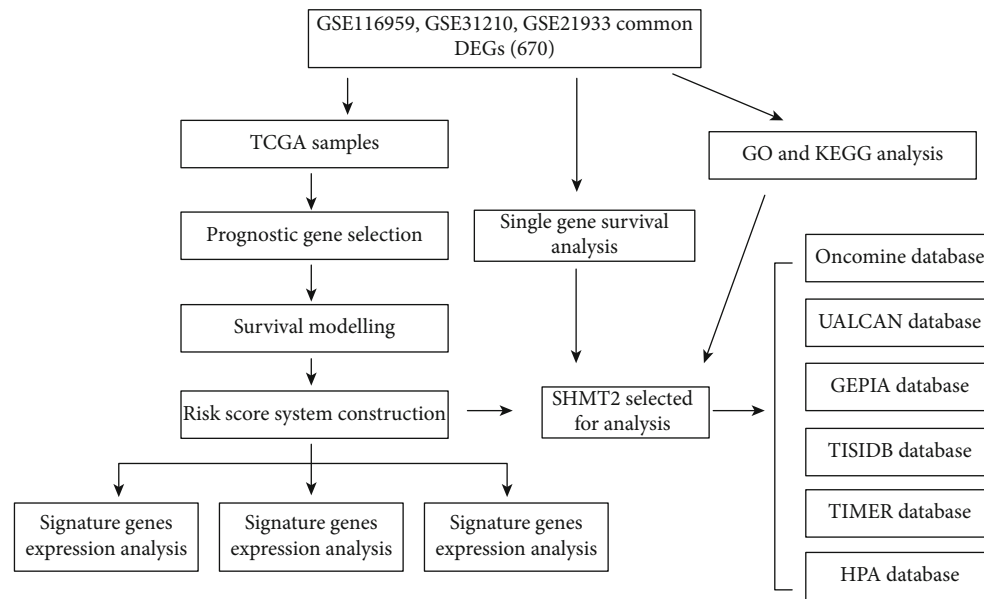


FIGURE 1: Flowchart for this study. DEGs: differential expression genes; GEPIA: Gene Expression Profiling Interactive Analysis; GO: Gene Ontology; GSEA: gene set enrichment analysis; KEGG: Kyoto Encyclopedia of Genes and Genomes; KM: Kaplan–Meier; TCGA: The Cancer Genome Atlas; TIMER: Tumor Immune Estimation Resource; HPA: the Human Protein Atlas.

and metastasis. To be noted, amino acid and one-carbon metabolism are the basis of cancer biology, and hyperactivation of one-carbon metabolism has been proved to be driving factors of cell proliferation and related to the epigenetic state of the cell [3]. SHMT2 is one of SHMT genes, encodes a protein that localizes to the mitochondria [4], and is identified as a potential driving gene in diverse cancers in cell growth and aggressiveness [5]. As a key regulator of viral transcription, HIV-1 Tat levels are regulated through K63Ub-selective autophagy-mediated through SHMT1,2 and the BRCC36 deubiquitinase. Xu et al. has identified SHMT2 and BRCC36 as novel and important regulators of HIV-1 Tat protein levels in infected T cells [6]. Ji et al. proved expression levels of SHMT2 in HCC tissues were significantly correlated with tumor grade and hepatitis B virus (HBV) infection [7]. Besides, genetic ablation of SHMT2 causes strong increases in inflammatory cytokine signatures [8]. SHMT2 may alleviate the apoptosis and the release of damaging inflammatory factors after hepatic ischemia-reperfusion injury by inhibiting the activation of the JNK pathway and excessive activation of the NF- κ B pathway [9]. SHMT2 showed unfavorable overall survival to intrahepatic cholangiocarcinoma patients [10]. SHMT2 is a very crucial gene in many cancers, and proteomic profiling of breast cancer metabolism identifies SHMT2 as a prognostic factor [11], and it drives glioma cell survival in ischemia depending on glycine clearance [12, 13]. However, the immune-related SHMT2 in LUAD and its potential use in prognosis are still largely unknown.

In recent years, the combination of immunotherapy and high-throughput gene microarray has been widely employed for oncology and other disease areas to analyze deeper correlation to predict more insight for research. So, analysis of available high-throughput data in many databases has

become an effective and low-cost method to discover biomarkers for many diseases. Immune cells have an intimate connection with the prognosis in various cancers. Mounting evidence supports that the malignant phenotype is not only determined by the intrinsic activities of cancer cells but also by components in the tumor microenvironment, especially tumor-infiltrating immune cells [14], which is an important determinant of prognosis and immunotherapy response of lung cancer [15]. For example, CD83+ dendritic cells and Foxp3+ regulatory T cells in primary lesions and regional lymph nodes are negatively correlated with the prognosis of gastric cancer [16]. Increased tumor-infiltrating tumor-associated macrophages (TAMs) are associated with a poor prognosis of NSCLC [17]; DC and T cells are connected with better prognosis [18, 19]. Meanwhile, high-throughput gene microarray makes it accessible for us to further explore the tumors at multiple levels.

In this study, we downloaded the LUAD-related data sets from the GEO database (Gene Expression Omnibus) and TCGA (The Cancer Genome Atlas) database and conducted bioinformatics statistical analysis to select different expression genes (DEGs) between normal tissue and tumor tissue. Subsequently, functional analysis and survival analysis were subsequently carried out to select and verify signature genes with biological and clinical signatures. In addition, we took full advantage of convenient online site tools to explore the relationship between signature and immune cells and verify the suppose at multiple levels especially.

2. Methods

2.1. Data Collection and Preprocess. We obtained the LUAD-related microarray profiles (GSE116959 [20], GSE21933 [21], and GSE31210 [22]) from the GEO database (<https://www>

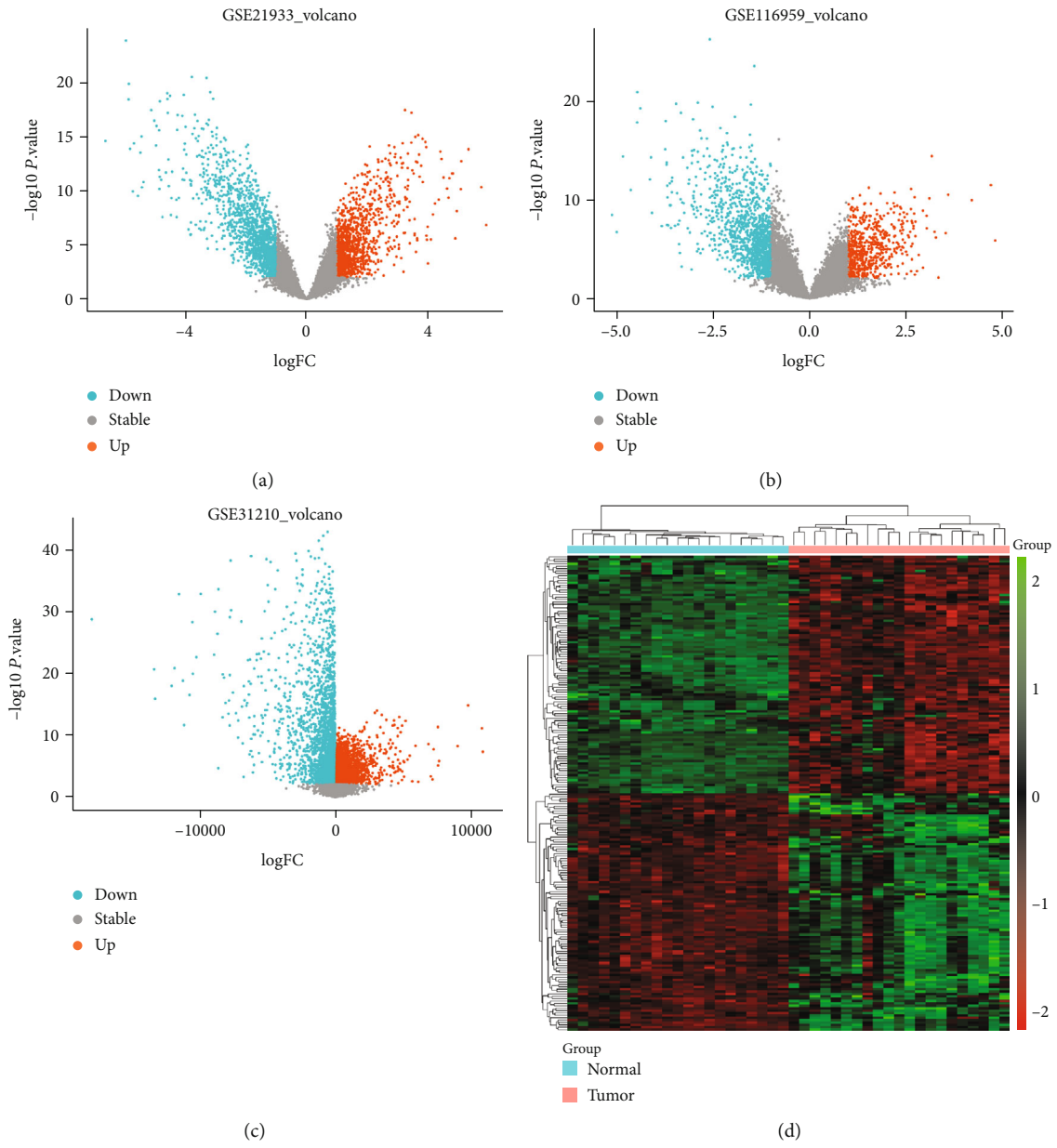


FIGURE 2: Continued.

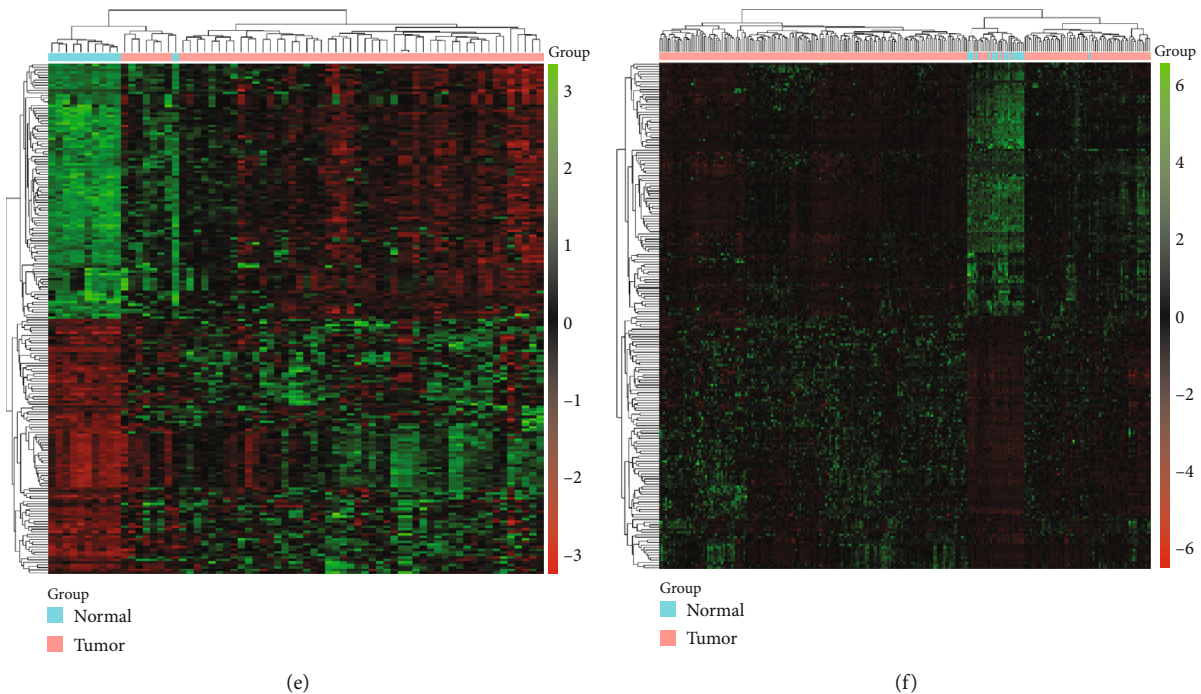


FIGURE 2: DEGs in three data sets. (a–c) The volcano plots visualize the DEGs in GSE116959, GSE21933, and GSE31210, respectively. The red nodes represent upregulated genes while the blue nodes represent downregulated genes. (d–f) Heatmap of the top 100 DEGs according to the value of $|\log_{2}FC| > 1$ and $P < 0.01$. The green color indicates lower expression and red color indicates high expression.

.ncbi.nlm.nih.gov/geo/). In this study, the datasets that met the following criteria were selected: (a) studies of comparing gene expression between human LUAD cancer samples and corresponding normal tissues; (b) the number of samples in each gene expression profiling dataset should be more than 30.

The microarray data were normalized and analyzed via the R “limma” package, which implements empirical Bayesian methods for analyzing microarray data [23]. We set \log_{2} fold change (FC) ≥ 1 with an adjusted P value less than 0.01 as the threshold to define important differentially expressed genes (DEGs) which are selected for subsequent analysis. We named the DEGs that overlapped in the three data matrixes as common DEGs. In addition, multiple probes corresponded to the same gene in the annotation file; the average expression of these probes was used as the expression value of the corresponding gene. Analyzing and processing these abovementioned data by R language.

Furthermore, we obtained the LUAD transcriptome RNA-seq data set and corresponding clinical data set from the TCGA database (<https://cancergenome.nih.gov/>) containing 521 tumor samples and 46 normal samples.

2.2. Functional Enrichment Analysis of DEGs

2.2.1. GO and KEGG Pathway Analysis. In order to investigate biological processes functions and pathways associated with the selected DEGs, we also performed Gene Ontology (GO) and the Kyoto Encyclopedia of Genes and Genomes (KEGG) enrichment analyses. The GO analyses classified the common DEGs into three categories, including biological

process (BP), cellular component (CC), and molecular function (MF). The KEGG analysis was conducted to determine significantly enriched the pathways of DEGs which was defined as the cutoff significant criteria with P value < 0.05 . Besides, the Cytoscape software (version 3.8.0) was used to screen hub genes. The GO and KEGG analyses were both based on the online database DAVID (version 6.8) (<https://david.ncifcrf.gov>) and visually display through R software (version 3.6.1).

2.2.2. Screening Hub Genes by Cytoscape Software. Cytoscape software (version 3.8.0) is an open-source bioinformatic software platform for visualizing molecular interaction networks and biological pathways and integrating these networks with annotations, gene expression profiles, and other state data. MCODE is a Cytoscape APP that finds clusters (highly connected areas) in the network.

2.2.3. Gene Set Enrichment Analysis. Gene Set Enrichment Analysis (GSEA) (<http://software.broadinstitute.org/gsea/index.jsp>) is a computational method that determines whether an a priori defined set of genes shows statistically significant, concordant differences between two biological states [24] (e.g., phenotypes) (from the official GSEA website). We used this computational method to analyze the function and potential pathway of signature genes. In order to find out the relationship between the gene set and the function we are interested in, we conducted GSEA analysis based on “C5: GO gene sets” for three groups of GSEs by GSEA software version 4.0.3. The false discovery rate (FDR

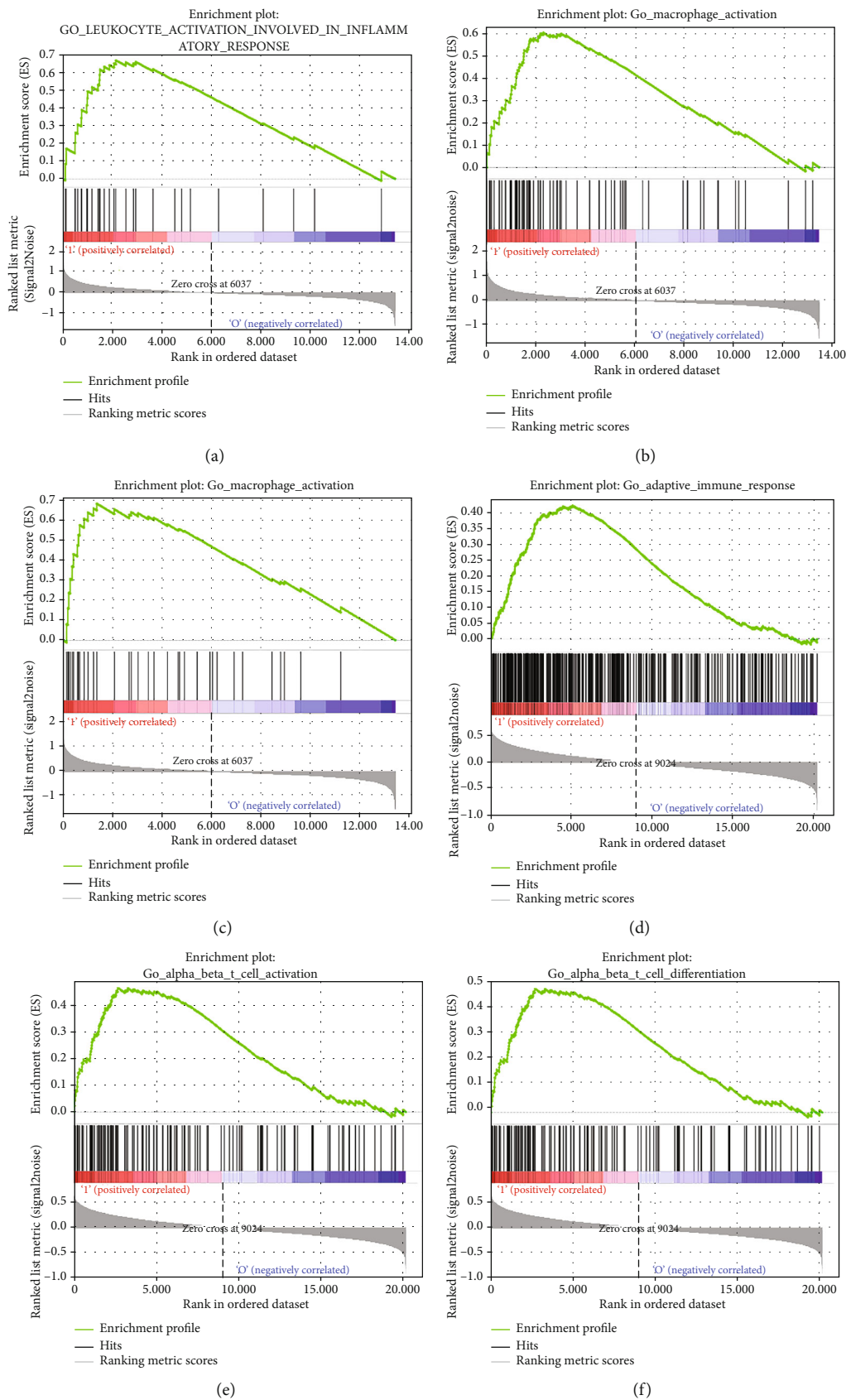


FIGURE 3: Continued.

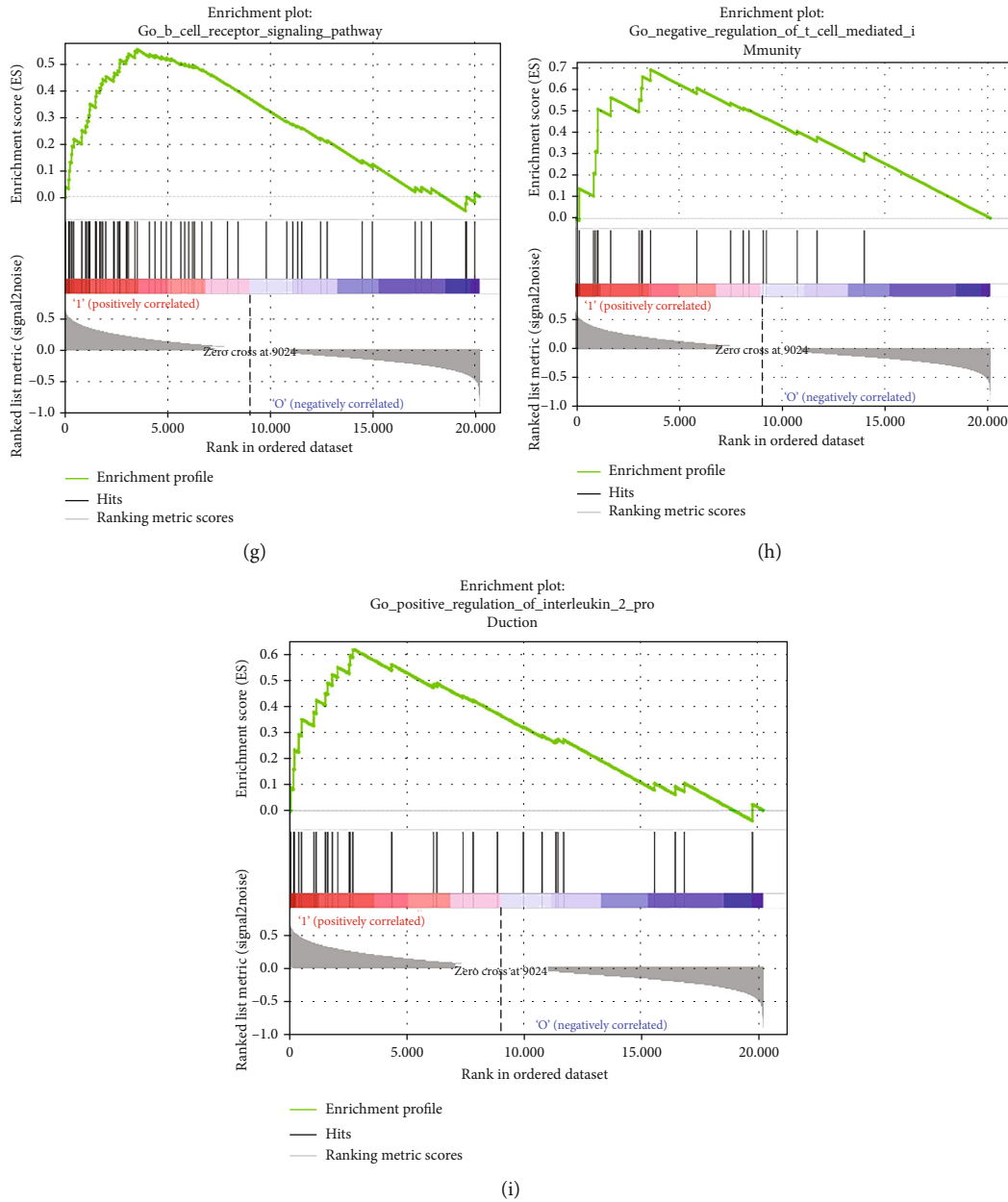


FIGURE 3: Upregulated gene expression was associated with an immunologic process and was validated by GSEA of GO gene sets analysis of high expression of SHMT2 in GSE21933, GSE31210, and GSE116959. (a) Leukocyte activation involved in inflammatory response, (b) macrophage activation, (c) response to interleukin 6, (d) adaptive immune response, (e) alpha beta T cell activation, (f) alpha beta T cell differentiation, (g) B cell receptor signaling pathway, (h) negative regulation of T cell mediated immunity, and (i) positive regulation of interleukin 2 production.

) < 25% and nominal $P < 0.05$ were regarded as the cut-off criteria.

2.3. Survival Analysis

2.3.1. Risk Score Formula Establishment. The clinical information of the original 521 TCGA patients with lung adenocarcinoma was sorted out and 270 cases were screened out, and the patients with lung adenocarcinoma were randomly divided into the training group ($n = 135$) and the testing group ($n = 135$). We further investigated the potential roles in clinical outcomes after screening out the genes. We used

a risk-score formula to predict LUAD patients' survival. The risk score formula is as follows: Risk score = $(1.43 \times \text{expression level of AC069513.4}) + (0.81 \times \text{expression level of AC003092.1}) + (1.64 \times \text{expression level of RP11 - 507 K2.3}) + (-6.56 \times \text{expression level of CTC - 205 M6.2}) + (-1.72 \times \text{expression level of U91328.21})$ [25].

2.3.2. Risk Score Formula Validation. To validate the gene risk signature in the internal validation data sets, we calculated the risk score for each patient in the complete TCGA cohort. The patients were then divided into high-risk and low-risk groups based on the corresponding median risk

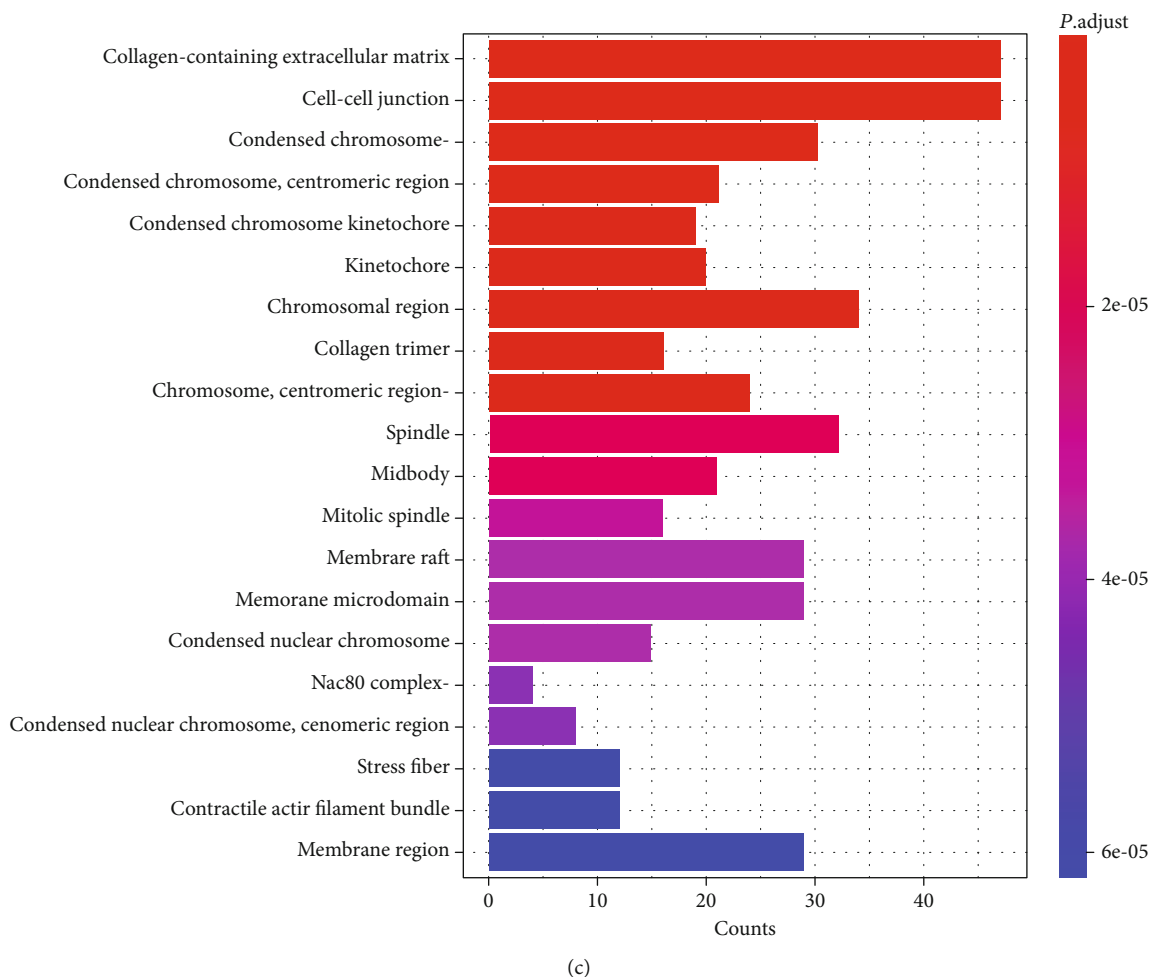
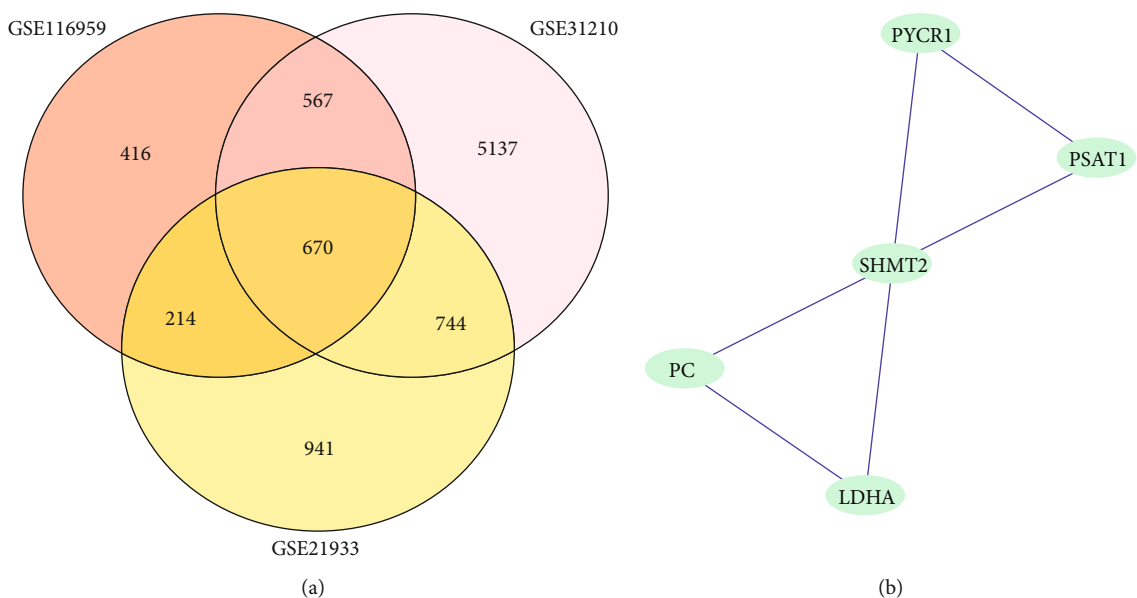


FIGURE 4: (a) Common DEGs in three data sets. A total of 670 commons in the intersection of three gene sets. (b) Hub gene of common DEGs. There are five hub genes in 670 common genes, including SHMT2, PSAT1, PYCR1, PC, and LDHA. (c) GO analysis of common DEGs.

score. The prediction accuracy of this risk model was determined by a time-dependent receiver operating characteristic (ROC) analysis.

2.3.3. *Statistical Analysis.* Statistical analysis and graphical plotting were conducted by R software. Differences in pathological and molecular characteristics between different

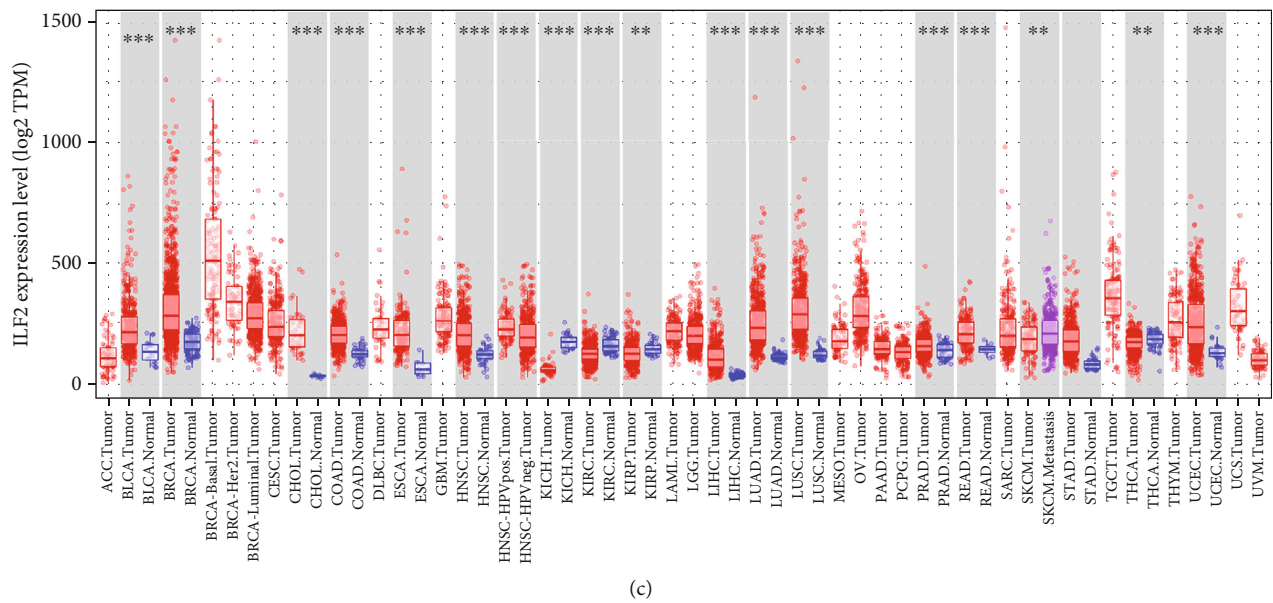
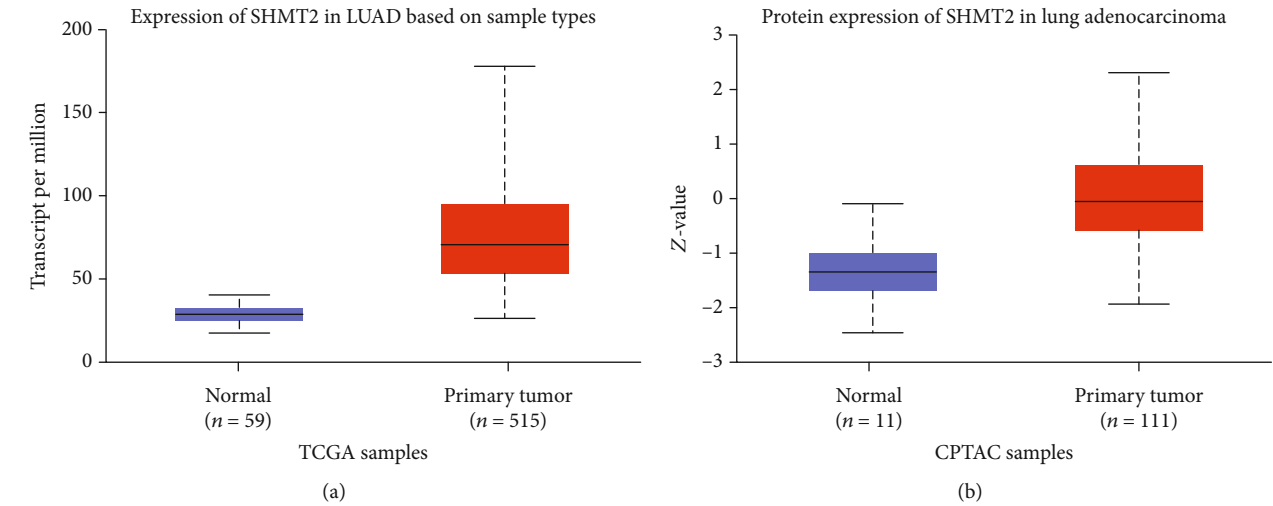


FIGURE 5: Continued.

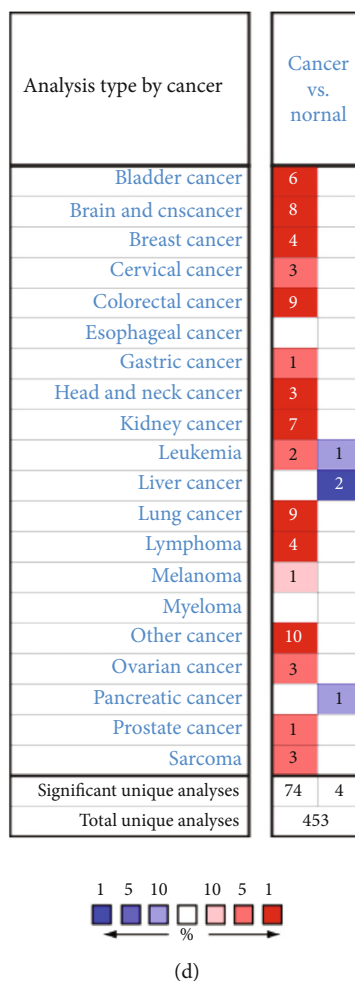


FIGURE 5: SHMT2 expression level (a) mRNA expression of SHMT2 in LUAD. The mRNA expression of SHMT2 is higher in tumor but lower in normal based on TCGA samples; (b) protein expression of SHMT2 in LUAD. The protein expression of SHMT2 is higher in tumor while lower in normal based on CPTAC samples; (c) the mRNA expression level of SHMT2 in various cancer. Color images are available online. Fold change = 2 and P value = 0.01; (d) SHMT2 different expression between tumor and adjacent normal tissue. * $P < 0.05$, ** $P < 0.01$, *** $P < 0.001$.

groups of patients were compared using chi-squared and Fisher's exact tests. Prognostic factors were assessed by Cox regression analysis and the Kaplan-Meier method. The survival rates were calculated by Kaplan-Meier method curves and compared using the log-rank test. The significance of prognostic factors was evaluated through a multivariate Cox proportional hazard regression, with a P value less than 0.05 considered as statistical significant.

Then, the Kaplan-Meier plotter was applied to examine the prognostic value of SHMT2. Kaplan-Meier plotter database (<http://kmpplot.com/analysis/>) is an online analysis tool containing microarray profiles and mRNA-seq data with patients' survival information, including overall survival (OS) and progression-free survival (RFS), summarized from TCGA, Gene Expression Omnibus, and the Cancer Biomedical informatics Grid [26]. Kaplan-Meier plotter database was used to analyze the correlation between SHMT2 expression and survival in LUAD. A log-rank P value and the hazard ratio (HR) with confidence intervals of 95% were also calculated.

2.4. Signature Gene Online Validation and Analysis

2.4.1. Oncomine Database Analysis. The expression level of SHMT2 in various types of cancers was analyzed in the Oncomine database (<https://www.oncomine.org/>), especially in lung cancer. Oncomine database is an online cancer database with powerful analytical capabilities for computing gene expression signatures, clusters, and gene-set modules, automatically extracting biological insights from the data [27]. The mRNA expression difference between tumors and normal tissues were analyzed with thresholds as follows: P value of 0.01, fold change of 2, gene ranking of all, and the data from mRNA.

2.4.2. GEPIA Database Analysis. The Gene Expression Profiling Interactive Analysis (GEPIA) database (<http://gepia.cancer-pku.cn/>) is an interactive web for analyzing the expression data of RNA based on 9,736 tumors and 8,587 normal samples from the cancer genome atlas (TCGA) and the GTE projects [28]. We conducted an online survival

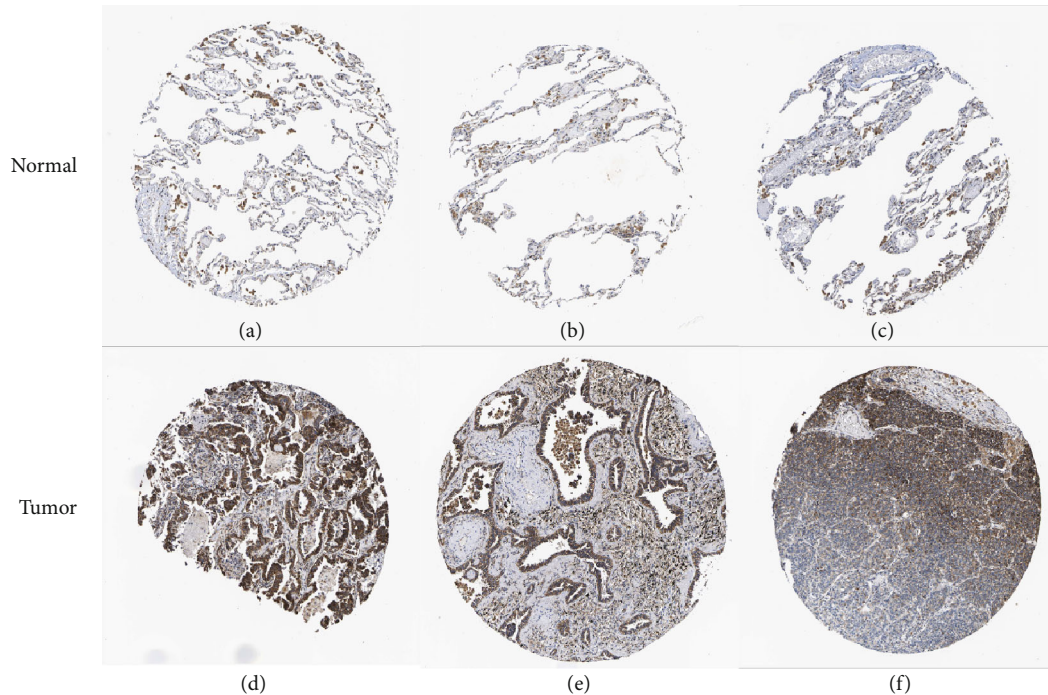


FIGURE 6: Immunohistochemistry (IHC) of SHMT2 expression in LUAD tissues and corresponding normal tissues based on The Human Protein Atlas (HPA). (a–c) Normal lung (T-28000) tissue and (d–f) lung (T-28000) tumor tissue.

analysis of the gene SHMT2 on the functional section named as the Survival plot in the GEPIA database. The threshold is determined by the following principles: Gene of SHMT2, Methods of Overall Survival, Group Cutoff of Median, Cutoff-High (%) and Cutoff-Low (%) both are 50, Hazards Ratio (HR) of yes, 95% Confidence Interval of yes, Axis Units of month, and Datasets set as LUAD.

2.4.3. UALCAN Database Analysis. UALCAN database (<http://ualcan.path.uab.edu>) is a user-friendly and interactive database, providing easy access to RNA-seq and clinical data of 31 cancer types from The Cancer Genome Atlas (TCGA) [29]. We checked the RNA-seq expression of SHMT2 again and further explored the correlation between SHMT2 protein expression and LUAD in this database.

2.4.4. TIMER Database Analysis. The correlations between SHMT2 expression and the abundance of immune infiltrates were explored by the Gene module in the TIMER database (<https://cistrome.shinyapps.io/timer/>), which is a comprehensive tool established for systematically analyzing immune infiltrates across diverse types of cancer [30]. Meanwhile, we also analyzed the relationship between the expression of SHMT2 and gene markers of tumor-infiltrating immune cells by a correlation module. Besides, the expression level of SHMT2 in various types of cancers was examined in the TIMER database once more.

2.4.5. TISIDB Database Analysis. To further investigate the correlations among SHMT2 expression, lymphocytes, and other immunomodulators, the TISIDB database (<http://cis.hku.hk/TISIDB>), known as a web portal for tumor and

immune system interaction, was applied to analyze. TISIDB integrates multiple heterogeneous data types, including 988 reported immune-related antitumor genes, high-throughput screening techniques, molecular profiling, and paracancerous multiomics data, as well as various resources for immunological data retrieved from seven public databases [31]. We used the TISIDB database to analyze the link between SHMT2 and immune cell infiltration and to learn the GO function in LUAD.

2.4.6. Human Protein Atlas Analysis. The protein expression of SHMT2 in both LUAD and normal tissues was retrieved from the Human Protein Atlas database (HPA) (<https://www.proteinatlas.org/>), which is a program with the aim to map all the human proteins in cells, tissues, and organs using an integration of various omics technologies, including antibody-based imaging, mass spectrometry-based proteomics, transcriptomics, and systems biology [32, 33]. In this study, we used the HPA database to analyze the protein expression and performed immunohistochemistry (IHC) analysis of SHMT2 between normal lung tissues and LUAD tissues.

3. Results

3.1. Identification of Common Differentially Expressed Genes (DEGs). The flow chart of the study was generalized in Figure 1. After performing difference analysis with dataset collection (GSE116959, GSE21933, and GSE31210) in the GEO database, a total of 577 samples (521 tumor samples and 46 normal samples) from TCGA database were explored. There were 1868 DEGs filtered from the GSE116959 data set,

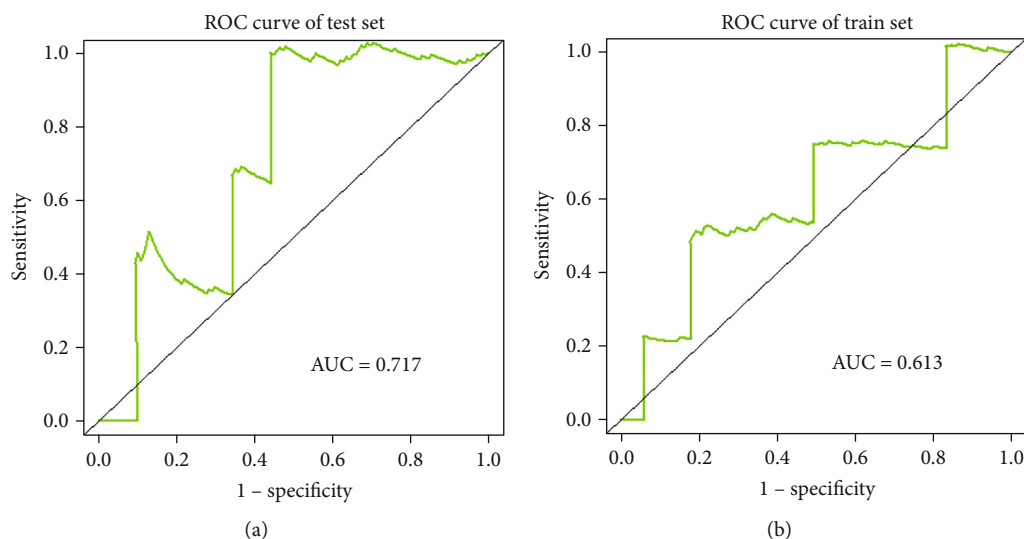


FIGURE 7: The time-dependent receiver operating characteristic (ROC) analysis. The AUC (area under ROC) score for the training dataset was 0.842, indicating the better performance of survival prediction in the training dataset.

including 624 upregulated and 1244 downregulated genes; 2570 DEGs screened from the GSE21933 data set, including 1193 upregulated and 1377 downregulated genes; and 7220 DEGs selected from the GSE31210 data set, including 4107 upregulated and 3013 downregulated genes. In order to make the results more intuitive, we visualized them. We displayed the DEGs among each data set via volcano plots (Figures 2(a)–2(c)). What is more, cluster analysis of DEGs showed two obvious different distribution patterns between the tumor and normal samples, suggesting crucial roles of DEGs in the occurrence and progression of LUAD (Figures 2(d)–2(f)). Through Venn diagram analysis, 670 common DEGs in the intersection of the three data sets were identified and selected for further analysis.

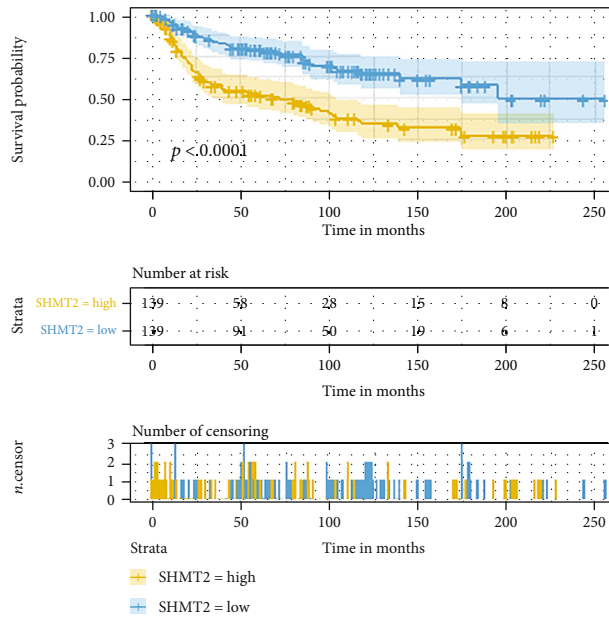
3.2. The Selection of Signature Genes. In order to search for the signature gene, we performed gene set enrichment analysis on GSE21933, GSE31210, and GSE116959. Afterward, with GSEA, we found that there were nine sets of results related to immunity closely, and all of them were highly expressed gene sets. In particular, GSE21933 was associated with macrophage, which is one of our focuses. The information of GSEA results was listed in Figure 3. Next, we selected upregulated genes for further analysis of the differences between genes and enrichment.

We conducted GO analysis and KEGG pathway enrichment analysis of DEGs from differential analysis to explore their potential biological functions and pathways associated with LUAD. The results of GO analysis in Figure 4(c) showed that DEGs were significantly related to mitotic nuclear division, cell-substrate adhesion, organelle fission, mitotic sister chromatid segregation, nuclear division, regulation of cell-substrate adhesion, regulation of mitotic nuclear division, microtubule cytoskeleton organization involved in mitosis, chromosome segregation, regulation of chromosome segregation, sister chromatid segregation, mitotic spindle organization, extracellular structure organization, urogenital system development, regulation of nuclear division, DNA-

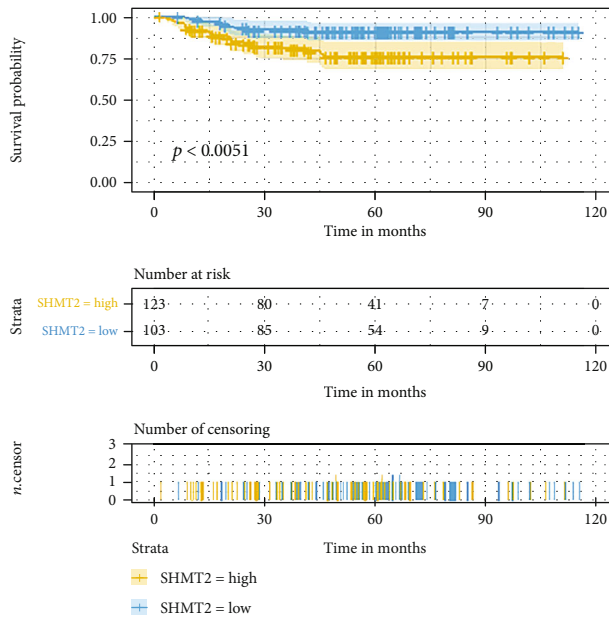
dependent DNA replication, and cell junction assembly, which were essential for the rapid growth of tumors. Additionally, as shown in Figure 4(b), MCODE was used to screen out cluster 15 containing all the upregulated 5 common DEG hub genes (SHMT2, PYCR1, PSA T1, PC, and LDHA) from Cytoscape software, and it was found that SHMT2 gene was located in the specific center of Figure 4(b), indicating that SHMT2 plays an important role in regulating cell behavior. In a function model of TISIDB, we verified the SHMT2 involved in the metabolism of glycine, serine, and threonine, metabolic pathways, carbon metabolism, biosynthesis of amino acids, providing the crucial basis for protein and nucleic acid production for cancer growth and metastasis. Thus, we believe that SHMT2 plays an important role in regulating the growth of LUAD.

3.3. High Expression Level of SHMT2 in Tumors. The expression level of SHMT2 in tumor and adjacent normal tissues was verified on the Oncomine database. As shown in Figure 5(d), SHMT2 displayed a higher expression level in bladder cancer, breast cancer, colorectal cancer, kidney cancer, lung cancer, and lymphoma, while the expression level was lower in liver cancer and pancreatic cancer. We also analyzed the mRNA-seq expression data in tumors by UALCAN database and TIMER database (Figures 5(a) and 5(c)). These results consistently showed that SHMT2 displays obviously high expression in LUAD. Besides, we explored the protein expression of SHMT2 between LUAD and normal tissues in UALCAN database (Figure 5(b)) and investigated immunohistochemistry (IHC) on The Human Protein Atlas (HPA) (Figures 6(a)–6(f)). Through the above analysis, we summarized the protein expression of SHMT2 was significantly elevated in tumors which may possess diverse functions in various tumors, especially in LUAD.

3.4. Prognostic Value of SHMT2 in LUAD. We calculated the area under the curve (AUC) of the receiver operating curve (ROC) to evaluate the discriminative ability of prediction

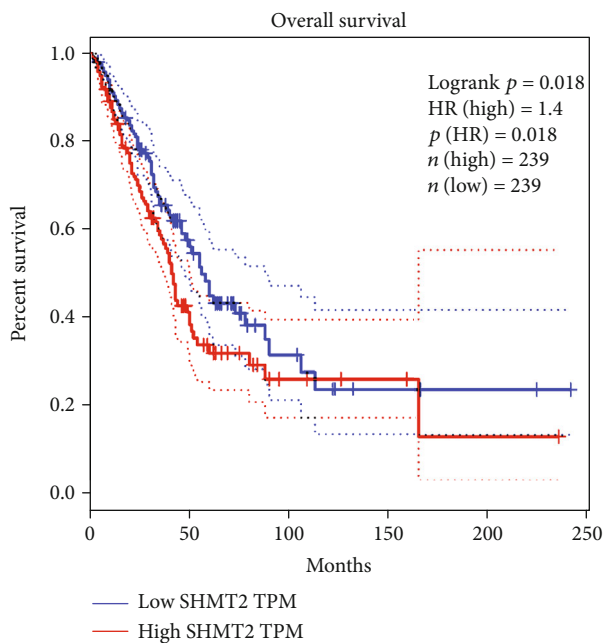


(a)

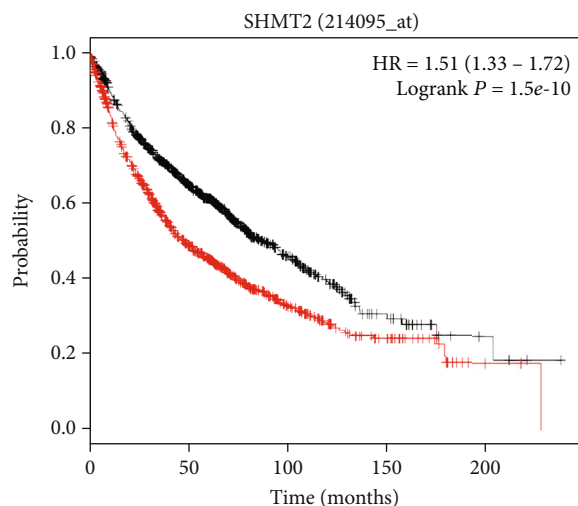


(b)

FIGURE 8: Continued.



(c)



Number at risk

Low	964	466	110	24	4
High	961	361	93	33	3

Expression

- Low
- High

(d)

FIGURE 8: Kaplan-Meier survival analysis. (a) OS (overall survival) of SHMT2 in GSE21933. (b) OS (overall survival) of SHMT2 in GSE31210. The numbers below the figures represent the number of patients at risk in each group. (c and d) Kaplan-Meier survival curves comparing the high and low expression of SHMT2 in LUAD in the Kaplan-Meier plotter database and GEPIA database.

rules. And the AUC score for the training dataset was 0.613 (Figure 7), indicating better survival prediction performance of the training data set. A Kaplan-Meier analysis showed an unfavorable effect on overall patient survival. Multivariate analysis and the Cox proportional hazard regression model uncovered that the expression of SHMT2 is an independent

prognostic indicator for patients with LUAD (Figures 8(a) and 8(b)).

We then examined the prognostic value of SHMT2 using the Kaplan-Meier plotter and the Gene Expression Profiling Interactive Analysis (GEPIA) database. We calculated the Cox *P*/log-rank *P* value and hazard ratio with 95% intervals.

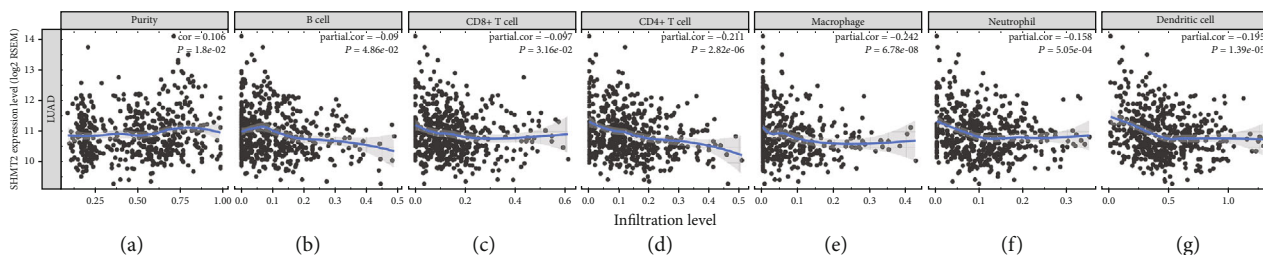


FIGURE 9: Correlation between SHMT2 expression and immune cell infiltration in LUAD from TCGA sample. Tumor purity, B cell abundance, CD8 + T cells, CD4 + T cells, macrophages, neutrophils, and dendritic cells relative to SHMT2 expression.

We set Cox P /log-rank $P = 0.05$ as the thresholds. The patients were divided into two groups based on the median level of the SHMT2 expression in each queue. Univariate analysis was carried out to assess the impact of SHMT2 on various cancer survival rates by GEPIA and the Kaplan-Mayer plotter database (Figures 8(c) and 8(d)). The results indicated that the expression level of SHMT2 has a significant effect on the prognosis of LUAD. Moreover, the low level of SHMT2 indicated a longer survival period for patients with LUAD. Given all that, these results suggested that high expression of SHMT2 was related to the poor prognosis of LUAD.

3.5. SHMT2 Immune Regulation Molecules. The result of GESA analysis based on 3 datasets in Figure 3 showed that the upregulated gene in GSE21933, GSE31210 was apparently correlated with immune-related biological functions and SHMT2 was proved as a significantly upregulated gene in 3 datasets, suggesting SHMT2 is possibly connected with immune regulation.

In order to explore whether SHMT2 exerts potential biological roles in immune infiltration, we conducted an integrated analysis based on the TIMER database and TISIDB database, analyzing the link between SHMT2 and immune cell infiltration as well as the gene markers of immune cell subtypes in LUAD. The results in Figure 3 suggested high levels of SHMT2 mRNA expression were associated with high immune infiltration in LUAD. SHMT2 mRNA expression level was significantly negatively correlated with infiltrating levels of immune cells, CD4+ T cells ($r = -0.055$, $P = 2.22e - 01$), macrophages ($r = -0.17$, $P = 1.65e - 04$), and dendritic cells (DCs) ($r = -0.111$, $P = 1.44e - 02$) (Figure 9). Besides, Supplemental Table 1 also demonstrated the SHMT2 mRNA expression level had significant correlations with immune cells, TAMs, DCs, CD4+ T cells, neutrophils, Th1, Th2, Thf, and T cell exhaustion in LUAD.

For further investigation, we found the expression of SHMT2 was associated with tumor-infiltrating lymphocytes (TILs), including activated Type 1 T helper cell, nature killer cell, T follicular helper cell, active B cell, immature B cell, active CD4 T cell, Type 17 T helper cell, Tem CD8 cell, and CD56dim nature killer cell (Figures 10(a)–10(i)). Particularly, the P value of the abovementioned cells is all less than 0.001. Overall, these results suggested that the SHMT2 and its associated genes were important for immune cell infiltra-

tion in the LUAD microenvironment and possibly have a more significant effect on the prognosis of LUAD.

4. Discussion

As an important branch of glycolysis and an essential source of one-carbon metabolism [3], serine was essential to support tumor cell proliferation [34]. SHMT, an essential enzyme that catalyze the conversion of serine to glycine, regulates serine metabolism and one-carbon metabolism, to provide important precursors for protein and nucleic acid synthesis for cancer growth and metastasis [3]. SHMT2, a type of SHMT gene found in the human genome, is associated with the prognosis of various tumors [10]. It is reported that SHMT2 is a key enzyme in the serine/glycine synthesis pathway, catalyzing the transformation of serine into glycine in mammalian mitochondria [12]. SHMT2 may serve as a prognostic factor and as a potential therapeutic target for human gliomas in clinical practice [13, 35]. However, there is still no study on the relationship between SHMT2 and LUAD. Therefore, it is of great significance to analyze the role of SHMT2 in LUAD.

As the most common LUAD, dense lymphocytic infiltrate is one of the most obvious characteristics of LUAD, indicating the immune system exerts an active role in the development and growth of LUAD. In this study, we screened out the key gene SHMT2 through difference analysis, functional enrichment analysis, and survival analysis based on the GEO database and TCGA database. Next, we used the Oncomine database and TIMER database to compare the expression level of SHMT2 among different cancers and verify its increased expression level in LUAD. Univariate analyses of this study were carried out to evaluate the effect of SHMT2 expression on the survival rates in LUAD via the R software and Kaplan-Meier plotter database. The high expression level of SHMT2 had a more significant effect on the prognosis of LUAD patients. After screening tumor prognosis related to SHMT2, the relationship between SHMT2 and immune infiltration levels in different tumors was investigated in the TIMER database and TISIDB database. The levels of infiltration of immune cells in LUAD were performed on the TIMER database, revealing that SHMT2 is obviously related to the immune filtration in this cancer.

Besides, multivariate analysis and the Cox proportional hazard regression model validated that SHMT2 could be an independent prognostic factor of patients with LUAD. The expression level of SHMT2 also had a significantly negative

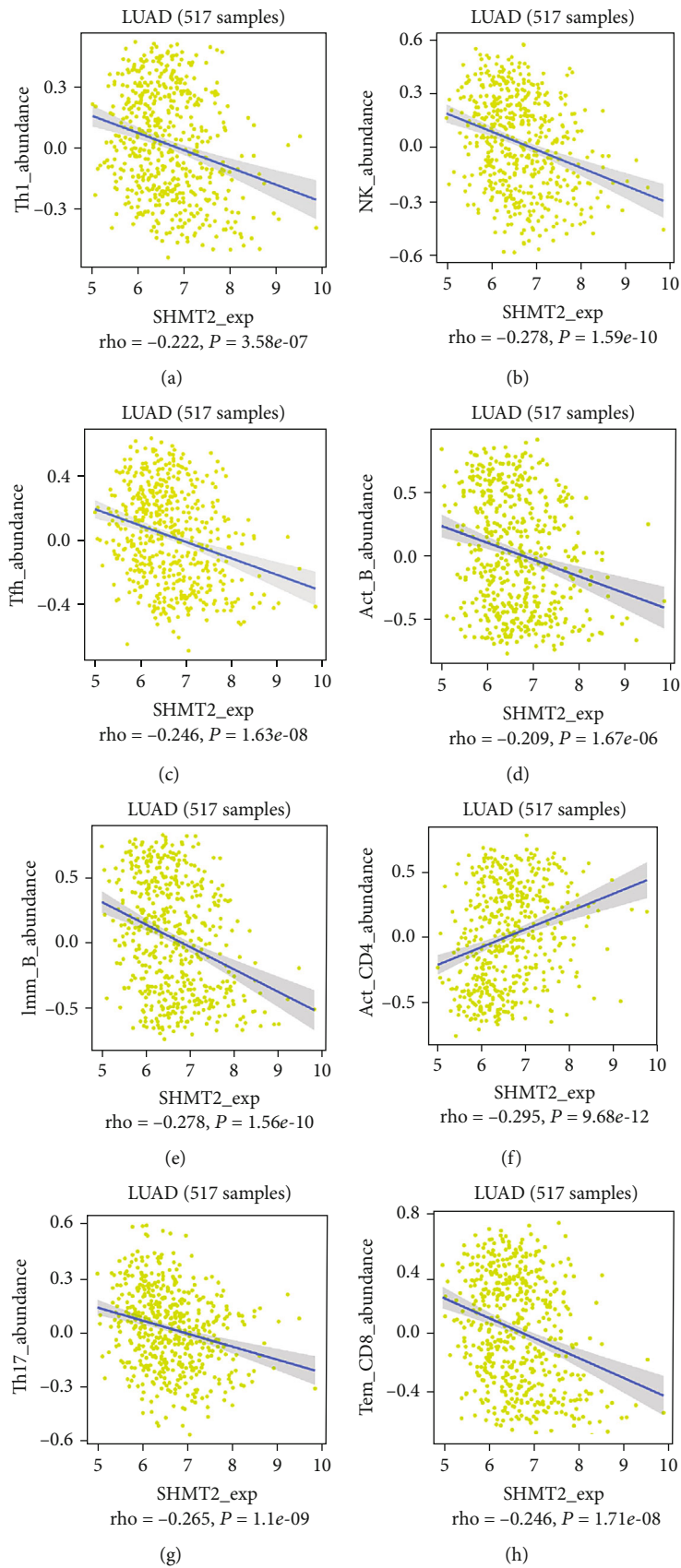


FIGURE 10: Continued.

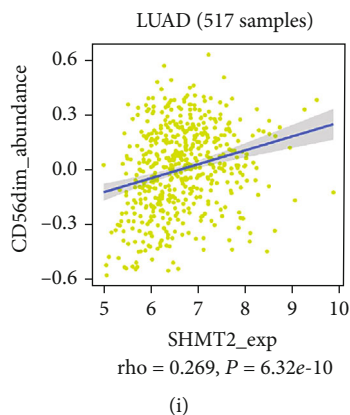


FIGURE 10: Relations between the abundance of tumor-infiltrating lymphocytes (TILs) and SHMT2 expression, including (a) Type 1 T helper cell, (b) nature killer cell, (c) T follicular helper cell, (d) active B cell, (e) immature B cell, (f) active CD4 T cell, (g) Type 17 T helper cell, (h) Tem CD8, and (i) CD56 dim nature killer cell.

correlation with tumor-infiltrating lymphocytes like immature B cell, active CD4 T cell, Th17, CD56dim nature killer cell (all $Cor > 0.2$; $P < 0.01$). Additionally, the results of correlation between SHMT2 and gene markers of immune cells showed that the SHMT2 was closely related with T cells (CD8+ T cells, Th1 cells, Th2 cells, Thf cell, general T cells, and exhausted T cells), TAM, NK cells, and DCs (Supplemental Table 1). Tumor-infiltrating lymphocytes (TILs), including T cells and B cells, are another important component of immune cells that exhibit antitumoral functions, especially CD8 and CD4 T cells. Some studies revealed that Th1 cells were associated with prolonged survival. SHMT2 regulating immune infiltration may be involved in these immune cells, especially T cell receptor interaction. The analysis mentioned above suggested that SHMT2 could serve as a potential overall prognostic marker for patient survival, improving the survival and prognosis of LUAD; SHMT2 may also play an important role in the microenvironment of LUAD via regulating tumor infiltration of immune cells.

At present, according to the known research results, the high expression of SHMT2 could be detected in different types of cancers, as reported, playing pivotal roles in migration and invasion. Knocking out SHMT2 in hepatocellular cancer cell lines was validated that reduces cell growth and tumorigenicity in vitro and vivo. Gene set enrichment analysis revealed that SHMT2 had a strong correlation with cancer invasion and poor survival among breast cancer patients. Besides, SHMT2 also was reported to control inflammatory cytokine signaling via its interaction with the BRISC deubiquitylase (DUB) and its important catalyst [36]. And SHMT2 impaired T cell survival in culture and antigen-specific T cell abundance in vivo [37]. Overall, these studies provide evidence that SHMT2 participated in different diseases via immune mechanisms.

5. Conclusion

In this study, we showed SHMT2 as an independent prognostic factor and found its high expression was associated with poor prognosis of LUAD. And further analysis conjectured that SHMT2 may mediate the immune cell infiltration

via regulation of macrophages and T cell in the LUAD micro-environment. Although there are some shortcomings in this study, such as our lack of experimental verification, we also demonstrate some highlights, which deserve more attention. We take full advantage of available public online datasets to verify our conjecture. However, further exploration and research to study the specific mechanism are also required. We hope this article can contribute to the following research.

Data Availability

The data that support the findings of this study are available from the corresponding author upon reasonable request.

Conflicts of Interest

The authors declare that they have no competing interests.

Authors' Contributions

LX Luo conceived the idea; XL Li, LX Luo, YS Zheng, ZP Lin, XD Li, and XL Li contributed to the acquisition, analysis, and interpretation of data. LX Luo and YS Zheng wrote the manuscript; MY Li, H Luo, L Cui, and LX Luo reviewed the paper and provided comments, and all authors reviewed the manuscript.

Acknowledgments

This project was supported by the PhD Start-up Fund of Guangdong Medical University (B2019016), Administration of Traditional Chinese Medicine of Guangdong Province (20201180), Administration of Traditional Chinese Medicine of Guangdong Province (20211223), Science and Technology Special Project of Zhanjiang (2019A01009), Natural Science Foundation of Guangdong Province (2016B030309002), Basic and Applied Basic Research Program of Guangdong Province (2019A1515110201), GDNRC [2020]038, and Fund of Southern Marine Science and Engineering Guangdong Laboratory (Zhanjiang) (ZJW-2019-007).

Supplementary Materials

Supplementary Table 1: correlation analysis between SHMT2 and related gene markers of immune cells. (*Supplementary Materials*)

References

- [1] R. D. Neal, W. Hamilton, and T. K. Rogers, "Lung cancer," *BMJ*, vol. 349, p. g6560, 2014.
- [2] J. J. Lin, S. Cardarella, C. A. Lydon et al., "Five-year survival in EGFR_{T790M}-mutant metastatic lung adenocarcinoma treated with EGFR-TKIs," *Journal of Thoracic Oncology*, vol. 11, no. 4, pp. 556–565, 2016.
- [3] I. Amelio, F. Cutruzzolá, A. Antonov, M. Agostini, and G. Melino, "Serine and glycine metabolism in cancer," *Trends in Biochemical Sciences*, vol. 39, no. 4, pp. 191–198, 2014.
- [4] D. D. Anderson and P. J. Stover, "Shmt1 and shmt2 are functionally redundant in nuclear de novo thymidylate biosynthesis," *PLoS One*, vol. 4, no. 6, p. e5839, 2009.
- [5] X. Yang, Z. Wang, X. Li et al., "Shmt2 desuccinylation by sirt5 drives cancer cell proliferation," *Cancer Research*, vol. 78, no. 2, pp. 372–386, 2018.
- [6] M. Xu, J. J. Moresco, M. Chang et al., "Shmt2 and the brcc36/brisc deubiquitinase regulate hiv-1 tat k63-ubiquitylation and destruction by autophagy," *PLoS Pathogens*, vol. 14, no. 5, pp. e1007071–e1007071, 2018.
- [7] L. Ji, Y. Tang, X. Pang, and Y. Zhang, "Increased expression of serine hydroxymethyltransferase 2 (shmt2) is a negative prognostic marker in patients with hepatocellular carcinoma and is associated with proliferation of hepg2 cells," *Medical Science Monitor*, vol. 25, pp. 5823–5832, 2019.
- [8] E. Balsa, E. A. Perry, C. F. Bennett et al., "Defective NADPH production in mitochondrial disease complex i causes inflammation and cell death," *Nature communications*, vol. 11, no. 1, p. 2714, 2020.
- [9] Y. Jiang, A. Wang, H. Bai, and M. Ye, "Protective effect of serine methyltransferase against hepatic ischemia-reperfusion injury in mice," *Nan Fang Yi Ke Da Xue Xue Bao*, vol. 40, no. 4, pp. 506–512, 2020.
- [10] S. Ning, S. Ma, A. Q. Saleh, L. Guo, Z. Zhao, and Y. Chen, "Shmt2 overexpression predicts poor prognosis in intrahepatic cholangiocarcinoma," *Gastroenterology Research and Practice*, vol. 2018, Article ID 4369253, 6 pages, 2018.
- [11] S. Bernhardt, M. Bayerlová, M. Vetter et al., "Proteomic profiling of breast cancer metabolism identifies shmt2 and asct2 as prognostic factors," *Breast Cancer Research*, vol. 19, no. 1, p. 112, 2017.
- [12] D. Kim, B. P. Fiske, K. Birsoy et al., "Shmt2 drives glioma cell survival in ischaemia but imposes a dependence on glycine clearance," *Nature*, vol. 520, no. 7547, pp. 363–367, 2015.
- [13] M. Wu, S. Wanggou, X. Li, Q. Liu, and Y. Xie, "Overexpression of mitochondrial serine hydroxyl-methyltransferase 2 is associated with poor prognosis and promotes cell proliferation and invasion in gliomas," *Oncotargets and Therapy*, vol. - Volume 10, pp. 3781–3788, 2017.
- [14] A. Mantovani, P. Allavena, A. Sica, and F. Balkwill, "Cancer-related inflammation," *Nature*, vol. 454, no. 7203, pp. 436–444, 2008.
- [15] X. Liu, S. Wu, Y. Yang, M. Zhao, G. Zhu, and Z. Hou, "The prognostic landscape of tumor-infiltrating immune cell and immunomodulators in lung cancer," *Biomedicine & Pharmacotherapy*, vol. 95, pp. 55–61, 2017.
- [16] J. Candido and T. Hagemann, "Cancer-related inflammation," *Journal of clinical immunology*, vol. 33, pp. S79–S84, 2013.
- [17] M. R. Rähkä and P. A. Puolakkainen, "Tumor-associated macrophages (tams) as biomarkers for gastric cancer: a review," *Chronic diseases and translational medicine*, vol. 4, no. 3, pp. 156–163, 2018.
- [18] N. Inoshima, Y. Nakanishi, T. Minami et al., "The influence of dendritic cell infiltration and vascular endothelial growth factor expression on the prognosis of non-small cell lung cancer," *Clinical Cancer Research*, vol. 8, no. 11, pp. 3480–3486, 2002.
- [19] R. P. Petersen, M. J. Campa, J. Sperlizza et al., "Tumor infiltrating Foxp3⁺ regulatory t-cells are associated with recurrence in pathologic stage i NSCLC patients," *Cancer*, vol. 107, no. 12, pp. 2866–2872, 2006.
- [20] L. Moreno Leon, M. Gautier, R. Allan et al., "The nuclear hypoxia-regulated nlucatl long non-coding rna contributes to an aggressive phenotype in lung adenocarcinoma through regulation of oxidative stress," *Oncogene*, vol. 38, no. 46, pp. 7146–7165, 2019.
- [21] F.-Y. Lo, J.-W. Chang, I. S. Chang et al., "The database of chromosome imbalance regions and genes resided in lung cancer from Asian and Caucasian identified by array-comparative genomic hybridization," *BMC Cancer*, vol. 12, no. 1, 2012.
- [22] H. Okayama, T. Kohno, Y. Ishii et al., "Identification of genes upregulated in ALK-positive and EGFR/KRAS/ALK-negative lung adenocarcinomas," *Cancer Research*, vol. 72, no. 1, pp. 100–111, 2012.
- [23] G. K. Smyth, J. Michaud, and H. S. Scott, "Use of within-array replicate spots for assessing differential expression in microarray experiments," *Bioinformatics*, vol. 21, no. 9, pp. 2067–2075, 2005.
- [24] A. Subramanian, H. Kuehn, J. Gould, P. Tamayo, and J. P. Mesirov, "GSEA-P: a desktop application for gene set enrichment analysis," *Bioinformatics*, vol. 23, no. 23, pp. 3251–3253, 2007.
- [25] D. Shi, Q. Qu, Q. Chang, Y. Wang, Y. Gui, and D. Dong, "A five-long non-coding RNA signature to improve prognosis prediction of clear cell renal cell carcinoma," *Oncotarget*, vol. 8, no. 35, pp. 58699–58708, 2017.
- [26] A. Lánckzy, Á. Nagy, G. Bottai et al., "Mirpower: a web-tool to validate survival-associated miRNAs utilizing expression data from 2178 breast cancer patients," *Breast Cancer Research and Treatment*, vol. 160, no. 3, pp. 439–446, 2016.
- [27] D. R. Rhodes, S. Kalyana-Sundaram, V. Mahavisno et al., "OncoPrint 3.0: genes, pathways, and networks in a collection of 18,000 cancer gene expression profiles," *Neoplasia*, vol. 9, no. 2, pp. 166–180, 2007.
- [28] Z. Tang, C. Li, B. Kang, G. Gao, C. Li, and Z. Zhang, "Gepia: a web server for cancer and normal gene expression profiling and interactive analyses," *Nucleic acids research*, vol. 45, no. W1, pp. W98–W102, 2017.
- [29] D. S. Chandrashekar, B. Bashel, S. A. H. Balasubramanya et al., "UALCAN: a portal for facilitating tumor subgroup gene expression and survival analyses," *Neoplasia*, vol. 19, no. 8, pp. 649–658, 2017.
- [30] T. Li, J. Fan, B. Wang et al., "Timer: a web server for comprehensive analysis of tumor-infiltrating immune cells," *Cancer Research*, vol. 77, no. 21, pp. e108–e110, 2017.

- [31] B. Ru, C. N. Wong, Y. Tong et al., "TISIDB: an integrated repository portal for tumor-immune system interactions," *Bioinformatics*, vol. 35, no. 20, pp. 4200–4202, 2019.
- [32] M. Uhlen, L. Fagerberg, B. M. Hallström et al., "Tissue-based map of the human proteome," *Science*, vol. 347, no. 6220, p. 1260419, 2015.
- [33] M. Uhlen, C. Zhang, S. Lee et al., "A pathology atlas of the human cancer transcriptome," *Science*, vol. 357, no. 6352, p. - ean2507, 2017.
- [34] C. F. Labuschagne, N. J. F. van den Broek, G. M. Mackay, K. H. Vousden, and O. D. K. Maddocks, "Serine, but not glycine, supports one-carbon metabolism and proliferation of cancer cells," *Cell Reports*, vol. 7, no. 4, pp. 1248–1258, 2014.
- [35] B. Wang, W. Wang, Z. Zhu et al., "Mitochondrial serine hydroxymethyltransferase 2 is a potential diagnostic and prognostic biomarker for human glioma," *Clinical Neurology and Neurosurgery*, vol. 154, pp. 28–33, 2017.
- [36] M. Walden, L. Tian, R. L. Ross et al., "Metabolic control of brisc-shmt2 assembly regulates immune signalling," *Nature*, vol. 570, no. 7760, pp. 194–199, 2019.
- [37] J. Cao, L. Sun, P. Aramsangtienchai et al., "Hdac11 regulates type i interferon signaling through defatty-acylation of shmt2," *Proceedings of the National Academy of Sciences of the United States of America*, vol. 116, no. 12, pp. 5487–5492, 2019.

Review Article

Application of Bionanomaterials in Tumor Immune Microenvironment Therapy

Jiawei Wang ^{1,2}, Yan Bao ², and Yandan Yao ^{1,2}

¹Breast Tumor Center, Sun Yat-sen Memorial Hospital, Sun Yat-sen University, Guangzhou 510120, China

²Guangdong Provincial Key Laboratory of Malignant Tumor Epigenetics and Gene Regulation, Guangdong-Hong Kong Joint Laboratory for RNA Medicine, Sun Yat-sen Memorial Hospital, Sun Yat-sen University, Guangzhou 510120, China

Correspondence should be addressed to Yan Bao; baoy5@mail.sysu.edu.cn and Yandan Yao; yaoyand@mail.sysu.edu.cn

Received 6 October 2020; Revised 20 December 2020; Accepted 7 January 2021; Published 11 February 2021

Academic Editor: Xianyang Li

Copyright © 2021 Jiawei Wang et al. This is an open access article distributed under the Creative Commons Attribution License, which permits unrestricted use, distribution, and reproduction in any medium, provided the original work is properly cited.

Targeted therapy for the cancer immune system has become a clinical reality with remarkable success. Immune checkpoint blockade therapy and chimeric antigen receptor T-cell (CAR-T) immunotherapy are clinically effective in a variety of cancers. However, the clinical utility of immunotherapy in cancer is limited by severe off-target toxicity, long processing time, limited efficacy, and extremely high cost. Bionanomaterials combined with these therapies address these issues by enhancing immune regulation, integrating the synergistic effects of different molecules, and, most importantly, targeting and manipulating immune cells within the tumor. In this review, we will summarize the most current researches on bionanomaterials for targeted regulation of tumor-associated macrophages, myeloid-derived suppressor cells, dendritic cells, T lymphocyte cells, and cancer-associated fibroblasts and summarize the prospects and challenges of cell-targeted therapy and clinical translational potential in a tumor immune microenvironment in cancer treatment.

1. Introduction

The tumor immune microenvironment (TIME) is broadly populated with immune cells including tumor-associated macrophages (TAMs) and myeloid-derived suppressor cells (MDSCs) which suppress cancer immunity, leading to failure of immunotherapy [1]. Targeted therapy of the immune subset of TIME not only can efficiently remodel the TIME and activate the immune system against tumors but is also accompanied by adverse side effects mostly due to off-target toxicity [2]. For instance, the approved immune checkpoint blockade drugs which target cytotoxic T-lymphocyte antigen 4 (CTLA-4) and programmed cell death 1 (PD-1) or its ligand, programmed cell death ligand 1 (PD-L1), have shown efficacy in prolonging the overall survival of patients with various cancers. However, it also increases immune-related adverse events in patients, including the gastrointestinal tract and liver toxicity and endocrine dyscrasia [2, 3].

To enhance the curative effect and overcome the side effects of and traditional immunology therapy, developments in nanotechnology and bioengineering have provided a new

approach that could greatly improve the safety and efficacy of cancer immunotherapy [4, 5]. Most clinical applications of bionanomaterials are as carriers of therapeutic and imaging agents in the treatment of cancer. Bionanomaterials have not only improved the delivery and efficacy of a series of pharmaceutical ingredients including drugs, antibodies, peptides, nucleotide, and enzymes but have also been designed to extend the duration of the release therapy and can be further modified to target specific sites in the body, thereby reducing the amount of the drug to achieve the desired therapeutic effect and reducing toxicity to the patients.

Bionanomaterials and related drug-delivery solutions focus the action of payloads on specific cell types and to specific anatomical locations to reduce adverse effects. Polymers and nanoparticles have become a focus of research in cancer therapy due to their potential ability to alter the pharmacokinetics and also accumulate in tumors through enhanced permeability and retention (EPR) effects [6, 7]. The EPR effect is that particles with sizes from 10 to 100 nm transport from the bloodstream, extravasate into tumors through the dysfunctional vasculature, and remain in tumors due to defective

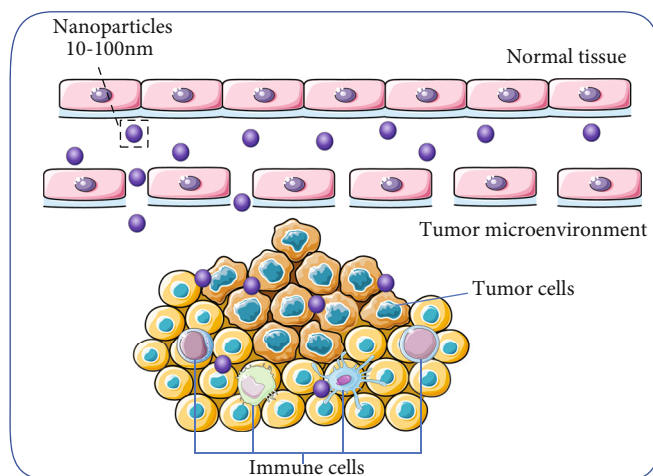


FIGURE 1: Overview of nanoparticles' permeation and retention effect (EPR). Nanoparticles ranging in size from 10 to 100 nm are aggregated by EPR effect through the immature blood vessels of the tumor and targeting the cells in the tumor microenvironment.

lymphatics, as shown in Figure 1. Besides, for the EPR effect, nanoparticle surface modification of specific markers is conducive to drug penetration into target immune cells. For example, the mannose receptor (CD206) has been demonstrated as an appealing target for M2 TAM in tumors and can be used in immunotherapy for TAMs and achieve good efficacy [8].

This review will summarize some of the recent advances in nanomaterial-based strategies of targeting immune cells in TIME, including TAMs, MDSCs, dendritic cells (DCs), T lymphocyte cells, and cancer-associated fibroblasts (CAFs). Instead of material design, we will focus on providing an overview of the material systems under development that is aimed at enhancing the effectiveness of cancer immunotherapy. Finally, we will summarize the prospects and challenges of targeting immune cells and clinical translational potential in TIME for cancer treatment.

2. The Mechanisms/Strategies for the Bionanomaterials in Regulating the Immune Cells

Many factors affect drug administration which may influence treatment outcomes, including pharmacokinetics, distribution, cellular uptake and metabolism, excretion and clearance, and toxicity [9]. In terms of this issue, bionanomaterials can be a good solution to treat cancer by delivering components to targeted immune cells and activate the immune system against tumors. Mostly, delivering small molecule immune activator/inhibitor or associated drug may be the most common way to regulate the immune cell in TIME, such as chemotherapy drug like Doxorubicin [10]. And recently, exosomes, nucleotides, antigens, and so on have been joined in the nanodelivery system [11–13]. Except for acting as the carriers, some nanoparticles (mostly mental nanoparticles) can regulate the immune cell directly. For instance, some nanoparticles could generate reactive oxygen species (ROS) and reprogram TAMs to an antitumor M1 phenotype directly, eradicating tumors effectively [14].

3. Targeted Therapy of Cells in the Tumor Immune Microenvironment

3.1. Tumor-Associated Macrophages (TAMs). While immune infiltrates vary in different cancer types, monocyte/macrophages represent the major infiltrating population in most human cancers [15]. Recently, many studies have demonstrated their close relation with tumor progression and protumoral functions [16, 17], including tumor cell activation, angiogenesis, immunosuppression, tumor invasion, and metastasis [18]. Tumor-associated macrophages that differentiate from myeloid cells driven by the growing tumor signals are mostly classified as classically activated (M1) alternatively activated (M2) macrophages. Clinical immunohistochemical data has indicated that a higher density of total TAMs or M2 TAMs is associated with a poorer prognosis, while tumor infiltration with M1 TAMs may be a good prognostic factor in specific environments [16, 19–21]. Therapies targeted at TAMs are mostly divided into two strategies, including depletion and reprogramming [18]. However, the poor specific accumulation in tumors and significant toxicity of these agents have limited their use in the clinic.

Colony-stimulating factor 1 receptor (CSF-1R) is a canonical expressive marker of macrophages. Because macrophages are dependent on the CSF-1R signal, it is an attractive target for selectively depleting macrophages, and many associated small molecules targeting CSF-1R are under clinical trial and development [22–24]. For instance, platinum-(Pt-) prodrug conjugated small particles and BLZ-945, a small molecule inhibitor of CSF-1R, not only induce apoptosis of tumor cells but also modulate the tumor immune environment to eventually augment the antitumor effect of CD8+ cytotoxic T cells through TAM depletion [25]. Besides CSF-1R inhibitors, bisphosphonates are the drugs most commonly used to deplete TAMs in the clinic. To improve the overall effect and decrease toxicity, liposomal clodronate was created to promote TAM depletion and antitumor efficiency [26]. A more accurate way to specifically block the

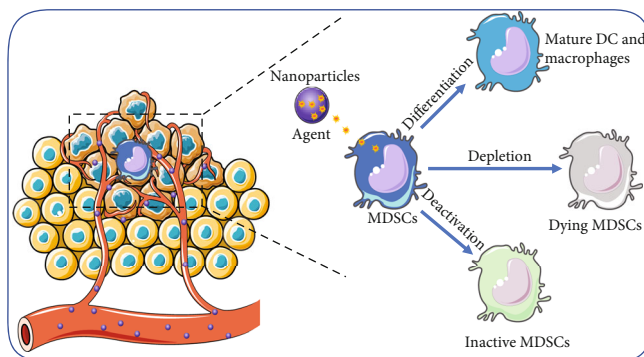


FIGURE 2: Nanomaterials for modulation of myeloid-derived suppressor cells (MDSCs). The immunotherapy strategy based on MDSC mainly includes the following three aspects: (i) induced to differentiate into mature DC and macrophages, (ii) depleted or blocked its amplification, and (iii) inhibited the immunosuppressive function.

survival signal of M2 TAMs and deplete them from melanoma is to load anti-CSF-1R small interfering RNA (siRNA) on nanoparticles [11].

In addition to TAM depletion, reprogramming TAMs from M2 to M1 via nanomaterials have also been widely developed. Azide-modified exosomes derived from M1 macrophages, which are conjugated with antibodies of CD47 and SIRP α , actively target tumors, improve phagocytosis of macrophages, and reprogram macrophages from protumoral M2 to antitumoral M1 [12]. The trastuzumab-modified mannosylated liposomal system was able to repolarize the protumor M2 phenotype to the antitumor M1, reversing the resistance to tyrosine kinase inhibitor treatment in EGFR-mutated non-small-cell lung cancer [8]. Ferumoxytol, an iron oxide nanoparticle compound approved by the FDA for the treatment of iron deficiency, was found to have an intrinsic therapeutic effect on cancer growth due to macrophage polarization into proinflammatory M1 phenotypes [27]. Some nanomaterials can also directly stimulate the repolarization of TAMs. Nanoparticle-based reactive oxygen species photogeneration can reprogram TAMs to an antitumor M1 phenotype, effectively eradicating tumors [14].

It is worth noting that TAMs cannot be simply divided into two subtypes because TAMs may express both M1 and M2 markers [28, 29]. M1 and M2 may only represent two extreme examples of macrophage phenotype. Ratios of M1/M2 in tumor tissues and normal tissues might be a more suitable way to evaluate TAM phenotype-modulating nanomaterials.

3.2. Myeloid-Derived Suppressor Cells (MDSCs). Among cancer patients, there is an increase in immature myeloid cell proportion within TIME [30]. These cells, which express myeloid markers (Gr1+/CD11b+ in mice and CD11b+/CD33+ in human) [31], are named myeloid-derived suppressor cells because of their immunosuppressive and protumor characteristics. MDSCs can prevent immune cells from infiltrating tumors and also suppress effector T cell infiltration [32]. A meta-analysis has shown that a high level of MDSCs might be related to poor clinical outcomes of cancer patients; that is, MDSCs might be a potential biomarker in cancer treatment [33]. Similar to TAMs, various agents tar-

geted at MDSCs have been developed, according to the strategies of depletion, differentiation, and deactivation, as shown in Figure 2.

Direct targeting and elimination of immunosuppressive MDSCs in TIME by signaling pathway regulation provide a new approach for tumor immunotherapy. PAH/RGX-104@PDM/PTX, a dual-pH-sensitive codelivery nanocarrier, not only causes apoptosis of cancer cells but also alleviates the immunosuppression of the TIME and finally enhances the antitumor effect of cytotoxic T lymphocytes (CTLs) through the depletion of MDSCs [34]. CpG-ODN/Poly(I:C)/RB6-8C5 nanoparticles have been developed which improve treatment outcome and have significantly reduced established B16 melanoma lung metastases through local depletion of MDSCs or reduction of immunosuppressive molecules (IFN- α , IL-10, Arg-1, and Nos2) which directly activate the natural killer (NK) cells and macrophages in the lung [35].

The polarization of immunosuppressive MDSCs in TIME of proinflammatory phenotype would be a better strategy than inhibiting or depleting it [36]. A designer scaffold encapsulated with Resiquimod (iNCV (R848)), which leads to the activation and maturation of antigen-presenting cells and induces the secretion of proinflammatory cytokines, can not only reduce the frequency of immunosuppressive cells in tumors but also increase systemic antitumor immune response while minimizing systemic toxicity [37]. Besides, zinc-doped iron oxide nanoparticles destroy glioma cells and repolarize MDSCs from an immunosuppressive phenotype to a proinflammatory phenotype *in vivo*, which promotes antitumor effects and synergistically promotes radiotherapy effects [38].

Some nanomaterials not only act as carriers for MDSC regulatory molecules but also directly silence or interfere with MDSCs. Low molecular weight heparin-tocopherol succinate nanoparticles prevent premetastatic niche formation by interfering with granulocytic myeloid-derived suppressor cells (G-MDSCs), effectively inhibiting implantation and colonization of circulating tumor cells [39].

Many nanomaterial agents have been developed for immunology cells as previously described; however, limited knowledge about the derivation and characteristics of

myeloid-derived cells (TAMs and MDSCs) restricts accurate nanomaterial targeting.

3.3. Dendritic Cells (DCs). DCs are a type of antigen-presenting cells (APC) that play an important role in the uptake and present tumor-associated antigens (TAAs) to the major histocompatibility complex (MHC), initiating antigen-specific T cell immune responses [40]. Cancer vaccines, composed of TAAs and adjuvants, act as the tumor antigen to stimulate DCs to generate TAA-specific CTL responses for killing tumor cells efficiently. Current cancer vaccines are designed to produce antibodies against cancer-causing viruses to reduce the risk of suffering from cancer. The best known is the human papillomavirus (HPV) vaccine, which can stimulate the body to produce antibodies to prevent HPV related to cervical, anal, oropharyngeal, vaginal, vulvar, and penile cancers. To date, three HPV vaccines (Gardasil, Cervarix, and Gardasil 9) have been approved by the United States Food and Drug Administration (FDA) [41]. Despite promising safety and immunogenicity profiles, the efficacy of the DC vaccine in clinical trials has not been satisfactory for several reasons, including method of loading, insufficient antigen presentation, poor accumulation in lymphatic tissues, and immunosuppression [42, 43]. Nanomaterials have obvious advantages in delivery capability and tissue targeting and have good application prospects in the development of tumor vaccines.

After intradermal injection, interstitial fluid flow transports ultrasmall nanoparticles highly efficiently into lymphatic capillaries and their draining lymph nodes (DLN), where dendritic cells were effectively activated [44]. Therefore, nanomaterial-based vaccines are capable of successfully transporting antigens to professional APCs in the DLN and enhancing immunogenicity [44, 45]. Silica nanoparticles as a lymph node targeting platform for vaccine delivery can accumulate in antigen-presenting cells in the draining lymph nodes after injection, greatly reducing the production of systemic proinflammatory cytokines and completely abrogating splenomegaly [13]. Besides receptor-mediated endocytosis, macropinocytosis is another way to take up exogenous antigens. For example, the biomimetic nanovaccine (R837- α OVA-ApoE3-HNP) can be taken into DCs through the macropinocytosis pathway and significantly promote DC maturation, antigen presentation, and strong T cell immune responses (including the generation of antigen-specific CD8 + T cells, expansion of IFN- γ + CD8+ T cells, and the secretion of IFN- γ +) [46]. In addition, the nanoparticle can also be used as an adjuvant or immune enhancer and has the ability to activate cellular, humoral immunity and promote antigen presentation. For example, it has been proven that poly-L-lysine-coated nanoparticles were effective adjuvants and greatly enhance DNA immunogenicity [47].

3.4. T Lymphocyte Cells. Lymphocyte-mediated adaptive immune response plays an important role in the development of tumors and the dysfunction of the immune response in the TIME. CD8+ T cells differentiate to cytotoxic T cells, immigrate into the tumor microenvironment, and exhibit cytotoxicity and the ability to kill tumor cells. However,

CD8+ T cells gradually produce a dysfunctional state known as T cell exhaustion after they infiltrate tumor tissues, characterized by losing robust effector functions and expressing multiple inhibitory receptors [48]. Mostly, the development of CD8+ T cell exhaustion could be due to persistent antigen exposure, inhibitory receptors, soluble mediators, and regulatory cells [48]. Substantially higher expressions of inhibitory receptors, including PD-1, CTLA-4, and T cell immunoglobulin, are the hallmarks of exhausted T cells. Immune checkpoint blockade therapy, which mostly targets PD-1/PD-L1 and CTLA-4/CD28 pathways in T cells to enhance antitumor immune responses, has led to important clinical advances and provided a new strategy against cancer [49]. However, multiple immune-related adverse events, including the gastrointestinal tract and liver toxicity, autoimmune disease, and endocrine dyscrasia, have been found in patients treated with immune checkpoint blockade, due to off-target effects [2]. Nanomaterial-engineered drug delivery systems and controlled release strategies can improve drug accumulation and retention within target cells and tissues and amplify their anticancer efficacy while reducing toxicities and off-target effects [50].

Controlled-release strategies for immune checkpoint blockade therapy may be an efficient way to enhance the anti-tumor effect. Spatiotemporally controlled nanodevices increase intratumoral drug concentrations and achieve sequential drug release, which enhances T cell infiltration in tumor tissues and thus prolongs the survival of mice [51]. Furthermore, a potent antitumor chemoimmunotherapy has been developed which utilizes tumor microenvironment-sensitive micelles bearing a sheddable PEG layer to mediate the site-specific sequential release of PD-1 monoclonal antibodies (MAbs) and Paclitaxel, resulting in a synergistic antitumor chemoimmunotherapy [52].

Materials not only enable controlled release of checkpoint blockade MAbs but can also be used to regulate the tumor microenvironment and promote checkpoint blockade MAb delivery and functions, such as increasing proinflammatory cytokine levels and T cell infiltration [53]. For example, photodynamic therapy (PDT) is able to stimulate antitumor immune responses by efficient photodynamic destruction of tumors to generate a mass of tumor-associated antigens and R837-containing nanoparticles as the adjuvants promote strong antitumor immune responses [54]. It has been shown that PDT with UCNP-Ce6-R837 in combination with CTLA-4 checkpoint blockade not only has excellent efficacy in eliminating tumors exposed to the near-infrared laser but also results in strong antitumor immunity to inhibit the growth of distant tumors left behind after PDT treatment [54].

Nanomaterial which delivers or loads cytokines acting on T cells provides another immunotherapy strategy. For example, transforming growth factor- β (TGF- β) and interleukin-2 (IL-2), which, respectively, suppress local tumor immune responses and amplify the activation of melanoma-specific T-cell responses, can be combined to treat metastatic melanoma [55]. Combination delivery of TGF- β inhibitor and IL-2 by nanoscale liposomal polymeric gels can deliver small hydrophobic molecular inhibitors and water-soluble protein

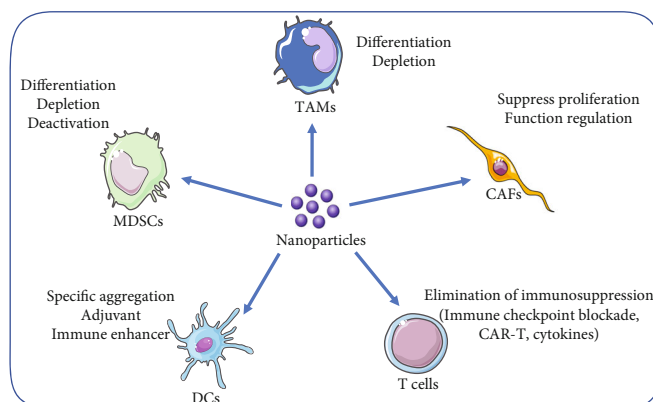


FIGURE 3: Some strategies of biomaterials in targeting different cells in a tumor immune microenvironment. Nanoparticles can target immune cells in TIME, including tumor-associated macrophages (TAMs), myeloid-derived suppressor cells (MDSCs), dendritic cells (DCs), T lymphocyte cells (T cells), and cancer-associated fibroblasts (CAFs), through various pathways or methods enumerated as shown.

cytokines in a sustained way to the tumor microenvironment to enhance tumor immunotherapy [55].

Besides immune checkpoint blockade therapy, chimeric antigen receptor T-cell (CAR-T) immunotherapy is another way to amplify cytotoxic T lymphocyte responses. CAR-T therapy, by genetically modifying and expanding T cells *ex vivo* before being infused back into patients, can concentrate tumor-specific CTLs in the tumor microenvironment. It has recently been approved by the FDA to treat large B-cell lymphoma and B-cell precursor acute lymphoblastic leukemia [56, 57] but is limited by low response rates, severe off-target side effects, cumbersome process, and extremely high cost [58]. For CAR-T therapy, biomaterials have been used to shorten the processing time, amplify the expansion of T cells *in vitro*, and promote the survival and proliferation of infused T cells [59]. For example, ionizable lipid nanoparticles (LNPs) are designed for *ex vivo* mRNA delivery to human T cells to induce functional protein expression, with substantially reduced cytotoxicity and potent cancer-killing activity [60]. The scarcity of tumor vessels and the immunosuppressive tumor microenvironment are often the reasons for the reduced efficacy of CAR-T cells in solid tumors. A combination of photothermal therapy with the adoptive transfer of CAR-T cells has superior antitumor activity in mice engrafted with human melanoma WM115 cell lines because it increases blood perfusion, releases antigens, and promotes the recruitment of endogenous immune cells [61].

3.5. Cancer-Associated Fibroblasts (CAFs). The interaction between tumor cells and the surrounding stroma promotes the acquisition of an invasive phenotype, neoangiogenesis, progression, metastasis, immunosuppression, and chemoresistance of tumors [62]. Cancer-associated fibroblasts (CAFs) are the predominant cells in the tumor stroma (up to 80% in pancreatic cancer) [63] and exert an important influence on tumor growth by regulating the tumor microenvironment. It was found that the genes associated with colorectal cancer (CRC) recurrence and poor prognosis were upregulated mainly in CAFs, rather than in tumor cells [64]. Therefore, it has also been widely studied as a nanomaterial target for enhanced immunotherapy.

Recently, some of the biological properties of CAFs have been used to study and design new therapeutics and nanotherapeutics to modify TIME and improve the therapeutic activity of chemotherapy [65]. For example, due to the scarcity of tumor vessels and extensive deposits of extracellular matrix components, pancreatic ductal adenocarcinoma (PDA) may impute its unique chemoresistance to inefficient drug delivery [66]. PEGPH20 combined with IPI-926 specifically decreases the proliferation of stromal myofibroblasts, inhibits tumor growth, and prolongs survival when combined with gemcitabine in a genetically engineered mouse model of PDA. It does this by impeding the intratumoral vasculature of PDA and increasing the delivery of the chemotherapeutic drug [67]. Besides the combination therapy of nanomaterials and chemotherapy, nanoparticles affect the gene expression and secretion of CAFs, thereby altering their intrinsic interactions with malignant cells and affecting the protumor activity of the TIME. It has been demonstrated that Au-Ag nanoparticles achieve remarkable metastasis-suppressing activity by directly inhibiting adenocarcinoma cell proliferation, as well as indirectly by affecting cancer-associated fibroblasts by reducing their cancer-promoting function and regulating their secretory profiles [68]. In addition, due to the off-target distribution of anticancer nanoparticles to CAFs, researchers have exploited nanoparticles that can genetically modify CAFs into cells producing secretable TNF-related apoptosis-inducing ligand (sTRAIL) efficiently *in situ*, leading to apoptosis in the adjacent tumor cells in mice [69].

4. Future Outlook and Perspective

For decades, cancer treatment has focused on killing tumor cells while ignoring other nontumor cells in the tumor microenvironment. In recent years, great attention has been paid to nontumor factors in the tumor microenvironment, as shown in Figure 3. Both CAR-T therapy and immune checkpoint blockade therapy, as well as treatments for other immune cells, have provided new solutions for cancer treatment which show efficacy for prolonging the overall survival of patients with various cancers. However, it also causes

TABLE 1: Examples of nanomaterial in modulation of TIME components.

TIME component	Strategy	Nanocarrier	Type	Active ingredient	Tumor model	Refs
TAMs	Depletion	Platinum - prodrug conjugated small particles	Pro-drug	BLZ-945	4T1, CT26	[25]
		SR-B1 linked with an M2 macrophage binding peptide	Liposome	Clodronate	-	[26]
MDSCs	Reprogramming	Azide-modified exosomes	Exosome	Antibodies of CD47 and SIRP α	B16F10	[11]
		Trastuzumab-modified, mannosylated liposomal ICG and titanium dioxide mannose-modified PEGylated PLGA nanoparticles	Liposome	Vorinostat	4T1	[12]
		Polymer of PEG-PDPA and PEG-PAEMA	Inorganic nanoparticle	ICG	H1975	[8]
		Porous scaffolds crosslinked with acid matrix	Polymer	RGX-104	4T1	[14]
DCs	Deactivation	Zinc-doped iron oxide nanoparticles	Polymer	Poly(I:C), RB6-8C5	4T1	[34]
		LWMMH - tocopherol succinate nanoparticle	Polymer scaffold	Resiquimod (R848)	B16	[35]
		Silica nanoparticle co-loading negatively charged oligonucleotide adjuvant and OVA antigen	Iron oxide nanoparticle	Zinc	4T1, TC1	[37]
T lymphocyte cells	Enhanced delivery and function	R837-loaded 26 DMPC-PLGA hybrid nanoparticles	Polymeric nanoparticle	D- α -tocopheryl succinate	U87 MG, CT-2A	[38]
		Copolymer of azide-terminated polyethylene glycol and polyaspartic acid sheddable long-chain PEG	Micelle/liposome	HY-19991	B16	[39]
CAF	Genetically modify	Upconversion nanoparticles by co-loading chlorin e6, and imiquimod	Inorganic conversion	Imiquimod (R837)	EG7-OVA	[13]
		lipid bilayer surrounding a hydrogel core fabricated from a degradable polymer	liposomal polymeric	IL-2	B16-OVA	[46]
CAF	Deactivation	Ionizable lipid nanoparticles	lipid nanoparticle	mRNA	EG7	[47]
		PEGylated human recombinant PH20 hyaluronidase	Polymer	CSPG-4	MCF-7	[51]
CAF	Genetically modify	Gold-core silver-shell-structured hybrid nanoparticle system	Gold/polymer hybrid	Au, Ag	B16F10	[52]
		Lipid-coated protamine DNA complexes	Liposome	sTRAIL	CT26	[54]

Abbreviation: TAMs: tumor-associated macrophages, MDSCs: myeloid-derived suppressor cells, DCs: Dendritic cells, CAFs: Cancer-associated fibroblasts, SIRP α : signal regulatory protein; SR-B1: scavenger receptor B type 1; PLGA: poly(lactic-co-glycolic) acid; ICG: indocyanine green; CpG-ODN/Poly(I:C): oligodeoxynucleotides containing CpG motifs/ polyinosinic-polycytidylic acid; LWMMH: low molecular weight heparin; OVA: ovalbumin; CSPG4: antigen chondroitin sulfate proteoglycan-4; IL-2: interleukin-2; sTRAIL:secretable form of tumor necrosis factor related apoptosis-inducing ligand.

TABLE 2: Main overexpressing receptors that could be targeted in TIME.

Type of cells	Receptors
Tumor-associated macrophages	CD86, CD206, CD163, HLA-DR, CD11b, F4/80, MHC-II
Myeloid-derived suppressor cells	CD11b, CD14, CD15, CD66b, Ly6C, Ly6G
Dendritic cells	CD11c, MHC-II, CD1a
T lymphocyte cells	CD3, CD4, CD8, FOXP3, CD45RO, PD-1
Cancer-associated fibroblasts	GPR77, CD10, α SMA, FAP

TABLE 3: Some applications of bio-nanomaterial approved by FDA or in clinical trials in microenvironment therapy.

Name	Component	Immunotherapy effect	Clinical trial status	Ref
Dex	Nanoparticulate DC-derived exosomes	Stimulate CTLs and CD4+ T cells, NK cell activation	Phase 2, completed (NCT01159288)	[73]
Ferumoxytol	IONP	Transfer M2-like macrophages to M1-like in TME	Approved by FDA for anemia and kidney diseases	[27]
RNA-LPX (Lipoplexfi)	RNA-loaded liposomes	DC maturation, T cell response, inflammatory response	Phase 1, recruiting (NCT04503278)	[74]
DOXIL	Doxorubicin-loaded liposomes	Increased intratumoral CD8+ T cell infiltration, decreased the proportion of regulatory T cells (Treg cells), and increased CD80 expression by myeloid cells	Approved by FDA for cancer treatment	[10]
TRQ15-01	Nanogels	Ex vivo modification of T cells prior to adoptive-cell transfer	Phase 1, active (NCT03815682)	[75]
AST-008	CpG oligonucleotide nanoparticulate	Activating NK cells and inducing IFN- α production from plasmacytoid DC precursors, enhance B cell stimulatory property	Phase 1/2, recruiting (NCT03684785)	[76]

IONP: iron oxide nanoparticle; CTL: cytotoxic T lymphocyte; NK cell: natural killer cell; FDA: Food and Drug Administration; DC: dendritic cell.

immune-related side-effects in patients and only benefits a fraction of patients.

Biomaterial carriers of immunotherapy can address the side effects of delivery and off-target effects, enhance immune regulation, integrate the synergistic effects of different molecules, and manipulate immune cells *in vivo* [70], as shown in Table 1. However, significant challenges remain to achieve a wide range of clinical outcomes for immune cell-targeted biomaterials. Firstly, the immune system has the paradoxical ability to have both tumor-suppressing and tumor-promoting roles, just as TAMs can be the proinflammatory M1 type and/or the anti-inflammatory M2 type. Furthermore, it is difficult to define MDSCs and TAMs through cell surface markers alone [28, 29]. There are some types of TIME cells and their main overexpressing receptors that could be targeted as shown in Table 2. The application of traditional fluorescence-based flow cytometry is limited by the number of phenotypic markers that can be detected. High-throughput approaches, such as mass spectrometry (CyTOF), that have emerged in recent years, should help further identify cell surface markers. Secondly, a tumor immune microenvironment is a complex system with mutual regulation among components, targeting only one kind of cells to antitumor seemed to be incomprehensive. Many other types of cells, particularly natural killer cells and B cells, may also provide effective targets for cancer immunotherapy [71] but have not been widely explored as targets for immunoregulatory materials. Finally, the short-

comings of nanomaterials themselves remain to be addressed, including damage to the cell directly or by initiating internal signaling pathways, the release of toxic material that impacts the organism's enzyme functions or cell DNA, and the generation of reactive oxygen species and subsequent oxidative stress [72].

Despite their potential advantages, only a handful of bio-nanomaterials have so far been used in clinical trials or received regulatory approval which affects the immune cell (Table 3). For now, a bionanomaterial drug like DOXIL, a kind of Doxorubicin-loaded liposomes, has been widely used in the clinic, which has the ability to kill the tumor directly meanwhile regulate T cells and myeloid cells [10]. With the recent outstanding achievements of the treatment of immune microenvironment cells and immune checkpoints, it is believed that nanomedicine materials will be widely used in clinical practice in the near future.

Conflicts of Interest

The authors declare that they have no conflicts of interest.

Acknowledgments

This work was supported by grants from the Fundamental Research Funds of the Central Universities (20ykjc03 and 19ykpy102), the National Science Foundation of China (81772837 and 82071859), the Science and Technology

Foundation of the Guangdong Province (2019A050510016), Guangdong Innovation and Entrepreneurship Team Projects (2019BT02Y198), and Guangdong Science and Technology Department (2020B1212060018 and 2020B1212030004).

References

- [1] M. Binnewies, E. W. Roberts, K. Kersten et al., "Understanding the tumor immune microenvironment (TIME) for effective therapy," *Nature Medicine*, vol. 24, no. 5, pp. 541–550, 2018.
- [2] M. A. Postow, R. Sidlow, and M. D. Hellmann, "Immune-related adverse events associated with immune checkpoint blockade," *The New England Journal of Medicine*, vol. 378, no. 2, pp. 158–168, 2018.
- [3] J. S. Weber, F. S. Hodi, J. D. Wolchok et al., "Safety profile of nivolumab monotherapy: a pooled analysis of patients with advanced melanoma," *Journal of Clinical Oncology*, vol. 35, no. 7, pp. 785–792, 2017.
- [4] L. Jeanbart and M. A. Swartz, "Engineering opportunities in cancer immunotherapy," *Proceedings of the National Academy of Sciences of the United States of America*, vol. 112, no. 47, pp. 14467–14472, 2015.
- [5] R. S. Riley, C. H. June, R. Langer, and M. J. Mitchell, "Delivery technologies for cancer immunotherapy," *Nature Reviews. Drug Discovery*, vol. 18, no. 3, pp. 175–196, 2019.
- [6] H. Maeda, H. Nakamura, and J. Fang, "The EPR effect for macromolecular drug delivery to solid tumors: improvement of tumor uptake, lowering of systemic toxicity, and distinct tumor imaging in vivo," *Advanced Drug Delivery Reviews*, vol. 65, no. 1, pp. 71–79, 2013.
- [7] V. P. Chauhan and R. K. Jain, "Strategies for advancing cancer nanomedicine," *Nature Materials*, vol. 12, no. 11, pp. 958–962, 2013.
- [8] H. Peng, B. Chen, W. Huang et al., "Reprogramming tumor-associated macrophages to reverse EGFR790MResistance by dual-targeting codelivery of gefitinib/vorinostat," *Nano Letters*, vol. 17, no. 12, pp. 7684–7690, 2017.
- [9] M. W. Tibbitt, J. E. Dahlman, and R. Langer, "Emerging frontiers in drug delivery," *Journal of the American Chemical Society*, vol. 138, no. 3, pp. 704–717, 2016.
- [10] D. J. Irvine and E. L. Dane, "Enhancing cancer immunotherapy with nanomedicine," *Nature Reviews Immunology*, vol. 20, pp. 321–334, 2020.
- [11] Y. Qian, S. Qiao, Y. Dai et al., "Molecular-targeted immunotherapeutic strategy for melanoma via dual-targeting nanoparticles delivering small interfering RNA to tumor-associated macrophages," *ACS Nano*, vol. 11, no. 9, pp. 9536–9549, 2017.
- [12] W. Nie, G. Wu, J. Zhang et al., "Responsive exosome nanobioconjugates for synergistic cancer therapy," *Angewandte Chemie*, vol. 59, no. 5, pp. 2018–2022, 2020.
- [13] M. An, M. Li, J. Xi, and H. Liu, "Silica nanoparticle as a lymph node targeting platform for vaccine delivery," *ACS Applied Materials & Interfaces*, vol. 9, no. 28, pp. 23466–23475, 2017.
- [14] C. Shi, T. Liu, Z. Guo, R. Zhuang, X. Zhang, and X. Chen, "Reprogramming tumor-associated macrophages by nanoparticle-based reactive oxygen species photogeneration," *Nano Letters*, vol. 18, no. 11, pp. 7330–7342, 2018.
- [15] A. J. Gentles, A. M. Newman, C. L. Liu et al., "The prognostic landscape of genes and infiltrating immune cells across human cancers," *Nature Medicine*, vol. 21, no. 8, pp. 938–945, 2015.
- [16] Y. Komohara, M. Jinushi, and M. Takeya, "Clinical significance of macrophage heterogeneity in human malignant tumors," *Cancer Science*, vol. 105, no. 1, pp. 1–8, 2014.
- [17] J. W. Pollard, "Tumour-educated macrophages promote tumour progression and metastasis," *Nature Reviews Cancer*, vol. 4, no. 1, pp. 71–78, 2004.
- [18] Y. Komohara, Y. Fujiwara, K. Ohnishi, and M. Takeya, "Tumor-associated macrophages: potential therapeutic targets for anti-cancer therapy," *Advanced drug delivery reviews*, vol. 99, no. Part B, pp. 180–185, 2016.
- [19] M. Heusinkveld and S. H. van der Burg, "Identification and manipulation of tumor associated macrophages in human cancers," *Journal of Translational Medicine*, vol. 9, p. 216, 2011.
- [20] X. Yuan, J. Zhang, D. Li et al., "Prognostic significance of tumor-associated macrophages in ovarian cancer: a meta-analysis," *Gynecologic Oncology*, vol. 147, no. 1, pp. 181–187, 2017.
- [21] J. G. Quatromoni and E. Eruslanov, "Tumor-associated macrophages: function, phenotype, and link to prognosis in human lung cancer," *American Journal of Translational Research*, vol. 4, no. 4, pp. 376–389, 2012.
- [22] *JNJ-40346527 in Treating Participants With Relapsed or Refractory Acute Myeloid Leukemia*, 2020, ClinicalTrials.org <https://clinicaltrials.gov/show/NCT03557970>.
- [23] *Microglial Colony Stimulating Factor-1 Receptor (CSF1R) in Alzheimer's Disease (MICAD)*, 2020, ClinicalTrials.org <https://clinicaltrials.gov/show/NCT04121208>.
- [24] *Nivolumab and the Antagonistic CSF-1R Monoclonal Antibody Cabiralizumab (BMS-986227) in Patients With Relapsed/Refractory Peripheral T Cell Lymphoma*, 2020, ClinicalTrials.org <https://clinicaltrials.gov/show/NCT03927105>.
- [25] S. Shen, H. J. Li, K. G. Chen et al., "Spatial targeting of tumor-associated macrophages and tumor cells with a pH-sensitive cluster nanocarrier for cancer chemoimmunotherapy," *Nano Letters*, vol. 17, no. 6, pp. 3822–3829, 2017.
- [26] N. M. La-Beck, X. Liu, H. Shmeeda, C. Shudde, and A. A. Gabizon, "Repurposing amino-bisphosphonates by liposome formulation for a new role in cancer treatment," in *Seminars in Cancer Biology*, 2019.
- [27] S. Zanganeh, G. Hutter, R. Spitler et al., "Iron oxide nanoparticles inhibit tumour growth by inducing pro-inflammatory macrophage polarization in tumour tissues," *Nature Nanotechnology*, vol. 11, no. 11, pp. 986–994, 2016.
- [28] B. Z. Qian and J. W. Pollard, "Macrophage diversity enhances tumor progression and metastasis," *Cell*, vol. 141, no. 1, pp. 39–51, 2010.
- [29] A. Mantovani, A. Sica, S. Sozzani, P. Allavena, A. Vecchi, and M. Locati, "The chemokine system in diverse forms of macrophage activation and polarization," *Trends in Immunology*, vol. 25, no. 12, pp. 677–686, 2004.
- [30] S. Brandau, K. Moses, and S. Lang, "The kinship of neutrophils and granulocytic myeloid-derived suppressor cells in cancer: cousins, siblings or twins?," *Seminars in Cancer Biology*, vol. 23, no. 3, pp. 171–182, 2013.
- [31] R. Wesolowski, J. Markowitz, and W. E. Carson 3rd, "Myeloid derived suppressor cells - a new therapeutic target in the treatment of cancer," *Journal for Immunotherapy of Cancer*, vol. 1, no. 1, p. 10, 2013.
- [32] D. I. Gabrilovich and S. Nagaraj, "Myeloid-derived suppressor cells as regulators of the immune system," *Nature Reviews Immunology*, vol. 9, no. 3, pp. 162–174, 2009.

- [33] L. Ai, S. Mu, Y. Wang et al., "Prognostic role of myeloid-derived suppressor cells in cancers: a systematic review and meta-analysis," *BMC Cancer*, vol. 18, no. 1, p. 1220, 2018.
- [34] D. Wan, Y. Yang, Y. Liu et al., "Sequential depletion of myeloid-derived suppressor cells and tumor cells with a dual-pH-sensitive conjugated micelle system for cancer chemimmunotherapy," *Journal of Controlled Release*, vol. 317, pp. 43–56, 2020.
- [35] V. Le Noci, M. Sommariva, M. Tortoreto et al., "Reprogramming the lung microenvironment by inhaled immunotherapy fosters immune destruction of tumor," *Oncoimmunology*, vol. 5, no. 11, article e1234571, 2016.
- [36] H. Phuengkham, C. Song, S. H. Um, and Y. T. Lim, "Implantable synthetic immune niche for spatiotemporal modulation of tumor-derived immunosuppression and systemic antitumor immunity: postoperative immunotherapy," *Advanced Materials*, vol. 30, no. 18, article e1706719, 2018.
- [37] H. Phuengkham, C. Song, and Y. T. Lim, "A designer scaffold with immune nanoconverters for reverting immunosuppression and enhancing immune checkpoint blockade therapy," *Advanced Materials*, vol. 31, no. 42, article e1903242, 2019.
- [38] C. Wu, M. E. Muroski, J. Miska et al., "Repolarization of myeloid derived suppressor cells via magnetic nanoparticles to promote radiotherapy for glioma treatment," *Nanomedicine*, vol. 16, pp. 126–137, 2019.
- [39] Y. Long, Z. Lu, S. Xu et al., "Self-delivery micellar nanoparticles prevent premetastatic niche formation by interfering with the early recruitment and vascular destruction of granulocytic myeloid-derived suppressor cells," *Nano Letters*, vol. 20, no. 4, pp. 2219–2229, 2019.
- [40] C. R. Perez and M. De Palma, "Engineering dendritic cell vaccines to improve cancer immunotherapy," *Nature Communications*, vol. 10, no. 1, p. 5408, 2019.
- [41] J. Paavonen, P. Naud, J. Salmerón et al., "Efficacy of human papillomavirus (HPV)-16/18 AS04-adjuvanted vaccine against cervical infection and precancer caused by oncogenic HPV types (PATRICIA): final analysis of a double-blind, randomised study in young women," *Lancet*, vol. 374, no. 9686, pp. 301–314, 2009.
- [42] M. Saxena, S. Balan, V. Roudko, and N. Bhardwaj, "Towards superior dendritic-cell vaccines for cancer therapy," *Nature Biomedical Engineering*, vol. 2, no. 6, pp. 341–346, 2018.
- [43] R. A. Belderbos, J. Aerts, and H. Vroman, "Enhancing dendritic cell therapy in solid tumors with immunomodulating conventional treatment," *Molecular Therapy-Oncolytics*, vol. 13, pp. 67–81, 2019.
- [44] S. T. Reddy, A. J. van der Vlies, E. Simeoni et al., "Exploiting lymphatic transport and complement activation in nanoparticle vaccines," *Nature Biotechnology*, vol. 25, no. 10, pp. 1159–1164, 2007.
- [45] A. V. Li, J. J. Moon, W. Abraham et al., "Generation of effector memory T cell-based mucosal and systemic immunity with pulmonary nanoparticle vaccination," *Science translational medicine*, vol. 5, no. 204, article 204ra130, 2013.
- [46] S. Zhou, Y. Huang, Y. Chen et al., "Engineering ApoE3-incorporated biomimetic nanoparticle for efficient vaccine delivery to dendritic cells via macropinocytosis to enhance cancer immunotherapy," *Biomaterials*, vol. 235, p. 119795, 2020.
- [47] G. Minigo, A. Scholzen, C. K. Tang et al., "Poly-L-lysine-coated nanoparticles: a potent delivery system to enhance DNA vaccine efficacy," *Vaccine*, vol. 25, no. 7, pp. 1316–1327, 2007.
- [48] E. J. Wherry and M. Kurachi, "Molecular and cellular insights into T cell exhaustion," *Nature Reviews Immunology*, vol. 15, no. 8, pp. 486–499, 2015.
- [49] P. Sharma and J. P. Allison, "The future of immune checkpoint therapy," *Science*, vol. 348, no. 6230, pp. 56–61, 2015.
- [50] D. M. Francis and S. N. Thomas, "Progress and opportunities for enhancing the delivery and efficacy of checkpoint inhibitors for cancer immunotherapy," *Advanced Drug Delivery Reviews*, vol. 114, pp. 33–42, 2017.
- [51] T. Lang, Y. Liu, Z. Zheng et al., "Cocktail strategy based on spatio-temporally controlled nano device improves therapy of breast cancer," *Advanced Materials*, vol. 31, no. 5, article e1806202, 2019.
- [52] Z. Su, Z. Xiao, Y. Wang et al., "Codelivery of anti-PD-1 antibody and paclitaxel with matrix metalloproteinase and pH dual-sensitive micelles for enhanced tumor chemimmunotherapy," *Small*, vol. 16, no. 7, article e1906832, 2020.
- [53] Q. Chen, L. Xu, C. Liang, C. Wang, R. Peng, and Z. Liu, "Photothermal therapy with immune-adjuvant nanoparticles together with checkpoint blockade for effective cancer immunotherapy," *Nature Communications*, vol. 7, no. 1, p. 13193, 2016.
- [54] J. Xu, L. Xu, C. Wang et al., "Near-infrared-triggered photodynamic therapy with multitasking upconversion nanoparticles in combination with checkpoint blockade for immunotherapy of colorectal cancer," *ACS Nano*, vol. 11, no. 5, pp. 4463–4474, 2017.
- [55] J. Park, S. H. Wrzesinski, E. Stern et al., "Combination delivery of TGF- β inhibitor and IL-2 by nanoscale liposomal polymeric gels enhances tumour immunotherapy," *Nature Materials*, vol. 11, no. 10, pp. 895–905, 2012.
- [56] N. Bouchkouj, Y. L. Kasamon, R. A. de Claro et al., "FDA approval summary: axicabtagene ciloleucel for relapsed or refractory large B-cell lymphoma," *Clinical Cancer Research*, vol. 25, no. 6, pp. 1702–1708, 2019.
- [57] M. C. O'Leary, X. Lu, Y. Huang et al., "FDA approval summary: tisagenlecleucel for treatment of patients with relapsed or refractory B-cell precursor acute lymphoblastic leukemia," *Clinical Cancer Research*, vol. 25, no. 4, pp. 1142–1146, 2019.
- [58] S. S. Neelapu, S. Tummala, P. Kebriaei et al., "Chimeric antigen receptor T-cell therapy - assessment and management of toxicities," *Nature Reviews Clinical Oncology*, vol. 15, no. 1, pp. 47–62, 2018.
- [59] M. T. Stephan, J. J. Moon, S. H. Um, A. Bershteyn, and D. J. Irvine, "Therapeutic cell engineering with surface-conjugated synthetic nanoparticles," *Nature Medicine*, vol. 16, no. 9, pp. 1035–1041, 2010.
- [60] M. M. Billingsley, N. Singh, P. Ravikumar, R. Zhang, C. H. June, and M. J. Mitchell, "Ionizable lipid nanoparticle-mediated mRNA delivery for human CAR T cell engineering," *Nano Letters*, vol. 20, no. 3, pp. 1578–1589, 2020.
- [61] Q. Chen, Q. Hu, E. Dukhovlinova et al., "Photothermal therapy promotes tumor infiltration and antitumor activity of CAR T cells," *Advanced Materials*, vol. 31, no. 23, article e1900192, 2019.
- [62] Y. Mao, E. T. Keller, D. H. Garfield, K. Shen, and J. Wang, "Stromal cells in tumor microenvironment and breast cancer," *Cancer Metastasis Reviews*, vol. 32, no. 1-2, pp. 303–315, 2013.
- [63] M. E. Fiori, S. di Franco, L. Villanova, P. Bianca, G. Stassi, and R. de Maria, "Cancer-associated fibroblasts as abettors of tumor progression at the crossroads of EMT and therapy resistance," *Molecular Cancer*, vol. 18, no. 1, p. 70, 2019.

- [64] A. Calon, E. Lonardo, A. Berenguer-Llargo et al., “Stromal gene expression defines poor-prognosis subtypes in colorectal cancer,” *Nature Genetics*, vol. 47, no. 4, pp. 320–329, 2015.
- [65] X. Chen and E. Song, “Turning foes to friends: targeting cancer-associated fibroblasts,” *Nature Reviews Drug Discovery*, vol. 18, no. 2, pp. 99–115, 2019.
- [66] K. P. Olive, M. A. Jacobetz, C. J. Davidson et al., “Inhibition of Hedgehog signaling enhances delivery of chemotherapy in a mouse model of pancreatic cancer,” *Science*, vol. 324, no. 5933, pp. 1457–1461, 2009.
- [67] M. A. Jacobetz, D. S. Chan, A. Neesse et al., “Hyaluronan impairs vascular function and drug delivery in a mouse model of pancreatic cancer,” *Gut*, vol. 62, no. 1, pp. 112–120, 2012.
- [68] D. Kovács, N. Igaz, A. Marton et al., “Core-shell nanoparticles suppress metastasis and modify the tumour-supportive activity of cancer-associated fibroblasts,” *Journal of nanobiotechnology*, vol. 18, no. 1, p. 18, 2020.
- [69] L. Miao, Q. Liu, C. M. Lin et al., “Targeting tumor-associated fibroblasts for therapeutic delivery in desmoplastic tumors,” *Cancer Research*, vol. 77, no. 3, pp. 719–731, 2017.
- [70] H. Wang and D. J. Mooney, “Biomaterial-assisted targeted modulation of immune cells in cancer treatment,” *Nature Materials*, vol. 17, no. 9, pp. 761–772, 2018.
- [71] B. A. Helmink, S. M. Reddy, J. Gao et al., “B cells and tertiary lymphoid structures promote immunotherapy response,” *Nature*, vol. 577, no. 7791, pp. 549–555, 2020.
- [72] J. T. Buchman, N. V. Hudson-Smith, K. M. Landy, and C. L. Haynes, “Understanding nanoparticle toxicity mechanisms to inform redesign strategies to reduce environmental impact,” *Accounts of Chemical Research*, vol. 52, no. 6, pp. 1632–1642, 2019.
- [73] J. M. Pitt, F. André, S. Amigorena et al., “Dendritic cell-derived exosomes for cancer therapy,” *The Journal of Clinical Investigation*, vol. 126, no. 4, pp. 1224–1232, 2016.
- [74] L. M. Kranz, M. Diken, H. Haas et al., “Systemic RNA delivery to dendritic cells exploits antiviral defence for cancer immunotherapy,” *Nature*, vol. 534, no. 7607, pp. 396–401, 2016.
- [75] L. Tang, Y. Zheng, M. B. Melo et al., “Enhancing T cell therapy through TCR-signaling-responsive nanoparticle drug delivery,” *Nature Biotechnology*, vol. 36, no. 8, pp. 707–716, 2018.
- [76] A. M. Krieg, “CpG motifs in bacterial DNA and their immune effects,” *Annual Review of Immunology*, vol. 20, no. 1, pp. 709–760, 2002.

Research Article

High-Expressed Macrophage Scavenger Receptor 1 Predicts Severity Clinical Outcome in Transplant Patient in Idiopathic Pulmonary Fibrosis Disease

Mingfeng Zheng,¹ Tian Tian,² Jialong Liang,¹ Shugao Ye,¹ Jingyu Chen ^{1,3},
and Yong Ji ^{1,3,4}

¹Department of Cardiothoracic Surgery in Affiliated Wuxi People's Hospital, Wuxi, China

²Department of Dermatology, The Affiliated Sir Run Run Hospital of Nanjing Medical University, Nanjing, China

³Department of Lung Transplant Center, Key Laboratory of Human Organ Transplant in Jiangsu Province, Affiliated Wuxi People's Hospital, Wuxi, China

⁴Key Laboratory of Pathogen Biology of Jiangsu Province, Nanjing, China

Correspondence should be addressed to Jingyu Chen; chenjingyu333@sina.com and Yong Ji; jiyongmyp@163.com

Received 5 November 2020; Revised 5 December 2020; Accepted 30 December 2020; Published 31 January 2021

Academic Editor: Juming Yan

Copyright © 2021 Mingfeng Zheng et al. This is an open access article distributed under the Creative Commons Attribution License, which permits unrestricted use, distribution, and reproduction in any medium, provided the original work is properly cited.

Background. Lung transplantation has been performed worldwide and admitted as an effective treatment for patients with various end-stage lung diseases. However, limit reliable clinical indicators exist to identify patients at high risk for allograft failure in lung transplant recipients. The recent advances in the knowledge of immunological aspects of the pulmonary diseases, for that innate macrophage activation, are induced by pathogen or pathogen-derived molecules and widely accepted as the critical evidence among the pathogenesis of lung inflammation and fibrosis. This study was aimed at evaluating the clinical significance of CD86- and macrophage scavenger receptor 1- (MSR1-) positive cells during the development of idiopathic pulmonary fibrosis (IPF) and pulmonary arterial hypertension (PAH), and their potential roles in the prediction of the outcomes after lung transplantation were examined. **Methods.** Tissues from lung transplantation for 37 IPF and 15 PAH patients from the Department of Cardiothoracic Surgery in Wuxi People's Hospital from December 2015 to December 2016 were analyzed by immunohistochemistry (IHC) for detecting the expression and CD86 and MSR1 and correlated with clinical events after lung transplantation. **Results.** IHC results showed that the expression of MSR1, IL-13, and arginase-1 (Arg1) but not CD86 in the lung section of IPF patients was dramatically enhanced when compared with that of PAH patients. The expression of MSR1, IL-13, and Arg1 but not CD86 in the lung from IPF patients with smoking was significantly increased when compared with that from nonsmoking subjects. In addition, the expression of MSR1-positive cells in IPF subjects with *Klebsiella pneumoniae* infection was dramatically enhanced than that in noninfection subjects. MSR1-positive macrophages were negatively associated with FEV1 and with FVC but not associated with TLC and with TL_{CO}. However, CD86-positive macrophages were not significantly associated with the above lung function-related factors. Furthermore, MSR1 had a higher area under the ROC curve (AUC) than CD86 for IPF diagnosis. Survival analysis indicated that high levels of MSR1-positive macrophages had a worse prognostic effect for IPF patients with lung transplantation. **Conclusion.** Our study indicates the clinical significance of *Klebsiella pneumoniae* infection-related MSR1-positive cells in IPF progression, and it could be a prognostic marker in IPF after the lung transplant; development strategies to reduce the expression of MSR1-positive macrophages in IPF may be beneficial for the lung transplant.

1. Introduction

Idiopathic pulmonary fibrosis (IPF) is a progressive and fatal illness characterized by the development of extracellular

matrix deposition resulting in severe dyspnea and impairment of lung function [1]. The median survival of patients with IPF ranges from 2.84 to 4.8 years after diagnosis, depending on the stage of the disease and histopathologic features [2–4]. The

pathologic processes that cause disease progression are thought possibly related to individual genetic and nongenetic factors (e.g., pathogen infection and smoking) [5]. Pulmonary arterial hypertension (PAH) is a progressive disease of the pre-capillary pulmonary vasculature, which occurs when most of the very small arteries throughout the lungs narrow in diameter, resulting in resistance to blood flow and eventually right heart failure and death [6]. Despite a large spectrum of drug targets and compounds, lung transplantation is the only intervention shown to increase life expectancy for patients with IPF and severe PAH, when medical therapy is no longer effective. Thus, understanding the accurate indicators for disease progression might improve the clinical management of lung transplantation.

The prognosis of individual patient underlines that lung transplantation is difficult to predict because there are no reliable clinical parameters or biomarkers to reflect disease progression. As the most abundant immune cells in the lungs (approximately 70% of the immune cells), macrophage phagocyte pathogenic microorganisms play a central role in airway remodeling in wound healing and pulmonary fibrosis [7]. Lung macrophages display polarized phenotypes by which they can be divided into two distinct populations, alveolar macrophages (AMs) and interstitial macrophages (IMs) [8]. AMs are located on the luminal surface and initiate the immune responses in the lungs during encounter with various pathogens, while IMs are located in the lung tissue interstitium and remodel the lung tissues [9]. Evidence has pointed towards a potential role of an altered lung microbiome in triggering IPF progression [10], suggesting that some pathogens or pathogen-derived molecules have the potential roles in IPF development that is associated with lung macrophage activation [11]. Depending on the micro-environment, macrophages can be polarized into classically activated (M1) macrophages and alternatively activated (M2) macrophages [12]. M1 macrophages are activated by microbial agents and/or Th1 cytokines, such as interferon gamma (IFN- γ), can increase the phagocytic capacity along with the expression of costimulatory molecules (such as CD86) and secrete proinflammatory cytokines (TNF- α , IL-6, and IL-12), and play essential roles in clearing bacterial, viral, or fungal infections and causing tissue damage [13]. On the other hand, M2 macrophages are stimulated by Th2 cytokines and involved in tissue repair and remodeling, angiogenesis, and metabolic responses [13–15]. Macrophage polarization is implicated in promoting and regulating lung fibrosis. M1 macrophages induced by MMP28 gene knock-out attenuate the bleomycin-induced lung fibrosis [16]. In addition, bleomycin-induced fibrosis is impaired in ST2-deficient mice, which is accompanied by increased M1 macrophages [17]. Pulmonary fibrosis is associated with a distinct type of M2 activation, suggesting a profibrotic role of M2 macrophages in the development of lung fibrosis [18, 19].

Previous studies showed that MSR1, one marker for M2 polarization [20], plays a critical role in the induction of inflammatory reactions and innate and adaptive immune responses by recognition of exogenous pathogen-associated molecular patterns (PAMP) and endogenous ligands [21, 22]. MSR1 plays vital roles in the process of silica-induced

fibrosis, for that the MSR1-deficient mice exhibited little to deposition of collagen [23]. The expression of MSR1 was increased in unilateral ureteral obstruction- (UUO-) induced renal fibrosis [24]. It was reported that the expression of MSR1 was significantly increased in the whole blood of IPF patients [25]. Stimulation with collagen-type monomers significantly upregulated MSR1 expression in alveolar macrophages from patients with idiopathic pulmonary fibrosis, suggesting a potential role of MSR1 for the development of lung fibrosis [26]. However, little is known about the potential clinical role of such macrophage subsets in the clinical manifestations and outcomes of individual IPF patients after lung transplantation.

On the background of these findings, we became interested in investigating the activation type of macrophages from 15 IPF patients using immunochemical staining containing pulmonary arterial hypertension patients, which is evolving as an important factor that can adversely affect outcomes in chronic lung disease [27], and 37 severe IPF from December 2015 to December 2016. We assess not only the correlation between MSR1- or CD86-expressed macrophages and clinicopathological factors of lung fibrosis but also its influence on the survival after lung transplantation. We hypothesized the MSR1-positive macrophages in IPF patients could be used as a new prognostic biomarker and a potential therapeutic target for lung transplantation.

2. Materials and Methods

2.1. Study Design and Human Tissue Samples. Voluntary lung donation after the brain and cardiac death of citizens has become the sole source of organ transplants in Mainland China from January 2015 [28]. This study is approved by the ethics committee of Wuxi People's Hospital and performed in accordance with the ethical principles originating in the Declaration of Helsinki, consistent with Good Clinical Practice and applicable regulatory requirements. And these procedures and samples involved in this study were performed by surgical teams at the Department of Cardiothoracic Surgery in Wuxi People's Hospital from December 2015 to December 2016. Protocols and informed consent forms for this study were approved by appropriate institutional review boards. All patients provided written informed consent prior to participating in any study procedures.

A total of 52 patients' lung samples from 37 severe IPF patients and 15 PAH (patients having a mean pulmonary arterial pressure of greater than 25 mmHg [29]), both of which diagnosed according to the published consensus statements through combined clinical, radiological, and pathological examination [29, 30], were included in the study. Demographic and clinical data of patients with IPF and PAH patients were obtained from paper records. All the patients' key clinical characteristics and the data, such as age, sex, smoking history, and BMI, were duly matched (Table 1). No patients received disease-modifying treatment (pirfenidone or nintedanib) prior to surgery. Among these 37 IPF patients, 11 subjects were evaluated to positive infection (*Klebsiella pneumoniae*) according to previous criteria [31].

TABLE 1: Clinical characteristics of cases in this study.

	Pulmonary arterial hypertension secondary to IPF (PAH)	IPF patients with severe fibrosis (lung transplant patients)	<i>p</i> value
Clinical data			
<i>N</i>	15	37	
Sex	3 females; 12 males	5 females; 32 males	0.870
Age (yr) (mean ± SEM)	59.67 ± 2.90	58.35 ± 1.46	0.725
Smoking in history (percent)	26.7%(4/15)	32.4% (12/37)	0.683
BMI (mean ± SEM)	22.27 ± 0.60	22.69 ± 0.62	0.661
Lung function			
FEV1 (mean ± SEM)	1.36 ± 0.03	0.86 ± 0.04	<i>p</i> ≤ 0.001
FVC (mean ± SEM)	1.32 ± 0.02	0.99 ± 0.04	<i>p</i> ≤ 0.001
TLC (mean ± SEM)	1.69 ± 0.03	1.41 ± 0.06	<i>p</i> ≤ 0.001
TL _{CO} (mean ± SEM)	1.94 ± 0.03	1.41 ± 0.07	<i>p</i> ≤ 0.001
Medication			
Prednisolone	100%	100%	
Azathioprine	0	0	
N-Acetylcysteine	100%	100%	

Definitions of abbreviations: PAH = pulmonary arterial hypertension; IPF = idiopathic pulmonary fibrosis; TL_{CO} = diffusing capacity of carbon monoxide. ^a Significant differences between the groups: *p* < 0.05.

All the lung tissue samples were selected from transplant explants according to the patient's informed consent and showed features of excellent tissue preservation and adequate lung inflation. Lung resections were fixed in 4% paraformaldehyde, immersed in 20% sucrose, mounted in OCT compound, and sectioned with microtome at 5 μm; then, all lung tissue samples were kept at 4°C.

2.2. Immunohistochemistry. After removing OCT or paraffin, all the lung tissue slides were dewaxed and hydrated using a graded series of ethanol and water. Then, antigen retrieval was performed with citrate buffer at a pH level of 6 for 5 minutes. After that, the slide was fixed with 4% paraformaldehyde and permeabilized with 0.4% Triton X-100 in PBS for 15 min at room temperature. Unspecific binding sites were blocked with PBS+2% BSA for 30 min at 4°C. Then, the rabbit anti-human CD86 antibody, rabbit anti-human MSR1 antibody (CST, 1:1000 dilution), rabbit anti-human IL-13 antibody (CST, 1:800 dilution), or rabbit anti-human arginase-1 antibody (Invitrogen, 1:1000 dilution) was used as the primary antibody and cocultured overnight. Then, the excess antibody was removed with PBS, and then, the slide was stained with HRP-conjugated goat anti-rabbit IgG, followed by incubation at room temperature for 30 minutes. Finally, the slices were observed under the microscope. The positive reaction of the CD86 or MSR1 protein was visible as yellow-brown staining of the cytoplasm.

Six random (100x) digital images captured from each sample were prepared for detecting the intensity of CD86- and MSR1-positive cells in the lung using Image-Pro Plus software 6.0 (Media Cybernetics, Silver Spring, MD, USA). Then, the average IOD was calculated for each sample.

2.3. Statistical Analysis. All statistical methods were performed using SPSS software, version 21.0 (SPSS Inc., Chicago, IL). Results are expressed as means ± standard error of the mean (SEM). Comparisons of characteristics and CD86/MSR1 expression between patients with PH and IPF subjects were performed using independent *t*-tests for normally distributed data and Mann-Whitney *U* tests for not normally distributed data. The chi-squared test was used to analyze the correlation between CD86/MSR1 expression and clinicopathologic characteristics in IPF. The levels of biomarkers were further analyzed by receiver operating characteristic (ROC) curves to determine the cut-off levels that resulted in the optimal diagnostic accuracy for each marker (CD86/MSR1) between the patients with IPF and PH subjects. Survival analysis was evaluated using the Kaplan-Meier method, and differences in outcome for each variable were evaluated using the log-rank test. *p* < 0.05 was considered statistically significant.

3. Results

3.1. Patient Demographics. Table 1 provides the details of all individuals whose lung samples were subjected to immunohistochemical staining. These parameters include number, age, sex, smoking history, pulmonary function, body mass index, and treatment. The ages of the 15 PAH subjects (59.67 ± 2.90 year old) were near-identical to those of subjects with IPF (58.35 ± 1.46, year old). The proportion of females (80.0%) among the IPF subjects was nearly the same as PAH subjects (86.5%). The proportion of subjects with smoking histories was similar among the IPF (32.4%) and PAH (26.7%) subjects (*p* = 0.68),

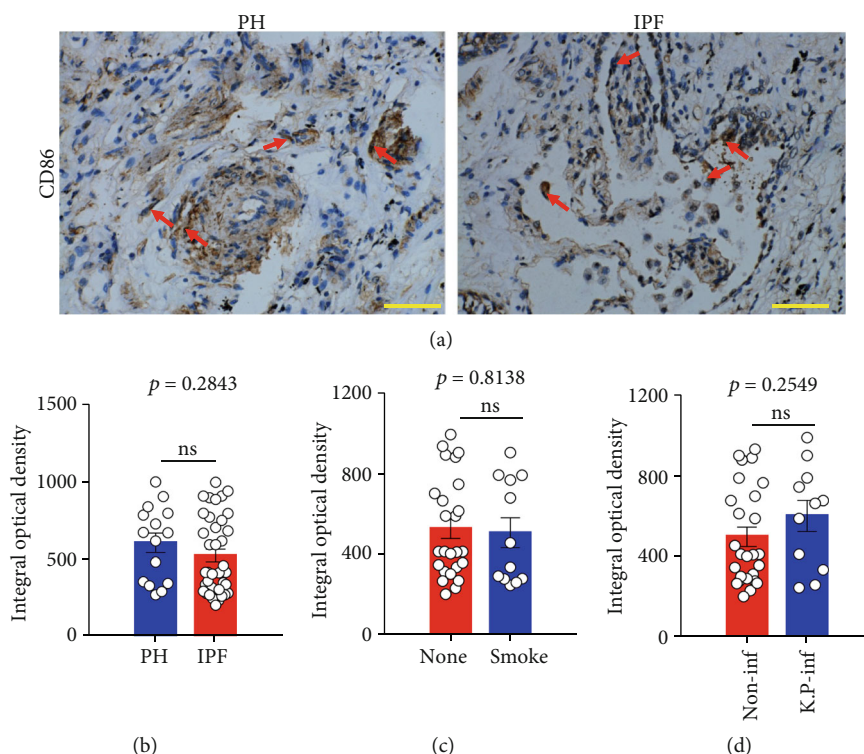


FIGURE 1: The expression of CD86 in the lung tissue samples from PH and IPF patients. (a) Representative figure of CD86 expression in the fibrotic lung in the samples from the PAH or IPF patient. Bar: 100 μm . (b) The mean optical density of CD86-positive cells between PH and IPF subjects was digitized and analyzed on Image-Pro Plus software. (c) The mean optical density of CD86-positive cells in IPF subjects with (smoke) or without (none) smoke was analyzed. Data are expressed as the mean \pm SEM for each group, PAH, $n = 15$; IPF, $n = 37$. ns: not significant (Student's t -test). (d) The mean optical density of CD86-positive cells in IPF subjects with noninfection (non-inf, $n = 25$) and smoke subjects ($n = 12$) in IPF patients was analyzed. (e) The mean optical density of CD86-positive cells in IPF subjects with (*K.P*-inf, $n = 11$) or without *Klebsiella pneumoniae* infection (non-inf, $n = 26$) was analyzed. ns: not significant (Student's t -test).

3.2. Enhanced Expression of MSR1 in IPF Patients with *Klebsiella pneumoniae* Infection. Previous studies have shown that CD86 and MSR1 are specifically expressed on macrophages and are useful as M1 and M2 macrophage markers, respectively, [32, 33]. Therefore, we performed immunostaining of CD86 or MSR1 using lung sections from IPF and PAH patients who underwent lung transplantation. As shown in Figures 1(a) and 1(b), the expression of CD86-positive macrophages in the lung sections from IPF patients was similar to that from PAH patients, suggesting that M1 macrophage polarization may not involve in the pathogenesis of IPF. In addition, there was no significant difference of CD86-positive cells in IPF subjects between with and without smoking (Figure 1(c)) or *Klebsiella pneumoniae* infection (Figure 1(d)).

However, there was a visible significant increased expression of MSR1 expression in lung tissues from IPF patients when compared to PAH patients (Figures 2(a) and 2(b)). The expression of MSR1 in the lung tissue from smokers was significantly increased than that from nonsmokers in IPF patients (Figure 2(c)), suggesting that smoke-induced M2 macrophage polarization is associated with the development of IPF pathogenesis. Interestingly, the expression of MSR1-positive cells in IPF subjects with *Klebsiella pneumoniae* infection was enhanced than that in noninfection subjects (Figure 2(d)). Since MSR1 is the critical marker for M2

macrophages, we next detected other M2 macrophage-related factors in lung tissues from IPF patients and found that the expression of IL-13 and Arg-1 in lung tissues from IPF patients was also significantly increased in IPF patients when compared with PAH patients (Figures 2(e)–2(h)).

3.3. The Expression of MSR1 Is Negatively Correlated with the Lung Function in IPF Patients. Next, we analyzed the connection between the expression of CD86 or MSR1 and parameters related to pulmonary function. As shown in Figures 3(a)–3(d), there was no association between the expression of CD86 and FEV1, FVC, TLC, or TL_{CO} in IPF subjects ($r = 0.076$, $p = 0.5831$; $r = 0.099$, $p = 0.2258$; $r = -0.023$, $p = 0.3495$; $r = 0.029$, $p = 0.3956$). However, FEV1, and FVC were found to be significantly negative correlated to MSR1 expression in fibrotic lungs from IPF subjects ($r = -0.781$, $p \leq 0.001$; $r = -0.734$, $p \leq 0.001$; Figures 4(a) and 4(b)), while there were no significant correlations between the expression of MSR1 and TLC or TL_{CO} in IPF subjects ($r = 0.155$, $p = 0.360$; $r = 0.226$, $p = 0.178$; Figures 4(c) and 4(d)).

3.4. MSR1 Expression in the Lung of IPF Patients Is Significantly Associated with the Severity of Fibrosis and Lung Function. The mean survival of patients with stable IPF after lung transplantation was 25.03 ± 20.02 months.

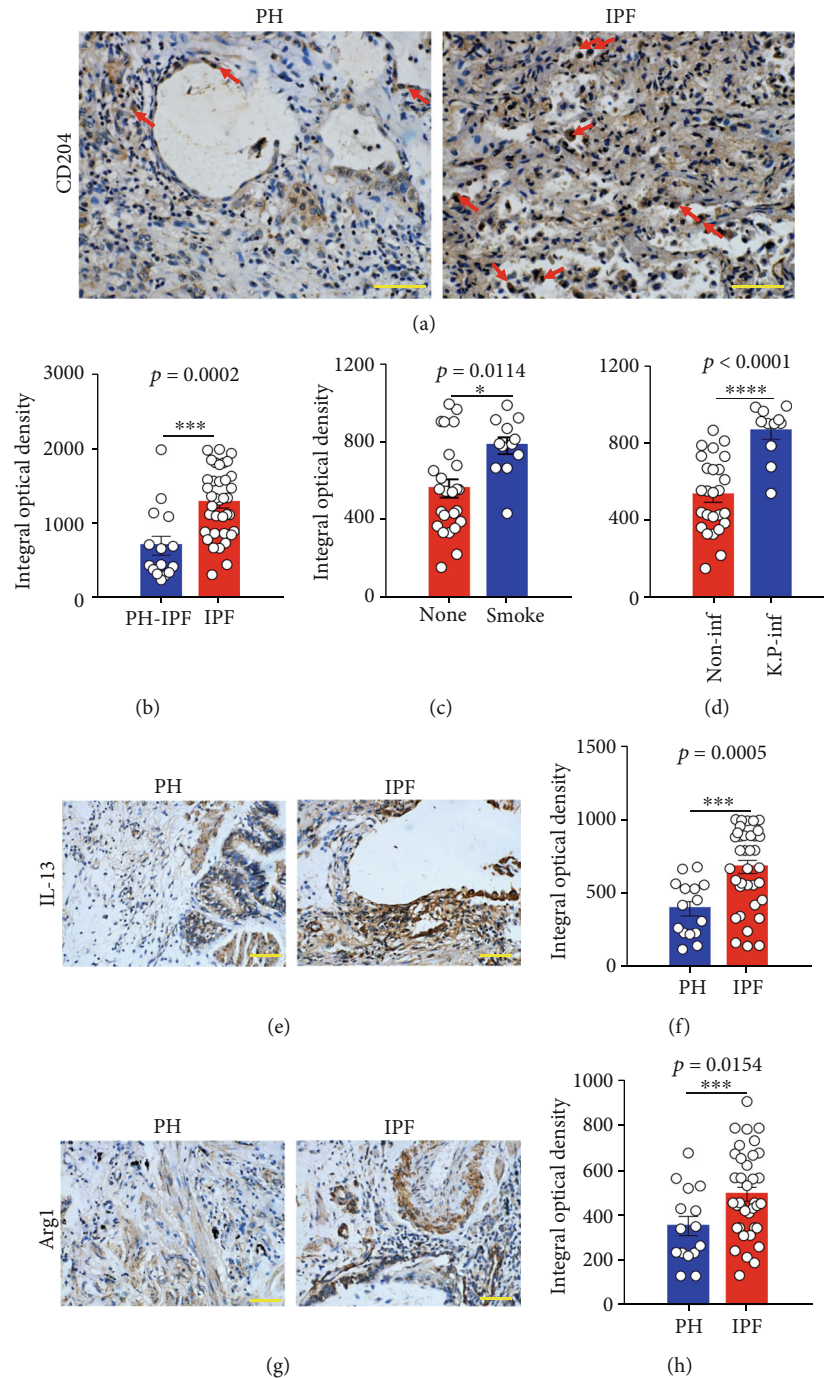


FIGURE 2: The expression of MSRI in the lung tissue samples from PAH and IPF patients. (a) Representative figure of MSRI expression in the fibrotic lung in the samples from a PAH or IPF patient. Bar: $100\ \mu\text{m}$. (b) The mean optical density of MSRI-positive cells between PAH and IPF subjects was digitized and analyzed on Image-Pro Plus software. (c) The mean optical density of MSRI-positive cells in IPF subjects with (smoke) or without (none) smoke was analyzed. (d) The mean optical density of MSRI-positive cells in IPF subjects with (*K.P*-inf, $n = 11$) or without *Klebsiella pneumoniae* infection (non-inf, $n = 26$) was analyzed. (e, f) Representative figure of the expression of IL-13 and arginase-1 (Arg1) in the fibrotic lung in the samples from a PAH or IPF patient. Bar: $100\ \mu\text{m}$. (g, h) The mean optical density of IL-13- and Arg1-positive cells between PAH and IPF subjects was digitized and analyzed on Image-Pro Plus software. Data are expressed as the mean \pm SEM for each group, PAH, $n = 15$; IPF, $n = 37$. * $p < 0.05$ and *** $p < 0.001$ (Student's *t*-test).

We next examined the prognostic roles of smoke and BMI, which were closely related to the outcome of IPF [34, 35], in IPF patients after lung transplantation. Results showed that patients with smoke ($n = 12$) had a significantly decreased life expectancy compared with nonsmokers

($n = 25$) in IPF patients after lung transplantation (Figure 5(a); $p = 0.011$). However, no difference in survival on comparing subgroups of patients with IPF between low BMI ($n = 30$) and high BMI ($n = 7$) was observed (Figure 5(b); $p = 0.433$).

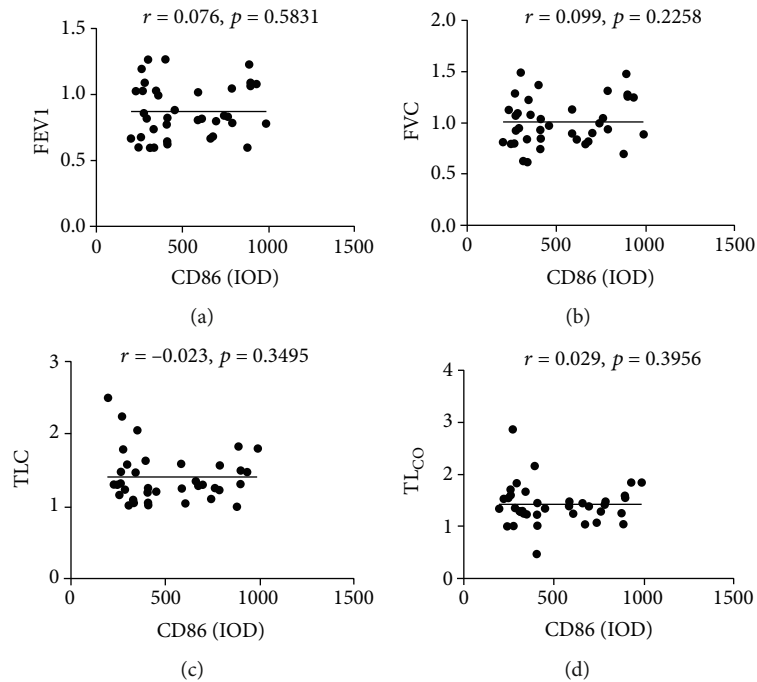


FIGURE 3: Correlation between the expression of CD86 and lung function-related factors in IPF patients ($n = 37$). (a) The correlation of CD86 and FEV1 ($r = 0.076, p = 0.5831$), (b) the correlation of CD86 and FVC ($r = 0.099, p = 0.2258$), (c) the correlation of CD86 and TLC ($r = -0.023, p = 0.3495$), and (d) the correlation of CD86 and TL_{CO} ($r = 0.029, p = 0.3956$) in fibrotic lungs from IPF subjects were evaluated by Pearson's chi-squared test.

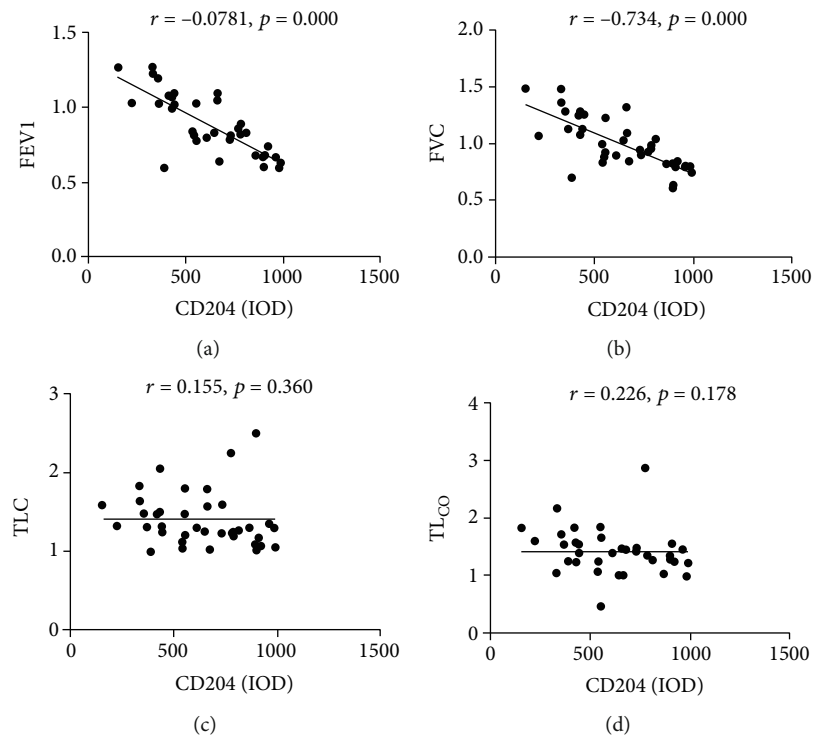


FIGURE 4: Correlation between the expression of MSR1 and lung function-related factors in IPF patients ($n = 37$). (a) The correlation of MSR1 and FEV1 ($r = -0.076, p = 0.5831$), (b) the correlation of MSR1 and FVC ($r = -0.099, p = 0.2258$), (c) the correlation of MSR1 and TLC ($r = -0.023, p = 0.3495$), and (d) the correlation of MSR1 and TL_{CO} ($r = 0.029, p = 0.3956$) in fibrotic lungs from IPF subjects were evaluated by Pearson's chi-squared test.

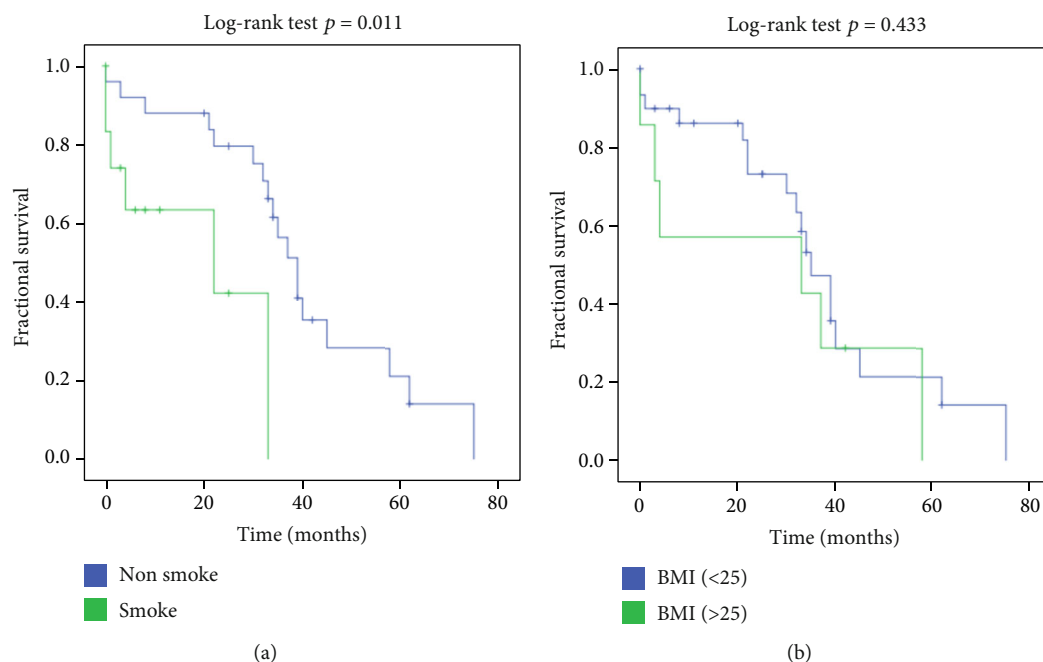


FIGURE 5: Survival curves of patients with idiopathic pulmonary fibrosis (IPF) grouped by smoking or BMI: (a) survival curves of patients with IPF nonsmoke (blue line, $n = 25$) and patients with smoke (green line, $n = 12$). (b) Survival curves of patients with IPF low BMI (blue line, $n = 30$) and patients with high BMI (green line, $n = 7$). Log-rank test was used.

To assess whether the expression of MSR1 or CD86 would predict survival after transplantation in IPF patients, ROC curve analysis was used to evaluate the discriminating capability of the two biomarkers to differentiate IPF patients from PAH subjects. Results showed that the integrated optical density (IOD) value of MSR1 ≥ 638 is the cut-off point (Figures 6(a) and 6(b)). This value represents the best compromise between the best sensitivity (90.0%) and specificity (94.1%) (MSR1: AUC = 0.921, 95% CI: 0.672-0.964, $p < .0001$). However, there is no apparent distributional difference between the CD86 values of the two groups (CD86: AUC = 0.399, 95% CI: 0.235-0.564, $p = 0.258$).

Subsequently, we divided patients into two groups according to the expression of MSR1, as demonstrated by less than 638 integrated optical density (IOD) or more than 638 IOD as low expression and high expression, respectively. The Kaplan-Meier survival analysis showed that patients with high expression of MSR1 (21 patients) had a significantly lower disease-specific survival rate than those with low expression (16 patients) (Figure 6(b); $p = 0.004$).

4. Discussion

In this study, we have evaluated macrophage-specific markers in the lungs from PAH patients and patients with severe-stage IPF undergoing lung transplant. Results show that M2 macrophage-related markers (MSR1, IL-13, and Arg1) are abnormally expressed in patients with IPF than PAH. Moreover, the expression of MSR1 in the lung tissues from IPF patients is also highly associated with the lung functions of afflicted individuals. Other demonstrations here are that the cases with higher numbers of M2 macrophages in the lungs from IPF patients had a poor clinical outcome after

lung transplant. Our data are supported by a study on a small group of patients with IPF, who had increased MSR1 expression of alveolar macrophages from bronchoalveolar lavage [26]. There is further evidence of a potential role for M2 macrophage polarization in the fibrotic tissue response including liver fibrosis [36, 37], renal fibrosis [38], pulmonary fibrosis [16, 39], pancreatic fibrosis [40], and cardiac interstitial fibrosis [41].

Different macrophage subsets contribute important activities towards the initiation, maintenance, and resolution phase of fibrosis [42]. M2 macrophages are crucial in the pathogenesis of IPF by providing profibrogenic factors, favoring cell growth, collagen formation, and wound-healing function [43]. Gharib et al. reported that MMP28 promotes lung fibrosis associated with induction of M2 programming by using MMP28 knockout mice [16]. Another article reported that lung fibrosis induced by IL-10 overexpression increased the expression of M2 macrophages in both BAL and whole lung tissues [44]. However, the expression of CD86 (M1 macrophages) was weakly detected in/around areas of fibrosis [45]. These observations may explain the enhanced M2 but not M1 macrophage invasion into the lung in the development of fibrosis in our study. The reason why M2 macrophage-related markers are higher in IPF than in PAH patients is probably involved in many diverse mediators, including prostaglandin (PG) E₂, endothelin 1 (ET-1), transforming growth factor- β (TGF- β), or IL-6, in the development of PH [46], which need further study in the future.

We found that the numbers of MSR1-positive macrophages were negatively correlated with the lung functions (FEV1 and FVC) in IPF patients; however, there was no association between CD86⁺ macrophages and lung functions.

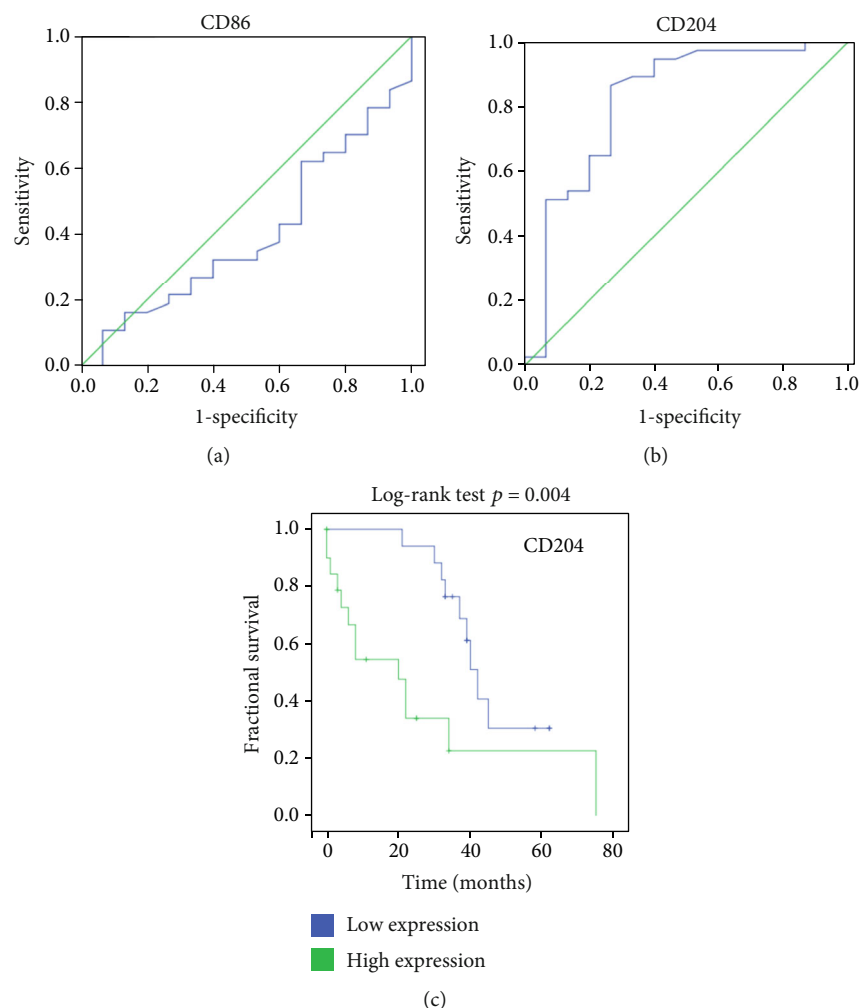


FIGURE 6: ROC and survival curves of patients with idiopathic pulmonary fibrosis (IPF) grouped by CD86 or MSR1 expression: (a, b) area under the receiver operating characteristic curve (AUC-ROC) of CD86 and MSR1 for distinguishing IPF patients from PAH; (c) survival curves of patients with IPF low expression of CD86 (blue line, $n = 16$) and patients with high expression of CD86 (green line, $n = 21$). Log-rank test was used.

Kaku et al. showed similar results that M2 macrophages ($CD163^+$ or $MSR1^+$) had significant negative correlation with FEV1 in COPD patients [47]. Cigarette smoking has been reported to be one risk factor for idiopathic pulmonary fibrosis [48], and the previous study provided transcriptome-based evidence that macrophages likely contribute to lung disease pathogenesis due to the smoking-induced reprogramming towards M2-polarized phenotype [49]. Our data show that MSR1 expression but not CD68 in the lungs from smokers was dramatically increased compared with MSR1 expression from nonsmoking IPF patients. To the best of our knowledge, this is the first study showing a smoking-related upregulation of MSR1 expression in IPF patients. One potential mechanism involved might be endotoxin (LPS) exposure by cigarette smoking, as MSR1 is required for LPS-induced TLR4-mediated NF- κ B activation in macrophages [50]. In addition, smoking was reported to affect a number of biological mediators of inflammation through its effect on immune-inflammatory cells, such as neutrophils, natural killer (NK) cells, dendritic cells, and mast cells, as well

as macrophages; we speculated that MSR1 is affected by the activation of the above cells [51]. Similar results of alveolar macrophages from patients with COPD were found and more CD204 was expressed in COPD smokers than non-COPD smokers and nonsmokers [52]. Consistent with this, IPF in patients with smoke history was associated with poor clinical prognoses after lung transplantation. However, the present study only illustrated the representative markers (MSR1 and CD86) in patients, while there existed various macrophage phenotypic markers, including cytokines, chemokines, soluble cytokine receptors, and other surface receptors [53], which needs further evaluation in the future. A study had indicated that the obvious pathogen infection, such as *Klebsiella pneumoniae*, *Mycobacterium tuberculosis*, and *Acinetobacter baumannii*, was associated with the IPF patients with deteriorating symptoms [31]. It is very interesting to explore the potential roles between the expression of MSR1 and the pathogen infection in IPF patients. Our data indicate that the expression of MSR1 in IPF subjects with *Klebsiella pneumoniae* infection was more than that in

noninfection subjects, probably due to *Klebsiella pneumoniae*-produced various endotoxins (LPS) that may involve in MSR1 activation [50].

Although several soluble molecules and bronchoalveolar lavage fluid (BALF) marker, including CXCL11 [54], KL-6 [55], IL-7 [56], and YKL-40 [57], for IPF have been investigated, however, there is an urgent need to discover new biomarkers to predict the clinical outcome of IPF patients after lung transplantation. Only a few reports indicated that factors associated with the survival after lung transplantation for IPF have been examined, including preoperative pulmonary artery pressure [58] and lung allocation score [59]. In fact, we speculate that the microenvironment of lungs from IPF patients offers them the best chance of survival. So, looking for the potential markers in the lungs might be one meaningful prognostic indicator. When patients with IPF were determined to undergo lung transplantation, we can get adequate pathological lung tissue to examine special markers. A further question is whether posttransplant survival should be given increased or decreased weight in the pro- or anti-inflammatory macrophages, which might be affected by various pathogens and pathogen-derived molecules. Our data show that higher expression of MSR1 in the lung was associated with worse clinical prognoses in IPF patients after lung transplantation, suggesting that MSR1 might serve as one potential quantitative tool to gauge posttransplant survival.

5. Conclusions

In summary, our data imply that an increased MSR1, IL-13, and Arg1 expression occurs in patients with IPF, an observation that could suggest a possible role for M2 macrophages in the pathogenesis of pulmonary fibrosis. Since the expression of MSR1 correlated significantly with functional indices (FEV1, FVC) of lung fibrosis severity, it could be a useful biomarker in the assessment of the clinical status of patients with IPF. More importantly, M2 macrophages seem to be one potential disease severity marker after lung transplant, suggesting the predictive value of MSR1 in the survival.

Abbreviations

PAH: Pulmonary arterial hypertension
 MSR1: Macrophage scavenger receptor 1
 IPF: Idiopathic pulmonary fibrosis
 IHC: Immunohistochemistry
 AMs: Alveolar macrophages
 IMs: Interstitial macrophages
 M1: Classically activated macrophages
 M2: Alternatively activated macrophages
 FVC: Forced vital capacity
 TLC: Total lung capacity
 FEV1: Forced expiratory volume in one second
 TL_{CO}: Transfer factor of the lung for carbon monoxide.

Data Availability

No data were used to support this study.

Conflicts of Interest

The authors declare that they have no competing financial interests.

Authors' Contributions

Mingfeng Zheng and Tian Tian contributed equally to this work.

Acknowledgments

This work was supported by the Key Laboratory of Pathogen Biology of Jiangsu Province (Grant No. KLPBJP-K202002) and the Natural Science Foundation of the Jiangsu Higher Education Institutions of China (Grant No. 20KJB320020).

References

- [1] L. Richeldi, H. R. Collard, and M. G. Jones, "Idiopathic pulmonary fibrosis," *Lancet*, vol. 389, no. 10082, pp. 1941–1952, 2017.
- [2] American Thoracic Society, "Idiopathic pulmonary fibrosis: diagnosis and treatment. International consensus statement. American Thoracic Society (ATS), and the European Respiratory Society (ERS)," *American journal of respiratory and critical care medicine*, vol. 161, pp. 646–664, 2000.
- [3] G. Thabut, H. Mal, Y. Castier et al., "Survival benefit of lung transplantation for patients with idiopathic pulmonary fibrosis," *The Journal of thoracic and cardiovascular surgery*, vol. 126, no. 2, pp. 469–475, 2003.
- [4] C. Neurohr, P. Huppmann, D. Thum et al., "Potential functional and survival benefit of double over single lung transplantation for selected patients with idiopathic pulmonary fibrosis," *Transplant international: official journal of the European Society for Organ Transplantation*, vol. 23, no. 9, pp. 887–896, 2010.
- [5] G. Sgalla, B. Iovene, M. Calvello, M. Ori, F. Varone, and L. Richeldi, "Idiopathic pulmonary fibrosis: pathogenesis and management," *Respiratory Research*, vol. 19, no. 1, p. ???, 2018.
- [6] S. Sakao, N. Tanabe, and K. Tatsumi, "Hypoxic pulmonary vasoconstriction and the diffusing capacity in pulmonary hypertension secondary to idiopathic pulmonary fibrosis," *Journal of the American Heart Association*, vol. 8, no. 16, p. e013310, 2019.
- [7] K. S. Smigiel and W. C. Parks, "Macrophages, wound healing, and fibrosis: recent insights," *Current Rheumatology Reports*, vol. 20, no. 4, 2018.
- [8] N. Mukaida, T. Nosaka, Y. Nakamoto, and T. Baba, "Lung macrophages: multifunctional regulator cells for metastatic cells," *International journal of molecular sciences*, vol. 20, no. 1, p. 116, 2019.
- [9] P. L. Loyher, P. Hamon, M. Laviron et al., "Macrophages of distinct origins contribute to tumor development in the lung," *The Journal of experimental medicine*, vol. 215, no. 10, pp. 2536–2553, 2018.
- [10] M. L. K. Han, Y. Zhou, S. Murray et al., "Lung microbiome and disease progression in idiopathic pulmonary fibrosis: an analysis of the COMET study," *The Lancet Respiratory Medicine*, vol. 2, no. 7, pp. 548–556, 2014.

- [11] E. G. Findlay and T. Hussell, "Macrophage-mediated inflammation and disease: a focus on the lung," *Mediators of Inflammation*, vol. 2012, Article ID 140937, 6 pages, 2012.
- [12] T. Lawrence and G. Natoli, "Transcriptional regulation of macrophage polarization: enabling diversity with identity," *Nature reviews. Immunology*, vol. 11, no. 11, pp. 750–761, 2011.
- [13] A. Sica and A. Mantovani, "Macrophage plasticity and polarization: in vivo veritas," *The Journal of clinical investigation*, vol. 122, no. 3, pp. 787–795, 2012.
- [14] T. Satoh, O. Takeuchi, A. Vandenbon et al., "The Jmjd3-Irf4 axis regulates M2 macrophage polarization and host responses against helminth infection," *Nature immunology*, vol. 11, no. 10, pp. 936–944, 2010.
- [15] S. J. Van Dyken and R. M. Locksley, "Interleukin-4- and interleukin-13-mediated alternatively activated macrophages: roles in homeostasis and disease," *Annual review of immunology*, vol. 31, no. 1, pp. 317–343, 2013.
- [16] S. A. Gharib, L. K. Johnston, I. Huizar et al., "MMP28 promotes macrophage polarization toward M2 cells and augments pulmonary fibrosis," *Journal of leukocyte biology*, vol. 95, no. 1, pp. 9–18, 2014.
- [17] D. Li, R. Guabiraba, A. G. Besnard et al., "IL-33 promotes ST2-dependent lung fibrosis by the induction of alternatively activated macrophages and innate lymphoid cells in mice," *The Journal of allergy and clinical immunology*, vol. 134, no. 6, pp. 1422–1432.e11, 2014.
- [18] A. Prasse, D. V. Pechkovsky, G. B. Toews et al., "A vicious circle of alveolar macrophages and fibroblasts perpetuates pulmonary fibrosis via CCL18," *American journal of respiratory and critical care medicine*, vol. 173, no. 7, pp. 781–792, 2006.
- [19] A. L. Mora, E. Torres-González, M. Rojas et al., "Activation of alveolar macrophages via the alternative pathway in herpesvirus-induced lung fibrosis," *American journal of respiratory cell and molecular biology*, vol. 35, no. 4, pp. 466–473, 2006.
- [20] Z. Xu, L. Xu, W. Li et al., "Innate scavenger receptor-A regulates adaptive T helper cell responses to pathogen infection," *Nature communications*, vol. 8, no. 1, p. ???, 2017.
- [21] M. P. de Winther, K. W. van Dijk, L. M. Havekes, and M. H. Hofker, "Macrophage scavenger receptor class A," *Arterioscler Thromb Vasc Biol*, vol. 20, no. 2, pp. 290–297, 2000.
- [22] H. Yi, D. Zuo, X. Yu et al., "Suppression of antigen-specific CD4+ T cell activation by SRA/CD204 through reducing the immunostimulatory capability of antigen-presenting cell," *Journal of Molecular Medicine*, vol. 90, no. 4, pp. 413–426, 2012.
- [23] C. A. Beamer and A. Holian, "Scavenger receptor class A type I/II (CD204) null mice fail to develop fibrosis following silica exposure," *American journal of physiology. Lung cellular and molecular physiology*, vol. 289, no. 2, pp. L186–L195, 2005.
- [24] T. KUSHIYAMA, T. ODA, M. YAMADA et al., "Alteration in the phenotype of macrophages in the repair of renal interstitial fibrosis in mice," *Nephrology*, vol. 16, no. 5, pp. 522–535, 2011.
- [25] B. Desai, et al. J. Mattson, H. Paintal et al., "Differential expression of monocyte/macrophage-selective markers in human idiopathic pulmonary fibrosis," *Experimental lung research*, vol. 37, no. 4, pp. 227–238, 2011.
- [26] M. Stahl, J. Schupp, B. Jäger et al., "Lung collagens perpetuate pulmonary fibrosis via CD204 and M2 macrophage activation," *PLoS one*, vol. 8, no. 11, p. e81382, 2013.
- [27] M. M. Hoepfer, M. Humbert, R. Souza et al., "A global view of pulmonary hypertension," *The Lancet Respiratory Medicine*, vol. 4, no. 4, pp. 306–322, 2016.
- [28] J. Huang, J. M. Millis, Y. Mao, M. A. Millis, X. Sang, and S. Zhong, "Voluntary organ donation system adapted to Chinese cultural values and social reality," *Liver transplantation : official publication of the American Association for the Study of Liver Diseases and the International Liver Transplantation Society*, vol. 21, no. 4, pp. 419–422, 2015.
- [29] A. F. Shorr, J. L. Wainright, C. S. Cors, C. J. Lettieri, and S. D. Nathan, "Pulmonary hypertension in patients with pulmonary fibrosis awaiting lung transplant," *The European respiratory journal*, vol. 30, no. 4, pp. 715–721, 2007.
- [30] G. Raghu, H. R. Collard, J. J. Egan et al., "An official ATS/ERS/JRS/ALAT statement: idiopathic pulmonary fibrosis: evidence-based guidelines for diagnosis and management," *American journal of respiratory and critical care medicine*, vol. 183, no. 6, pp. 788–824, 2011.
- [31] D. Weng, X.-Q. Chen, H. Qiu et al., "The role of infection in acute exacerbation of idiopathic pulmonary fibrosis," *Mediators of Inflammation*, vol. 2019, Article ID 5160694, 10 pages, 2019.
- [32] S. K. Biswas and A. Mantovani, "Macrophage plasticity and interaction with lymphocyte subsets: cancer as a paradigm," *Nature Immunology*, vol. 11, no. 10, pp. 889–896, 2010.
- [33] Y. Komohara, K. Ohnishi, J. Kuratsu, and M. Takeya, "Possible involvement of the M2 anti-inflammatory macrophage phenotype in growth of human gliomas," *The Journal of pathology*, vol. 216, no. 1, pp. 15–24, 2008.
- [34] K. M. Antoniou, D. M. Hansell, M. B. Rubens et al., "Idiopathic pulmonary fibrosis," *American journal of respiratory and critical care medicine*, vol. 177, no. 2, pp. 190–194, 2008.
- [35] Y. Kondoh, H. Taniguchi, T. Katsuta et al., "Risk factors of acute exacerbation of idiopathic pulmonary fibrosis," *Sarcoidosis, vasculitis, and diffuse lung diseases : official journal of WASOG*, vol. 27, pp. 103–110, 2010.
- [36] F. Tacke and H. W. Zimmermann, "Macrophage heterogeneity in liver injury and fibrosis," *Journal of hepatology*, vol. 60, no. 5, pp. 1090–1096, 2014.
- [37] L. Barron and T. A. Wynn, "Macrophage activation governs schistosomiasis-induced inflammation and fibrosis," *European journal of immunology*, vol. 41, no. 9, pp. 2509–2514, 2011.
- [38] T. T. Braga, M. Correa-Costa, Y. F. S. Guise et al., "MyD88 signaling pathway is involved in renal fibrosis by favoring a TH2 immune response and activating alternative M2 macrophages," *Molecular Medicine*, vol. 18, no. 8, pp. 1231–1239, 2012.
- [39] D. V. Pechkovsky, A. Prasse, F. Kollert et al., "Alternatively activated alveolar macrophages in pulmonary fibrosis—mediator production and intracellular signal transduction," *Clin Immunol*, vol. 137, no. 1, pp. 89–101, 2010.
- [40] J. Xue, V. Sharma, M. H. Hsieh et al., "Alternatively activated macrophages promote pancreatic fibrosis in chronic pancreatitis," *Nature communications*, vol. 6, no. 1, p. ???, 2015.
- [41] P. Shivshankar, G. V. Halade, C. Calhoun et al., "Caveolin-1 deletion exacerbates cardiac interstitial fibrosis by promoting M2 macrophage activation in mice after myocardial infarction," *Journal of molecular and cellular cardiology*, vol. 76, pp. 84–93, 2014.
- [42] T. A. Wynn and T. R. Ramalingam, "Mechanisms of fibrosis: therapeutic translation for fibrotic disease," *Nature Medicine*, vol. 18, no. 7, pp. 1028–1040, 2012.

- [43] T. T. Braga, J. S. Agudelo, and N. O. Camara, "Macrophages during the fibrotic process: M2 as friend and foe," *Frontiers in immunology*, vol. 6, p. 602, 2015.
- [44] L. Sun, M. C. Louie, K. M. Vannella et al., "New concepts of IL-10-induced lung fibrosis: fibrocyte recruitment and M2 activation in a CCL2/CCR2 axis," *American journal of physiology. Lung cellular and molecular physiology*, vol. 300, no. 3, pp. L341–L353, 2011.
- [45] S. Furukawa, M. Moriyama, A. Tanaka et al., "Preferential M2 macrophages contribute to fibrosis in IgG4-related dacryoadenitis and sialoadenitis, so-called Mikulicz's disease," *Clin Immunol*, vol. 156, no. 1, pp. 9–18, 2015.
- [46] S. D. Collum, J. Amione-Guerra, A. S. Cruz-Solbes et al., "Pulmonary hypertension associated with idiopathic pulmonary fibrosis: current and future perspectives," *Canadian respiratory journal*, vol. 2017, Article ID 1430350, 12 pages, 2017.
- [47] Y. Kaku, H. Imaoka, Y. Morimatsu et al., "Overexpression of CD163, CD204 and CD206 on alveolar macrophages in the lungs of patients with severe chronic obstructive pulmonary disease," *PloS one*, vol. 9, no. 1, p. e87400, 2014.
- [48] K. B. Baumgartner, J. M. Samet, C. A. Stidley, T. V. Colby, and J. A. Waldron, "Cigarette smoking: a risk factor for idiopathic pulmonary fibrosis," *American journal of respiratory and critical care medicine*, vol. 155, no. 1, pp. 242–248, 1997.
- [49] R. Shaykhiev, A. Krause, J. Salit et al., "Smoking-dependent reprogramming of alveolar macrophage polarization: implication for pathogenesis of chronic obstructive pulmonary disease," *The Journal of Immunology*, vol. 183, no. 4, pp. 2867–2883, 2009.
- [50] H. Yu, T. Ha, L. Liu et al., "Scavenger receptor A (SR-A) is required for LPS-induced TLR4 mediated NF- κ B activation in macrophages," *Biochimica et biophysica acta*, vol. 1823, no. 7, pp. 1192–1198, 2012.
- [51] R. B. Gonçalves, R. D. Coletta, K. G. Silvério et al., "Impact of smoking on inflammation: overview of molecular mechanisms," *Inflammation Research*, vol. 60, no. 5, pp. 409–424, 2011.
- [52] K. Hu, Y. Jin, Z. Chroneos, X. Han, H. Liu, and L. Lin, "Macrophage functions and regulation: roles in diseases and implications in therapeutics," *Journal of immunology research*, vol. 2018, Article ID 7590350, 2 pages, 2018.
- [53] S. Arora, K. Dev, B. Agarwal, P. Das, and M. A. Syed, "Macrophages: their role, activation and polarization in pulmonary diseases," *Immunobiology*, vol. 223, no. 4-5, pp. 383–396, 2018.
- [54] L. J. Vuga, J. R. Tedrow, K. V. Pandit et al., "C-X-C motif chemokine 13 (CXCL13) is a prognostic biomarker of idiopathic pulmonary fibrosis," *American journal of respiratory and critical care medicine*, vol. 189, no. 8, pp. 966–974, 2014.
- [55] A. YOKOYAMA, K. KONDO, M. NAKAJIMA et al., "Prognostic value of circulating KL-6 in idiopathic pulmonary fibrosis," *Respirology*, vol. 11, no. 2, pp. 164–168, 2006.
- [56] K. Tachibana, Y. Inoue, A. Nishiyama et al., "Polymyxin-B hemoperfusion for acute exacerbation of idiopathic pulmonary fibrosis: serum IL-7 as a prognostic marker," *Sarcoidosis, vasculitis, and diffuse lung diseases : official journal of WASOG*, vol. 28, pp. 113–122, 2011.
- [57] N. M. Korthagen, C. H. M. van Moorsel, N. P. Barlo et al., "Serum and BALF YKL-40 levels are predictors of survival in idiopathic pulmonary fibrosis," *Respiratory Medicine*, vol. 105, no. 1, pp. 106–113, 2011.
- [58] T. P. Whelan, J. M. Dunitz, R. F. Kelly et al., "Effect of preoperative pulmonary artery pressure on early survival after lung transplantation for idiopathic pulmonary fibrosis," *The Journal of Heart and Lung Transplantation*, vol. 24, no. 9, pp. 1269–1274, 2005.
- [59] E. S. Weiss, J. G. Allen, C. A. Merlo, J. V. Conte, and A. S. Shah, "Lung allocation score predicts survival in lung transplantation patients with pulmonary fibrosis," *The Annals of thoracic surgery*, vol. 88, no. 6, pp. 1757–1764, 2009.

Research Article

Club Cell Protein 16 Attenuates CD16^{bright}CD62^{dim} Immunosuppressive Neutrophils in Damaged Tissue upon Posttraumatic Sepsis-Induced Lung Injury

Nils Becker ^{1,2}, Philipp Störmann ², Andrea Janicova,¹ Kernt Köhler,³ Klemens Horst ⁴, Ildiko Rita Dunay,⁵ Claudia Neunaber ⁶, Ingo Marzi,² Jan Tilmann Vollrath,² and Borna Relja ^{1,2}

¹Experimental Radiology, Department of Radiology and Nuclear Medicine, Otto von Guericke University, Magdeburg, Germany

²Department of Trauma, Hand and Reconstructive Surgery, University Hospital Frankfurt, Germany

³Institute of Veterinary Pathology, Justus Liebig University Giessen, Giessen, Germany

⁴Department of Trauma Surgery, Hospital of the RWTH University, Aachen, Germany

⁵Institute of Inflammation and Neurodegeneration, Otto von Guericke University, Magdeburg, Germany

⁶Trauma Department, Hannover Medical School, Hannover, Germany

Correspondence should be addressed to Borna Relja; info@bornarelja.com

Received 1 November 2020; Revised 24 December 2020; Accepted 13 January 2021; Published 28 January 2021

Academic Editor: Zhipeng Xu

Copyright © 2021 Nils Becker et al. This is an open access article distributed under the Creative Commons Attribution License, which permits unrestricted use, distribution, and reproduction in any medium, provided the original work is properly cited.

Background. Recently, identification of immunosuppressive polymorphonuclear leukocytes (PMNL) that were traditionally described as proinflammatory cells emerged in the field of posttraumatic immunity. To understand their local and remote distribution after trauma, PMNL-subsets and the impact of immunomodulatory Club Cell protein (CC)16 that correlates with pulmonary complications were assessed. **Methods.** C57BL/6N mice were divided into three groups, receiving isolated blunt chest trauma (TxT), undergoing TxT followed by cecal ligation and puncture (CLP, TxT + CLP) after 24 h, or sham undergoing analgesedation ($n = 18/\text{group}$). Further, each group was subdivided into three groups receiving either no treatment (ctrl) or intratracheal neutralization of CC16 by application of anti-CC16-antibody or application of an unspecific IgG control antibody ($n = 6/\text{group}$). Treatment was set at the time point after TxT. Analyses followed 6 h post-CLP. PMNL were characterized via expression of CD11b, CD16, CD45, CD62L, and Ly6G by flow cytometry in bone marrow (BM), blood, spleen, lung, liver, and bronchoalveolar and peritoneal lavage fluid (BALF and PL). Apoptosis was assessed by activated (cleaved) caspase-3. Results from untreated ctrl and IgG-treated mice were statistically comparable between all corresponding sham, TxT, and TxT + CLP groups. **Results.** Immature (CD16^{dim}CD62L^{bright}) PMNL increased significantly in BM, circulation, and spleen after TxT vs. sham and were significantly attenuated in the lungs, BALF, PL, and liver. Classical-shaped (CD16^{bright}CD62L^{bright}) PMNL increased after TxT vs. sham in peripheral tissue and were significantly attenuated in circulation, proposing a trauma-induced migration of mature or peripheral differentiation of circulating immature PMNL. Immunosuppressive (CD16^{bright}CD62L^{dim}) PMNL decreased significantly in the lungs and spleen, while they systemically increased after TxT vs. sham. CLP in the TxT + CLP group reduced immunosuppressive PMNL in PL and increased their circulatory rate vs. isolated TxT, showing local reduction in affected tissue and their increase in nonaffected tissue. CC16 neutralization enhanced the fraction of immunosuppressive PMNL following TxT vs. sham and decreased caspase-3 in the lungs post-CLP in the TxT + CLP group, while apoptotic cells in the liver diminished post-TxT. Posttraumatic CC16 neutralization promotes the subset of immunosuppressive PMNL and antagonizes their posttraumatic distribution. **Conclusion.** Since CC16 affects both the distribution of PMNL subsets and apoptosis in tissues after trauma, it may constitute as a novel target to beneficially shape the posttraumatic tissue microenvironment and homeostasis to improving outcomes.

1. Introduction

In 2016, more than 3 million people worldwide died directly after trauma or in consequence from its clinical complications [1]. The posttraumatic mortality has been illustrated by a biphasic distribution with direct or early and late in-hospital mortality [2]. As early mortality is mainly caused by injury severity, seriously injured trauma patients, surviving the initial phase, are at high risk for complications, e.g., multiple organ dysfunction syndrome, multiple organ failure (MOF), or sepsis caused by immunological dysregulations [2, 3]. Trauma-induced tissue damage provokes a massive release of endogenous damage-associated molecular patterns to initiate the resolution of nonpathogenic and pathogenic inflammation with subsequent tissue repair. Simultaneous abundance of a proinflammatory state and a compensatory, anti-inflammatory response syndrome results in a complex postinjury immune response. However, a systemic hyperinflammation may induce the remote organ damage and MOF [4, 5], while an excessive immunosuppression promotes the development of infectious complications and sepsis [6, 7]. Here, improved understanding of the regulatory mechanisms is crucial for the development of therapeutic strategies to prevent complications caused by the posttraumatic inflammatory dysregulation.

It is known that distinct protein levels correlate with specific damage patterns, e.g., systemic elevation of the Club Cell protein (CC)16 in patients suffering traumatic lung injury exemplifies [8]. CC16 is a 15.8 kDa protein secreted primarily by nonciliated club cells along the tracheobronchial epithelium, especially in distal respiratory and terminal bronchioles [9, 10]. It may serve as a biomarker to indicate the development of secondary pulmonary complications after trauma, but it also exerts anti-inflammatory and immunosuppressive properties [11–13]. Due to its anti-inflammatory effects, CC16 has been described to be protective in the development of chronic obstructive pulmonary disease in human and mouse [13, 14].

Latest findings suggest that myeloid-derived suppressive cells (MDSC) with immunosuppressive properties are increased in patients suffering from persistent inflammation, immunosuppression, and catabolism syndrome (PICS), which is associated with macrophage paralysis and recurrent infections [15–17]. The heterogeneous MDSC populations are divided into cells with characteristics of monocytes, Mo-MDSC, and so-called granulocyte- (G-) MDSC or polymorphonuclear- (PMN-) MDSC with granulocyte characteristics, respectively [18]. PMN-MDSC are defined as a subpopulation of PMNL [19], bringing a new diversity into the most frequent leukocyte fraction in human circulation, that has traditionally been considered a proinflammatory population of early effector cells [20]. However, the identification of immunosuppressive PMNL remains challenging, since different surface markers were shown to indicate immunosuppressive features. In mice, MDSC are described as Gr-1⁺CD11b⁺ [21, 22], with Ly6G⁺Ly6C^{high} defining Mo-MDSC and Ly6G⁺Ly6C^{low} defining PMN-MDSC [18]. As Ly6G is a neutrophil marker only expressed on murine PMNL, the identification of human MDSC and especially

human PMNL with similar immunosuppressive functions is more complicated and still lacking an internationally approved unified surface recognition pattern [23]. A promising strategy to identify immunosuppressive PMNL in human was described by Pillay et al. in healthy volunteers who have been challenged with endotoxin, inducing a CD16^{bright}CD62L^{dim}-expressing population with a nuclear morphology of hyper-segmented, mature PMNL. This cell population was shown to exhibit immunosuppressive properties as it reduced the T-cell proliferation [24]. CD16^{dim}CD62L^{bright} cells had a banded nucleus morphology as described for immature PMNL [24], while CD16^{bright}CD62L^{bright} exhibited a classical, segmented nuclear morphology, both without immunosuppressive properties. As PMNL are rapidly responding immune cells [25], their recently described functional heterogeneity is likely to affect the early immune regulation and priming of the long-term immune dysregulation after trauma.

We hypothesized that local trauma will change the dynamic distribution of PMNL subsets in affected and unaffected tissue in a murine trauma model of sepsis after blunt chest trauma. Due to its local and systemic immunomodulating characteristics, we also hypothesized the lung injury-associated CC16 to influence the PMNL subset distribution. Thus, a possible prevention of the posttraumatic immune dysregulation via CC16 may uncover a novel therapeutic approach to improve outcomes in the future.

2. Experimental Section

2.1. Animals and Ethics. 54 male C57BL/6N mice (25 ± 5 g), 6–8 weeks of age, were provided by Janvier Labs (France) and held at the *Zentrale Forschungseinrichtung* at the University Hospital of the Goethe University Frankfurt, Germany. All animal experiments were approved by the Veterinary Department of the regional council *Regierungspräsidium Darmstadt* and were performed according to the German Federal Law and in consent with the ARRIVE guidelines [26]. The mice had access to water and food *ad libitum*. After experiments, mice received analgesia as described before [27].

2.2. Group Allocation and Experimental Model. The animals were randomly assigned into the isolated blunt chest/thoracic trauma (TxT) group ($n = 18$) with sterile laparotomy, the double-hit group consisting of TxT with subsequent cecal ligation and puncture (CLP, TxT + CLP) ($n = 18$) or the sham group undergoing analgosedation only ($n = 18$). All mice received analgesia with buprenorphin and a general mask anesthesia with isoflurane as described before [27, 28]. TxT and the double-hit groups of mice (TxT + CLP) received a bilateral blunt chest trauma as described before [28, 29]. Briefly, after supine positioning, 2.5 cm under a cylinder, a standardized blast wave was focused centrally to the chest. The air blast wave perforates the 0.05 mm Mylar polyester film and provides the air blast to the thorax (Du Pont, Bad Homburg, Germany).

Mice in the sham, TxT, or TxT + CLP groups underwent a randomization each into three further subgroups of $n = 6$

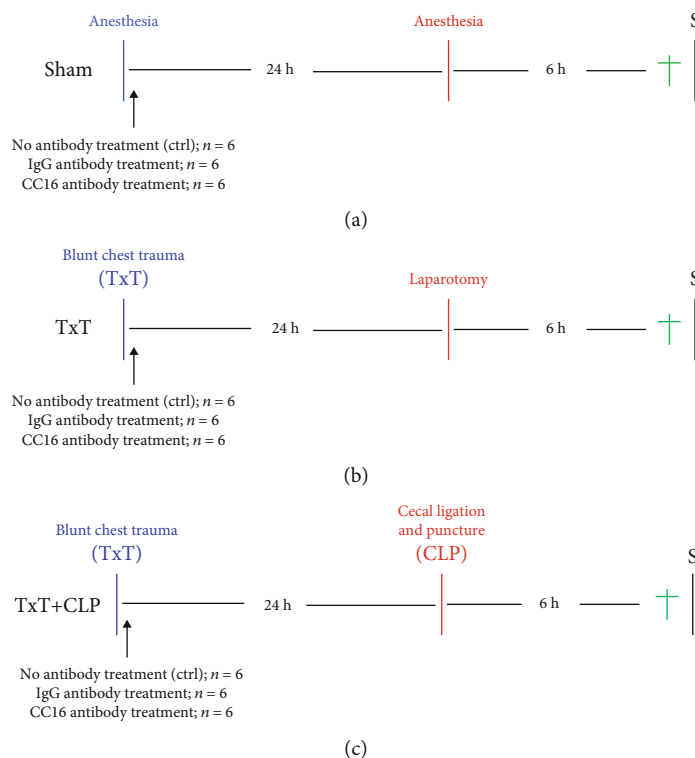


FIGURE 1: Experimental design. (a) In the sham group, eighteen animals underwent analgesedation, while 18 animals were randomly assigned into the isolated blunt chest/thoracic trauma (TxT) group ($n = 18$) with sterile laparotomy (b) and 18 animals into the double-hit group consisting of TxT with subsequent cecal ligation and puncture (TxT + CLP, c). In each of those groups, three further subgroups were created with $n = 6$ per group. One control subgroup received no treatment with antibodies (ctrl), the second subgroup received an unspecific IgG antibody, and the third group underwent intratracheal neutralization of CC16 by application of anti-CC16-antibody. The treatment was performed subsequently to TxT or corresponding to that timing in the sham subgroups.

per group. One group of mice received no treatment (ctrl, $n = 6$), and the second group underwent intratracheal neutralization of CC16 by application of anti-CC16 antibody ($n = 6$), while a third subgroup received an unspecific IgG control antibody ($n = 6$). This treatment was performed subsequently to TxT or corresponding to that timing in the sham subgroups. Local application of $50 \mu\text{l}$ Uteroglobin/SCGB1A1 (CC16 Ab, LS Biosciences) antibody in the intervention group or $50 \mu\text{l}$ of the IgG (IgG) control antibody ($10 \mu\text{g}/\text{ml}$, R&D Systems) was administered using an intratracheally placed buttoned cannula at the beginning of the trachea. Antibody distribution was ensured by positioning the mice in a supine position and keeping thoroughly the tongue aside. After a careful administration of the antibody, the mice were kept in the reverse Trendelenburg position for 30 seconds to assure the antibody distribution inside the lungs. 24 hours later, in general anesthesia (intraperitoneal application of ketamine, Zoetis, Berlin, Germany and xylazin, Bayer, Leverkusen, Germany), the double hit group (TxT + CLP) received additional CLP as described before [28, 30]. Briefly, after median laparotomy, the distal cecum underwent ligation and puncture with a 25-gauge cannula (Braun, Melsungen, Germany). The TxT group underwent sterile laparotomy using identical general anesthesia. Sham animals received only anesthesia. Six hours later all mice received intraperitoneal analgesic sedation as described above and euthanasia followed to facilitate sampling. For randomization of the ani-

mals, one animal per each group underwent the experimental procedure, and by this protocol, the group allocation was done. The experimental design is shown in Figure 1. For assessing relative changes in the PMNL distribution, sham animals receiving no antibodies were compared against the TxT or TxT + CLP groups with no antibody application. The results from those untreated controls and IgG-treated mice were statistically comparable between all corresponding sham, TxT, and TxT + CLP groups; therefore, in the following manuscript, the data are provided for the IgG-groups. Thus, to examine the effect of CC16 neutralization, animals receiving the IgG-control antibody were taken as the reference cohort and compared with animals receiving the anti-CC16 antibody.

2.3. Sampling. Intraperitoneal lavage (PL) was gained by puncturing the peritoneum with a 23-gauge cannula (Braun, Melsungen, Germany), flushing the abdominal cavity with 1.5 ml of phosphate-buffered saline (PBS). To collect the bronchoalveolar lavage fluid (BALF), the trachea was intubated using a 20-gauge indwelling venous cannula (Braun, Melsungen, Germany) and the lungs were flushed with 1.2 ml PBS. BALF and PL were centrifuged (1164 g at 4°C for 5 minutes). Cell pellets were resuspended in $100 \mu\text{l}$ PBS supplemented with 0.5% bovine serum albumin (FACS buffer). $40 \mu\text{l}$ was transferred into polystyrene FACS tubes (BD Pharmingen™) for further staining as described below.

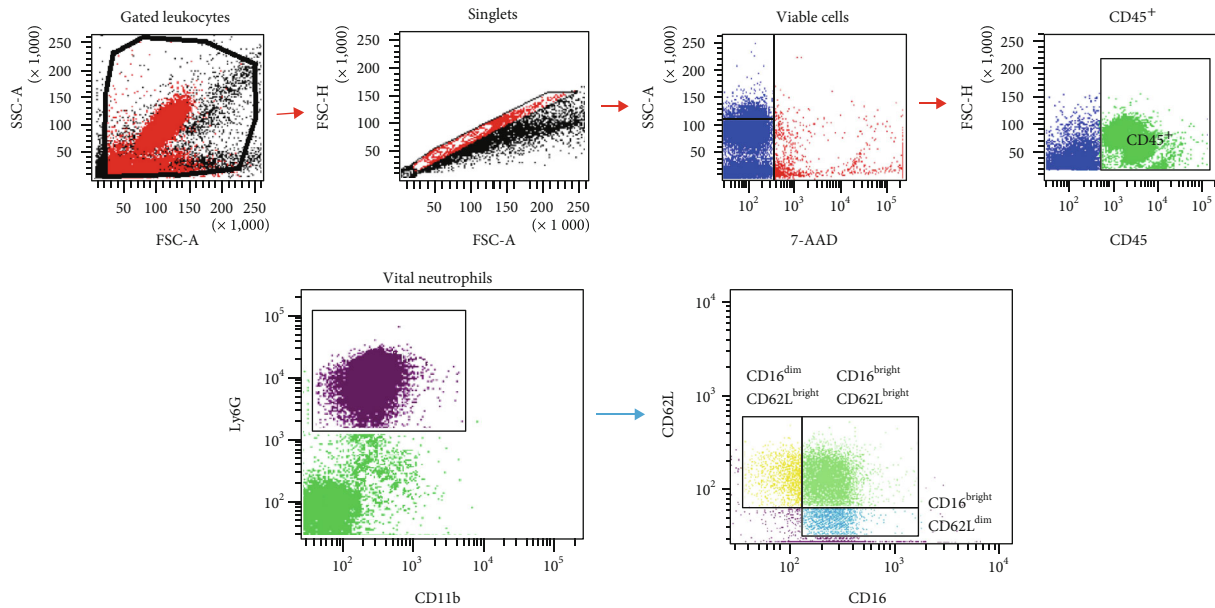


FIGURE 2: Gating strategy. Singlet leukocytes were identified by using forward and side scatter scan. Viability was detected by 7-AAD. Then, CD45⁺ cells (leukocytes) were gated by their Ly6G-expression to identify Ly6G⁺ population (PMNL fraction). Among the PMNL fraction, CD11b⁺ cells were divided by their relative expression of CD16 and CD62L, and distribution of CD16^{dim}CD62L^{bright} (immature PMNL), CD16^{bright}CD62L^{bright} (classical PMNL), and CD16^{bright}CD62L^{dim} (immunosuppressive PMNL) cells among viable CD11b⁺PMNL was measured.

Blood collection was performed by a *Vena cava* puncture with a 23-gauge cannula and heparinized syringe. Samples were centrifuged for 15 minutes at 1164 g and 4°C. The cellular pellet was resuspended in PBS (isovolume), and 30 μ l of whole blood (WB) was stored in FACS tubes for staining.

After blood sampling, the mice were perfused with 20 ml PBS *via* the cannula located in the *vena cava*. 25 mg of one lung lobe, one liver lobe, and spleen were taken and processed by Minute Single Cell Isolation protocol (Invent Biotechnologies, Minnesota, US). 40 μ l of isolated and in FACS buffer resuspended single cell pellets was stained for flow cytometric analysis as described below. For bone marrow (BM) sampling, the femoral bone was taken, and both diaphyses were removed. The bone cavity was subsequently flushed with 1 ml of PBS. To remove remaining bone material, the bone marrow was filtered using single cell isolation kit filter tubes (Invent Biotechnologies). The filtrate was centrifuged at 1164 g at 4°C for 5 minutes, and the pellet was resuspended in 100 μ l FACS buffer. 40 μ l was taken for further staining.

After blood withdrawal, one lung lobe was filled with 4% formalin for overnight fixation and immunohistological caspase-3 staining as described below. Since the left liver lobe was ligated and processed for FACS stainings, the remaining liver was flushed with 20 ml 10% buffered formalin solution and removed for further handling for immunohistology as described below.

2.4. FACS Staining. All samples were stored on ice and incubated with Alexa Fluor[®] 647-conjugated anti-mouse CD11b antibody (Ab) (BioLegend, San Diego, California, US), APC/Fire 750 conjugated anti-mouse CD45 Ab (BioLegend),

Pacific Blue-conjugated anti-mouse Ly-6G/Ly6C Ab (Gr-1, RB6-8C5, BioLegend), Alexa Fluor[®] 488-conjugated anti-mouse CD62L Ab (Biolegend), and phycoerythrin- (PE-) conjugated anti-mouse CD16/CD32 Ab (BD Biosciences, Franklin Lakes, USA). After 30 minutes in the dark, 5 μ l 7-AAD (BD Biosciences) was added and samples were incubated for additional 15 minutes. 2 ml of FACS buffer was used for washing at room temperature (RT) with centrifugation at 423 g. After discarding of the supernatant 1 ml FACS Lysing Solution (BD Biosciences) was added to the cell pellet and incubated for 10 minutes at RT. The stained samples were centrifuged for 7 minutes at 400 g and washed twice with 2 ml FACS buffer. The remaining cell pellet was resuspended in 80 μ l FACS buffer and stored light-protected on ice until flow cytometric analysis.

2.5. FACS Analyzing and Gating Strategy. Stained single-cell isolations were analyzed using BD FACS Canto 2[™] and BD FACS DIVA[™] software. Cut-offs for fluorescence intensity were set by using the corresponding isotype control antibodies. In each sample, a minimum of 3.0×10^4 cells were measured, despite few samples with lower total cellular amount. Singlets were identified by using a forward and side scatter scan. Viability was identified by isotype-controlled 7-AAD negativity. Next, CD45⁺ cells were gated by their Ly6G-expression to identify percentage of Ly6G⁺ cells (referred to as PMNL fraction). Among the PMNL fraction, CD11b⁺ cells were divided by their relative expression of CD16 and CD62L. In every sample, gating was performed by individual expression intensity according cell distribution as described by Pillay et al. [24] and as shown in Figure 2. Percentual distribution of CD16^{dim}CD62L^{bright} cells (immature PMNL),

CD16^{bright}CD62L^{bright} cells (classical PMNL), and CD16^{bright}CD62L^{dim} cells (immunosuppressive PMNL), among CD11b⁺ PMNL, was measured.

2.6. Immunohistological Staining of Caspase-3. For the determination of the caspase-3 expression in the liver and lungs, paraffin-embedded sections were deparaffinized, rehydrated, and stained with antibodies as described below. Antigen retrieval was performed by R-universal solution (Aptum Biologics) and under steam atmosphere for 20 minutes (Retriever 2010). In order to block the endogenous peroxidase activity, hydrogen peroxide was applied (Peroxidase UltraVision Block). Anti-Cleaved Caspase-3 (Asp175) (#9661, Cell Signaling Technology) in Antibody Diluent with Background Reducing Components (Dako) were used as primary antibodies for 1 hour at room temperature. The secondary horseradish peroxidase-linked antibody (rabbit, Histofine Simple Stain, Nichirei Biosciences Inc.) was used to detect the cleaved caspase-3. 3-Amino-9-ethylcarbazol (AEC, DCS Innovative Diagnostik-Systeme, Hamburg) was applied as a substrate to detect specific binding. The samples were finally counterstained with hematoxylin. The mean number of positively stained cells/high power field was assessed from 25 different fields per slide.

2.7. Statistical Analysis. Statistical analysis was performed using GraphPad Prism 6 (GraphPad Software, Inc., San Diego, CA). Based on the histogram and Shapiro-Wilk test, the nonparametric Kruskal-Wallis test, not assuming a normal distribution of the residuals, followed by Dunn's post hoc test for the correction of multiple comparisons was applied. Results are given as the mean and standard error of the mean (SEM). A p value below 0.05 was considered statistically significant.

3. Results

3.1. Main Findings. For assessing relative changes in the PMNL distribution, sham animals receiving no antibodies were compared against the TxT or TxT + CLP groups with no antibody application. The results from those untreated controls and IgG-treated mice were statistically comparable between all the corresponding sham, TxT, and TxT + CLP groups (data not shown); therefore, in the following manuscript, the data are provided for the IgG-groups. Thus, to examine the effect of CC16 neutralization, animals receiving the IgG-control antibody were taken as the reference cohort and compared with animals receiving the anti-CC16 antibody.

3.1.1. Trauma Induced Systemic Recruitment of PMNL Out of the Bone Marrow. Following blunt chest trauma, the PMNL fraction was significantly reduced in the bone marrow ($p < 0.05$, Figure 3(a)) and significantly increased in the blood, spleen, BALF, lung, PL, and liver ($p < 0.05$, Figures 3(b)–3(g)). After induction of systemic inflammation, the PMNL fraction trended to a further attenuation in the bone marrow but was significantly increased compared to monotrauma in the blood, spleen, BALF, and PL. In the lungs (Figure 3(c)), systemic inflammation resulted in PMNL

reduction compared to isolated chest trauma, while in the liver (Figure 3(f)) additional CLP in the TxT + CLP group induced a significant PMNL reduction ($p < 0.05$).

3.1.2. Production and Systemic Release of Immature PMNL Were Induced by Trauma. In mice undergoing blunt chest trauma, relative levels of immature PMNL (Figure 4) were significantly increased in the bone marrow, blood, and spleen, while systemic inflammation caused further significant enhancement in the bone marrow and blood, but a decrease to sham levels in the spleen ($p < 0.05$, Figures 4(a), 4(b), and 4(e)). TxT induced a significant reduction of immature PMNL in the BALF, lung, PL, and liver ($p < 0.05$, Figures 4(c), 4(d), 4(f), and 4(g)). Following CLP in the TxT + CLP group, levels in the BALF and lung remained decreased, while the level in PL was significantly further attenuated. CLP enhanced the hepatic ratio of immature PMNL to levels comparable to sham (Figure 4(f)).

3.1.3. Circulating Classical PMNL Migrated in Tissues after Isolated Chest Trauma and Systemic Inflammation. Monotrauma induced a significant increase of classical PMNL in the bone marrow, lungs, PL, and liver ($p < 0.05$, Figures 5(a), 5(c), 5(f), and 5(g)) that changed to pretraumatic levels in PL and bone marrow after CLP in the TxT + CLP group. Lung levels (Figure 5(c)) significantly decreased during systemic inflammation but remained significantly elevated compared to sham animals ($p < 0.05$). A similar trend was observed in the liver (Figure 5(f)). Monotrauma and systemic inflammation caused a significant decrease of circulating classical PMNL in the blood and after CLP in the TxT + CLP group in the BALF ($p < 0.05$, Figures 5(b) and 5(d)).

3.1.4. Local Injury Caused Attenuation of Immunosuppressive PMNL in Damaged Tissue and Their Increase in Unaffected Tissue. Following chest trauma, the relative amount of immunosuppressive PMNL (Figure 6) was significantly reduced in the lungs and spleen ($p < 0.05$, Figures 6(c) and 6(e)). Trends to increased levels were detected in the blood and liver (Figures 6(b) and 6(f)), while this effect was significant in the BALF, PL, and bone marrow ($p < 0.05$, Figures 6(a), 6(d), and 6(g)). During CLP-induced systemic inflammation in the lungs in the TxT + CLP group, the ratio was significantly increased compared to isolated chest trauma but remained significantly reduced compared to sham animals ($p < 0.05$, Figure 6(c)). In the blood, there was a further trend to an increase compared to monotrauma and sham (Figure 6(b)). Additional CLP in the TxT + CLP group reduced immunosuppressive PMNL significantly in PL compared to the sham and TxT groups ($p < 0.05$, Figure 6(g)), while the ratio in the spleen and bone marrow normalized towards sham levels (Figures 6(a) and 6(e)).

3.1.5. Local Inhibition of CC16 Antagonizes Posttraumatic Attenuation of Immunosuppressive PMNL. In mice receiving posttraumatic local application of CC16 Ab, distribution of the PMNL fraction increased in the BALF and lungs compared to mice receiving IgG-control antibodies (Figures 3(c), 3(c#), 3(d), and 3(d#)). Pulmonary CC16

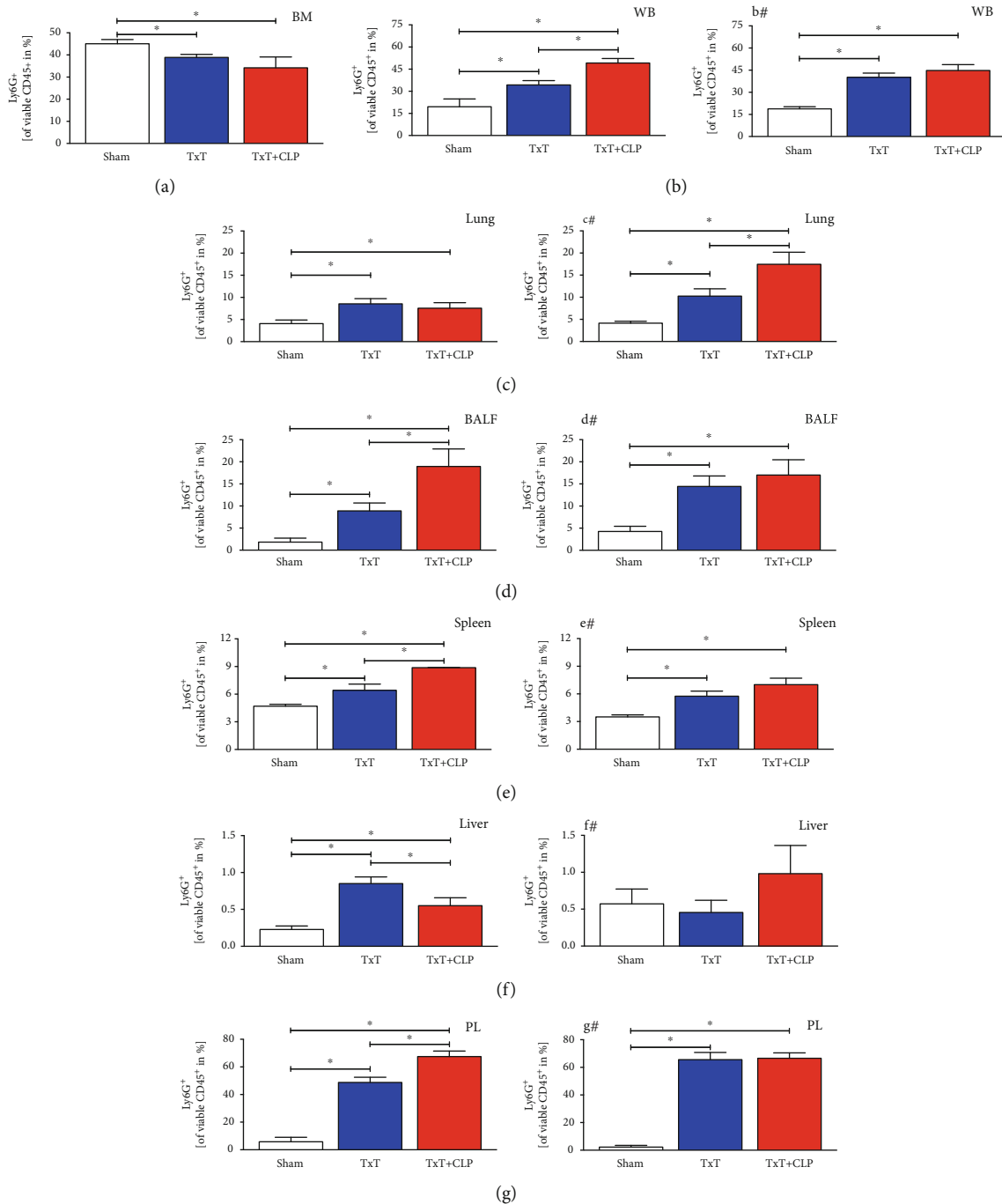


FIGURE 3: Percental ratio of PMNL fraction among leukocytes in sham (white bars), isolated chest trauma (TxT, blue bars), and systemic inflammation model (TxT + CLP, red bars) was assessed (a) in the bone marrow, (b) in the whole blood (WB), (c) in the lungs, (d) in the bronchoalveolar lavage fluid (BALF), (e) in the spleen (f), in the liver (g), and in peritoneal lavage (PL) by the expression of Ly6G⁺ in flow cytometry. * $p < 0.05$ vs. indicated. (b#–g#) Corresponding groups with intratracheal application of the neutralizing CC16 antibody. Data are represented as the mean \pm standard error of the mean.

neutralization following TxT increased the induction of the PMNL fraction in PL (Figures 3(g) and 3(g#)). Regarding the changing distribution of immature PMNL, the inhibition of CC16 was able to reduce immature PMNL in sham BALF and PL, in the spleen after TxT and in the blood and liver following CLP in the TxT + CLP group (Figures 4(b), 4(d)–4(g), and #, respectively). In mice receiving CC16 Ab compared to

mice receiving control antibodies, increases of immature PMNL were observed after CC16 neutralization in BALF. In the lungs (Figures 4(c) and 4(c#)), they increased towards sham levels following TxT and CLP in the TxT + CLP group. Among the ratio of classical PMNL in mice receiving CC16 neutralization, cells were reduced in the spleen, PL, and blood of sham animals (Figures 5(b), 5(e), 5(g), and #,

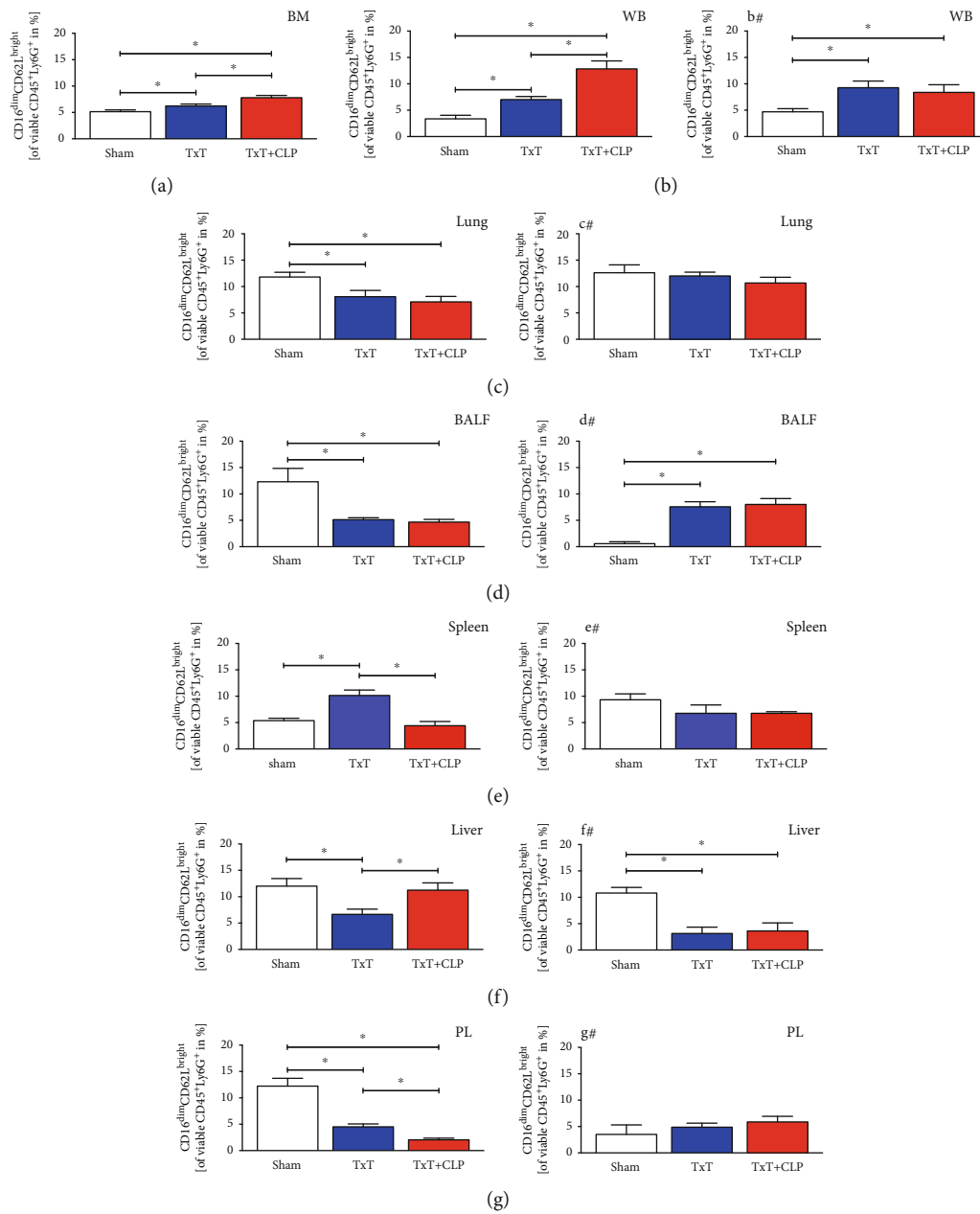


FIGURE 4: Percental ratio of immature PMNL among the CD11b⁺ PMNL fraction in sham (white bars), isolated chest trauma (TxT, blue bars), and systemic inflammation model (TxT + CLP, red bars) was assessed (a) in the bone marrow, (b) in the whole blood (WB), (c) in the lungs, (d) in the bronchoalveolar lavage fluid (BALF), (e) in the spleen, (f) in the liver, and (g) in the peritoneal lavage (PL) by flow cytometry. * $p < 0.05$ vs. indicated. (b#–g#) Corresponding groups with intratracheal application of the neutralizing CC16 antibody. Data are represented as the mean \pm standard error of the mean.

respectively). CC16 neutralization caused an increase of classical PMNL in the blood following CLP in the TxT + CLP group. In the lungs (Figures 5(c) and 5(c#)), the ratio of classical PMNL was not changed through CC16 Ab application after TxT and CLP in the TxT + CLP group. In the liver (Figures 5(f) and 5(f#)), classical PMNL were reduced after TxT and CLP in the TxT + CLP group following CC16 neutralization. Concerning immunosuppressive PMNL, neutralization of CC16 reduced the ratio in sham BALF (Figures 6(d) and 6(d#)), after TxT in the liver and PL (Figures 6(f), 6(f#), 6(g), and 6(g#)), following CLP in the

TxT + CLP group in the blood (Figures 6(b) and 6(b#)). CC16 Ab-related increase of immunosuppressive PMNL was only seen in the spleen and lungs after TxT towards sham levels (Figures 6(c), 6(c#), 6(e), and 6(e#)).

3.1.6. Trauma Causes Apoptosis in Damaged and Remote Organs. Apoptotic caspase-3 positive cells were significantly induced by blunt chest trauma in the lungs and liver ($p < 0.05$, Figures 7(b) and 7(c)). In the lung, CLP in the TxT + CLP group significantly increased apoptosis. Apoptosis rates in liver cells were significantly attenuated but

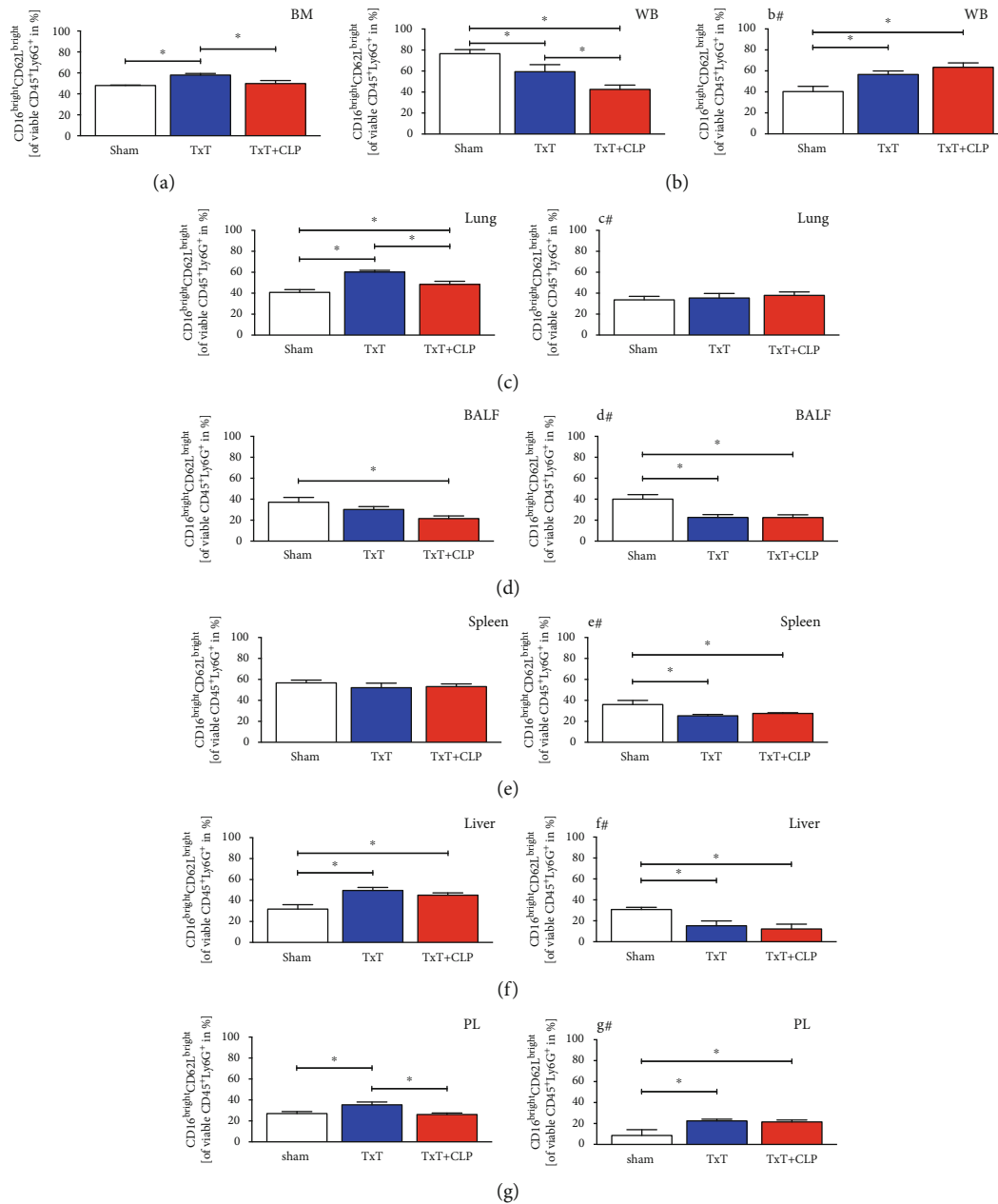


FIGURE 5: Percentual ratio of classical PMNL among the CD11b⁺ PMNL fraction in sham (white bars), isolated chest trauma (TxT, blue bars), and systemic inflammation model (TxT + CLP, red bars) was assessed (a) in the bone marrow (BM), (b) in the whole blood (WB), (c) in the lungs, (d) in the bronchoalveolar lavage fluid (BALF), (e) in the spleen, (f) in the liver, and (g) in the peritoneal lavage (PL) by flow cytometry. * $p < 0.05$ vs. indicated. (b#, c#) Corresponding groups with intratracheal application of the neutralizing CC16 antibody. Data are represented as the mean \pm standard error of the mean.

remained significantly increased towards sham animals ($p < 0.05$). In comparison to that, the numbers of caspase-3-positive cells in mice receiving pulmonic CC16 neutralization were reduced in the lungs and liver following TxT and in lungs after additional CLP in the TxT + CLP group (Figures 7(b#) and 7(c#)).

4. Discussion

4.1. Posttraumatic Neutrophil Subset Distribution. Trauma significantly affects the immune system by initiating an early

proinflammatory systemic reaction that appears within the first days after trauma. This response to traumatic injury is associated with a strong inflammation that may lead to increased damage of local tissues and remote organ damage [5, 31, 32]. In parallel, an immunosuppressive response is induced, which in fact again promotes PICS and posttraumatic infections [17]. Although both were traditionally described as occurring in sequelae, more recent findings suggest the simultaneous appearance of a proinflammatory and an immunosuppressive reaction [33], thus emphasizing the importance of their early regulation to prevent potential

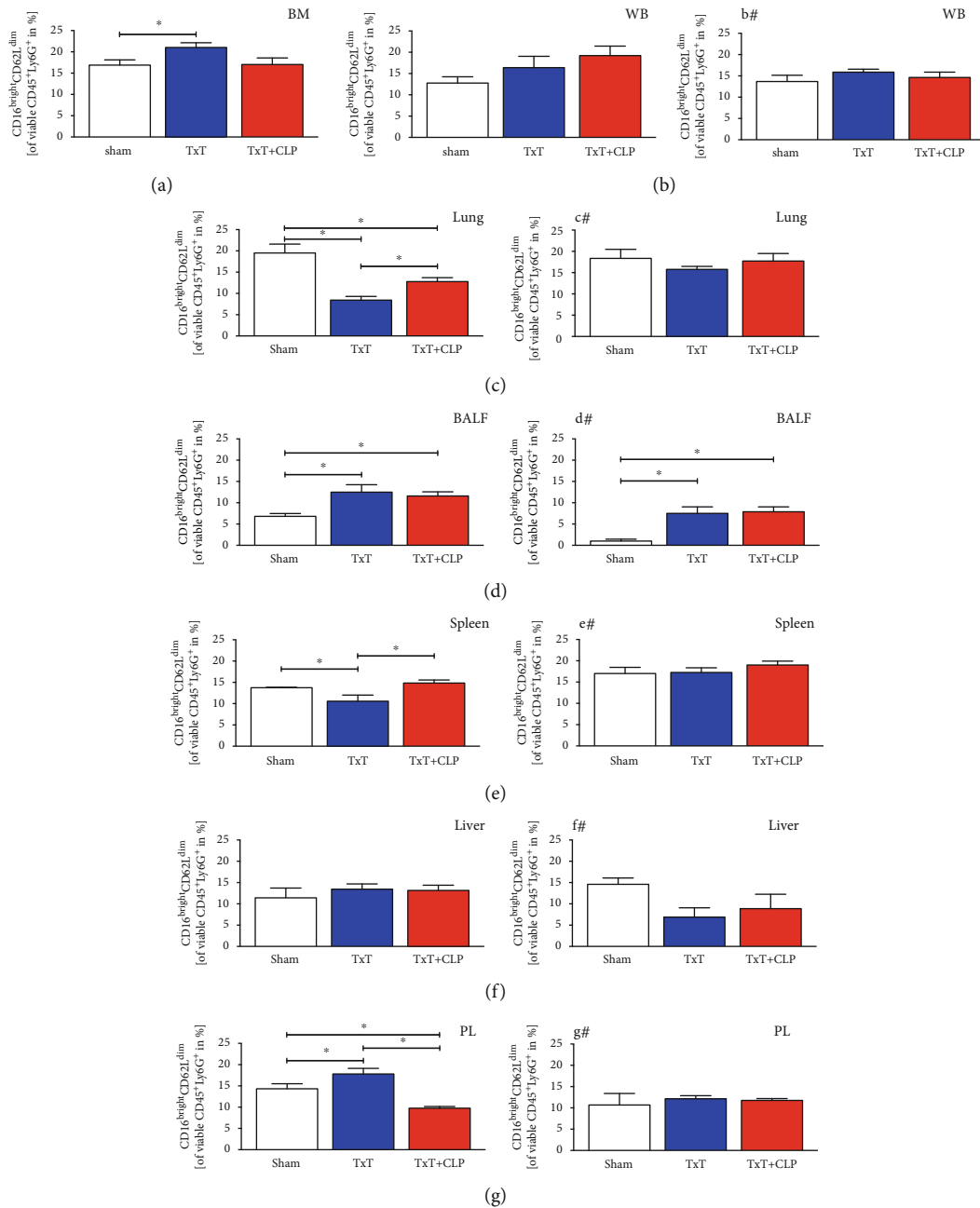


FIGURE 6: Percental ratio of immunosuppressive PMNL among the CD11b⁺ PMNL fraction in sham (white bars), isolated chest trauma (TxT, blue bars), and systemic inflammation model (TxT + CLP, red bars) was assessed (a) in the bone marrow (BM), (b) in the whole blood (WB), (c) in the lungs, (d) in the bronchoalveolar lavage fluid (BALF), (e) in the spleen, (f) in the liver, and (g) in the peritoneal lavage (PL) by flow cytometry. * $p < 0.05$ vs. indicated. (b#–g#) Corresponding groups with intratracheal application of the neutralizing CC16 antibody. Data are represented as the mean \pm standard error of the mean.

dysregulations and clinical complications. PMNL with their capability to regulate early inflammation are among the first nonresidual cells infiltrating the site of tissue damage and infections. As described before [32], we observed that local blunt chest trauma induces the systemic recruitment of PMNL out of the bone marrow; however, the posttraumatic increase of PMNL in damaged or remote organs [32] must be carefully reconsidered. Considering the systemic PMNL recruitment, potential local dysbalances in the distribution of three heterogeneous PMNL subsets [34] might promote

posttraumatic complications. Immature (CD16^{dim}CD62L^{bright}) PMNL are endotoxin-induced and display a banded nuclear morphology [24]. Compared to other PMNL subsets, they possess the highest intracellular bacterial containment capacity [35, 36]. The largest population among circulating PMNL is classical (CD16^{bright}CD62L^{bright}) PMNL [24]. These cells are characterized by a segmented nuclear morphology and referred to as mature PMNL [37]. The most recently described immunosuppressive subpopulation (CD16^{bright}CD62L^{dim}), with a hyper-segmented nuclear

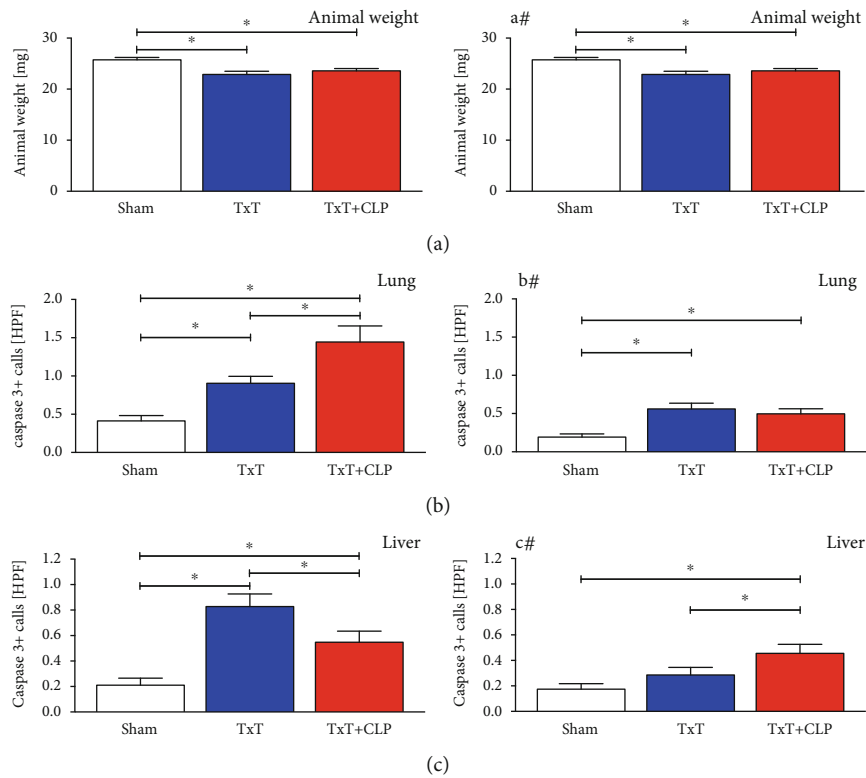


FIGURE 7: (a) Animal weights in mg of sham (white bars), isolated chest trauma (TxT, blue bars) and systemic inflammation model (TxT + CLP, red bars). (b) Number of apoptotic (caspase-3-positive) cells per high power field (HPF) in lungs. (c) Number of apoptotic cells per high power field (HPF) in liver. (a#–c#): corresponding groups with intratracheal application of the neutralizing CC16 antibody. Data are represented as mean \pm standard error of the mean. *: $p < 0.05$ vs. indicated.

morphology, has lower intracellular bacterial containment capacity [36], but is able to suppress the proliferation of immune-meditating T-cells by direct cell-cell interaction [24]. A possible stimulator of human, endotoxin-induced immunosuppressive PMNL is interferon-gamma (IFN- γ), as it stimulates the expression of programmed death ligand (PD-L)1. PD-L1 is required in immunosuppressive PMNL to suppress T-cell proliferation via direct cell-cell-interaction [38]. In human and mice, a PMNL subpopulation with upregulated PD-L1 during inflammation provided immunosuppressive characteristics by inducing lymphocyte apoptosis. Interestingly, in the murine PD-L1^{high} population, CD16 was upregulated, while CD62L was downregulated [39], confirming a coexpression of CD16^{bright}CD62L^{dim} to indicate immunosuppressive features in human and mice.

Comparable to findings in the human population [40], immature PMNL were induced after TxT and DH in the bone marrow, blood, and spleen (Figures 4(a), 4(b), and 4(e)), while trauma affected their reduction in damaged and remote tissue. It remains elusive, whether trauma-induced reduction in affected and unaffected tissue may be caused by the local differentiation before homing or as seen in the early inflammatory state by a time delay compared to classical PMNL between cytokine release and their recruitment. However, given their higher bacterial containment capacity, increased circulating immature PMNL may potentially inhibit systemic bacterial dissemination. The increase of classical PMNL in several organs following TxT and DH may be

induced by trauma-associated danger-associated molecular patterns, which are known to prime PMNL to migrate towards the endothelial barrier and promote their proinflammatory characteristics [41, 42], displaying an early alarmed immune state. Reduction in PL after additional CLP could be a first sign of immune dysregulation in systemic hyperinflammation. Interestingly, blunt chest trauma significantly reduced immunosuppressive PMNL in the lungs, the main site of organ damage. Similar attenuation in the spleen may be associated with the intrathoracic location of this organ with a possible mechanical damage by chest trauma. As the spleen stores PMNL [43], a recruitment of immunosuppressive PMNL after trauma may be assumed. Since the attenuation was only observed in intrathoracic damaged organs, phenotypic changes due to cytokine patterns or emigration may be responsible. An increase of immunosuppressive PMNL in unaffected organs, as shown for PL, bone marrow, blood, and liver following chest trauma might act as an endogenous mechanism providing hyperinflammation. Due to reduced migratory capacity of immunosuppressive PMNL, they might migrate less effectively into affected organs and appear in a higher ratio in unaffected tissue as it was hypothesized before [35]. Attenuation in the PL following additional CLP underlines the declining effects of local damage on immunosuppressive PMNL. The increase of immunosuppressive PMNL following DH in the BALF did not correlate with our findings, suggesting a special role of the BALF in pulmonary injury, underlining recent findings about

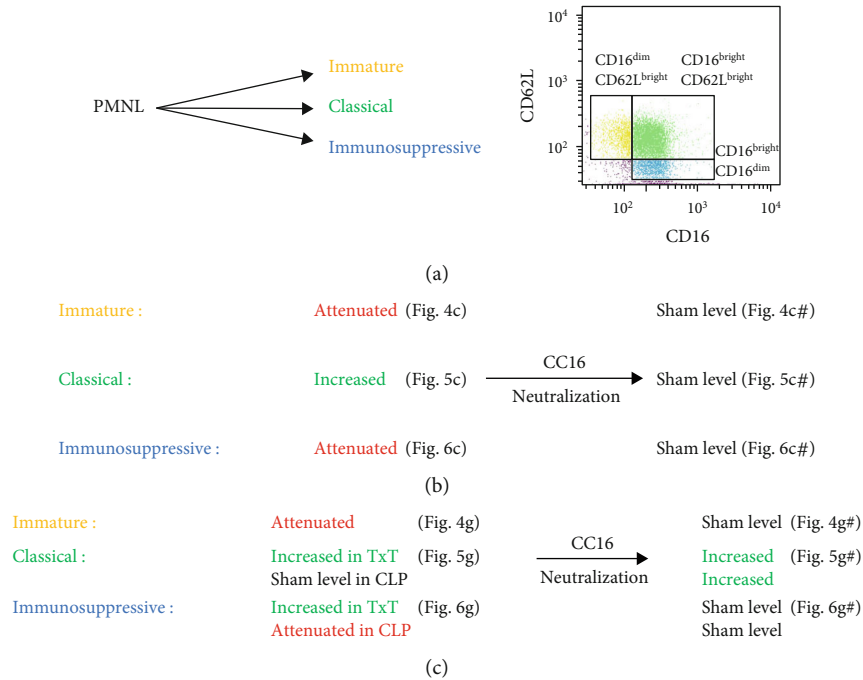


FIGURE 8: (a) Polymorphonuclear leukocytes (PMNL) were characterized by their relative expression of CD16 and CD62L into the three subsets (immature, CD16^{dim}CD62L^{bright}; classical, CD16^{bright}CD62L^{bright}; and immunosuppressive, CD16^{bright}CD62L^{dim}). (b) Changes in the subset distribution following trauma in the lungs representing affected tissue without and with CC16 neutralization. (c) Corresponding changes in cells in peritoneal (PL) undergoing thoracic trauma (TxT) and additional cecal ligation and puncture (CLP) representing unaffected tissue in TxT and affected tissue in CLP.

differences in PMNL behavior in BALF and parenchymal lung tissue [44].

Our data supports the existence of a trauma-induced distribution of the heterogeneous PMNL subsets with distinct characteristics, as highlighted above. Accumulation of cells with specific properties, distinguishing between damaged and unaffected tissues, is a potential method to emphasize inflammation and reduce uncontrolled systemic hyperinflammation after trauma.

4.2. Influence of CC16 on the Posttraumatic PMNL Subset Distribution. More than 50% of severely injured patients with physiologic problems suffer from a severe chest trauma [45], while the last constitutes as a risk factor for complex post-traumatic complications, i.e., acute respiratory distress syndrome [46]. Despite direct damage of the respiratory active tissue, systemic immunomodulation is likely to be involved in trauma-associated late mortality [47, 48]. After local trauma, the systemic effects seem reasonable considering the large contact area between the lungs and blood. CC16 is mainly produced in the lungs [49], and its elevated systemic levels were found in patients with lung damage, correlating with the size of damaged area [8]. Exact functions of CC16 are not entirely understood, but they are closely linked to its anti-inflammatory characteristics, e.g., attenuated IL-8-dependent PMNL chemotaxis [50], inhibited serum phospholipase A2 [51], reduced IFN- γ [52], and high affinity to Formyl Peptide Receptor (FPR)2 [53]. As long-term lower serum levels of baseline CC16 in adults are associated with deteriorated lung function [54], little is known about the

immunologic role of acutely elevated CC16 levels following chest trauma. The reported correlation of early elevated CC16 levels and elevated CC16 levels in the clinical course with the development of posttraumatic pneumonia [11] suggests that CC16 may act as a promising target to prevent complications in patients suffering from chest trauma. Despite its known immunosuppressive properties, we found that CC16 attenuated immunosuppressive PMNL, as its early neutralization following blunt chest trauma normalized the levels of immunosuppressive PMNL in the lungs. Similar normalizations were found systemically and in the spleen following TxT and in PL after CLP. Corresponding to the elevated rates of immunosuppressive PMNL, rates of classical PMNL were reduced after CC16 neutralization in lungs and spleen. Thus, we suggest CC16 to mediate “proinflammatory” properties during acute lung injury on the PMNL level. This was also highlighted by a reduced number of apoptotic cells after early application of the neutralizing CC16 antibody and supports our recently published data demonstrating that an early CC16 neutralization increased PMNL infiltration but prevented histologic lung damage 24 hours after blunt chest trauma [55]. Early proinflammatory properties are not entirely dissent with the anti-inflammatory properties described above. High local CC16 increase may affect FPR2 interference, as the FPR2 provides proinflammatory properties [56] or the coappearance of proinflammatory cytokines may modulate the immune response towards CC16. Since IFN- γ is delayed in its systemic increase compared to other proinflammatory cytokines after trauma [57], CC16 might also provide late immunosuppressive effects by suppressing

IFN- γ , while the immediate effects on PMNL-differentiation may be rather proinflammatory. Increased rates of immature PMNL following CC16 neutralization in the lungs, BALF, and blood might be associated with reducing effects of CC16 on PMNL migration [58]. On the other hand, it suggests the effect of CC16 to be influenced by the local immune state, as PMNL differentiation differs in unaffected tissue. This is highlighted by the attenuated fractions of immature and classical PMNL in the liver following CC16 neutralization (Figures 4(f) and 4(f#)), associated with a reduced tissue apoptosis in the liver. Taken together, this study is a first approach to characterize the diverse roles of PMNL in inflammation (summarized in Figure 8) and further promising effects of CC16 as a possible factor in their differentiation and as a pharmacologic target in the underlying model. Yet, the exact molecular mechanisms remain elusive.

As limitations of the study, it must be considered that the traditional gating strategy for murine MDSC (Gr-1⁺ and CD11b⁺) with promising human characterization of PMN-MDSC using CD16 and CD62L was applied. Dunay et al. applied CXCR4 and CD62L expression to stratifying two neutrophil populations [59]. Despite findings of murine CD16^{bright}CD62L^{dim}PD-L1⁺ PMNL with immunosuppressive properties, the comparison of human and murine CD16^{bright}CD62L^{dim} PMNL with immunosuppressive characteristics is necessary to allow transferability. One possible issue of identification is the shedding of CD62L [43] as it interferes with CD62L-staining, while shedding could also be a necessary step in the PMNL differentiation. In our gating strategy, we therefore extended the CD62L^{dim} gate towards low, isotype-positive fluorescent intensities, by considering the morphology of relative expression intensity.

5. Conclusions

Immature PMNL are released from the bone marrow following trauma and undergo specific subset differentiation at the site of their respective action, differing in damaged and undamaged organs. While classical PMNL were increased in damaged and remote organs, immunosuppressive PMNL were increased in unaffected and attenuated in damaged tissues following local blunt chest trauma (Figure 8(b)). CC16 neutralization affected the differentiation of immunosuppressive PMNL by inhibiting their attenuation in the lungs following TxT. Early CC16 neutralization following blunt chest trauma reduced the amount of apoptotic cells and might therefore be a promising target in preventing the post-traumatic immune dysregulation and improving outcomes.

Data Availability

Data are available upon a reasonable request to the corresponding author BR.

Disclosure

The funders had no role in the design of the study; in the collection, analyses, or interpretation of data; in the writing of

the manuscript; or in the decision to publish the results. Parts of this study have been published as meeting abstracts.

Conflicts of Interest

The authors state that they have no conflict of interest.

Authors' Contributions

B.R. is responsible for the conceptualization. N.B., P.S., A.J., and K.K. are responsible for the methodology. A.J. and B.R. performed the formal analysis. N.B., P.S., and A.J. did the investigation. N.B. acquired the data curation. N.B. wrote the original draft preparation. K.K., J.T.V., K.H., I.R.D., C.N., I.M., and B.R. did the writing of the review and editing. N.B. and B.R. did the visualization. B.R. did the supervision. B.R. is responsible for the project administration. All authors have read and agreed to the published version of the manuscript. Jan Tilmann Vollrath and Borna Relja contributed equally to this work.

Acknowledgments

We thank Katrin Jurida and Kerstin Kontradowitz for the outstanding technical assistance. The work was supported by the grant from the DFG RE 3304/8-1.

References

- [1] Geneva, World Health Organization, *Global Health Estimates 2016: Deaths by Cause, Age, Sex, by Country and by Region, 2000-2016*, 2018, https://terrance.who.int/mediacentre/data/ghe/GlobalCOD_method_2000_2016.pdf?ua=1.
- [2] M. Gunst, V. Ghaemmaghami, A. Gruszecki, J. Urban, H. Frankel, and S. Shafi, "Changing epidemiology of trauma deaths leads to a bimodal distribution," *Baylor University Medical Center Proceedings*, vol. 23, no. 4, pp. 349–354, 2017.
- [3] R. Lefering, T. Paffrath, O. Bouamra et al., "Epidemiology of in-hospital trauma deaths," *European Journal of Trauma and Emergency Surgery*, vol. 38, no. 1, pp. 3–9, 2012.
- [4] L. M. Napolitano, T. Ferrer, R. J. McCarter, and T. M. Scalea, "Systemic inflammatory response syndrome score at admission independently predicts mortality and length of stay in trauma patients," *The Journal of Trauma*, vol. 49, no. 4, pp. 647–653, 2000.
- [5] J. Cuschieri, E. Bulger, V. Schaeffer et al., "Early elevation in random plasma IL-6 after severe injury is associated with development of organ failure," *Shock*, vol. 34, no. 4, pp. 346–351, 2010.
- [6] A. Cheron, B. Floccard, B. Allaouchiche et al., "Lack of recovery in monocyte human leukocyte antigen-DR expression is independently associated with the development of sepsis after major trauma," *Critical Care*, vol. 14, no. 6, article R208, 2010.
- [7] A. Sousa, F. Raposo, S. Fonseca et al., "Measurement of cytokines and adhesion molecules in the first 72 hours after severe trauma: association with severity and outcome," *Disease Markers*, vol. 2015, Article ID 747036, 8 pages, 2015.
- [8] S. Wutzler, T. Lehnert, H. Laurer et al., "Circulating levels of Clara cell protein 16 but not surfactant protein D identify and quantify lung damage in patients with multiple injuries," *The Journal of Trauma*, vol. 71, no. 2, pp. E31–E36, 2011.

- [9] C. Hermans and A. Bernard, "Lung epithelium-specific proteins: characteristics and potential applications as markers," *American Journal of Respiratory and Critical Care Medicine*, vol. 159, no. 2, pp. 646–678, 1999.
- [10] F. Broeckaert, A. Clippe, B. Knoops, C. Hermans, and A. Bernard, "Clara cell secretory protein (CC16): features as a peripheral lung biomarker," *Annals of the New York Academy of Sciences*, vol. 923, no. 1, pp. 68–77, 2000.
- [11] S. Wutzler, L. Backhaus, D. Henrich et al., "Clara cell protein 16," *Journal of Trauma and Acute Care Surgery*, vol. 73, no. 4, pp. 838–842, 2012.
- [12] I. Dierynck, A. Bernard, H. Roels, and M. De Ley, "The human Clara cell protein: biochemical and biological characterisation of a natural immunosuppressor," *Multiple Sclerosis Journal*, vol. 1, no. 6, pp. 385–387, 1996.
- [13] M. Pang, H.-Y. Liu, T. Li et al., "Recombinant club cell protein 16 (CC16) ameliorates cigarette smoke-induced lung inflammation in a murine disease model of COPD," *Molecular Medicine Reports*, vol. 18, pp. 2198–2206, 2018.
- [14] M. E. Laucho-Contreras, F. Polverino, K. Gupta et al., "Protective role for club cell secretory protein-16 (CC16) in the development of COPD," *The European Respiratory Journal*, vol. 45, no. 6, pp. 1544–1556, 2015.
- [15] Y. Hüsecken, S. Muche, M. Kustermann et al., "MDSCs are induced after experimental blunt chest trauma and subsequently alter antigen-specific T cell responses," *Scientific Reports*, vol. 7, no. 1, article 12808, 2017.
- [16] L. F. Gentile, A. G. Cuenca, P. A. Efron et al., "Persistent inflammation and immunosuppression," *Journal of Trauma and Acute Care Surgery*, vol. 72, no. 6, pp. 1491–1501, 2012.
- [17] E. L. Vanzant, C. M. Lopez, T. Ozrazgat-Baslanti et al., "Persistent inflammation, immunosuppression, and catabolism syndrome after severe blunt trauma," *Journal of Trauma and Acute Care Surgery*, vol. 76, no. 1, pp. 21–30, 2014.
- [18] K. Movahedi, M. Guillemins, J. Van den Bossche et al., "Identification of discrete tumor-induced myeloid-derived suppressor cell subpopulations with distinct T cell-suppressive activity," *Blood*, vol. 111, no. 8, pp. 4233–4244, 2008.
- [19] J. Pillay, T. Tak, V. M. Kamp, and L. Koenderman, "Immune suppression by neutrophils and granulocytic myeloid-derived suppressor cells: similarities and differences," *Cellular and Molecular Life Sciences*, vol. 70, no. 20, pp. 3813–3827, 2013.
- [20] W. M. Nauseef, "How human neutrophils kill and degrade microbes: an integrated view," *Immunological Reviews*, vol. 219, no. 1, pp. 88–102, 2007.
- [21] E. Y. Enioutina, D. Bareyan, and R. A. Daynes, "A role for immature myeloid cells in immune senescence," *The Journal of Immunology*, vol. 186, no. 2, pp. 697–707, 2011.
- [22] V. Greifengberg, E. Ribechini, S. Rössner, and M. B. Lutz, "Myeloid-derived suppressor cell activation by combined LPS and IFN- γ treatment impairs DC development," *European Journal of Immunology*, vol. 39, no. 10, pp. 2865–2876, 2009.
- [23] V. Bronte, S. Brandau, S.-H. Chen et al., "Recommendations for myeloid-derived suppressor cell nomenclature and characterization standards," *Nature Communications*, vol. 7, no. 1, article 12150, 2016.
- [24] J. Pillay, V. M. Kamp, E. van Hoffen et al., "A subset of neutrophils in human systemic inflammation inhibits T cell responses through Mac-1," *The Journal of Clinical Investigation*, vol. 122, no. 1, pp. 327–336, 2012.
- [25] B. G. Yipp, J. H. Kim, R. Lima et al., "The lung is a host defense niche for immediate neutrophil-mediated vascular protection," *Science Immunology*, vol. 2, no. 10, article eaam8929, 2017.
- [26] C. Kilkenny, W. J. Browne, I. C. Cuthill, M. Emerson, and D. G. Altman, "Improving bioscience research reporting: the ARRIVE guidelines for reporting animal research," *PLoS Biology*, vol. 8, no. 6, article e1000412, 2010.
- [27] A. Janicova, N. Becker, B. Xu et al., "Endogenous uteroglobin as intrinsic anti-inflammatory signal modulates monocyte and macrophage subsets distribution upon sepsis induced lung injury," *Frontiers in Immunology*, vol. 10, article 2276, 2019.
- [28] P. Störmann, N. Becker, L. Künnemeyer et al., "Contributing factors in the development of acute lung injury in a murine double hit model," *European Journal of Trauma*, vol. 46, no. 1, pp. 21–30, 2020.
- [29] M. W. Knöferl, U. C. Liener, D. H. Seitz et al., "Cardiopulmonary, histological, and inflammatory alterations after lung contusion in a novel mouse model of blunt chest trauma," *Shock*, vol. 19, no. 6, pp. 519–525, 2003.
- [30] D. B. Danahy, S. P. Kurup, C. S. Winborn et al., "Sepsis-induced state of immunoparalysis is defined by diminished CD8 T cell-mediated antitumor immunity," *Journal of Immunology*, vol. 203, no. 3, pp. 725–735, 2019.
- [31] B. Relja, K. Mörs, and I. Marzi, "Danger signals in trauma," *European Journal of Trauma and Emergency Surgery*, vol. 44, no. 3, pp. 301–316, 2018.
- [32] P. Störmann, N. Wagner, K. Köhler et al., "Monotrauma is associated with enhanced remote inflammatory response and organ damage, while polytrauma intensifies both in porcine trauma model," *European Journal of Trauma*, vol. 46, no. 1, pp. 31–42, 2020.
- [33] W. Xiao, M. N. Mindrinos, J. Seok et al., "A genomic storm in critically injured humans," *The Journal of Experimental Medicine*, vol. 208, no. 13, pp. 2581–2590, 2011.
- [34] T. Tak, P. Wijten, M. Heeres et al., "Human CD62Ldim neutrophils identified as a separate subset by proteome profiling and in vivo pulse-chase labeling," *Blood*, vol. 129, no. 26, pp. 3476–3485, 2017.
- [35] V. M. Kamp, J. Pillay, J.-W. J. Lammers, P. Pickkers, L. H. Ulfman, and L. Koenderman, "Human suppressive neutrophils CD16bright/CD62Ldim exhibit decreased adhesion," *Journal of Leukocyte Biology*, vol. 92, no. 5, pp. 1011–1020, 2012.
- [36] P. H. C. Leliefeld, J. Pillay, N. Vrisekoop et al., "Differential antibacterial control by neutrophil subsets," *Blood Advances*, vol. 2, no. 11, pp. 1344–1355, 2018.
- [37] J. A. Fraser, S. Kemp, L. Young et al., "Silver nanoparticles promote the emergence of heterogeneous human neutrophil subpopulations," *Scientific Reports*, vol. 8, no. 1, pp. 7506–7506, 2018.
- [38] S. de Kleijn, J. D. Langereis, J. Leentjens et al., "IFN- γ -stimulated neutrophils suppress lymphocyte proliferation through expression of PD-L1," *PLoS One*, vol. 8, no. 8, article e72249, 2013.
- [39] J.-F. Wang, J.-B. Li, Y.-J. Zhao et al., "Up-regulation of programmed cell death 1 ligand 1 on neutrophils may be involved in sepsis-induced immunosuppression: an animal study and a prospective case-control study," *Anesthesiology*, vol. 122, no. 4, pp. 852–863, 2015.
- [40] E. van Grinsven, J. Textor, L. S. P. Hustin, K. Wolf, L. Koenderman, and N. Vrisekoop, "Immature neutrophils

- released in acute inflammation exhibit efficient migration despite incomplete segmentation of the nucleus," *Journal of Immunology*, vol. 202, pp. 207–217, 2019.
- [41] J. Manson, C. Thiemermann, and K. Brohi, "Trauma alarmins as activators of damage-induced inflammation," *British Journal of Surgery*, vol. 99, Supplement 1, pp. 12–20, 2012.
- [42] V. Schenten, S. Plançon, N. Jung et al., "Secretion of the phosphorylated form of S100A9 from neutrophils is essential for the proinflammatory functions of extracellular S100A8/A9," *Frontiers in Immunology*, vol. 9, p. 447, 2018.
- [43] S. H. Saverymuttu, A. M. Peters, A. Keshavarzian, H. J. Reavy, and J. P. Lavender, "The kinetics of ¹¹¹Indium distribution following injection of ¹¹¹Indium labelled autologous granulocytes in man," *British Journal of Haematology*, vol. 61, no. 4, pp. 675–685, 1985.
- [44] M. P. J. Teuben, M. Hofman, A. Shehu et al., "The impact of intramedullary nailing on the characteristics of the pulmonary neutrophil pool in rodents," *International Orthopaedics*, vol. 44, no. 3, pp. 595–602, 2020.
- [45] L. Rea, *TraumaRegister® DGU—Annual Report 2017*, 2017, http://www.traumaregister-dgu.de/fileadmin/user_upload/traumaregister-dgu.de/docs/Downloads/TR-DGU_Annual_Report_2017.pdf.
- [46] C. J. Tignanelli, M. R. Hemmila, M. A. M. Rogers, and K. Raghavendran, "Nationwide cohort study of independent risk factors for acute respiratory distress syndrome after trauma," *Trauma Surgery & Acute Care Open*, vol. 4, no. 1, article e000249, 2019.
- [47] C. Ehrnthaller, M. Flierl, M. Perl et al., "The molecular fingerprint of lung inflammation after blunt chest trauma," *European Journal of Medical Research*, vol. 20, no. 1, p. 70, 2015.
- [48] K. B. Thompson, L. T. Krispinsky, and R. J. Stark, "Late immune consequences of combat trauma: a review of trauma-related immune dysfunction and potential therapies," *Military Medical Research*, vol. 6, no. 1, p. 11, 2019.
- [49] A. Bernard, X. Dumont, H. Roels et al., "The molecular mass and concentrations of protein 1 or Clara cell protein in biological fluids: a reappraisal," *Clinica Chimica Acta*, vol. 223, no. 1–2, pp. 189–191, 1993.
- [50] O. Côté, M. E. Clark, L. Viel et al., "Secretoglobin 1A1 and 1A1A differentially regulate neutrophil reactive oxygen species production, phagocytosis and extracellular trap formation," *PLoS One*, vol. 9, no. 4, article e96217, 2014.
- [51] S. W. Levin, J. D. Butler, U. K. Schumacher, P. D. Wightman, and A. B. Mukherjee, "Uteroglobin inhibits phospholipase A₂ activity," *Life Sciences*, vol. 38, no. 20, pp. 1813–1819, 1986.
- [52] I. Dierynck, A. Bernard, H. Roels, and M. De Ley, "Potent inhibition of both human interferon-gamma production and biologic activity by the Clara cell protein CC16," *American Journal of Respiratory Cell and Molecular Biology*, vol. 12, no. 2, pp. 205–210, 1995.
- [53] G. Antico, M. Aloman, K. Lakota, L. Miele, S. Fiore, and S. Sodin-Semrl, "Uteroglobin, a possible ligand of the lipoxin receptor inhibits serum amyloid A-driven inflammation," *Mediators of Inflammation*, vol. 2014, Article ID 876395, 10 pages, 2014.
- [54] S. Guerra, M. Halonen, M. M. Vasquez et al., "Relation between circulating CC16 concentrations, lung function, and development of chronic obstructive pulmonary disease across the lifespan: a prospective study," *The Lancet Respiratory Medicine*, vol. 3, no. 8, pp. 613–620, 2015.
- [55] P. Störmann, N. Becker, J. T. Vollrath et al., "Early local inhibition of club cell protein 16 following chest trauma reduces late sepsis-induced acute lung injury," *Journal of Clinical Medicine*, vol. 8, no. 6, p. 896, 2019.
- [56] F. Cattaneo, M. Parisi, and R. Ammendola, "Distinct signaling cascades elicited by different formyl peptide receptor 2 (FPR2) agonists," *International Journal of Molecular Sciences*, vol. 14, no. 4, pp. 7193–7230, 2013.
- [57] J. Liu, J. Wang, H. Luo et al., "Screening cytokine/chemokine profiles in serum and organs from an endotoxic shock mouse model by LiquiChip," *Science China. Life Sciences*, vol. 60, no. 11, pp. 1242–1250, 2017.
- [58] B. Xu, A. Janicova, J. T. Vollrath et al., "Club cell protein 16 in sera from trauma patients modulates neutrophil migration and functionality via CXCR1 and CXCR2," *Molecular Medicine*, vol. 25, no. 1, pp. 45–45, 2019.
- [59] A. Biswas, T. French, H. P. Düsedau et al., "Behavior of neutrophil granulocytes during *Toxoplasma gondii* infection in the central nervous system," *Frontiers in Cellular and Infection Microbiology*, vol. 7, 2017.
- [60] F. H. Brennan, T. Jorgia, E. R. Gillespie et al., "Complement receptor C3aR1 controls neutrophil mobilization following spinal cord injury through physiological antagonism of CXCR2," *JCI Insight*, vol. 4, no. 9, 2019.

Research Article

DHX37 Impacts Prognosis of Hepatocellular Carcinoma and Lung Adenocarcinoma through Immune Infiltration

Yanni Xu ^{1,2}, Qiongchao Jiang ^{1,2}, Hejun Liu ³, Xiaoyun Xiao ¹, Dinghong Yang ¹, Phei Er Saw ⁴ and Baoming Luo ¹

¹Department of Ultrasound, Sun Yat-sen Memorial Hospital, Sun Yat-sen University, 107 Yanjiangxi Rd., Guangzhou, 510120 Guangdong Province, China

²Guangdong Provincial Key Laboratory of Malignant Tumor Epigenetics and Gene Regulation, Sun Yat-sen Memorial Hospital, Sun Yat-sen University, China

³Department of Hyperbaric Oxygen, Sun Yat-sen Memorial Hospital, Sun Yat-sen University, Guangzhou 510120, China

⁴Guangdong Provincial Key Laboratory of Malignant Tumor Epigenetics and Gene Regulation, Medical Research Center, Sun Yat-sen Memorial Hospital, Sun Yat-sen University, Guangzhou, China 510120

Correspondence should be addressed to Phei Er Saw; caipeie@mail.sysu.edu.cn and Baoming Luo; luobm@mail.sysu.edu.cn

Received 25 September 2020; Revised 31 October 2020; Accepted 17 December 2020; Published 31 December 2020

Academic Editor: Xianyang Li

Copyright © 2020 Yanni Xu et al. This is an open access article distributed under the Creative Commons Attribution License, which permits unrestricted use, distribution, and reproduction in any medium, provided the original work is properly cited.

Background. RNA helicases have various essential functions in basically all aspects of RNA metabolism, not only unwinding RNA but also disturbing the interaction of RNA with proteins. Recently, RNA helicases have been considered potential targets in cancers. So far, there has been no detailed investigation of the biological functions of RNA helicase DHX37 in cancers. **Objective.** We aim to identify the prognostic value of DHX37 associated with tumor microenvironments in cancers. **Methods.** DHX37 expression was examined via the Oncomine database and Tumor Immune Estimation Resource (TIMER). We explored the prognostic role of DHX37 in cancers across various databases. Coexpression genes, Gene Ontology (GO) and Kyoto Encyclopedia of Genes and Genomes (KEGG), and fundamental regulators were performed via LinkedOmics. Confirming the prognostic value of DHX37 in liver hepatocellular carcinoma (LIHC) and lung adenocarcinoma (LUAD), we explored the role of DHX37 in infiltrated lymphocytes in cancers using the Gene Expression Profiling Interactive Analysis (GEPIA) and TIMER databases. **Results.** Through GO and KEGG analyses, expression of DHX37 was also correlated with complex function-specific networks involving the ribosome and RNA metabolic signaling pathways. In LIHC and LUAD, DHX37 expression showed significant positive correlations with markers of T_{regs}, myeloid-derived suppressor cells (MDSCs), and T cell exhaustion, contributing to immune tolerance. **Conclusion.** These results indicate that DHX37 can serve as a prognostic biomarker in LIHC and LUAD while having an important role in immune tolerance by activating the function of T_{regs}, MDSC, and T cell exhaustion.

1. Introduction

Cancer is now known to be a disease which involves multiple players, including its relationship with micro- and macroenvironments. Tumor microenvironment (TME) is crucial in cancer progression and therapeutic responses [1, 2] and consists of complex components, among which inflammatory cells make up for the majority proportion and are valuable for diagnostic and prognostic assessment of tumors. The widely used therapy of immune checkpoint modulators, including programmed cell death protein 1 (PD-1), cytotoxic

T lymphocyte-associated antigen-4 (CTLA4), lymphocyte activation gene-3 (LAG-3), and T cell immunoglobulin mucin 3 (TIM-3) [3, 4], has become a promising anticancer therapy by reversing the suppressed immune status in tumors [5, 6]. However, immunotherapy failed to have satisfactory effects in that only 20% of cancer patients benefited with significantly increased survival rates [7, 8], due to a combination of different clinical and biological behaviors [9].

In recent years, cumulative evidence has revealed that RNA helicases can modulate physiological processes like innate immune reactions, carcinogenic disorders, and inflammatory

disorders [10–13]. For example, RNA helicase A/DHX9, as a potential therapeutic target, is associated with cancer risk and inflammation [14]. The abnormally high expression of RNA helicases has been tested in a variety of cancers [15]. DHX15 is significantly upregulated in HCC, and its high expression was correlated with poor prognosis. DDX3X drives posttranscriptional programming that dictates melanoma phenotype and poor disease prognosis. RNA helicases p68 and p72 show increased expression during colon carcinogenesis.

DHX37 is a highly conserved DEAH box RNA helicase essential for development of the ribosome [16]. It conjugates to the U3 small nucleolar RNA and is significant for remodeling the U3 snoRNA-pre-18S rRNA structure during 40S maturation [17]; this ensures the formation of the central pseudoknot structure. The production of eukaryotic ribosomes is a massively complicated and energy-draining intracellular activity responsible for the translation of mRNAs into proteins [18].

Previous immunological characterization of CD8 T cells indicated that DHX37 suppressed effector functions, cytokine production, and T cell activation by modulating NF- κ B [19], which first showed that DHX37 was related to the progression of cancers. This suggests that DHX37 may be a potential biomarker for cancers and is involved in the immune response.

However, the intrinsic mechanisms of effects of DHX37 on malignant tumor development and immune regulation have not been investigated. In this research, we conducted a comprehensive bioinformatic analysis of DHX37 expression profiles in multiple cancers. This is the first finding that reveals the association between DHX37 and Pan-Cancer in multidimensional biological functions. Our study has identified DHX37 as a potential marker of lung and liver cancers, which may guide the development of novel anticancer therapies.

2. Methods

2.1. Oncomine Database Analysis. We examined the gene expression of DHX37 in Pan-Cancer using the Oncomine database [20]. The gene was assessed for differential expression with *t*-statistics using Total Access Statistics 2002 (FMS Inc., Vienna, VA). *t*-tests were conducted both as two-sided for differential expression analysis and one-sided for specific overexpression analysis. A *P* value of 0.001 and a fold change of 1.5 were set as significance thresholds.

2.2. PrognScan Database Analysis. We utilized PrognScan database analysis [21] to assess the correlations between DHX37 expression and survival time in multiple cancers. Survival analysis in PrognScan employs the minimum *P* value approach to find the cut point in continuous gene expression measurement for grouping patients. An adjusted Cox *P* value < 0.05 was considered statistically significant.

2.3. Kaplan-Meier Plotter Database Analysis. The correlation between the gene level of DHX37 and overall survival as well as relapse-free survival in 21 types of tumors was performed by Kaplan-Meier Plotter [22]. The Kaplan-Meier Plotter was

set up by searching the GEO, EGA, TCGA, and PubMed repositories to identify datasets with published gene expression and clinical data. The hazard ratio (HR) with 95% confidence intervals (CI) was analyzed. The correlation was significant at the 0.05 level.

2.4. UALCAN Analysis. UALCAN [23] was used to obtain the relative expression of DHX37 both in normal and neoplastic tissues and in several clinicopathological subgroups. UALCAN analysis use the TCGA-Assembler to download the TCGA level 3 RNA-seq data related to 31 cancer types and used TPM as the measure of expression. The *P* value cutoff was 0.05.

2.5. GEPIA. Gene Expression Profiling Interactive Analysis (GEPIA) was applied to confirm the correlational analyses from TIMER [24]. GEPIA analyzed the RNA sequencing expression data of both tumor samples and normal samples from TCGA and the Genotype Tissue Expression projects. To solve the imbalance between the tumor and normal data which can cause inefficiency in various differential analyses, GEPIA downloaded the TCGA and GTEx gene expression data that are recomputed from raw RNA-seq data by the UCSC Xena project based on a uniform pipeline. The *P* value cutoff was 0.05.

2.6. TIMER Database Analysis. The Tumor Immune Estimation Resource aims to evaluate relative proportions of various immune cell subsets based on data from TCGA with a deconvolution approach [25]. We assessed DHX37 expression and the correlation of DHX37 expression with the density of 6 types of infiltrating immune cells in diverse cancers by the TIMER algorithm database. In addition, the “differential expression module” was used to evaluate clinical prognosis affected by overexpressed DHX37.

2.7. TISIDB Database Analysis. Tumor and immune system interactions [26] were performed to explore the abundance of 28 types of tumor-infiltrating lymphocytes (TILs) and MHC markers by precalculating for 30 TCGA cancer types. The relational coefficient between DHX37 and TILs as well as MHC markers was measured by Spearman’s test.

2.8. LinkedOmics Analysis. The LinkedOmics database is a publicly available web server for analyzing multidimensional datasets based on TCGA [27]. DHX37 coexpression was presented in heat maps with analysis of Pearson’s correlation coefficient. GO (CC (cellular component), BP (biological process), and MF (molecular function)) and KEGG (Kyoto Encyclopedia of Genes and Genomes) pathways and enrichment of cellular regulators including kinase targets and miRNA targets and transcription factor target were analyzed by gene set enrichment analysis (GSEA). The rank criterion was an FDR (false discovery rate) < 0.05, a minimum number of genes of 3, and a simulation of 500, using the LIHC and LUAD compared datasets.

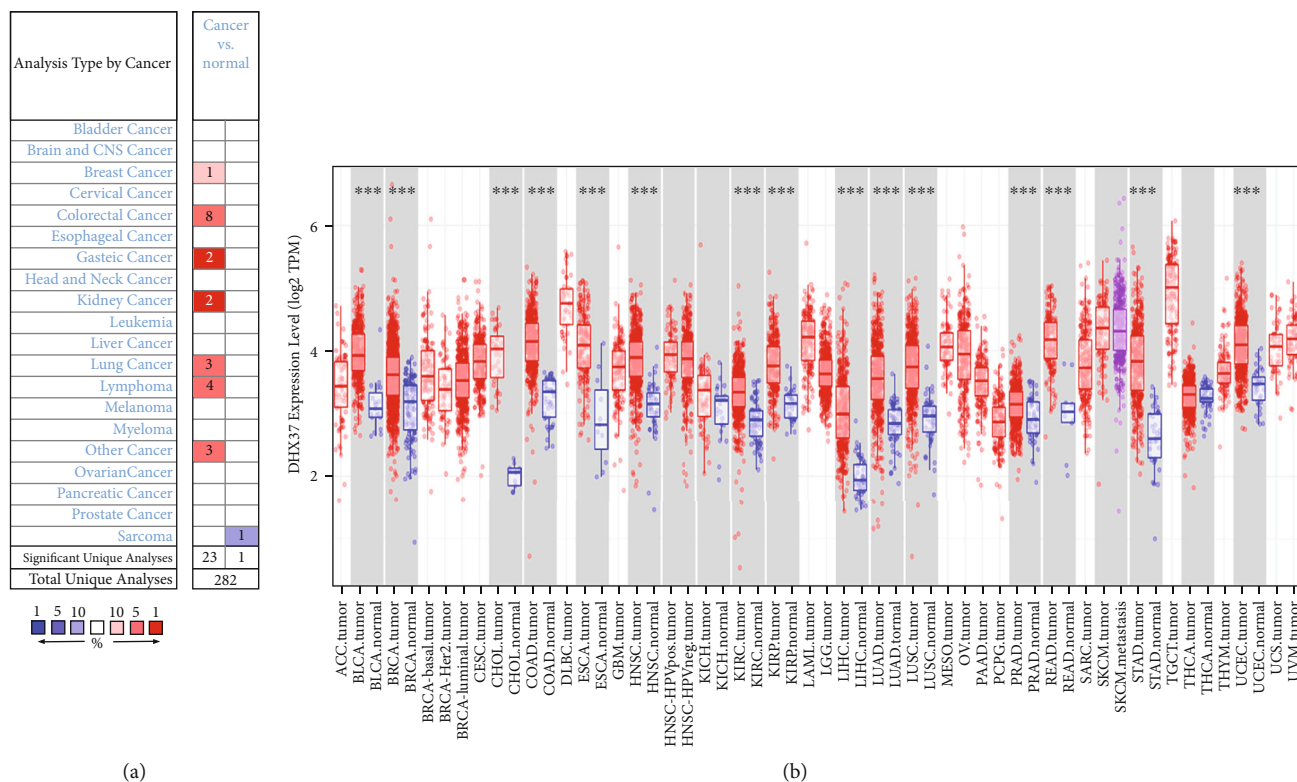


FIGURE 1: DHX37 expression levels in cancers. (a) Increased or decreased expression of DHX37 in different cancer tissues compared with normal tissues in the Oncomine database. Number in each cell is the number of datasets. Red indicates high expression and blue indicates low expression. (b) Human DHX37 expression levels in different cancer types from TCGA data in TIMER. * $P < 0.05$, ** $P < 0.01$, *** $P < 0.001$. Red indicates tumor and blue indicates normal tissue.

3. Results

3.1. DHX37 Expression in Various Cancers. DHX37 gene expression was retrieved using the Oncomine database to determine differences between tumor and normal tissues over a cancer-wide range. As depicted in Figure 1(a) and Table S1, the DHX37 expression was elevated in breast (1.5, $P = 5.45e - 9$), colorectal (3.526, $P = 5.14e - 5$), gastric (3.866, $P = 2.24e - 9$), kidney (3.023, $P = 5.81e - 4$), and lung cancers (2.357, $P = 6.95e - 5$) as well as lymphoma (2.032, $P = 3.03e - 7$), whereas DHX37 was only observed significantly reduced in the sarcoma dataset (-1.632, $P = 5.15e - 5$).

To validate DHX37 high expression in other databases, the RNA-seq data in TCGA from TIMER were investigated. The aberrant expression of tumor masses compared with adjacent normal tissues in Pan-Cancer is shown in Figure 1(b). DHX37 expression was significantly upregulated in cancer groups, including BLCA (bladder urothelial carcinoma), BRCA (breast invasive carcinoma), CHOL (cholangiocarcinoma), COAD (colon adenocarcinoma), ESCA (esophageal carcinoma), HNSC (head and neck squamous cell carcinoma), KIRC (head and neck squamous cell carcinoma), KIRP (kidney renal papillary cell carcinoma), LIHC (liver hepatocellular carcinoma), LUAD (lung adenocarcinoma), LUSC (lung squamous cell carcinoma), PRAD (prostate adenocarcinoma), READ (rectum adenocarci-

noma), STAD (stomach adenocarcinoma), and UCEC (uterine corpus endometrial carcinoma) as compared with the surrounding tissues.

3.2. Prognostic Value of DHX37 in Various Cancers. The association between DHX37 and survival time from PrognScan based on the Gene Expression Omnibus (GEO) database is summarized in Table S2. DHX37 expression significantly impacted prognosis in 5 types of cancers, including breast, colorectal, skin, blood, and lung cancers (Figures 2(a)–2(h)). Two cohorts (GSE31210 and GSE11117) comprising 204 samples and 41 samples, respectively, of lung cancer revealed that upregulated expression of DHX37 was related to poorer final outcome (RFS (relapse-free survival) HR (hazard ratio) = 2.83, 95%CI (confidence interval) = 1.05 to 7.66, Cox $P = 0.04$; OS HR = 2.02, 95%CI = 1.07 – 3.82, Cox $P = 0.03$) (Figures 2(a) and (b)). Therefore, increased DHX37 predicted poor outcomes in lung cancer.

Unlike the findings from PrognScan, we found a high expression of DHX37 reduced survival in BRCA (breast invasive carcinoma) (Figures 2(k) and 2(l)) by using the Kaplan-Meier Plotter database. Similarly, the poor outcome [28] in liver hepatocellular carcinoma (OS (overall survival) HR = 1.6, 95%CI = 1.06 to 2.42, $P = 0.025$; RFS HR = 1.23, 95%CI = 0.87 to 1.73, $P = 0.23$) and lung adenocarcinoma (OS HR = 1.83, 95%CI = 1.27 to 2.64, $P = 0.00095$; RFS HR = 1.25, 95%CI = 0.79 to 1.96, $P = 0.34$)

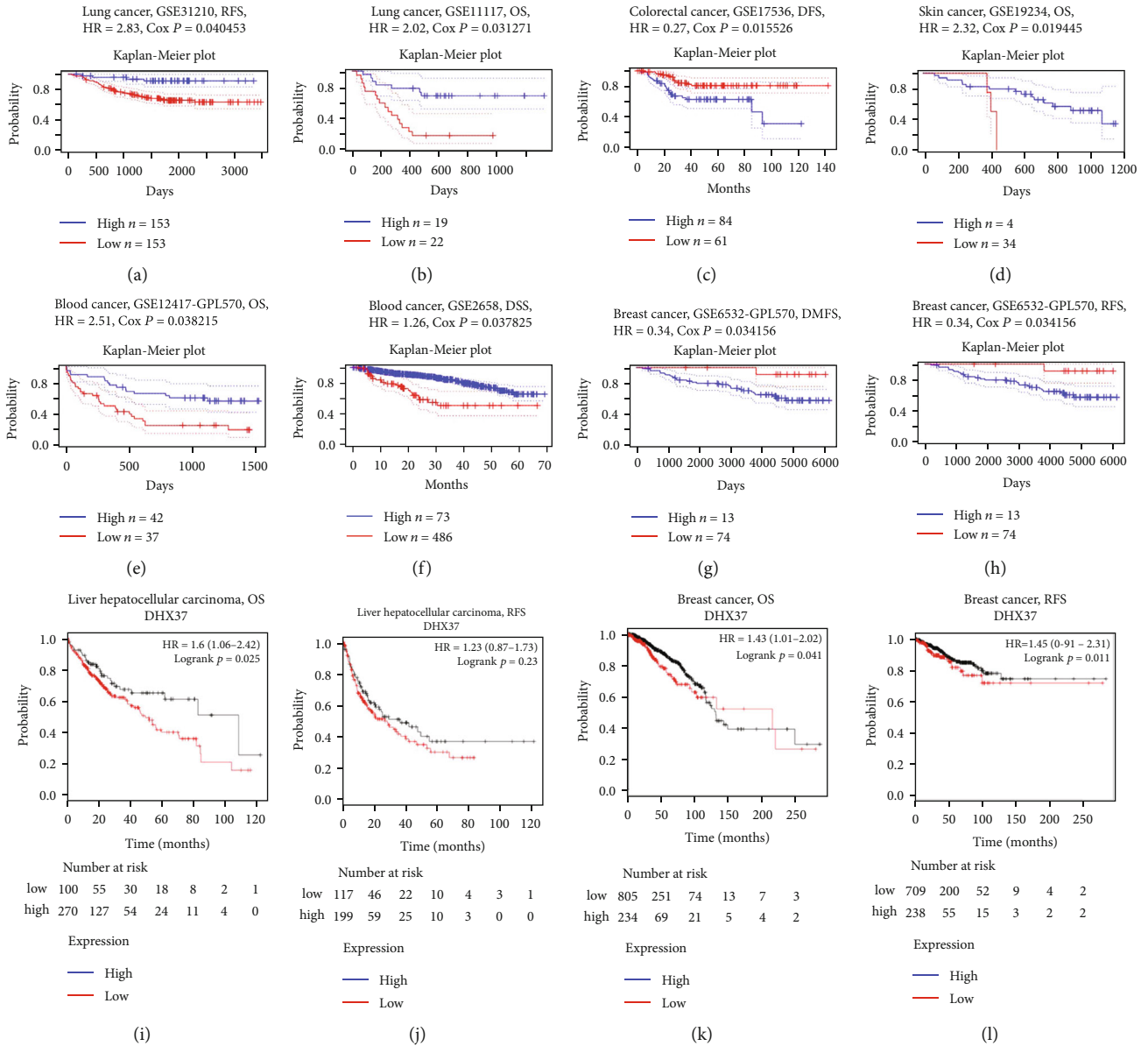


FIGURE 2: Continued.

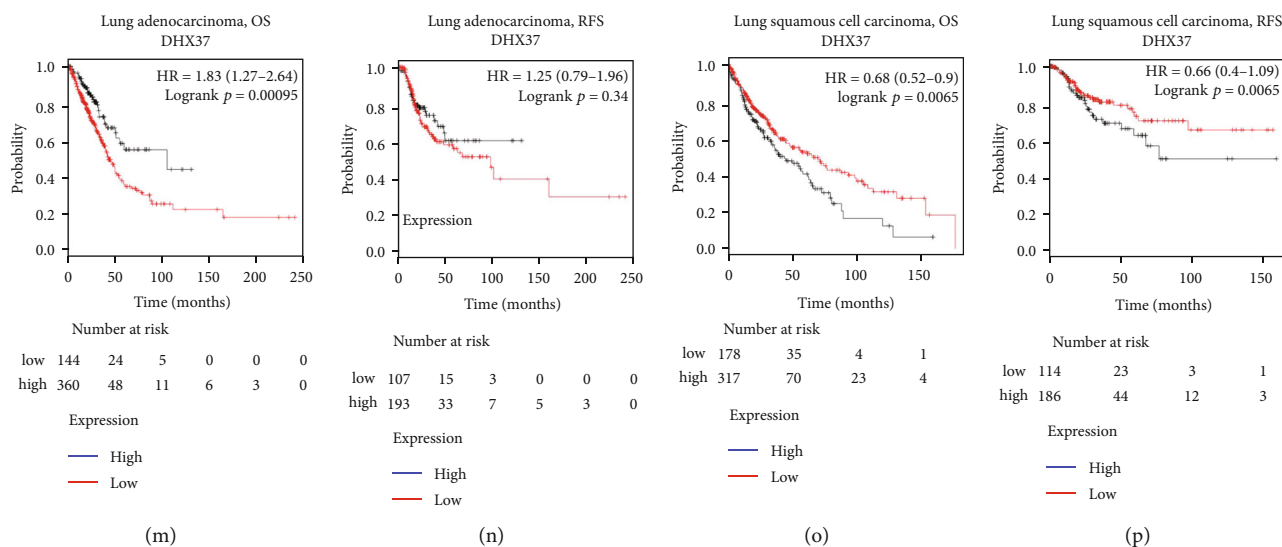


FIGURE 2: Kaplan-Meier survival curves comparing the high and low expression of DHX37 in different types of cancer in the Prognoscan (a–h) and Kaplan-Meier plotter databases (i–p). (a, b) Survival curves of RFS and OS in two lung cancer cohorts [GSE31210 ($n = 204$) and GSE11117 ($n = 41$)]. (c, d) Survival curves of DFS and OS in colorectal cancer cohort (GSE17536, $n = 145$) and skin cancer cohort (GSE19234, $n = 38$). (e, f) Survival curves of OS and DSS in two blood cancer cohorts [GSE12417-GPL570 ($n = 79$) and GSE2658 ($n = 559$)]. (g, h) Survival curves of DMSF and RFS in the breast cancer cohort (GSE6532-GPL570, $n = 87$). Kaplan-Meier survival curves comparing the high and low expression of DHX37 in Kaplan-Meier Plotter, OS, and RFS of (i, j) liver hepatocellular carcinoma (LIHC) (k, l) breast cancer (BRCA) (m, n) lung adenocarcinoma (LUAD) (o, p) lung squamous cell carcinoma (LUSC). Red curve represents patients with high expression of DHX37. OS: overall survival; DMSF: distant metastasis-free survival; DFS: disease-free survival; RFS: relapse-free survival; DSS: disease-specific survival.

was shown to be relevant to higher DHX37 expression (Figures 2(i), 2(j), 2(m), and 2(n)). However, DHX37 expression has less influence on head and neck squamous cell carcinoma (Figure S1C, D). For lung squamous cell carcinoma (Figures 2(o) and 2(p)), thyroid carcinoma (Figure S1E, F), rectum adenocarcinoma (Figure S1I, J), stomach adenocarcinoma (Figure S1M, N), and uterine corpus endometrial carcinoma (Figure S1O, P), DHX37 plays a protective role in their OS but not RFS. For esophageal adenocarcinoma, DHX37 was found to have a favorable effect on relapse-free survival while it worsened overall survival (Figure S1A, B). In addition, DHX37 only had significant correlation with RFS for pancreatic ductal adenocarcinoma and ovarian cancers (Figure S1G, H, S, T).

To further verify the value of differentially expressed DHX37 in the progression of different cancers, the RNA-seq data in TCGA were also exploited to confirm the prognostic implications of DHX37 in each cancer type via GEPIA (Gene Expression Profiling Interactive Analysis). We assessed correlations between DHX37 expression and clinical outcomes in 33 types of cancer (Figure S2). DHX37 overexpression was related to poor outcomes of OS (overall survival) and DFS (disease-free survival) in ACC (adrenocortical carcinoma), LGG (brain lower grade glioma), and LIHC (liver hepatocellular carcinoma); OS in LUAD (lung adenocarcinoma), MESO (mesothelioma), and THCA (thyroid carcinoma); and DFS (disease-free survival) in SKCM (Skin Cutaneous Melanoma). These results

validated the predictive value of DHX37 in particular types of cancer, such as LIHC and LUAD.

3.3. DHX37 Expression Is Associated with Advanced Clinicopathological Characteristics in LIHC and LUAD. To further reveal the potential relevance of DHX37 expression in cancers, we explored the relationship between DHX37 expression and several clinical features of LIHC and LUAD patients in TCGA cohorts by UALCAN. Subgroup analysis of several clinicopathological characteristics of 421 LIHC samples and 574 LUAD samples consistently showed significantly elevated DHX37 mRNA expression. As shown in Figure 3, the transcription level of DHX37 was significantly upregulated in LIHC and LUAD patients compared to the healthy group (with subgroup analysis based on gender, disease stages, pathological grade, cancer status, and TP53 mutation). Upregulated expression of DHX37 correlates with advanced stage and poor differentiation, particularly in older men and smokers.

Overall, these data analyses indicate that patients of LIHC and LUAD with high levels of DHX37 expression tend to have tumors with advanced clinicopathological parameters.

3.4. DHX37 Coexpression Networks in Patients with LIHC and LUAD. Given the above prognostic findings from multiple databases, we chose LIHC and LUAD as representative cancers for further research. To elucidate the biological function of DHX37, LinkedOmics was applied to

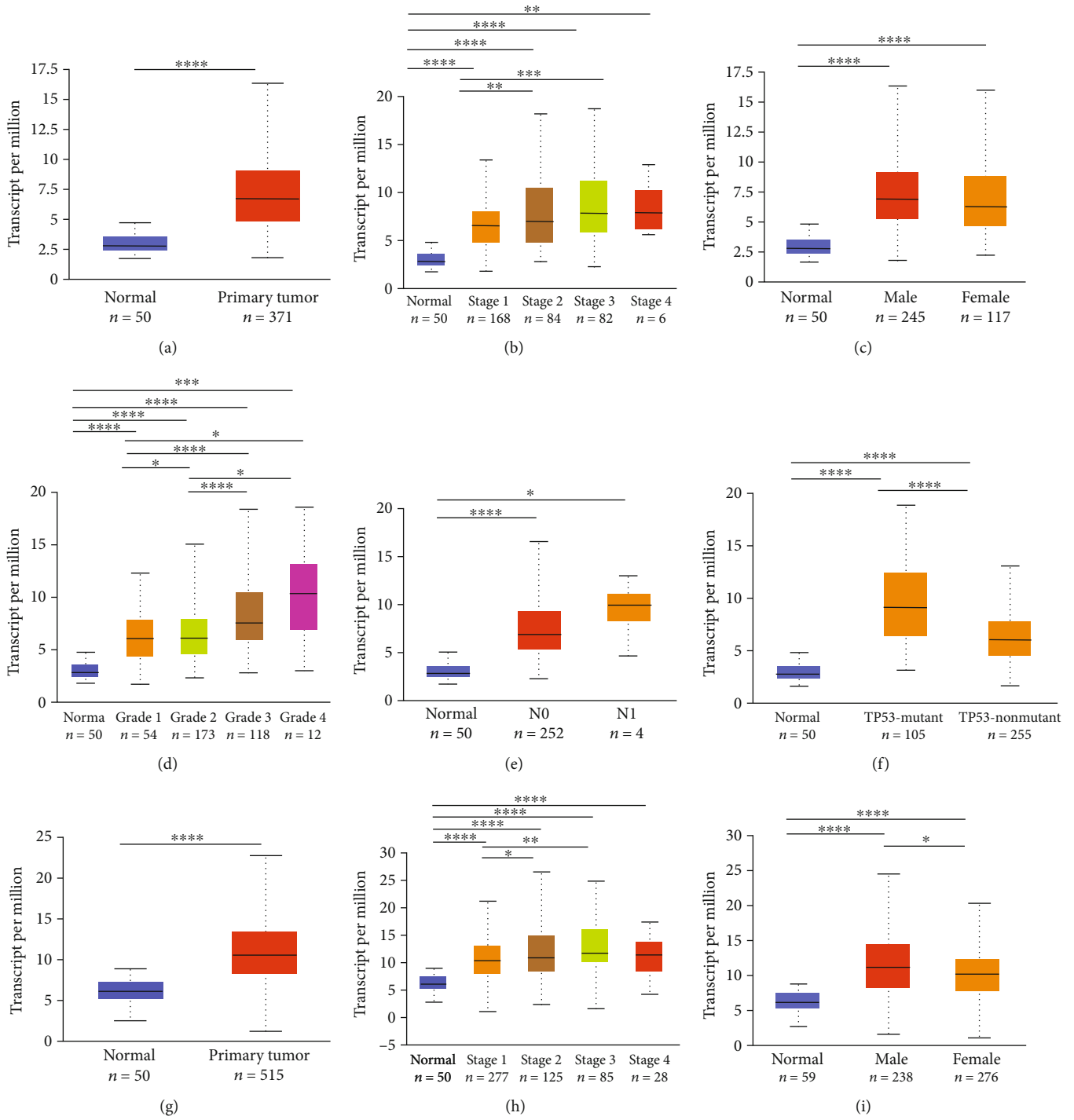


FIGURE 3: Continued.

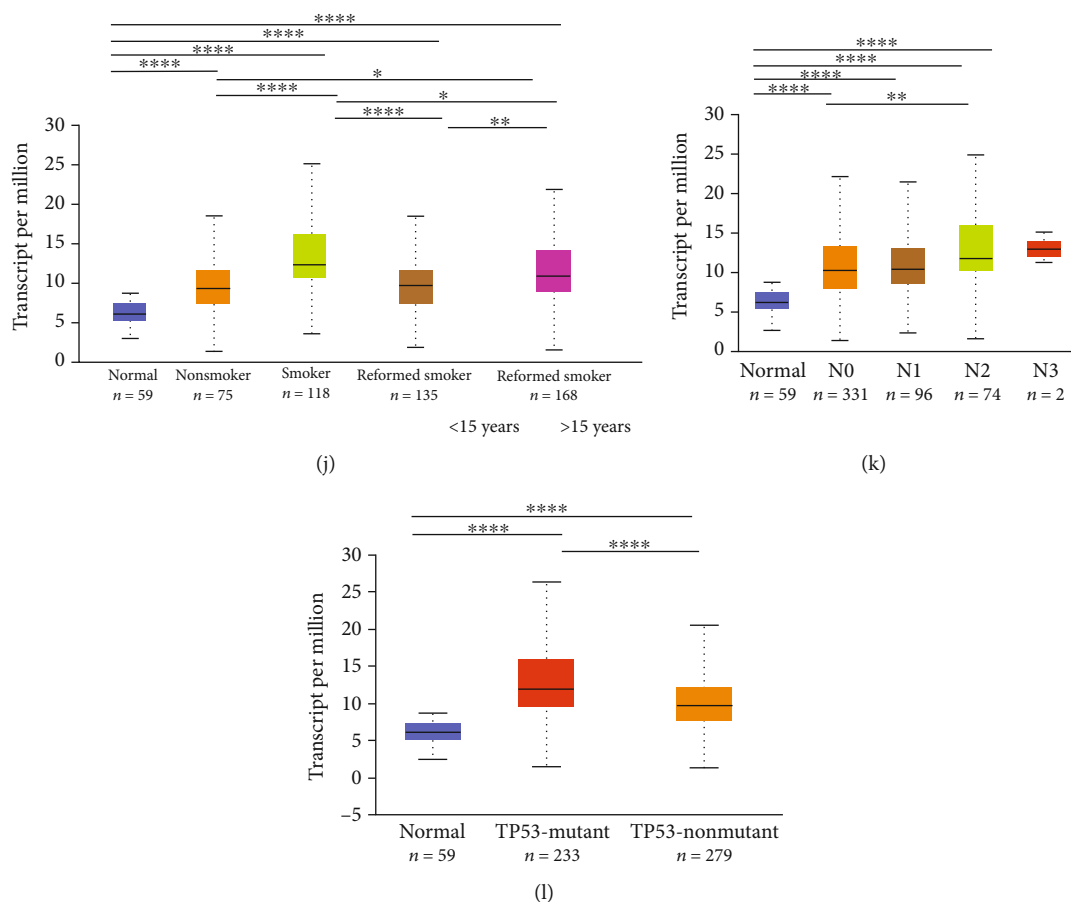


FIGURE 3: DHX37 transcription in subgroups of patients with hepatocellular carcinoma and lung adenocarcinoma, stratified based on gender, disease stages, pathological grade, tumor status, and TP53 mutation (UALCAN). (a, g) Boxplot showing relative expression of DHX37 in normal and LIHC or LUAD samples. (b, h) Boxplot showing relative expression of DHX37 in normal individuals and LIHC or LUAD patients in stages 1, 2, 3, or 4. (c, i) Boxplot showing relative expression of DHX37 in normal individuals of either gender and male or female LIHC and LUAD patients. (e, k) Boxplot showing relative expression of DHX37 in normal individuals and LIHC or LUAD patients with lymph node metastasis. (f, l) Boxplot showing relative expression of DHX37 in normal individuals and LIHC or LUAD patients with mutant TP53 or nonmutant TP53. (d) Boxplot showing relative expression of DHX37 in normal individuals or LIHC patients with grade 1, 2, 3, or 4 tumors. (j) Boxplot showing relative expression of DHX37 in normal individuals or LUAD patients with or without smoking habits. * $P < 0.05$, ** $P < 0.01$, *** $P < 0.001$, and **** $P < 0.0001$.

analyze DHX37 coexpression genes by comparing LIHC and LUAD cohorts. We found that 3682 overlap genes were positively correlated with DHX37, whereas 2002 overlap genes were negatively correlated (Table S4). This result suggests an extensive influence of DHX37 on the transcriptome. A heat map (Figures 4(a) and 4(b)) provides details about the top 50 significant (positively and negatively correlated) genes with DHX37. DHX37 expression had a strong positive association with expression of DDX54, GCN1L1, and PUS1, which reflect changes in mRNA modifications, transcriptional regulation, and DNA repair [29–31]. In line with the fact that DHX37 suppresses the immune system by modulating NF- κ B, DHX37 expression is positively correlated with the expression of PDCD11, which is known as the NF- κ B binding protein (Figure 4(a)). Notably, 43/50 and 18/50 genes in LIHC and LUAD, respectively, had high HR ($P < 0.05$) in the top 50 significantly positive genes. Instead, there were 12/50 and

13/50 genes with low HR ($P < 0.05$) in negatively significant ones (Figure 4(c)).

The functions of DHX37 were predicted by analyzing GO and KEGG by GSEA. The most highly enriched signaling pathway was determined by their normalized enrichment score (NES). As illustrated in Table 1 and Figure S3B, the biological processes, cellular components, and molecular functions strongly associated with DHX37 were cell cycle regulation, DNA replication, mRNA processing, and respiratory activity. Interestingly, GO analysis also uncovered that MHC (major histocompatibility complex), which plays a crucial role in antigen presenting in cancers, was one of the negatively correlated categories. KEGG analysis defined enrichment in DNA replication, cell cycle, ribosome biogenesis in eukaryotes, homologous recombination, Fanconi anemia pathway, notch signaling pathway, and microRNAs in cancers, while the activities like fatty acid degradation, drug metabolism, metabolism of

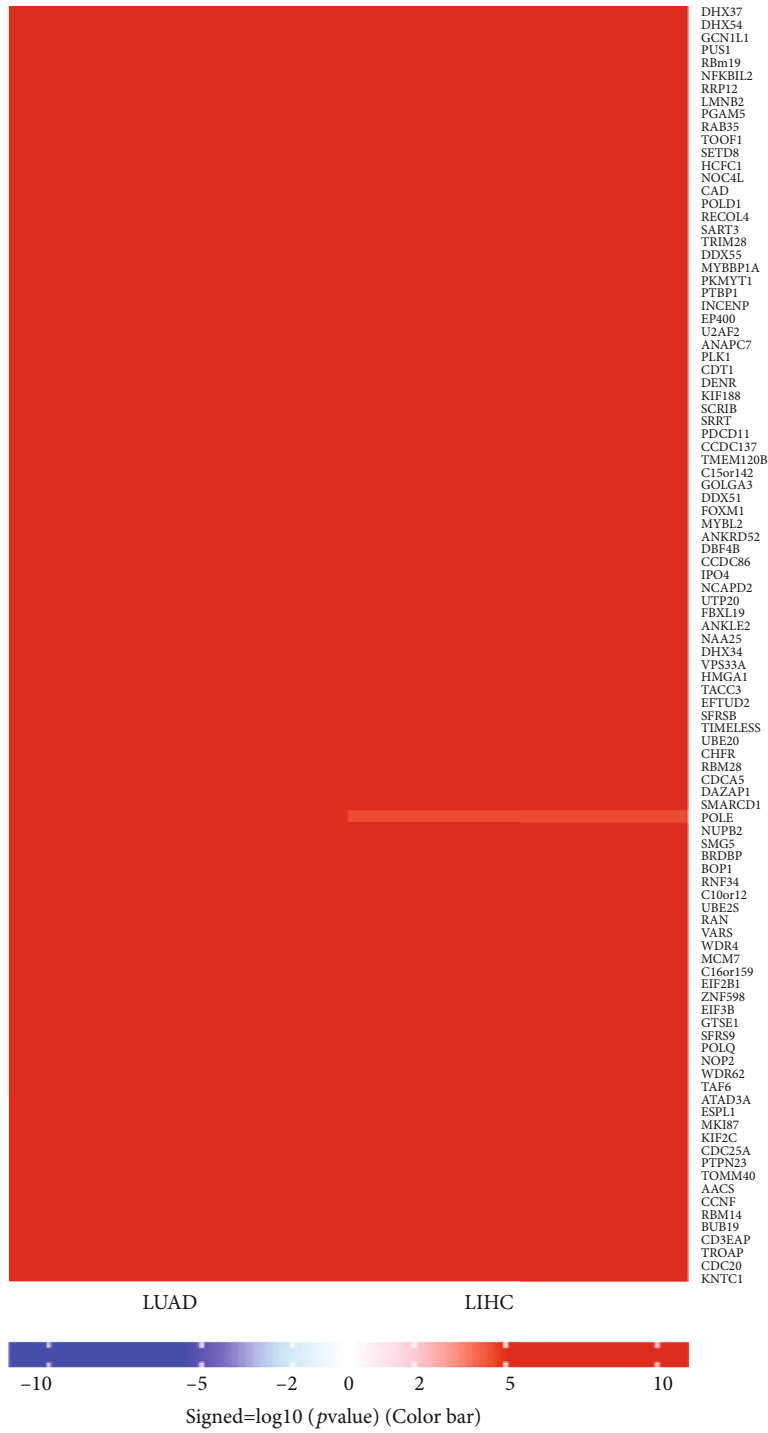


FIGURE 4: Continued.

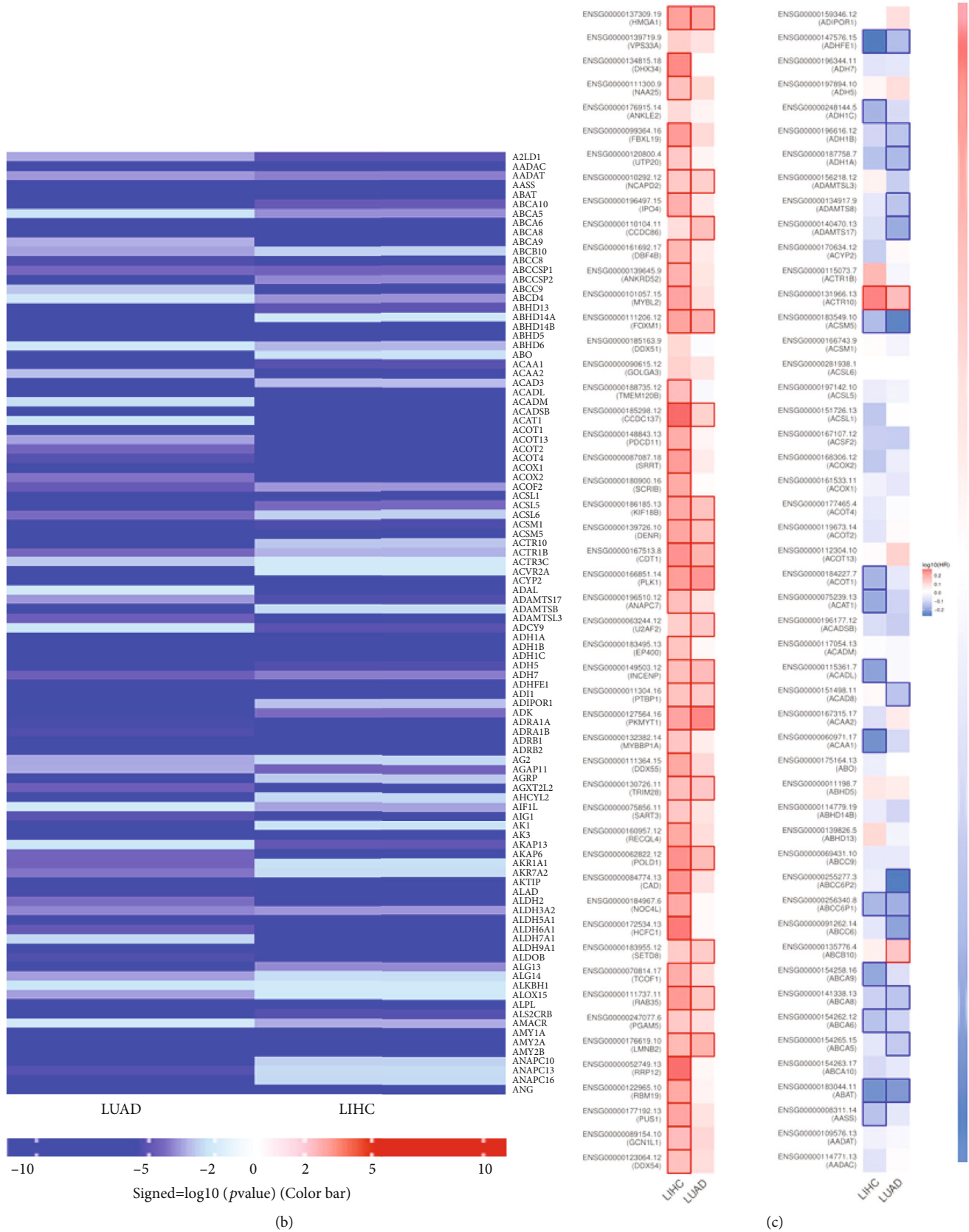


FIGURE 4: DHX37 coexpression genes in LIHC and LUAD (LinkedOmics). (a, b) Heat maps showing top 50 genes positively and negatively correlated with DHX37. (c) Survival map of the top 50 genes positively and negatively correlated with DHX37 in LIHC and LUAD.

TABLE 1: Signaling pathways most significantly correlated with DHX37 expression based on their normalized enrichment score (NES) and *P* value.

	GO name (BP)	NES	<i>P</i> value	FDR
Positive	Protein localization to chromosome	1.672	≤0.001	0.008
	CENP-A containing chromatin organization	1.665	≤0.001	0.004
	rRNA metabolic process	1.640	≤0.001	0.006
	Chromosome localization	1.635	≤0.001	0.005
	Chromosome segregation	1.634	≤0.001	0.004
	DNA replication	1.627	≤0.001	0.004
	Peroxisome organization	-1.916	≤0.001	0.107
Negative	Benzene-containing compound metabolic process	-1.809	≤0.001	0.137
	Peroxisomal transport	-1.729	≤0.001	0.151
	Mitochondrial respiratory chain complex assembly	-1.721	≤0.001	0.119
	GO name (CC)	NES	<i>P</i> value	FDR
Positive	Preribosome	2.404	≤0.001	0.000
	Condensed chromosome	2.309	≤0.001	0.000
	Replication fork	2.209	≤0.001	0.000
	Chromosomal region	2.173	≤0.001	0.000
	Heterochromatin	2.162	≤0.001	0.000
	NADH dehydrogenase complex	-2.478	≤0.001	0.000
	MHC protein complex	-2.371	≤0.001	0.000
Negative	Respiratory chain	-2.251	≤0.001	0.000
	Platelet dense granule	-2.212	≤0.001	0.000
	Basal part of cell	-2.042	≤0.001	0.007
	GO name (MF)	NES	<i>P</i> value	FDR
Positive	snoRNA binding	2.247	≤0.001	0.000
	tRNA binding	2.233	≤0.001	0.000
	Helicase activity	2.204	≤0.001	0.000
	Catalytic activity, acting on DNA	2.161	≤0.001	0.000
	Methyl-CpG binding	2.038	≤0.001	0.000
	Monooxygenase activity	-2.317	≤0.001	0.009
	Oxidoreductase activity, acting on NAD(P)H	-2.104	≤0.001	0.009
Negative	Steroid dehydrogenase activity	-2.089	≤0.001	0.006
	Tetrapyrrole binding	-2.075	≤0.001	0.005
	Oxidoreductase activity, acting on peroxide as acceptor	-2.051	≤0.001	0.009

xenobiotics by cytochrome, chemical carcinogenesis, complement and coagulation cascades, and activity of amino acid including histidine, arginine, and tyrosine were inhibited (Figure S3A). These results reveal that the functions involving cell cycle modulation, amino acid metabolism, and immune activity were highly correlated with DHX37 expression.

3.5. Regulators of DHX37 in LIHC and LUAD. To delve further into the regulators of DHX37 in LIHC and LUAD, we analyzed the kinase, miRNA, and transcription factor derived from positively correlated gene sets. The top 5 most important target networks were the kinase-target ones related mainly to the polo-like kinase 1, checkpoint kinase 2, cyclin dependent kinase 2, ATR serine/threonine kinase, and cyclin dependent kinase 1 (Table 2). The miRNA-target network was associated with (TCCGTCC) MIR-184, (TGCACGA)

MIR-517, (GTGGTGA) MIR-197, (CCAGGGG) MIR-331, and (CAGCAGG) MIR-370. The transcription factor-target network was related primarily to the E2F Transcription Factor family, including E2F1DP2_01, E2F1_Q6, E2F1DP1_01, E2F1DP2_01, and E2F4DP2_01. The gene set enriched for kinase is responsible mainly for regulating stability and integrity of the genome.

3.6. DHX37 Expression Impacts Immune Infiltration Level. DHX37 is expressed in immune cells and TILs (tumor infiltrating lymphocytes). These cells serve as independent prognostic factors of clinicopathological parameters and outcome in cancers [32]. Hence, we analyzed the correlation between DHX37 expression and immunophenotypic characteristics in Pan-Cancer from TIMER and TISIDB (tumor and immune system interaction). The comprehensive analysis indicated that the DHX37 expression had significant

TABLE 2: The kinase, miRNA, and transcription factor-target networks of DHX37 in LIHC and LUAD (LinkedOmics).

Enriched category	Gene set	LeadingEdgeNum	FDR
Kinase target	Polo-like kinase 1	45	0.000
	Checkpoint kinase 2	17	0.000
	Cyclin dependent kinase 2	139	0.000
	ATR serine/threonine kinase	42	0.000
	Cyclin dependent kinase 1	108	0.000
miRNA target	TCCGTCC, MIR-184	4	0.164
	TGCACGA, MIR-517A/C	13	0.097
	GTGGTGA, MIR-197	34	0.104
	CCAGGGG, MIR-331	32	0.080
	CAGCAGG, MIR-370	51	0.078
Transcription factor target	SGCGSSAAA_V\$E2F1DP2_01	74	0.000
	V\$E2F1_Q6	95	0.000
	V\$E2F1DP1_01	95	0.000
	V\$E2F1DP2_01	95	0.000
	V\$E2F4DP2_01	95	0.000

LeadingEdgeNum: the number of leading-edge genes; FDR: false discovery rate from Benjamini and Hochberg from gene set enrichment analysis (GSEA); VS: the annotation found in the Molecular Signatures Database for transcription factors.

correlations with tumor purity in 16 types of cancers. Moreover, DHX37 expression also significantly correlated with CD8 T cells, CD4 T cells, B cells, macrophages, neutrophils, and dendritic cells (DCs) in 16, 19, 12, 18, 16, and 14 types of cancer, respectively (Table S3 and Figure S4). Furthermore, we also found that DHX37 expression weakly to moderately negatively correlated with 28 types of TILs and MHC expression across all human heterogeneous cancers, except in KIRP (kidney renal papillary cell carcinoma), THCA (thyroid carcinoma), and LGG (brain lower grade glioma) (Figures 5(a) and 5(b)).

On the basis of the findings in immune infiltration landscapes, we further found that DHX37 expression level correlates with poorer clinical outcomes and specific immune cell infiltration in LIHC and LUAD (Figures 5(c) and 5(d)). The DHX37 expression level has significant positive correlations with infiltrating levels of CD8 T cells ($r=0.177$, $P=9.98e-04$), CD4T cells ($r=0.298$, $P=1.84e-08$), macrophages ($r=0.387$, $P=1.27e-13$), neutrophils ($r=0.349$, $P=2.46e-11$), B cells ($r=0.364$, $P=3.37e-12$), and DCs (dendritic cells) ($r=0.335$, $P=2.44e-10$) in LIHC. In LUAD, except for CD8 T cells ($r=-0.096$, $P=3.41e-02$), DHX37 expression positively correlated with infiltration levels of CD4 T cells ($r=0.126$, $P=5.46e-03$) and neutrophils ($r=0.097$, $P=3.33e-02$). Although DHX37 expression has no significant correlations with tumor purity in both LIHC ($r=0.032$, $P=5.57e-01$) and LUAD ($r=0.021$, $P=5.44e-01$), these findings strongly suggest that DHX37 may participate in immune response to affect patient survival in cancers like LIHC and LUAD.

3.7. Correlation Analysis between DHX37 Expression and Immune Markers. To broaden our understanding of DHX37 crosstalk with immune signatures, we assessed the correlations between DHX37 expression and immune

marker genes of CD8+ T cells, T cells (general), B cells, monocytes, tumor associated macrophages (TAMs), M1 and M2 macrophages, neutrophils, NK cells, myeloid-derived suppressor cells (MDSCs), cancer-associated fibroblasts (CAFs), and DCs in LIHC and LUAD (Table 3). We also analyzed the different functional T cells, including Th1 cells, Th2 cells, T_{regs} , and exhausted T cells. In TIMER, after adjustments for tumor purity, the DHX37 expression level was significantly correlated with 59 out of 72 immune cell markers in LIHC and 38 out of 72 in LUAD. In LIHC, B cells, macrophages, and various types of T cells were strongly correlated with DHX37 expression (Table 3) and less significant in LUAD. Moreover, we found that expression of DHX37 positively correlates with markers of CAFs including ACTA2 ($r=0.13$, $P=0.0098$), FAP ($r=0.32$, $P=4.5e-10$), PDGFR ($r=0.22$, $P=1.5e-05$), and S100A4 ($r=0.21$, $P=3.4e-05$) in LIHC.

The expression levels of most marker set of T_{regs} and exhausted T cells, such as forkhead box P3 (FOXP3), C-C chemokine receptor type 8 (CCR8), signal transducer and activator of transcription 5B (STAT5B), PD-1, CTLA4, and LAG3, have strong positive correlations with DHX37 expression in LIHC and LUAD (Figure 6). FOXP3 regulates the immune suppression and is a strong prognostic factor for distant metastases [33]. PD-1, a widely known marker related to T lymphocyte function, showed strong positive correlation with DHX37 expression, indicating that high DHX37 expression itself may be a novel predictor for immunotherapy response. In addition, DHX37 expression showed strong negative correlations with complement and strong positive correlations with markers of myeloid-derived suppressor cells. We further evaluated the correlation between DHX37 expression and the above strong significant markers in GEPIA (Table 3). Correlation results between DHX37 and the above markers are similar to this in TIMER. These findings

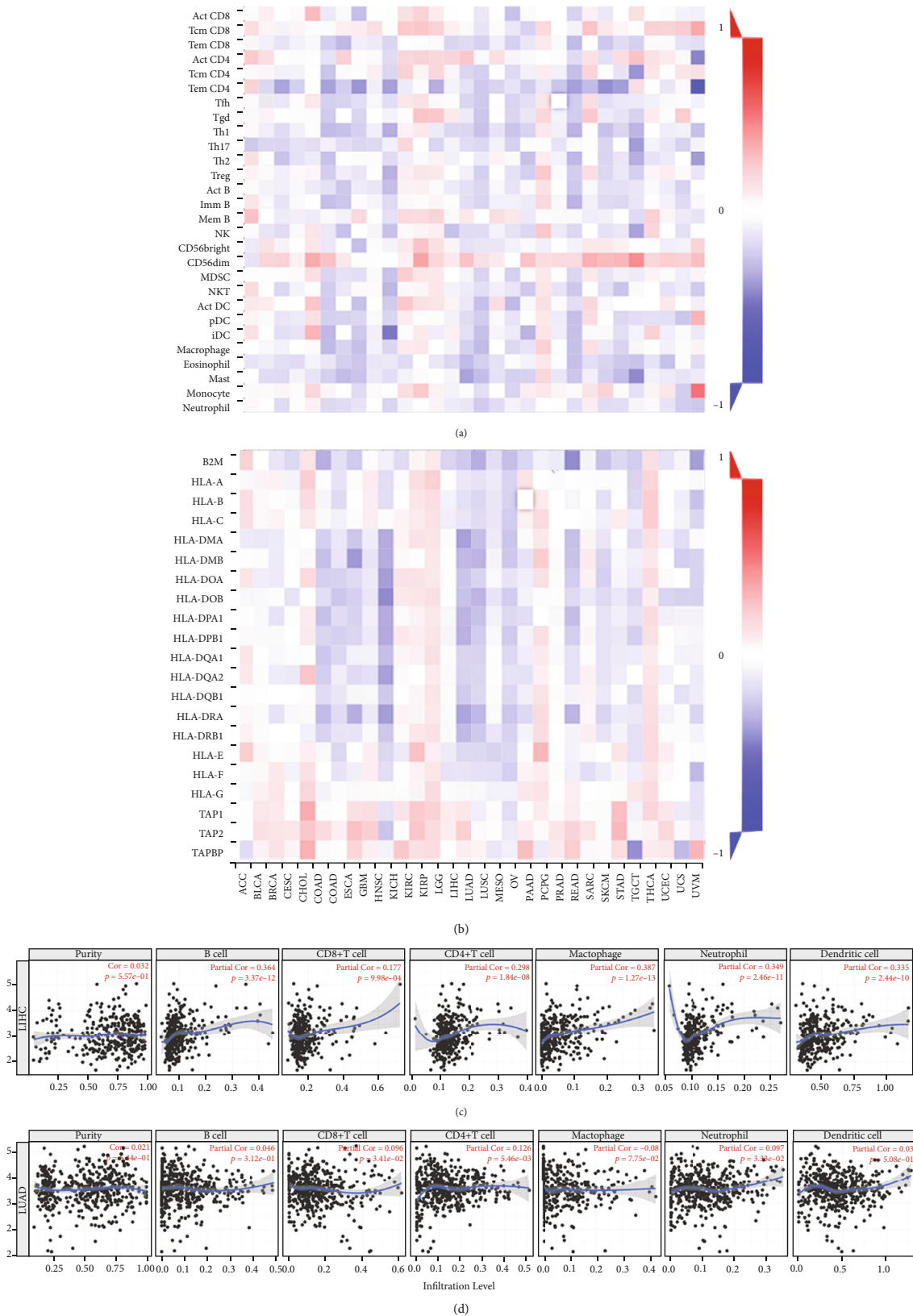


FIGURE 5: Correlations between DHX37 expression and TILs across human cancers. (a, b) Heat map showing relations between expression of DHX37 and 28 types of TILs as well as 21 types of MHC molecules. (c) DHX37 expression level has significant positive correlations with infiltrating levels of CD8+ T cells, CD4+ T cells, macrophages, neutrophils, B cells, and DCs in LIHC. (d) DHX37 expression level has significant positive correlations with infiltrating levels of CD4+ T cells and neutrophils and negative correlations with CD8+ T cells in LUAD. $P < 0.05$ is considered significant.

TABLE 3: Correlation analysis between DHX37 and related genes and markers of immune cells in TIMER.

	Markers	LIHC				LUAD			
		None		Purity		None		Purity	
		Cor	P	Cor	P	Cor	P	Cor	P
CD8+ T cell	CD8A	0.138	**	0.173	**	0.063	0.160	0.081	0.074
	CD8B	0.140	**	0.169	**	0.056	0.212	0.068	0.133
	CD3D	0.263	****	0.310	****	-0.067	0.140	-0.065	0.148
T cell (general)	CD3E	0.174	**	0.231	****	-0.020	0.658	-0.010	0.817
	CD2	0.176	**	0.225	****	-0.058	0.199	-0.055	0.222
B cell	CD19	0.177	***	0.199	***	0.025	0.576	0.041	0.366
	CD79A	0.090	0.096	0.120	*	-0.010	0.821	-0.001	0.986
Monocyte	CD86	0.314	****	0.386	****	-0.041	0.358	-0.036	0.427
	CSF1R	0.256	****	0.322	****	0.034	0.449	0.046	0.307
TAM	CCL2	0.078	0.145	0.112	*	-0.009	0.845	-0.002	0.965
	CD68	0.291	****	0.340	****	0.075	0.097	0.088	0.051
	IL10	0.256	****	0.307	****	-0.029	0.527	-0.022	0.629
M1 macrophage	NOS2	-0.071	0.186	-0.069	0.202	0.173	***	0.183	****
	IRF5	0.393	****	0.393	****	0.124	**	0.139	**
	PTGS2	0.111	*	0.147	**	0.038	0.397	0.039	0.392
M2 macrophage	CD163	0.132	*	0.168	**	0.117	**	0.136	**
	VSIG4	0.162	**	0.203	***	-0.050	0.264	-0.046	0.308
	MS4A4A	0.140	**	0.182	***	-0.101	*	-0.102	*
Neutrophils	CEACAM8	0.044	0.414	0.048	0.377	-0.199	****	-0.198	****
	ITGAM	0.370	****	0.403	****	0.029	0.524	0.039	0.388
	CCR7	0.014	0.797	0.038	0.486	-0.082	0.070	-0.083	0.065
	KIR2DL1	-0.036	0.508	-0.034	0.524	0.065	0.150	0.069	0.127
	KIR2DL3	0.150	**	0.159	**	0.121	**	0.129	**
Natural killer cell	KIR2DL4	0.149	**	0.157	**	0.286	****	0.300	****
	KIR3DL1	0.050	0.357	0.053	0.324	0.057	0.205	0.062	0.166
	KIR3DL2	0.081	0.132	0.090	0.094	0.168	***	0.178	****
	KIR3DL3	0.024	0.652	0.026	0.631	0.119	**	0.120	**
	KIR2DS4	0.052	0.336	0.053	0.325	0.059	0.189	0.064	0.155
	HLA-DPB1	0.154	**	0.195	***	-0.247	****	-0.259	****
	HLA-DQB1	0.141	**	0.174	**	-0.168	***	-0.172	***
Dendritic cell	HLA-DRA	0.154	**	0.193	***	-0.299	****	-0.316	****
	HLA-DPA1	0.152	**	0.191	***	-0.234	****	-0.244	****
	CD1C	0.102	0.058	0.128	*	-0.384	****	-0.393	****
	NRP1	0.239	****	0.251	****	0.032	0.472	0.035	0.442
	ITGAX	0.377	****	0.442	****	0.138	**	0.164	***
	TBX21	0.073	0.176	0.096	0.074	0.090	*	0.112	*
	STAT4	0.165	**	0.180	***	-0.030	0.504	-0.023	0.608
Th1	STAT1	0.278	****	0.290	****	0.301	****	0.326	****
	IFNG	0.255	****	0.277	****	0.158	***	0.177	****
	TNF	0.276	****	0.322	****	0.058	0.199	0.072	0.109
Th2	GATA3	0.137	*	0.177	***	0.095	*	0.113	*
	STAT6	0.185	***	0.185	***	0.091	*	0.091	*

TABLE 3: Continued.

	Markers	LIHC				LUAD			
		None		Purity		None		Purity	
		Cor	P	Cor	P	Cor	P	Cor	P
Tfh	STAT5A	0.334	****	0.353	****	0.110	*	0.130	**
	IL13	-0.022	0.677	-0.022	0.683	0.011	0.804	0.016	0.724
	BCL6	0.209	****	0.209	****	0.078	0.084	0.079	0.081
Th17	STAT3	0.160	**	0.172	**	0.144	**	0.143	**
	IL17A	0.069	0.203	0.070	0.195	0.047	0.299	0.053	0.240
	FOXP3	0.057	0.295	0.065	0.226	0.152	***	0.184	****
T _{reg}	CCR8	0.253	****	0.278	****	0.098	*	0.117	**
	STAT5B	0.208	****	0.206	***	0.246	****	0.250	****
	TGFB1	0.335	****	0.381	****	0.040	0.373	0.049	0.277
T cell exhaustion	PDCD1	0.304	****	0.351	****	0.242	****	0.279	****
	CTLA4	0.310	****	0.355	****	0.101	*	0.129	**
	LAG3	0.220	****	0.234	****	0.221	****	0.247	****
Myeloid-derived suppressor cells	HAVCR2	0.337	****	0.411	****	-0.033	0.470	-0.026	0.566
	GZMB	0.085	0.113	0.103	0.057	0.275	****	0.308	****
	CD14	-0.435	****	-0.434	****	0.078	0.084	0.093	*
	CD86	0.314	****	0.386	****	-0.041	0.358	-0.036	0.427
	FERMT3	0.328	****	0.413	****	0.077	0.088	0.100	*
	GPSM3	0.316	****	0.408	****	-0.127	**	-0.127	***
	IL18BP	0.215	****	0.281	****	0.160	***	0.187	****
	ITGAM	0.370	****	0.403	****	0.029	0.524	0.039	0.388
	PSAP	0.417	****	0.439	****	0.109	*	0.114	*
	PTGES2	0.496	****	0.496	****	0.538	****	0.538	****
Complement	CFD	0.227	****	0.257	****	-0.181	****	-0.181	****
	MBL2	-0.230	****	-0.228	****	-0.037	0.413	-0.036	0.429
	C2	-0.140	**	-0.147	**	-0.013	0.774	-0.011	0.813
	C5	-0.148	**	-0.146	**	0.028	0.537	0.027	0.552
	C8G	-0.309	****	-0.307	****	0.244	****	0.244	****
	MASP2	-0.424	****	-0.424	****	0.067	0.135	0.069	0.124
	C3	-0.425	****	-0.426	****	-0.202	****	-0.202	****
C1S	-0.362	****	-0.361	****	0.039	0.388	0.055	0.225	

* $P < 0.05$, ** $P < 0.01$, *** $P < 0.001$, and **** $P < 0.0001$.

further confirm that DHX37 plays a vital role in cancer immune escape.

4. Discussion

DHX37, a member of the DEAH box family of RNA helicases [34], plays indispensable roles in many aspects of gene expression [35]. Differential expression and dysfunction of RNA helicases have been reported in various cancers [36–39]. Although DHX37 functions have not been extensively elucidated, it was once discovered that it suppressed T cell activation in breast cancer [19]. As elucidated in other research, LAYN was identified as a prognostic biomarker and is highly correlated with immune infiltrates in gastric

and colon cancers [40]. Therefore, it might reasonably be assumed that DHX37 expression may influence patients' clinical outcomes through immune infiltration. Here, we report that aberrant expression level of DHX37 correlated to prognosis in multiple cancers. Overexpression of DHX37 predicted higher rates of recurrence and shorter survival times in LIHC and LUAD. Interestingly, increased levels of DHX37 expression were related to advanced clinicopathological characteristics, indicating that DHX37 can be used as a prognostic indicator of cancer stages and metastasis. In addition, this study found that in liver hepatocellular carcinoma and lung adenocarcinoma, immune infiltration levels and various immune marker sets were correlated with the level of DHX37 expression. Therefore, this study revealed

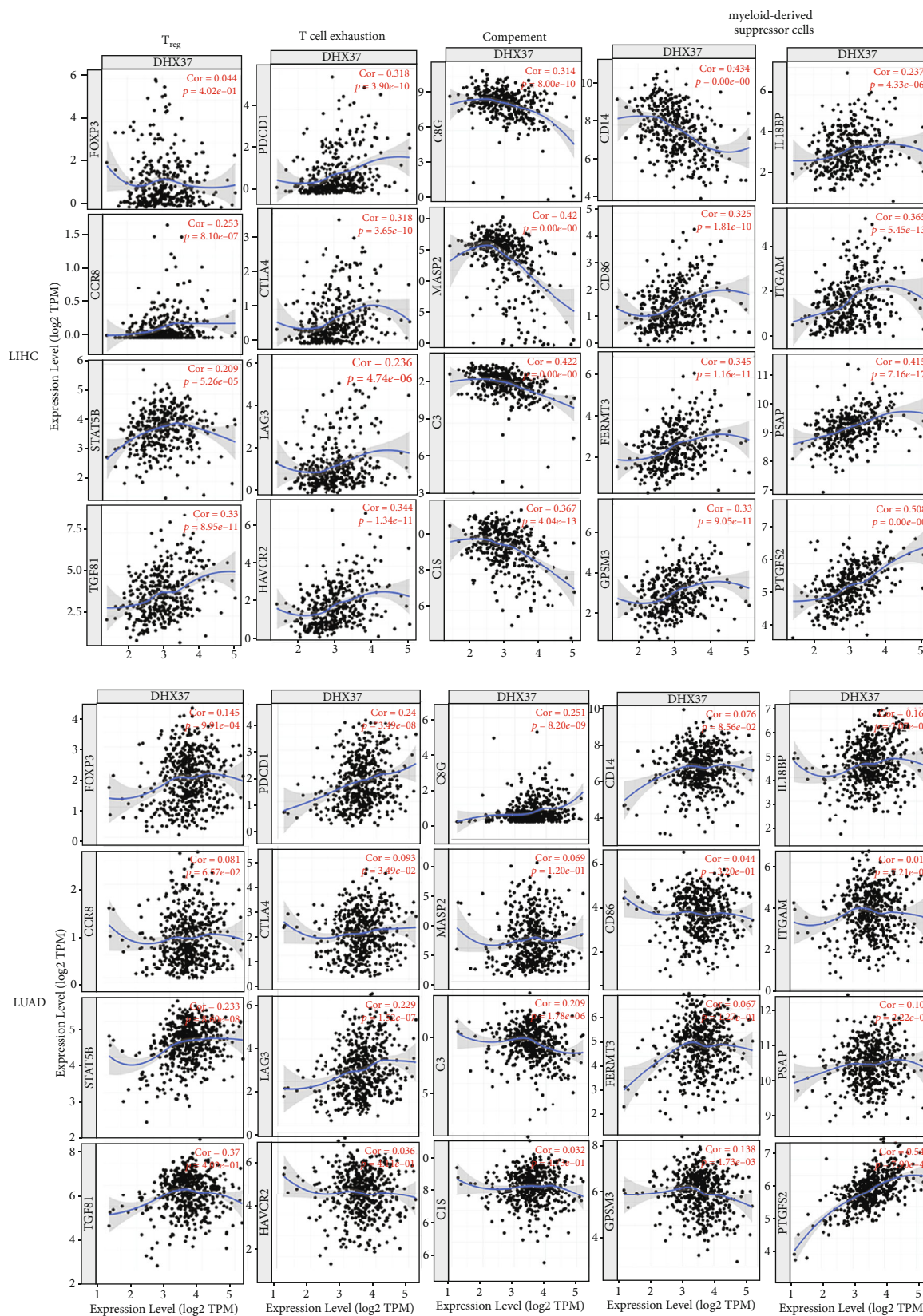


FIGURE 6: DHX37 expression correlates with T_{reg}, T cell exhaustion, complement, and myeloid-derived suppressor cells in LIHC and LUAD. Markers include FOXP3, CCR8, STAT5B and TGFB1 of T_{reg}, PDCD1, CTLA4, LAG3 of T cell exhaustion, CD14, CD86, FERMT3, GPSM3, IL18BP, ITGAM, PSAP and PTGES2 of myeloid-derived suppressor cells, C8G, MASP2, C3, and C1S of complement. $P < 0.05$ is considered significant.

TABLE 4: Correlation between DHX37 and gene markers of complement, T_{regs}, T cell exhaustion, and myeloid-derived suppressor cells.

Cell type	Gene marker	LIHC				LUAD			
		Tumor		Normal		Tumor		Normal	
		R	P	R	P	R	P	R	P
Complement	CFD	0.088	0.093	0.48	***	-0.095	*	0.044	0.74
	C2	-0.15	**	0.32	*	-0.069	0.13	0.29	*
	C5	-0.067	0.2	0.28	0.052	0.061	0.18	0.23	0.076
	C8G	-0.28	****	0.21	0.14	0.17	***	0.12	0.38
	MASP2	-0.35	****	0.079	0.59	0.12	**	0.41	**
	C4B	-0.24	****	-0.017	0.91	-0.11	*	0.25	0.056
	C3	-0.4	****	-0.31	*	-0.16	***	0.17	0.2
	C1S	-0.25	****	0.36	*	0.042	0.36	0.31	*
T _{reg}	FOXP3	-0.017	0.75	0.27	0.055	0.12	*	0.4	**
	CCR8	0.21	****	0.31	*	0.12	**	0.22	0.088
	STAT5B	0.23	****	0.69	****	0.32	****	0.59	****
	TGFB1	0.34	****	0.61	****	0.093	*	0.64	****
T cell exhaustion	PDCD1	0.18	***	0.42	**	0.26	****	0.32	*
	CTLA4	0.21	****	0.3	*	0.16	***	0.26	*
	LAG3	0.21	****	0.2	0.17	0.19	****	0.23	0.084
	HAVCR2	0.24	****	0.43	**	0.017	0.71	-0.039	0.77
	GZMB	0.15	**	0.49	***	0.25	****	-0.069	0.6
	CD14	-0.28	****	0.24	0.094	0.11	*	-0.081	0.54
	CD86	0.38	****	0.46	***	0.0043	0.93	-0.066	0.62
Myeloid-derived suppressor cells	FERMT3	0.3	****	0.45	**	0.065	0.15	0.28	*
	GPSM3	0.27	****	0.48	***	-0.098	*	0.36	**
	IL18BP	0.17	**	0.57	****	0.2	****	0.042	0.75
	ITGAM	0.33	****	0.63	****	0.12	*	0.44	***
	PSAP	0.46	****	0.62	****	0.22	****	0.22	0.1
	PTGES2	0.46	****	0.67	****	0.49	****	0.59	****
	ACTA2	0.13	**	0.51	****	0.007	0.88	0.058	0.66
CAFs	FAP	0.32	****	0.45	***	0.038	0.41	0.22	0.1
	PDGFR	0.22	****	0.52	****	0.087	0.055	0.37	**
	S100A4	0.21	****	0.35	*	-0.15	***	-0.33	*

* $P < 0.05$, ** $P < 0.01$, *** $P < 0.001$, **** $P < 0.0001$.

the potential usage of DHX37 expression as a novel predictive biomarker.

Notably, DHX37 expression is related to various immune infiltration levels in cancers, especially in liver cancer and lung adenocarcinoma (Tables 3 and 4 and Figures 5 and 6). Surprisingly, the expression level of DHX37 in LIHC and LUAD is not correlated with tumor purity, indicating that the expression of DHX37 in cancer cells and the tumor microenvironment is equally important. Our results suggest that there is weak to moderate positive correlations between DHX37 expression and infiltration levels of CD4⁺ T cells and neutrophils in LIHC and LUAD (Figures 5 and 6). Moreover, gene markers of T_{regs}, T cell exhaustion, and MDSCs (myeloid-derived suppressor cells) showed significantly

strong positive correlation with DHX37 expression, which gives clues about DHX37 function in modulating tumor immunology in LIHC and LUAD. Furthermore, significantly negative correlations can be found between DHX37 expression and several markers of complement. Immunotherapy based on checkpoint inhibitors yields significant clinical benefit for multiple cancers. However, PD-1 inhibition meets resistance partially resulting from the accumulation of MDSCs [41] or T_{regs} [42]. MDSCs, comprising macrophages, granulocytes, dendritic cells, and immature myeloid cells [43], were initially identified leading to tumor persistence and metastasis [44]. A set of microRNAs was associated with MDSCs and resistance to immunotherapy [45], which was consistent with our results that show expression of DHX37

induces microRNA in cancer (Figure S3A). C3 is an important component of the complement system [46]. Recent studies find that the complement activates and functions within cells [47], and that this takes effect in the induction of key metabolic pathways [48] and the regulation of cell death. Whether the complement fights cancer [49] or promotes the development of cancer [50] or both is yet undetermined raising the possibility that the function of complement depends on the type of cancer. A recent study [51] showed that C3d induced the antitumor immunological effect by increasing infiltrating CD8+ T cells, by decreasing T_{regs} and by suppressing expression of PD-1. Interestingly, other complement components, like anaphylatoxin C5a, contributed to cancer progression by promoting an immunosuppressive microenvironment in which MDSCs are involved [52, 53]. After adjustment for tumor purity, DHX37 in LIHC and LUAD showed negative correlations with C3 and other complement regulators but not significantly correlated with C5. Our results substantiate that DHX37 overexpression has far-reaching effects in the immune response and complement systems in cancers, which may ultimately affect patient clinical outcomes.

To probe regulators potentially responsible for DHX37, we performed enrichment analyses of target gene sets, which illustrated that DHX37 participated primarily in the spliceosome, ribosome, DNA replication, and cell cycle (Table 2). The aberrant expression of cell cycle regulatory factors in tumor cells leads to rapid multiplication and decreased apoptosis. The E2F family, always related to the progression of liver cancer [54], served as the main transcription factors for DHX37 dysregulation. In research into cancer biology and molecular pathways, we also found DHX37 expression was correlated with metabolic changes including inhibiting fatty acid degradation, amino acid (arginine, histidine valine, leucine, and isoleucine), metabolism, and mitochondrial function. These findings were in line with the molecular pathways illustrated in liver cancer oncogenes [55]. In addition, DHX37 is positively correlated with notch signaling that regulates cell proliferation, differentiation, and survival [56]. The notch pathway is an important target for many types of solid cancers [57]. The functional effects of DHX37 on cancer cell proliferation and survival of liver cancer and lung adenocarcinoma are probably partially modulated by notch signaling. Future studies may develop compounds targeting DHX37 for precision medicine in cancers.

However, even though we utilized online tools based on widely used bioinformatic theories from public databases, this study still had one major limitation. We only performed a bioinformatic analysis of DHX37 expression without further confirmation using *in vivo/in vitro* experiments. Future prospective studies focusing on these aspects in a comprehensive manner could help identify the function of DHX37 in cancers.

In conclusion, DHX37 can impact cancer prognosis by not only playing direct regulatory roles in cancer cells but also affecting the immune microenvironment. Based on multilevel evidence, DHX37 plays an oncogenic role and induces a suppressive tumor microenvironment in LIHC

and LUAD. These findings for the first time offer evidence that DHX37 serves as an immunobased potential therapeutic target for cancer treatment.

Abbreviations

OS:	Overall survival
DFS:	Disease-free survival
RFS:	Relapse-free survival
HR:	Hazard ratio
MDSCs:	Myeloid-derived suppressor cells
TCGA:	The Cancer Genome Atlas
TIMER:	Tumor Immune Estimation Resource
GEPIA:	Gene Expression Profiling Interactive Analysis
TISIDB:	Tumor and immune system interaction
GO:	Gene Ontology
CC:	Cellular component
BP:	Biological process
MF:	Molecular function
KEGG:	Kyoto Encyclopedia of Genes and Genomes
GSEA:	Gene set enrichment analysis
FDR:	False discovery rate
ACC:	Adrenocortical carcinoma
BLCA:	Bladder urothelial carcinoma
BRCA:	Breast invasive carcinoma
CESC:	Cervical squamous cell carcinoma
CHOL:	Cholangiocarcinoma
COAD:	Colon adenocarcinoma
ESCA:	Esophageal carcinoma
GBM:	Glioblastoma multiforme
HNSC:	Head and neck squamous cell carcinoma
KICH:	Kidney chromophobe
KIRC:	Kidney renal clear cell carcinoma
KIRP:	Kidney renal papillary cell carcinoma
AML:	Acute myeloid leukemia
LGG:	Brain lower grade glioma
LIHC:	Liver hepatocellular carcinoma
LUAD:	Lung adenocarcinoma
LUSC:	Lung squamous cell carcinoma
MESO:	Mesothelioma
OV:	Ovarian serous cystadenocarcinoma
PAAD:	Pancreatic adenocarcinoma
PCPG:	Pheochromocytoma and paraganglioma
PRAD:	Prostate adenocarcinoma
READ:	Rectum adenocarcinoma
SARC:	Sarcoma
SKCM:	Skin cutaneous melanoma
STAD:	Stomach adenocarcinoma
STES:	Stomach and esophageal carcinoma
THCA:	Thyroid carcinoma
THYM:	Thymoma
UCEC:	Uterine corpus endometrial carcinoma
UCS:	Uterine carcinosarcoma.

Data Availability

The datasets analyzed for this study can be found in the OncoPrint, PrognoScan, GEPIA, Kaplan-Meier Plotter,

UALCAN, TIMER, TISIDB, and LinkedOmics web resources.

Conflicts of Interest

The authors declare that they have no conflicts of interest.

Authors' Contributions

PS and BL designed the project and wrote and revised the manuscript. YX and QJ completed most of the data and analysis; XX, HL, XG, and DY participated in the data preparation and analysis. All authors have read and approved the final manuscript. Yanni Xu and Qionghao Jiang contributed equally to this work.

Acknowledgments

This study was supported by the National Natural Science Foundation of China (81701715, 81873899), the Natural Science Foundation of Guangdong Province (2017A030310200, 2018A030313097), and the People's Livelihood and Technology Planning Project of Guangzhou City of China (201803010035).

Supplementary Materials

Per the publisher's request, the details of the supplementary materials are added here. However, the editable version of each table and figure is given in a separate folder, as requested. Table S1: DHX37 expression in cancers versus normal tissue in the Oncomine database. The DHX37 expression was elevated in breast, colorectal, gastric, kidney, lung cancers as well as lymphoma, whereas DHX37 was only observed significantly reduced in the sarcoma dataset. Table S2: relationship between DHX37 expression and patient prognosis of different cancers in the Prognoscan database. Table S3: DHX37 cooccurrence genes shown in the PDF file. We found that 3682 overlap genes were positively correlated with DHX37, whereas 2002 overlap genes were negatively correlated. Table S4: summarization of correlation between DHX37 expression and immune infiltration level in diverse type cancers via the TIMER database. N: not significantly; * $P < 0.05$, ** $P < 0.01$, *** $P < 0.001$, and **** $P < 0.0001$. DHX37 expression showed significantly correlated with CD8 T cells, CD4 T cells, B cells, macrophages, neutrophils, and dendritic cells in 16, 19, 12, 18, 16, and 14 types of cancer, respectively. Figure S1: correlation of DHX37 expression with diverse types of cancer via Kaplan-Meier Plot. For esophageal adenocarcinoma, DHX37 was found to have a favorable effect on relapse-free survival while worsening overall survival. For head and neck squamous cell carcinoma, DHX37 expression has less influence. For thyroid carcinoma, rectum adenocarcinoma, stomach adenocarcinoma, and uterine corpus endometrial carcinoma, DHX37 plays a protective role in their OS but not RFS. DHX37 only had significant correlation with RFS for pancreatic ductal adenocarcinoma and ovarian cancer. Figure S2: correlation of DHX37 expression with diverse types

of cancer via GEPIA. Overall survival and disease-free survival comparing the high and low expression of DHX37 in various cancers. DHX37 overexpression was related to worsening outcome of OS and DFS in ACC, LGG, and LIHC; OS in LUAD, MESO, and THCA; and DFS in SKCM. These results validated the predictive value of DHX37 in particular types of cancer, such as LIHC and LUAD. Figure S3: KEGG pathways and GO of DHX37 in the LIHC and LUAD cohort. These results reveal that the functions involving cell cycle modulation, amino acid metabolism, and immune activity were highly correlated with DHX37 expression. Figure S4: correlation of the DHX37 expression with immune infiltration level in various cancers via the TIMER database. Diverse type of cancers via the TIMER database. DHX37 expression was shown as significantly correlated with CD8 T cells, CD4 T cells, B cells, macrophages, neutrophils, and dendritic cells in 16, 19, 12, 18, 16, and 14 types of cancer, respectively. (*Supplementary Materials*)

References

- [1] D. Zeng, R. Zhou, Y. Yu et al., "Gene expression profiles for a prognostic immunoscore in gastric cancer," *The British Journal of Surgery*, vol. 105, no. 10, pp. 1338–1348, 2018.
- [2] Y. Jiang, Q. Zhang, Y. Hu et al., "Immunoscore signature: a prognostic and predictive tool in gastric cancer," *Annals of Surgery*, vol. 267, no. 3, pp. 504–513, 2018.
- [3] S. L. Topalian, C. G. Drake, and D. M. Pardoll, "Immune checkpoint blockade: a common denominator approach to cancer therapy," *Cancer Cell*, vol. 27, no. 4, pp. 450–461, 2015.
- [4] B. Huang, H. Zhang, L. Gu et al., "Advances in immunotherapy for glioblastoma multiforme," *Journal of Immunology Research*, vol. 2017, Article ID 3597613, 11 pages, 2017.
- [5] G. Bindea, B. Mlecnik, M. Tosolini et al., "Spatiotemporal dynamics of intratumoral immune cells reveal the immune landscape in human cancer," *Immunity*, vol. 39, no. 4, pp. 782–795, 2013.
- [6] J. Liu, M. Xu, and Z. Yuan, "Immunoscore guided cold tumors to acquire "temperature" through integrating physicochemical and biological methods," *BIO Integration*, vol. 1, no. 1, pp. 6–14, 2020.
- [7] S. Bayraktar, S. Batoo, S. Okuno, and S. Gluck, "Immunotherapy in breast cancer," *Journal of Carcinogenesis*, vol. 18, no. 1, p. 2, 2019.
- [8] T. W. Hulett, B. A. Fox, D. J. Messenheimer et al., "Future research goals in immunotherapy," *Surgical Oncology Clinics of North America*, vol. 28, no. 3, pp. 505–518, 2019.
- [9] D. F. Quail and J. A. Joyce, "Microenvironmental regulation of tumor progression and metastasis," *Nature Medicine*, vol. 19, no. 11, pp. 1423–1437, 2013.
- [10] S. Ahmad and S. Hur, "Helicases in antiviral immunity: dual properties as sensors and effectors," *Trends in Biochemical Sciences*, vol. 40, no. 10, pp. 576–585, 2015.
- [11] H. Kato and T. Fujita, "RIG-I-like receptors and autoimmune diseases," *Current Opinion in Immunology*, vol. 37, pp. 40–45, 2015.
- [12] M. M. Rahman, E. Bagdassarian, M. A. M. Ali, and G. McFadden, "Identification of host DEAD-box RNA helicases that regulate cellular tropism of oncolytic myxoma virus

- in human cancer cells,” *Scientific Reports*, vol. 7, no. 1, pp. 1–14, 2017.
- [13] M. Lewinsohn, A. L. Brown, L. M. Weinel et al., “Novel germ line DDX41 mutations define families with a lower age of MDS/AML onset and lymphoid malignancies,” *Blood*, vol. 127, no. 8, pp. 1017–1023, 2016.
- [14] T. Lee and J. Pelletier, “The biology of DHX9 and its potential as a therapeutic target,” *Oncotarget*, vol. 7, no. 27, pp. 42716–42739, 2016.
- [15] F. Raza, J. A. Waldron, and J. L. Quesne, “Translational dysregulation in cancer: eIF4A isoforms and sequence determinants of eIF4A dependence,” *Biochemical Society Transactions*, vol. 43, no. 6, pp. 1227–1233, 2015.
- [16] S. Ozgur, G. Buchwald, S. Falk, S. Chakrabarti, J. R. Prabu, and E. Conti, “The conformational plasticity of eukaryotic RNA-dependent ATPases,” *The FEBS Journal*, vol. 282, no. 5, pp. 850–863, 2015.
- [17] A. Roychowdhury, C. Joret, G. Bourgeois, V. Heurgue-Hamard, D. L. J. Lafontaine, and M. Graille, “The DEAH-box RNA helicase Dhr1 contains a remarkable carboxyl terminal domain essential for small ribosomal subunit biogenesis,” *Nucleic Acids Research*, vol. 47, no. 14, pp. 7548–7563, 2019.
- [18] A. M. Anger, J. P. Armache, O. Berninghausen et al., “Structures of the human and Drosophila 80S ribosome,” *Nature*, vol. 497, no. 7447, pp. 80–85, 2013.
- [19] M. B. Dong, G. C. Wang, R. D. Chow et al., “Systematic immunotherapy target discovery using genome-scale in vivo CRISPR screens in CD8 T cells,” *Cell*, vol. 178, no. 5, pp. 1189–1204.e23, 2019.
- [20] D. R. Rhodes, S. Kalyana-Sundaram, V. Mahavisno et al., “OncoPrint 3.0: genes, pathways, and networks in a collection of 18,000 cancer gene expression profiles,” *Neoplasia*, vol. 9, no. 2, pp. 166–180, 2007.
- [21] H. Mizuno, K. Kitada, K. Nakai, and A. Sarai, “PrognoScan: a new database for meta-analysis of the prognostic value of genes,” *BMC Medical Genomics*, vol. 2, no. 1, p. 18, 2009.
- [22] A. Lániczky, A. Nagy, G. Bottai et al., “miRpower: a web-tool to validate survival-associated miRNAs utilizing expression data from 2178 breast cancer patients,” *Breast Cancer Research and Treatment*, vol. 160, no. 3, pp. 439–446, 2016.
- [23] D. S. Chandrashekar, B. Bashel, S. A. H. Balasubramanya et al., “UALCAN: a portal for facilitating tumor subgroup gene expression and survival analyses,” *Neoplasia*, vol. 19, no. 8, pp. 649–658, 2017.
- [24] Z. Tang, C. Li, B. Kang, G. Gao, C. Li, and Z. Zhang, “GEPIA: a web server for cancer and normal gene expression profiling and interactive analyses,” *Nucleic Acids Research*, vol. 45, no. W1, pp. W98–W102, 2017.
- [25] T. Li, J. Fan, B. Wang et al., “TIMER: a web server for comprehensive analysis of tumor-infiltrating immune cells,” *Cancer Research*, vol. 77, no. 21, pp. e108–e110, 2017.
- [26] B. Ru, C. N. Wong, Y. Tong et al., “TISIDB: an integrated repository portal for tumor-immune system interactions,” *Bioinformatics*, vol. 35, no. 20, pp. 4200–4202, 2019.
- [27] S. V. Vasaikar, P. Straub, J. Wang, and B. Zhang, “LinkedOmics: analyzing multi-omics data within and across 32 cancer types,” *Nucleic Acids Research*, vol. 46, no. D1, pp. D956–D963, 2018.
- [28] L. J. van ’t Veer, H. Dai, M. J. van de Vijver et al., “Gene expression profiling predicts clinical outcome of breast cancer,” *Nature*, vol. 415, no. 6871, pp. 530–536, 2002.
- [29] M. Milek, K. Imami, N. Mukherjee et al., “DDX54 regulates transcriptome dynamics during DNA damage response,” *Genome Research*, vol. 27, no. 8, pp. 1344–1359, 2017.
- [30] T. D. Cambiaghi, C. M. Pereira, R. Shanmugam et al., “Evolutionarily conserved IMPACT impairs various stress responses that require GCN1 for activating the eIF2 kinase GCN2,” *Biochemical and Biophysical Research Communications*, vol. 443, no. 2, pp. 592–597, 2014.
- [31] T. M. Carlile, N. M. Martinez, C. Schaening et al., “mRNA structure determines modification by pseudouridine synthase 1,” *Nature Chemical Biology*, vol. 15, no. 10, pp. 966–974, 2019.
- [32] K. Yoshihara, M. Shahmoradgoli, E. Martínez et al., “Inferring tumour purity and stromal and immune cell admixture from expression data,” *Nature Communications*, vol. 4, no. 1, 2013.
- [33] A. Facciabene, G. T. Motz, and G. Coukos, “T-regulatory cells: key players in tumor immune escape and angiogenesis,” *Cancer Research*, vol. 72, no. 9, pp. 2162–2171, 2012.
- [34] A. Colley, J. D. Beggs, D. Tollervey, and D. L. J. Lafontaine, “Dhr1p, a putative DEAH-box RNA helicase, is associated with the box C+D snoRNP U3,” *Molecular and Cellular Biology*, vol. 20, no. 19, pp. 7238–7246, 2000.
- [35] A. Luking, U. Stahl, and U. Schmidt, “The protein family of RNA helicases,” *Critical Reviews in Biochemistry and Molecular Biology*, vol. 33, pp. 259–296, 2008.
- [36] K. V. Rosinski, N. Fujii, J. K. Mito et al., “DDX3Y encodes a class I MHC-restricted H-Y antigen that is expressed in leukemic stem cells,” *Blood*, vol. 111, no. 9, pp. 4817–4826, 2008.
- [37] S. Lin, L. Tian, H. Shen et al., “DDX5 is a positive regulator of oncogenic NOTCH1 signaling in T cell acute lymphoblastic leukemia,” *Oncogene*, vol. 32, no. 40, pp. 4845–4853, 2013.
- [38] J. Tang, H. Chen, C. C. Wong et al., “DEAD-box helicase 27 promotes colorectal cancer growth and metastasis and predicts poor survival in CRC patients,” *Oncogene*, vol. 37, no. 22, pp. 3006–3021, 2018.
- [39] Y. Xue, X. Jia, C. Li et al., “DDX17 promotes hepatocellular carcinoma progression via inhibiting Klf4 transcriptional activity,” *Cell Death & Disease*, vol. 10, no. 11, p. 814, 2019.
- [40] J. H. Pan, H. Zhou, L. Cooper et al., “LAYN is a prognostic biomarker and correlated with immune infiltrates in gastric and colon cancers,” *Frontiers in Immunology*, vol. 10, p. 6, 2019.
- [41] J. I. Youn, S. Nagaraj, M. Collazo, and D. I. Gabrilovich, “Subsets of myeloid-derived suppressor cells in tumor-bearing mice,” *Journal of Immunology*, vol. 181, no. 8, pp. 5791–5802, 2008.
- [42] M. Mkrtychyan, Y. G. Najjar, E. C. Raulfs et al., “Anti-PD-1 synergizes with cyclophosphamide to induce potent anti-tumor vaccine effects through novel mechanisms,” *European Journal of Immunology*, vol. 41, no. 10, pp. 2977–2986, 2011.
- [43] D. I. Gabrilovich and S. Nagaraj, “Myeloid-derived suppressor cells as regulators of the immune system,” *Nature Reviews Immunology*, vol. 9, no. 3, pp. 162–174, 2009.
- [44] S. Nagaraj and D. I. Gabrilovich, “Tumor escape mechanism governed by myeloid-derived suppressor cells,” *Cancer Research*, vol. 68, no. 8, pp. 2561–2563, 2008.
- [45] V. Huber, V. Vallacchi, V. Fleming et al., “Tumor-derived microRNAs induce myeloid suppressor cells and predict immunotherapy resistance in melanoma,” *The Journal of Clinical Investigation*, vol. 128, no. 12, pp. 5505–5516, 2018.
- [46] Q. Peng, K. Li, K. Anderson et al., “Local production and activation of complement up-regulates the allostimulatory

- function of dendritic cells through C3a-C3aR interaction,” *Blood*, vol. 111, no. 4, pp. 2452–2461, 2008.
- [47] M. K. Liszewski, M. Kolev, G. le Friec et al., “Intracellular complement activation sustains T cell homeostasis and mediates effector differentiation,” *Immunity*, vol. 39, no. 6, pp. 1143–1157, 2013.
- [48] M. Kolev, S. Dimeloe, G. le Friec et al., “Complement regulates nutrient influx and metabolic reprogramming during Th1 cell responses,” *Immunity*, vol. 42, no. 6, pp. 1033–1047, 2015.
- [49] R. Pio, L. Corrales, and J. D. Lambris, “The role of complement in tumor growth,” *Advances in Experimental Medicine and Biology*, vol. 772, pp. 229–262, 2014.
- [50] D. Ricklin, S. K. Ricklin-Lichtsteiner, M. M. Markiewski, B. V. Geisbrecht, and J. D. Lambris, “Cutting edge: members of the *Staphylococcus aureus* extracellular fibrinogen-binding protein family inhibit the interaction of C3d with complement receptor 2,” *Journal of Immunology*, vol. 181, no. 11, pp. 7463–7467, 2008.
- [51] J. L. Platt, I. Silva, S. J. Balin et al., “C3d regulates immune checkpoint blockade and enhances antitumor immunity,” *JCI Insight*, vol. 2, no. 9, 2017.
- [52] L. Corrales, D. Ajona, S. Rafail et al., “Anaphylatoxin C5a creates a favorable microenvironment for lung cancer progression,” *Journal of Immunology*, vol. 189, no. 9, pp. 4674–4683, 2012.
- [53] P. Berraondo, L. Minute, D. Ajona, L. Corrales, I. Melero, and R. Pio, “Innate immune mediators in cancer: between defense and resistance,” *Immunological Reviews*, vol. 274, no. 1, pp. 290–306, 2016.
- [54] Y. L. Chen, Y. H. Uen, C. F. Li et al., “The E2F transcription factor 1 transactivates stathmin 1 in hepatocellular carcinoma,” *Annals of Surgical Oncology*, vol. 20, no. 12, pp. 4041–4054, 2013.
- [55] T. Couri and A. Pillai, “Goals and targets for personalized therapy for HCC,” *Hepatology International*, vol. 13, no. 2, pp. 125–137, 2019.
- [56] S. Artavanis-Tsakonas and M. A. Muskavitch, “Notch: the past, the present, and the future,” *Current Topics in Developmental Biology*, vol. 92, pp. 1–29, 2010.
- [57] P. Ranganathan, K. L. Weaver, and A. J. Capobianco, “Notch signalling in solid tumours: a little bit of everything but not all the time,” *Nature Reviews Cancer*, vol. 11, no. 5, pp. 338–351, 2011.